PROTON MAGNETIC RELAXATION INVESTIGATIONS OF CORRELATION AMONG MOLECULAR STRUCTURE AND DYNAMICS IN LIQUID CRYSTALS AND FABRICATION OF FIELD CYCLING NMR SPECTROMETER

A Thesis Submitted
for the award of the Degree of

DOCTOR OF PHILOSOPHY

By

A. SESHA SAILAJA

SCHOOL OF PHYSICS
UNIVERSITY OF HYDERABAD
HYDERABAD- 500 134, INDIA

APRIL 1994

TO ...

MY PARENTS

DECLARATION

I hereby declare that the work reported in this thesis has been carried out by me independently in the School of Physics, University of Hyderabad, under the supervision of Dr. K. Venu. I also declare that this work is original and has not formed the basis for the award of any degree, diploma, fellowship, associateship or similar title of any University or Institution.

A. S. Sailaja.

(A. Sesha Sailaja)

Date : 21/4/'94

Place : Hyderabad.

Certificate

This is to certify that the work reported in this thesis has been carried out by Ms. A. Sesha Sailaja, under my supervision and it is her bonafide work. The work is original and has not been submitted for any other degree of this or any other university.

K. Venu 21/04/09

(Dr. K. Venu)
Thesis Supervisor

Dean 21.4.09
School of Physics
Univeristy of Hyderabad.

ACKNOWLEDGEMENTS

I wish to express my thanks to Dr. K. Venu for his guidance in completing this project successfully. I also acknowledge him for all the encouragement throughout the period of this work.

No words are adequate to express my gratitude to Prof. V.S.S. Sastry who impressed upon me the beauty of physics in general, and in particular liquid crystals. I make an honest attempt to thank him for all the inspiring discussions I had with him, which helped me to pursue the course with perseverance.

I thank the Dean, School of Physics for the facilities provided during the project. I also express my thanks to other faculty members and staff of the school.

I thank the staff of the Central workshop and Central Instruments Laboratory for their timely cooperation.

I would like to thank all my friends and colleagues in the laboratory and department who helped me a lot during the course of the work. I express my thanks to Mr. R.K. Subramanian for all the fruitful discussions and encouragement he offered during the difficult times. I am also grateful to him for patiently and speedily typing the many versions of the manuscript which helped me in submitting the thesis within the stipulated time.

My special thanks to Mrs. Veena Tejaswini, whose help was immense during the fabrication of the field cycling spectrometer. I also wish to thank my friends Ms. M.V. Sailaja, Ms. K. Karunasree and Ms. Padma with whom I have shared many a happy occasion during my stay in the campus.

To my loving parents and brothers, whose patience and constant encouragement induced confidence in me during many a depressing time, I attempt to say thanks. Their love and affection helped me in completing the course successfully.

Finally, I would like to thank the Council of Scientific and Industrial Research, India for providing me financial support during the course of the work.

CON-TENTS

PREFACE

Liquid crystals have been systems of immense interest in recent years due to the numerous physical phenomena involved, like phase transitions leading to rich polymorphism, ferroelectricity, nonlinear dynamics, reentrant phenomena, incommensurate structures etc., apart from their wide ranging technical applications like in electro-optical devices, digital logic devices (due to fast switching times), surface temperature detectors, etc. Particularly, there have been major efforts to understand the influence of microscopic details (like molecular structure) on various phenomena exhibited by these systems, which is far from accomplished at present. This is an important aspect necessary to understand the nature of these systems in order to be able to optimize their properties for specific applications. An important step in this direction is to study the relation between the molecular structure and microscopic dynamics.

Liquid crystals, with mesophases in between a solid (X) and liquid (I) are characterized by molecular dynamics intermediate to them resulting in a complicated fluctuation spectrum. The long rod like molecular conformation in them leads to long range cooperative interactions, and hence collective fluctuations of the partially ordered molecules. These collective fluctuations (order director fluctuations, ODF), - perceived as hydrodynamic phenomena influenced by elastic and viscosity coefficients of the medium - make these systems unique and interesting. Along with the other molecular motions, like translational self diffusion (SD) and molecular reorientations (R) which are sensitive to the nature of anisotropic interactions, the collective fluctuations are known to provide a novel contribution to the dynamics. Attempts to understand the manner in which the order affects the individual motions in liquid crystals are rather meagre. Even though a large number of liquid crystals have been studied with a view to obtaining information about these dynamic processes, there have been very few attempts to understand the influence of microscopic structure and physical properties on these dynamic processes. At present, a number of unsolved problems exist in this regard like for example (i) the dependence of order director

fluctuations on the details of the end chains or on the core, (ii) the effect of order on individual reorientations, (iii) the influence of varying degrees of order on molecular translational diffusion, etc. In this regard, a systematic investigation of several systems in different mesophases within a homologous series seems to be necessary to obtain definite information about these molecular mechanisms. The present work aims at such a systematic study in two homologous series, viz., alkyloxy benzilidene alkylanilines and alkyloxy benzoic acids.

Since the above mentioned fluctuations have power spectra with intensities in the radio frequency (rf) region, nuclear magnetic resonance (NMR) is best suited to probe such processes. NMR relaxation rates reflect the time dependence of intra and intermolecular interactions among nuclear spins arising due to underlying molecular motions (lattice). Thus, the details of the spin lattice relaxation processes lead to the mapping of spectral densities of the various fluctuations perturbing the spin system. An elaborate study of frequency (over a few decades) and temperature dependent relaxation rates thus gives detailed information on the different mechanisms mediating the relaxation processes, and the associated dynamic parameters. In the present studies, proton spin lattice relaxation measurements performed as a function of frequency and temperature have been used to obtain information about the molecular dynamics.

The correlation times of all the above mentioned mechanisms are comparable to the conventional NMR frequency range, resulting in a complicated power spectrum as seen by the NMR spin probe. Such a situation necessitates an elaborate frequency and temperature dependent study of relaxation times to decouple the contributions from different dynamic processes. In this regard conventional NMR, though versatile in its own right, is limited by the range of accessible time scales and hence frequencies. Extension of the frequency dispersion measurements to the low frequency region (< 5 MHz, where conventional NMR fails due to weakening of the signal strength) is more rewarding, particularly since the major contribution to relaxation from ODF lies in the low frequency region. Field cycling NMR (FCNMR) facilitates such measurements

and part of the aim of the work reported in this thesis is to set up an FCNMK facility in the laboratory. This thesis presents the results of proton NMR investigations of molecular dynamics in two families of liquid crystals and the details of fabrication of the FCNMR spectrometer. The organization of the thesis which contains four chapters is as discussed below.

The first chapter aims at providing a comprehensive review of the various theoretical models available in literature connecting the NMR relaxation rates in different mesophases with molecular parameters associated with underlying dynamic processes in liquid crystals, viz., order director fluctuations, translational self diffusion and reorientations. The effects of phase transitions from isotropic liquid to nematic (N) phase and nematic to smectic (S_A) phase are also considered.

The details of the FCNMR instrumentation are presented in chapter 2. This Chapter consists of four sections. The first section discusses the general methodology of pulsed NMR measurements, providing a background of time domain NMR spectroscopy. The second section provides the details of the fabrication of FCNMR spectrometer. The third section provides a brief description of the high frequency spectrometer used in this work. The experimental procedures adopted for the present studies is discussed in the fourth section.

The third chapter presents the results of the proton NMR T_1 measurements (5 - 50 MHz) on three liquid crystals belonging to the homologous series, butyloxy benzilidene alkyl anilines (4O.m), viz. 40.4, 40.3 and 40.2. The first section of this chapter contains a brief review of the literature available on nO.m compounds. This, even though by no means is exhaustive, aims at providing the basic background needed to appreciate the results presented in the subsequent sections. The next three sections deal with the studies on 40.4, 40.3 and 40.2 respectively. The final outcome of these studies, particularly in comparison with the existing information on the other nO.m compounds is discussed in the last section.

The experimental results on two systems belonging to the homologous series alkyloxy benzoic acids, *p*-heptyloxy benzoic acid (pHepBA) and *p*-nonyloxy benzoic acid (pNBA) are presented in the fourth chapter. The first section attempts to briefly review the literature available on these compounds. The next two sections present the results of the measurements on pHepBA and PNBA, respectively. Conclusions arrived at from these studies by comparison with the existing literature on this homologous series are presented in the final section.

Chapter 1

NMR RELAXATION IN LIQUID CRYSTALS

Magnetic resonance spectroscopy probes the dynamics of condensed matter systems in time scales ranging from 10^{-11}sec to 10^{-1} sec (corresponding to atomic dimensions and to sizes of molecular aggregates respectively on the length scales). A typical time domain magnetic relaxation spectroscopic experiment consists of stimulating the system by external radiation to a known non equilibrium state and then monitoring the approach of the system (i.e. the response of the system) to equilibrium state. This process called relaxation, is characterized by the variation of one or more macroscopic variables in time. The finite life time of fluctuations and hence of the response function leads to a description of the dynamic properties like transport coefficients and responses for time dependent perturbations in terms of time dependent correlation functions. In other words, the correlation functions result in a knowledge of the details of instantaneous potential fields and hence of the dominant molecular interactions, intensity and duration of forces (torques) etc. Thus relaxation theory provides a link between the experiment performed at macroscopic time scales and useful parameters characterizing the microscopic dynamics at molecular level. This chapter gives a brief review of the relaxation mechanisms in liquid crystals. The basic NMR relaxation theory is discussed briefly in the first section. The second section discusses the relaxation due to various mechanisms in the different mesophases of a

liquid crystal. The theory connected with dipolar relaxation, which probes the slow molecular motions is explained in the third section.

Section - 1

1.1 *NMR relaxation theory*

NMR deals with the interaction between nuclei having a magnetic moment, μ (spin angular momentum, J and gyromagnetic ratio 7) and an external dc magnetic field resulting in equally spaced energy levels. The presence of these energy levels can be detected with a time dependent interaction causing transitions between these levels. The macroscopic process which causes the evolution of the system from the initial excited state (non equilibrium state) to the final equilibrium state through energy exchange with the surroundings is termed as relaxation. Depending on the agents of the energy exchange, the relaxation process can be spin-spin or spin-lattice relaxation process. Spin-spin relaxation (with a time constant, T_2) corresponds to relaxation through redistribution of energies within the spin system and hence no change in entropy of the system. On the other hand, spin-lattice relaxation (with a time constant, $T\backslash$) is the process of energy exchange between the perturbed spin system and other degrees of freedom of the system (lattice or bath) through fluctuations in the surrounding electromagnetic fields, resulting in a change of entropy of the system. The lattice can be of many possible forms such as molecular rotations, diffusion, lattice vibrations etc.

Thus, a measurement of T_1 gives information about the time modulation of the fluctuating local fields surrounding the spin system, $\mathbf{B}_{loc}(t)$. These local fields are the dipolar fields arising due to interaction with the surrounding dipoles. The different atomic or molecular interactions (leading to the fluctuating fields) can be described by the appropriate time dependent correlation functions or the related Fourier intensities (spectral densities). The characteristic time, τ_c associated with these motions can be obtained by measuring the correlation functions **over a time interval or the related power spectrum over a frequency range. Thus a frequency dependent study**

of NMR relaxation rate probes the power spectrum for possible information about the fluctuating molecular dynamics i.e., the measurement of nuclear spin-lattice relaxation time, T_1 yields the spectral density, $J(\omega)$, which is the Fourier transform of the autocorrelation function for the corresponding motions.

1.1.1 Spin lattice relaxation

Different approaches viz., quantum mechanical time dependent perturbation theory (Bloombergen et al. 1948 ; Abragam, 1961), spin temperature concept (Goldman, 1970 ; Wolf, 1979), density matrix formalism (Wangsness and Bloch, 1953 ; Slichter, 1978) etc. lead to the following expression for the spectral density and hence the spin lattice relaxation rate

$$\frac{1}{T_1} \propto J_m(\omega) \simeq \int_0^\infty G_m(\tau) e^{i\omega\tau} d\tau \qquad \textbf{(1.1)}$$

Here $G_m(\tau)$ qunatifies the correlation between the random functions $B_{loc}(t)$ at times t and $t + \tau$ and is given by the ensemble average of the corresponding fluctuating Hamiltonian as

$$G_m(\tau) = < B^*_{loc}(t) B_{loc}(t + \tau) >_{av} \qquad \textbf{(1.2)}$$

Considering the fluctuations in $B_{loc}(t)$ to be stationary and Markovian in time, the correlation function can be written as

$$G_m(\tau) = <| B_{loc}(0) |^2> e^{-t/\tau_c} \qquad (1.3)$$

where τ_c is the correlation time. The corresponding spectral density function is a Lorentzian (i.e $J(\omega) \propto \tau_c/(1+\omega^2\tau_c^2)$. In the case of dipole dipole interaction between two like spins separated by a distance r, the relaxation rate can be written as (Slichter, 1978)

$$\frac{1}{T_1} = C\left[J_1(\omega) + \frac{1}{2}J_2(2\omega)\right] \tag{1.4}$$

The constant C in eqn. (1.4) depends on the geometery of the spin system and the type of dynamics under consideration. $J_1(\omega)$ and $J_2(2\omega)$ are the spectral densities at frequencies ω and 2ω respectively. The subscripts 1 and 2 correspond to one spin flip and two spin flips respectively.

By considering the additional non-secular broadening effect (Kubo and Tomita 1954 ; Solomon, 1955), the above equation can be modified as

$$T_1^{-1} = C_1\,[J_1(\omega) + J_2(2\omega)] \tag{1.5}$$

If different molecular motions are present in a system (each one mediating the relaxation process with its own individual spectra] density function) which are independent of each other, the total relaxation rate is obtained as a sum of individual relaxation rates i.e.,

$$T_1^{-1} = \sum_{\lambda} (T_1^{-1})_{\lambda} \tag{1.6}$$

where A denotes the type of mechanism. Thus in any system, estimate of the total relaxation rate involves modelling different molecular motions and computing the corresponding contribution from each mecihanism to the relaxation.

Section - 2

1.2 *Spin lattice relaxation theory of liquid crystals*

The anisotropic nature of liquid crystalline medium leads to partial averaging of the different magnetic interactions. This results in a collection of different components of the interaction Hamiltonian with dissimilar correlation times. Thus, the anisotropic

nature of the medium complicates the separation of the different dynamics occuring in the medium and hence necessitates more experimental data to interpret the results in terms of the theoretical models when compared to either isortopic liquids or solids. Investigation of molecular dynamics in these systems have revealed the presence of three major dynamic processes contributing to relaxation. The T_1 profile of liquid crystals is usually dominated by collective fluctuations at low frequencies (normally a few MHz or below), molecular self diffusion at high frequencies (of the order of a few MHz and above) and molecular rotations about different axes in the high frequency region (order of MHz). Further cross relaxation due to other nuclei like nitrogen are also present at very low frequencies (< MHz). Apart from the above, pretransitional phenomena like onset of orientational order at nematic-isotropic transition, the layer formation at the nematic-smectic A transition show profound effect on the relaxation rate, close to the phase transition temperatures.

However, each of the mechanism described above has its own characteristic temperature and frequency dependence. Hence these contributions can be separated using an elaborate frequency and temperature depndent study of the relaxation rate (relaxation spectroscopy). The details of these mechanisms that become dominant at different temperature regions (as the liquid crystalline system is cooled from the isotropic phase to solid phase) are given below.

1.2.1 Isotropic phase

Well inside the isotropic phase, there is neither positional nor orientational ordering and all the dynamic processes except self diffusion are fast compared to normal NMR time scales (thus leading to a temperature and frequency independent relaxation rate).

Torrey's theory (1953) for isotropic diffusion of liquids can be extended to the anisotropic systems appropriately. The inter molecular dipole-dipole interactions are modulated by the self diffusion process, which can be considered as a limiting case of the random flights model (Chandrasekhar, 1943).

The correlation functions for the inter molecular dipolar interaction, modulated by the diffusive motion of the molecule are given by

$$K_\alpha(t) = \sum_j < F_{ij}^{\alpha}(t) F_{ij}^{\alpha *}(t+\tau) >_{Av(t)} \quad ; \qquad \alpha = 1,2 \tag{1.7}$$

where $< >_{Av(t)}$ represents the time average. The functions $F_{ij}^{\alpha}(t)$ which are the space part of the non-secular component of the dipolar interaction are given by (Slichter, 1978)

$$F_{ij}^{(1)}(t) = \sin\theta_{ij} \cos\theta_{ij} e^{i\phi_{ij}} / r_{ij}^3 \tag{1.8a}$$

$$F_{ij}^{(2)}(t) = \sin^2\theta_{ij} e^{2i\phi_{ij}} / r_{ij}^3 \tag{1.8b}$$

where r_{ij}, θ_{ij} and *faj* are the spherical coordinates of spin j relative to spin i. In evaluating the spectral density functions, the time averages in eqn. (1.7) are replaced by the ensemble averages. Thus

$$K_\alpha(t) = \int\int P(\mathbf{r}, \mathbf{r}_o, t) F_{ij}^{\alpha}(\mathbf{r}_o) F_{ij}^{(\alpha)*}(\mathbf{r}) f(\mathbf{r}_o) d\mathbf{r}_o d\mathbf{r} \tag{1.9}$$

where $P(\mathbf{r}, \mathbf{r}_o, t)d\mathbf{r}$ is the probability that the spin j located at $\mathbf{r}_o$ at t = 0 relative to spin i, will lie at time t within the volume elememt *dr* located at r relative to the new position of i. $f(\mathbf{r}_o)$ is the initial spin density. Considering N to be the total number of spins, $N^{-1} f(\mathbf{r}_o) d\mathbf{r}_o$ is the probability that at time t = 0, spin j is located in $d\mathbf{r}_o$ at $\mathbf{r}_o$ relative to spin i. The function $P(\mathbf{r}, \mathbf{r}_o, t)$ can be found from the theory of random flights as follows (Chandrasekhar, 1943).

Assuming that every position of the spin is statistically equivalent i.e., at any position the probability of the spins occupying a new position r in volume element *dr* relative to the previous position (after a single flight) is the same (designated by $P_1(\mathbf{r})d\mathbf{r}$), $P_n(\mathbf{r})d\mathbf{r}$ after n flights is given by

$$P_n(\mathbf{r})d\mathbf{r} = \frac{1}{8\pi^3} \int (A(\mathbf{q}))^n e^{-i\mathbf{r}.\mathbf{q}} d\mathbf{q} \tag{1.10}$$

Here the integration is over the entire $\mathbf{q}$ space and $A(\mathbf{q})$ is the Fourier transform of P_1 (r) given by

$$A(\mathbf{q}) = \int P_1(\mathbf{r}) e^{i\mathbf{q}\cdot\mathbf{r}} d\mathbf{r} \tag{1.11}$$

The probability $P(r,t)dr$ that a spin initially at the origin will be located at r in $d\mathbf{r}$ after a time t is

$$P(\mathbf{r}, t) = \sum_n P_n(\mathbf{r}) w_n(t) \tag{1.12}$$

where $w_n(t)$ is the probability that n flights take place in time t, for which a Poisson distribution is assumed i.e.,

$$w_n(t) = \frac{1}{n!} \left[\frac{t}{\tau}\right]^n e^{-t/\tau} \tag{1.13}$$

r being the time between the flights. The summation in eqn. (1.12) includes the term n = 0, where $P_o(\mathbf{r})$ = $S(r)$ and $6(r)$ is the three dimensional S function. Substituting eqn. (1.13) and eqn. (1.10) in eqn. (1.12), the expression for $P(\mathbf{r},t)$ and hence $P(\mathbf{r}, \mathbf{r}_o, t)$ can be calculated. Transforming to a relative centroidal coordinate system with r = $\mathbf{r}_i$ — $\mathbf{r}_j$ and R = $\frac{1}{2}(\mathbf{r}_j + \mathbf{r}_i)$ (where $\mathbf{r}_i$ and $\mathbf{r}_j$ are the position vectors of spins i and j relative to a common origin) and finally integrating over all positions and substituting for the correlation functions with appropriate initial spin density, $f(\mathbf{r}_o)$, the spectral density can be calculated.

For isotropic diffusion which corresponds to uniform spin density, the correlation function K_1 is given by

$$K_1(t) = \frac{n}{4\pi} \int\int\int \frac{\sin\theta_o \cos\theta_o \sin\theta \cos\theta}{r_o^3 r^3} e^{i(\phi_o - \phi)} \times \exp\left[-i\mathbf{q}(\mathbf{r} - \mathbf{r}_o) - \frac{2t}{\tau}[1 - A(\mathbf{q})]\right] d\mathbf{r} d\mathbf{r}_o d\mathbf{q} \tag{1.14}$$

where n = $f(\mathbf{r}_o)$ represents the uniform spin density. Expansion of $e^{-i\mathbf{q}.\mathbf{r}}$ and $e^{i\mathbf{q}.\mathbf{r}_o}$ in terms of Legendre and Bessel functions results in

$$e^{iqr\cos\phi} = \left[\frac{\pi}{2qr}\right]^{1/2} \sum_{n=0}^{\infty} (2n+1)\, i^n\, J_{n+1/2}(qr)\, P_n(\cos\phi) \tag{1.15}$$

Equation (1.14) can be simplified to

$$K_1(t) = \frac{8\pi n}{15a^3} \int_0^{\infty} \exp\left[-\frac{2t}{\tau}[1 - A(\mathbf{q})]\right] J^2_{3/2}(a\mathbf{q}) \frac{d\mathbf{q}}{\mathbf{q}} \tag{1.16}$$

where 'a' is assumed to be the closest possible distance of approach of two nuclei. The corresponding spectral density is given by

$$J_1(\omega) = 2\int_0^{\infty} \cos(\omega t) K_1(t)\, dt$$

$$= \frac{8\pi n\tau}{15a^3} \int_0^{\infty} J^2_{3/2}(a\mathbf{q}) \frac{[1 - A(\mathbf{q})]}{[1 - A(\mathbf{q})]^2 + (\omega\tau/2)^2} \frac{d\mathbf{q}}{\mathbf{q}} \tag{1.17}$$

A similar calculation for $K_2(t)$ results in

$$K_2(t) = 4K_1(t) \tag{1.18}$$

and

$$J_2(\omega) = 4J_1(\omega). \tag{1.19}$$

The possible choices of A(q) can be limited to three cases.

Case (i) : $\omega\tau > 1$

Since r is assumed to vary with temperature as r = $\tau_o e^{E_a/kT}$ for a thermally activated process, this case corresponds to the low temperature asymptote of T_1 i.e.

$$A(\mathbf{q}) \leq \int | e^{i\mathbf{q}.\mathbf{r}} | \; P_1(\mathbf{r})\, d\mathbf{r} = 1$$

Hence 1 — $A(\mathbf{q}) \ll 1$ can be neglected and the spectral density can be simplified as

$$T_1^{-1} \propto J_1(\omega) = \frac{32\pi n}{15a^3\omega^2\tau} \int_0^\infty J_{3/2}^2(a\rho)\, [1 - A(\mathbf{q})]\, \frac{d\mathbf{q}}{\mathbf{q}} \tag{1.21}$$

i.e., $J_1(\omega) \propto (\omega^2\tau)^{-1}$. Thus

$$T_1 \propto \omega^2\tau = \omega^2\tau_o e^{E_a/kT} \tag{1.22}$$

Case (ii) : $\omega\tau \ll 1$

In this case, $\omega\tau = 0$ and hence the spectral density is given by

$$J_1(\omega) = \frac{8\pi n\tau}{15a^3} \int_0^\infty J_{3/2}^2(a\mathbf{q})\, \frac{1}{[1 - A(\mathbf{q})]}\, \frac{d\mathbf{q}}{\mathbf{q}} \tag{1.23}$$

Since the integral in the above equation always converges, the spin lattice relaxation rate (T_1^{-1}) is given by

$$T_1^{-1} \propto J_1(\omega) \propto T \tag{1.24a}$$

or

$$T_1 \propto \frac{1}{\tau} = \frac{1}{\tau_o}\, e^{-E_a/kT} \tag{1.246}$$

This case corresponds to a higher temperature asymptote for T_1 which is just the opposite of case (i). It is seen that whenever the frequency ω is in between these two cases, there exist a particular r for which the relaxation rate is maximum (and hence T_1 is minimum).

Case (iii) : $< r^2 \gg a^2$

This is a special case for which the mean flight path is long. The function $[1 - A(\mathbf{q})]$ vanishes for q = 0 and approaches unity for large q. The value of $P_1(\mathbf{r})$ is very small and hence

$$J_1(\omega) = \frac{8\pi n}{45a^3} \frac{\tau/2}{1+(\omega\tau/2)^2} \tag{1.25a}$$

Thus

$$T_1^{-1} = \frac{8\pi n}{15a^3}\gamma^4\hbar^2 I(I+1)\left[\frac{\tau/2}{1+(\omega\tau/2)^2} + \frac{2\tau}{1+(\omega\tau)^2}\right]$$

The above two equations have the well known forms appropriate to an exponentially decaying correlation function with a correlation time τ_c = T/2 and the T_1 minimum obtained from eqn. (1.25b) when $\omega\tau = \sqrt{2}$ is given by

$$T_{1min}^{-1} = \frac{16\sqrt{2}\pi}{45}\gamma^4\hbar^2 I(I+1)\frac{n}{a^3\omega} \tag{1.26}$$

Case (iv) :

Assuming special forms for $P(r)$ and A(q), say

$$P_1(\mathbf{r}) = \frac{1}{4\pi D\tau r}\exp\left[-r/(D\tau)^{1/2}\right] \tag{1.27}$$

(where D is the diffusion coefficient) corresponds to $A(q) = [1 + D\tau q^2]^{-1}$ which is mathematically the simplest form for $A(\mathbf{q})$ satisfying all the conditions that can be imposed for an acceptable form. Substituting in eqn. (1.23), the spectral density is obtained as

$$J_1(\omega) = \frac{16\pi n}{15a^3} Re\,[J] \tag{1.28}$$

where J is the Bessel function given by

$$J = \int_0^\infty \frac{1 + D\tau q^2}{2Dq^2 - i\omega(1 + D\tau q)} \, J_{3/2}^2(aq) \, \frac{dq}{q} \tag{1.29}$$

Simplifying eqn. (1.28) (Torrey, 1953) results in

$$J_1(\omega) = \frac{8\pi n}{15a^3\omega} \, f(\alpha, x) \tag{1.30}$$

The function $f(\alpha, x)$ is given by

$$f(\alpha, x) = \frac{2}{x^2}\left[v\left(1 - \frac{1}{u^2 + v^2}\right) + \left(v\left(1 + \frac{1}{u^2 + v^2}\right) + 2\right) e^{-2v} \cos 2u \right.$$
$$\left. + u\left(1 - \frac{1}{u^2 + v^2}\right) e^{-2v} \sin 2u \right] \tag{1.31}$$

with u and v defined in terms of a and x as

$$\begin{pmatrix} u \\ v \end{pmatrix} = \frac{(\omega a^2/2D)^{1/2}}{(4 + \omega^2\tau^2)^{1/4}} \left\{1 \mp \frac{\omega\tau}{(4 + \omega^2\tau^2)^{1/2}}\right\}^{1/2} \tag{1.32a}$$

and

$$a = < r^2 > /12a^2 \; ; \; x = (\omega a^2/2D)^{1/2} \tag{1.32b}$$

Let

$$w = \frac{\omega\tau/2}{[1 + (\omega\tau/2)^2]^{1/2}} = \frac{\alpha x^2}{(1 + \alpha^2 x^4)^{1/2}}$$

Then, u and v can be expressed as

$$\begin{pmatrix} u \\ v \end{pmatrix} = \frac{1}{2}\left[\frac{w(1 \mp w)}{\alpha} \right]^{1/2} \tag{1.33}$$

Hence the expression for the relaxation rate (in terms of $J_1(\omega)$ and $J_2(2\omega)$) is given by

$$(T_1^{-1})_{Torrey} = \frac{4}{5}\gamma^4\hbar^2 I(I+1)\frac{n\pi}{a^3\omega}\phi(\alpha, x) \qquad \textbf{(1.34)}$$

where $\phi(\alpha, x) = f(\alpha, x) + f(\alpha, \sqrt{x})$. In the limit, $\omega\tau \gg 1$, the spectral density term and hence the relaxtion rate reduces to the ω^{-2} law. Similarly for $\omega\tau \gg 1$, it can be shown that $T_1^{-1} \propto \omega^{1/2}$, i.e.

$$T_1^{-1} = C - F\omega^{1/2} \qquad (1.35)$$

where F and C are constants related to the diffusion coefficient D and are given by (Harmon and Muller, 1969)

$$F = -4.77 \times 10^{-14}(1+\delta)D^{-3/2} \qquad (1.36a)$$

$$C \text{ oc } D^{-1} \qquad (1.366)$$

1.2.2 Near the Isotropic-nematic transition (TV/)

Not too far from the transition temperature (typically about 10 to 15°C above T_{NI}) local nematic clusters start forming (Wade, 1977). The molecules are locally parallel to each other along an average direction n, with a short range order described by a coherence length ξ. These clusters are stable for short intervals of time. The formation and breaking of the local nematic clusters gives rise to fluctuations in the dipolar interaction of the nuclear spins (ordered fluctuations) resulting in a significant contribution to the relaxation and hence pretransition phenomena (Luckhurst, 1988). If the short range order is long lived compared to the time scaleSof NMR measurement (ω^{-1}), then the T_1 is not sensitive to these fluctuations. On the other hand, if the order fluctuations are in the time scales of the Larmor frequency $(\sim\omega^{-1})$, then T_1 is sensitive to these fluctuations.

The above explained nematic order can be quantified in terms of the microscopic order parameter (de Gennes, 1974)

$$S_{ij}^{\alpha\beta} = \frac{1}{2} < (3i_\alpha i_\beta - \delta_{ij}\delta_{\alpha\beta}) > \quad (1.37)$$

i, j and k being the ortho normal unit vectors, a and β are the indices refering to the laboratory frame, the average is the ensemble average taken over all the molecules. δ_{ij} and $\delta_{\alpha\beta}$ represent the Kroneckar symbols. The symmetric nature of the liquid crystalline molecules (de Gennes, 1974), then a suitable transformation into a digaonalized form and finally the imposition of the uniaxial nature of the molecules reduces the order parameter into a simple scalar quantity given by

$$S = \frac{1}{2} < 3\cos^2\theta - 1 > \quad (1.38)$$

where *0* is the angle between the direction of the long molecular axes and the average direction of the medium n, called the director. This definition of the order parameter is compatible with the usual case of S = 0 for isotropic liquids and S = 1 for a solid.

The mean square amplitude of the fluctuations and the correlation times associated with these fluctuations can be obtained from Landau - de Gennes theory (de Gennes, 1974), according to which free energy density, g(S,T) which can be expanded in powers of order parameter, *S = S(r,t)* as

$$g(S,t) = g_o + \frac{1}{2}AS^2 + \frac{3}{2}BS^3 + \frac{1}{2}C\,(\nabla S)^2 + .. \quad (1.39)$$

The presence of the cubic term ensures that the transition is first order and the presence of ordered fluctuations are reflected in the gradient term where *C* is a positive elastic constant of the medium. The coefficient A should be small below the transition temperature and should diverge critically for T > T_{NI} and hence is expected to vary as

$$A = A(T) = a\,(T - T_{NI})^{\nu} \;\; ; \;\; a > 0 \quad (1.40)$$

For A > 0 i.e. T > T_{NI}, the equilibrium value of S is zero. The nematic order parameter, *S(r,t)* can be written in terms of the Fourier components $S(\mathbf{q},t)$as

$$\mathbf{S(r)} = \frac{1}{\sqrt{V}} Re \sum_{\mathbf{q}} S(\mathbf{q})\, e^{i\mathbf{q}.\mathbf{r}} \tag{1.41}$$

in order to explain the spatial dependence of the director. Replacing the summation by integration to include the entire volume, the free energy can be written as $F = \int g dV$ i.e.,

$$F - F_o = \frac{1}{2} A \sum_{\mathbf{q}} |\, S(\mathbf{q})\,|^2 \;\; [1 + q^2\xi^2] \tag{1.42}$$

where $\xi = \left(\frac{C}{A}\right)$ is the coherence length and it measures the distance over which the local nematic order persists in the isotropic phase. The characteristic time, $\tau_{\mathbf{q}}$ for the persistence of q modes is given from the Landau-Khalatnikov's equation (Landau and Khalatnikov, 1954) as

$$\frac{dS(\mathbf{q})}{dt} = -\Gamma \frac{dF}{|\, dS(\mathbf{q},t)\,|} = -\Gamma\, [1 + q^2\xi^2] \;\; |\, S(\mathbf{q})\,| \tag{1.43}$$

$\tau_{\mathbf{q}} = \Gamma^{-1}/[A(1 + q^2\xi^2)]$, where Γ^{-1} is average viscosity of the medium for long wavelength fluctuations and $\tau_{\mathbf{q}}$ tends to oo as T $\rightarrow$ T_{NI}.

The spin lattice relaxation rate due to the modulation of intra molecular dipolar interaction can be obtained from the corresponding correlation functions and hence the spectral densities. The interaction Hamiltonian for the pair wise dipolar interaction between two protons, i.e. protons of a benzene ring separated by a distance r is given by

$$H_D = -\frac{(\gamma\hbar)^3}{r^3} \;\; [3(I_1.\mathbf{n})(I_2.\mathbf{n}) - (I_1.I_2)] \tag{1.44}$$

Substituting eqn. (1.44) in the expression for the correlation function, $J_1(\omega)$ is obtained as

$$J_1(\omega) = \frac{1}{4}(\gamma H_L)^2 \int_{-\infty}^{\infty} < S(0)S(t) > e^{-i\omega t} dt \tag{1.45}$$

where $H_L = \gamma\hbar/r^3$ and the nematic director n is given in terms of the order parameter S of the system as

$$\overline{n^2}_z = \frac{1}{3} + \frac{2}{3}S$$

$$\overline{n_x^2} = \overline{n_y^2} = \frac{1}{3} - \frac{1}{3}S \tag{1.46}$$

and

$$\overline{n_x n_y} = \overline{n_x n_z} = \overline{n_y n_z} = 0$$

The autocorrelation function and the spectral density function for the above Hamiltonian are written as

$$< S(0)S(t) > = \frac{1}{V} \sum_{\mathbf{q}} <| S(\mathbf{q}) |^2> e^{-t/\tau_{\mathbf{q}}} \tag{1.47}$$

$$J_1(\omega) = \frac{1}{4}(\gamma H_L)^2 \frac{1}{V} \sum_{\mathbf{q}} <| S(\mathbf{q}) |^2> \frac{2\tau_q}{1 + (\omega\tau_q)^2} \tag{1.48}$$

Using the equipartition theorem in equ. (1.42), the mean square fluctuations in the order parameter are expressed as

$$<| S(\mathbf{q}) |^2>= \frac{kT}{A(T)(1 + q^2\xi^2)} \tag{1.49}$$

Replacing the summation in eqn. (1.48) by an integration from 0 to an upper cutoff

wave vector, $\mathbf{q}_m$ (which cannot be assumed to be oo due to the finite dimension of the molecule) to include all the q modes results in

$$J_1(\omega) = \frac{(\gamma H_L)^2}{2(2\pi)^3} \frac{kT}{\Gamma^{-1}} \int_0^{q_m} \frac{4\pi q^2 dq}{\omega^2 + [C\Gamma(q^2 + 1/\xi^2)]^2} \tag{1.50}$$

Here, $\mathbf{q}_m = \pi/l$ with / being the length of the molecule. The integral in the above equation is solved separately and is given by

$$I_1 = \frac{2\pi}{(C\Gamma)^{3/2}} \int_0^{x_m} \frac{\sqrt{x}dx}{\omega^2 + (x + r)^2} \tag{1.51}$$

Here r = $C\Gamma/\xi^2$ is the correlation frequency and $x_m = C\Gamma q_m^2$ is the upper cutoff frequency. For temperatures T away from the transition, $T_{NI}, r \ll x_m$ and $\omega \ll x_m$ and hence the upper limit can be taken as $x_m \rightarrow$ oo. Solving for I_1 gives

$$T_1^{-1} = \frac{2\pi}{(C\Gamma)^{3/2}} \frac{\sin(\frac{1}{2}\tan^{-1}(\omega/r))}{\sin(\tan^{-1}(\omega/r))} \frac{1}{(\omega^2 + r^2)^{1/4}} \tag{1.52}$$

In this context, two limiting cases can be considered depending on the relative values of Larrnor frequency and the cutoff frequencies.

Case (i) $\omega \ll$ r = ω_c

$$I_1 \propto \frac{1}{\sqrt{r}} \propto \xi$$

and hence

$$T_1 \propto \xi^{-1} \propto (T - T_{IN})^{\nu/2} \neq f(\omega) \tag{1.53}$$

Thus T_1 is strongly dependent on temperature but independent of frequency.

Case (ii) $\omega \gg r = \omega_c$

$$I \propto \frac{1}{\sqrt{\omega}}$$

Thus

$$T_1 \propto \sqrt{\omega} \neq f(T) \tag{1.54}$$

In this case, T_1 is proportional to the square root of frequency but is independent of temperature. This situation is close to T_{NI} where ξ becomes large and hence r is small (Blinc, 1976 ; Ghosh, 1976 ; Ghosh et al. 1980).

1.2.3 Nematic phase

The long axes of the molecules in the entire sample tend to align parallel to each other along an average direction and any unit vector $\mathbf{n_o}$ along this preferred direction is known as the nematic director, which may vary locally throughout the medium (Fig. 1.1). There is no long range correlation of molecular centers of mass and hence, the molecules move freely i.e., the nematic phase is fluid like. Thus, the nematic phase is characterized by long range orientational but no positional order. Due to the lack of translational order, the molecules are not rigidly fixed and hence any distortion (either due to external forces or boundary conditions) leads to simple rotation around the direction of molecular axis resulting in smaller elastic energies compared to solids. This small angle deformations from equilibrium postions are termed as curvature strains and the restoring forces are termed as curvature stresses or torques. The cooperative small angle rotations of the liquid crystalline molecules about their short axes, due to thermal fluctuations, result in a special kind of collective motions called order director fluctuations (ODF). Due to the large number of molecules involved, a major part of these fluctuations contribute to the relaxation at low frequencies compared to the Larmor frequencies of conventional NMR. These coherent fluctuations along

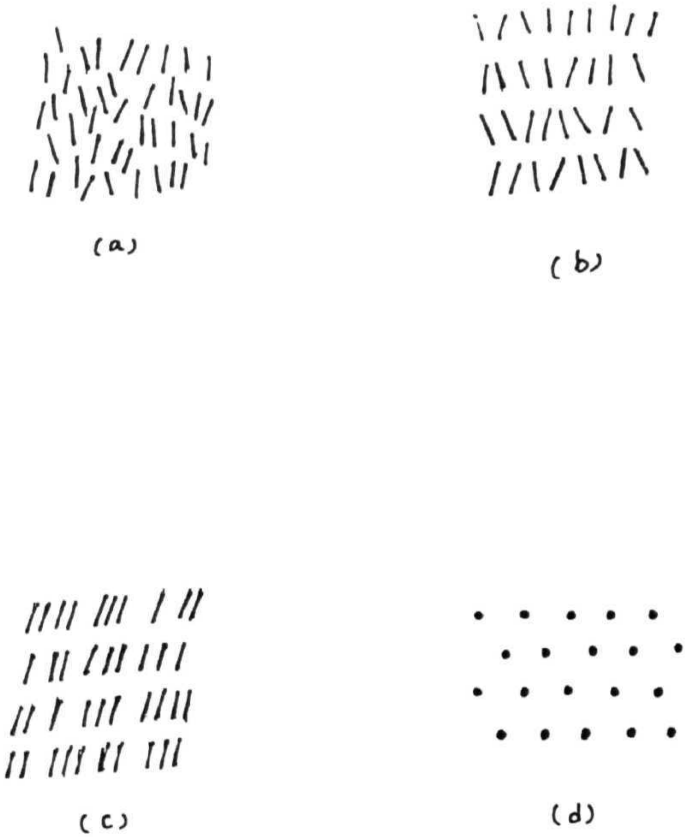

Fig. 1.1 The arrangement of molecules in different mesophases of liquid crystals
(a) Nematic phase, with orientational order but no positional order
(b) Smectic—A phase, with layer formation and nematic order in each layer
(c) Smectic — *C* phase, with tilted nematic order in each layer
(d) Smectic —*B* phase, with layer stacking and correlation among molecules in neighboring layers.

with **reorientations** and self diffusion form the dominant relaxation mechanisms in this phase and **the** details are discussed below.

Order director fluctuations

The precise role of the collective (coherent) **fluctuations** in mediating the spin lattice relaxation processes of **nematic** fluids continues to attract both theoretical and experimental attention. Though several theories describing this mechanism are available in literature, fundamental limitations regarding the separation of these coherent fluctuations from the individual molecular reorientations and the role of cutoff frequencies in deciding the range of frequency over which these fluctuations occur still exist.

The nematic director $\mathbf{n}(\mathbf{r}, t)$ is considered to be aligned along the direction of the magnetic field. The orientations of the molecule vary in space giving rise to fluctuations of the director around **the** equlibrium direction i.e. an average direction $\mathbf{n_o}$ parallel to the z-axis i.e.

$$\mathbf{n}(\mathbf{r}, t) = \mathbf{n}_o + \delta\mathbf{n}(\mathbf{r}, t). \tag{1.55}$$

$6n = (\delta n_x, \delta n_y, 0)$is the fluctuation around $\mathbf{n}_o$ and is normal to $\mathbf{n_o}$ with $| n |^2 = 1$.

Three distinct curvature strains can be defined in the nematic medium (Fig. 1.2) and any arbitrary deformation can be considered as a combination of these basic deformations (deGennes, 1974). Referring to a coordinate system x, y, z with the z-axis parallel to the director, the different possible components of curvature strains are splay $\left[\frac{\partial n_x}{\partial x}, \frac{\partial n_y}{\partial y}\right]$,bend $\left[\frac{\partial n_x}{\partial z}, \frac{\partial n_y}{\partial z}\right]$and twist $\left[\frac{\partial n_x}{\partial y}, -\frac{\partial n_y}{\partial x}\right]$(Fig. 1.2). Thus the free energy density of the medium associated with any deformation in the director can be expanded in terms of these curvature strains as (Doane and Johnson, 1970 ; Blinc, 1976)

$$g_n = \frac{1}{2}K_1\left[\frac{\partial n_x}{\partial x} + \frac{\partial n_y}{\partial y}\right]^2 + \frac{1}{2}K_2\left[\frac{\partial n_x}{\partial x} - \frac{\partial n_y}{\partial y}\right]^2 + \frac{1}{2}K_3\left[\left(\frac{\partial n_x}{\partial x}\right)^2 + \left(\frac{\partial n_y}{\partial y}\right)^2\right] \tag{1.56}$$

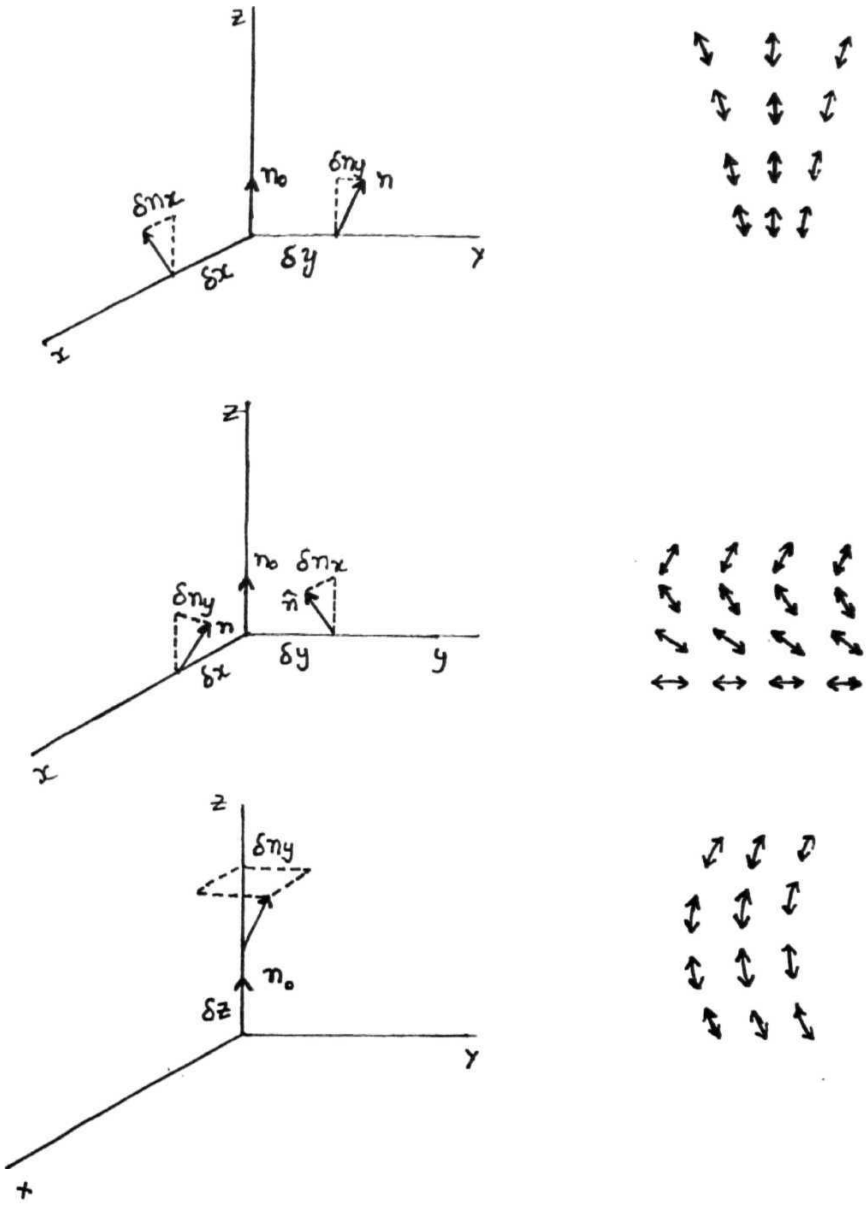

Fig. 1.2 The three types of deformations in nematic liquid crystals. The double arrows emphasize the non-polar nature of nematics.

(a) Splay deformation with V.n ≠0

(b) Twist deformation with n.(V x n) ≠0

(c) Bend deformation with n x (V x n) ≠0

The fluctuations are expressed in terms of a set of periodic distortion modes (though this description is not reliable when the fluctuations are really large i.e., close to T_{NI}) so as to empahsize the spatial dependence of the orientations of the local director (Blinc, 1976) as

$$\delta n_x(\mathbf{r}) = \frac{1}{\sqrt{V}} \sum_q n_x(\mathbf{q}) e^{-i\mathbf{q}.\mathbf{r}} \tag{1.57a}$$

$$\delta n_y(\mathbf{r}) = \frac{1}{\sqrt{V}} \sum_q n_y(\mathbf{q}) e^{-i\mathbf{q}.\mathbf{r}} \tag{1.576}$$

where V is the volume. The total deformational energy responsible for restoring the instantaneous director to its equilibrium direction is then given by

$$F_n = \frac{1}{2} \sum_q \Big\{ K_1 \mid n_x(\mathbf{q}) q_x + n_y(\mathbf{q}) q_y \mid^2 + K_2 \mid n_x(\mathbf{q}) q_y - n_y(\mathbf{q}) q_x \mid^2 + K_3 q_z^2 \left[\mid n_x(\mathbf{q}) \mid^2 + \mid n_y(\mathbf{q}) \mid^2 \right] \Big\} \tag{1.58}$$

$$F_n = \frac{1}{2} \sum_q \sum_{\alpha=1}^{2} \mid n_\alpha(\mathbf{q}) \mid^2 \left[K_3 q_z^2 + K_\alpha q_\perp^2 \right] \tag{1.59}$$

Here $q_\perp^2 = q_x^2 + q_y^2$. The transverse modes $n_\alpha(\mathbf{q}, t)$ relax exponentially as $n_\alpha(\mathbf{q}, t) = n_\alpha(\mathbf{q}, 0) \exp(-t/(\tau_\alpha(\mathbf{q}))$ with a damping time given by

$$\tau_\alpha(\mathbf{q}) = \frac{\eta_\alpha}{K_3 q_z^2 + K_\alpha q_\perp^2} \qquad \alpha = 1, 2 \tag{1.60}$$

where $\eta_\alpha = \Gamma^{-1}$ is closely related to the appropriate viscosity coefficient. The frequencies of the two transverse modes go to zero in the long wavelength limit ($q \rightarrow 0$)

in the nematic phase (l)oane and Johnson, 1970). The mean square amplitude of each mode is obtained from the equipartition theorem as

$$<|\, \mathbf{n}_\alpha(\mathbf{q})\,|^2>= \frac{kT}{K_3 q_z^2 + K_\alpha q_\perp^2} \qquad \alpha = 1,2 \tag{1.61}$$

The spectral densities as before are obtained from the correlation functions associated with these fluctuations leading to the modulation of the intramolecular dipolar interactions. However, these correlation functions have to be transformed from the magnetic field fixed frame (laboratory frame) to the director fixed frame and finally to the molecular fixed frame through proper Wigner rotation matrix elements (Doane and Johnson, 1970). Such a transformation results in

$$G(t) = < F_h(0)F_h^*(t) > = f_h(\Delta) < F_1(0)F_1^*(t) > \tag{1.62a}$$

$$= f_h(\Delta)\, S^2 < \delta\mathbf{n}(\mathbf{r},0)\, \delta\mathbf{n}(\mathbf{r},t) > \tag{1.626}$$

Here $S = \frac{1}{2} < 3\cos^2 0 — 1 >$ is the nematic order parameter and the term A in the function /(A) is the angle between the magnetic field and the director. The functions /(A) are given by

$$\begin{aligned} f_o(\Delta) &= 18\ (\cos^2\Delta - \cos^4\Delta) \\ f_1(\Delta) &= \frac{1}{2}\ (1 - \cos^2\Delta + 4\cos^4\Delta) \\ f_2(\Delta) &= 2(1 - \cos^4\Delta) \end{aligned} \tag{1.63}$$

The corresponding spectral density is given by

$$J_h(p\omega) = f_h(\Delta)S^2 \int_{-\infty}^{\infty} e^{-ipwt} < \delta\mathbf{n}(\mathbf{r},0)\delta\mathbf{n}(\mathbf{r},t) > dt \tag{1.64}$$

Introducing the Fourier components of the director fluctuations of the nematic order (eqn. (1.57)) the spectral density is given by

$$J_h(p\omega) = f_h(\Delta)S^2 \int_{-\infty}^{\infty} e^{-ipwt} dt \sum_{\mathbf{q}} \sum_{\alpha=1}^{2} <| n_\alpha(\mathbf{q}) |^2> e^{-t/\tau_\alpha(\mathbf{q})} \qquad (1.65)$$

Isotropic visco-elastic *coefficients*

Earlier theories (**Pincus,** 1969 ; Doane and Johnson, 1970, Doane et **al. 1974** ; **Ukeleja et** al. 1976) which considered the visco-elastic coefficients to be isotropic (i.e., $K_1 = K_2 = K_3$ = A' and $\eta_1 = \eta_2 = 77$), resulted in a simplified expression for the lifetime of each mode as

$$\tau_q = \frac{\eta}{Kq^2} \qquad (1.66)$$

By considering the upper cutoff frequencies of the modes to be infinity, these theories predicted a $\omega^{-1/2}$ dependence for the relaxation rate due to colective fluctuations. However, since the ODF modes should be restricted by a longest and shortest possible wavelenghts, the existence of an upper and lower bound for frequencies is to be considered. The limitations for short wavelength and hence upper cutoff frequency come from the molecular dimensions, a^{-1} (a being the size of the molecule). **However,** it is inconsistent to allow for cutoff wavevectors upto a^{-1} and at the same time assume that molecules undergo free rotational diffusion about the local director. By considering suitable high cutoff frequency ω_c (**Blinc** et al. 1969 ; Doane and Johnson, 1970 ; Lubensky, 1970), the expression for $J_1(\omega)$ can be written as

$$J_1(\omega) = \frac{3kTS^2}{2\pi^2 K} \int_{-\infty}^{\infty} dt \int_0^{q_c} dq e^{-tKq^2/\eta} e^{-iwt} \qquad (1.67a)$$

$$= A_c S^2 \omega^{-1/2} U\left(\frac{\omega_c}{\omega}\right) \qquad (1.67b)$$

where A_c - $(3kT)/(2\pi^2 K)\omega_c$ = (q_c^2/η) and the cutoff function $U(\omega_c/\omega)$ is given by

$$U\left(\frac{\omega_c}{\omega}\right) = \frac{1}{2\pi} \ln \frac{\omega_c/\omega - (2\omega_c/\omega)^{1/2} + 1}{\omega_c/\omega + (2\omega_c/\omega)^{1/2} + 1}$$
$$+\frac{1}{\pi}\left\{\tan^{-1}\left[(2\omega_c/\omega)^{1/2} - 1\right] + \tan^{-1}\left[(2\omega_c/\omega)^{1/2} + 1\right]\right\} \quad (1.68)$$

The high frequency cutoff ω_c is usually assumed to be determined by the length of the molecule i.e., $\lambda_c = 2\pi/q_c \sim 30\mathring{A}$. For typical values of $K \sim 0.1$ to 1 μdyne and η = 0.1 poise ; this corresponds to cutoff frequencies in the range of *rf* frequencies, (1-200 MHz).

Anisotropic viscoelastic constants :

For nematics which have underlying smectic phases, the elastic constants are no more isotropic (the bend (K_3) and twist (K_2) elastic coefficients diverge critically as the nematic - smectic-A transition is approached) (de Gennes, 1972 ; Brochard, 1973 ; de Jeu et al. 1973). Hence the one constant approximation is no longer adequate in evaluating the spectral density (Brochard, 1973 ; Blinc et al. 1975 ; Blinc, 1976)

Thus to include the anisotropic nature of the viscoelastic coefficients, the summation over the modes in eqn. (1.65) is replaced by integration over a cylindrical volume from zero to the high cutoff frequencies ($q_{zc} = 7r//, q_{\perp c} = n/a$, l and a being of the order of the molecular length and width respectively) instead of the originally assumed spherical volume (Pincus, 1969). The resulting spectral density can be written as

$$J_h(p\omega) = f_h(\Delta)\, S^2\, \frac{1}{(2\pi)^3} \sum_\alpha \int_0^{q_{zc}} \int_0^{q_{\perp c}} \frac{kT}{(K_3 q_z^2 + K_\alpha q_\perp^2)}$$
$$\times \frac{2\tau_\alpha(\mathbf{q}) 2\pi q_\perp}{1 + p^2\omega^2\tau_\alpha^2(\mathbf{q})}\, dq_\perp dq_z \quad (1.69)$$

Neglecting the wave vector dependence of viscoelastic coefficients, the above equation can be simplified for different limiting cases given below. The cutoff frequencies ω_{ac} and ω_{zc} are given by

$$\omega_{ac} = \frac{K_1 q_{\perp c}^2}{\eta_\alpha} \quad ; \quad \omega_{zc} = \frac{K_3 q_{zc}^2}{\eta_3} \quad (1.70)$$

Case (i) $\omega \ll \omega_{ac}, \omega_{z\,c}$

This case is in general valid for normal range of Larmor frequencies (< 100 MHz) and the spectral density (and hence relaxation rate) results in a square root dependence of frequency i.e.

$$J_h(p\omega) = \sum_{\alpha=1}^{2} C' \frac{\sqrt{2}\pi}{2K_\alpha} \sqrt{\frac{\eta_\alpha}{K_3}} \frac{1}{\sqrt{p\omega}} \tag{1.71}$$

where $C' = (f_h(\Delta)S^2kT)/(2\pi^2)$. In other words, the elastic continuum theory can be used for the whole range of q values and the integration over q can be performed from zero to oo in the nematic phase.

Case (ii) : $\omega_{ac} \gg \omega \gg \omega_{zc}$

In this case

$$J_h(p\omega) = \frac{C'\pi q_{zc}}{4K_1 p\omega} \tag{1.72a}$$

and hence

$$J_h(p\omega) \propto \frac{1}{\omega} \tag{1.726}$$

Case (iii) : $\omega \gg \omega_{ac}, \omega_{z_s}$

$$J_h(p\omega) = C' \frac{q_{\perp c}^2 q_{zc}^2}{2p^2\omega^2} \left[\frac{1}{\eta_1} + \frac{1}{\eta_2}\right]$$

and hence

$$J_h(p\omega) \propto \frac{1}{\omega^2} \tag{1.73}$$

case (iv) $\omega_{zc} \gg \omega \gg \omega_{\alpha c}$

case (iv) $\omega_{zc} \gg \omega > \omega_{\alpha c}$

In this case

$$J_h(p\omega) = \frac{C' q_{\perp c}^2}{2K_3^2 q_{zc}^2}(\eta_1 + \eta_2) \tag{1.74}$$

i.e., the spectral density is independent of frequency.

Since the Blinc's expression (1976) does not reduce to the one constant approximation (Pincus, 1969), Vold and Vold (1988) modified Blinc's treatment given above by integrating over **a** rotational ellipsoid instead of a cylindrical volume to obtain the spectral density as .

$$J_1(\omega) = \frac{3}{16\pi^2}\frac{3}{4} kTS^2 \sum_\alpha \eta_\alpha \int_0^{q_{zc}} dq_z \int^{q_{\perp c0}(1-q_z^2/q_{zc}^2)^{1/2}} \frac{\mathbf{q}_\perp d\mathbf{q}_\perp}{(K_3\mathbf{q}_z^2 + K_\alpha \mathbf{q}_\perp^2)^2 + \eta_\alpha^2\omega^2} \tag{1.75}$$

The above equation differs from that of Blinc's expression (1976) in that the upper limit of the integral over $\mathbf{q}_\perp$ has been modified to represent an ellipsoidal volume, whose cross section in the (q_x, q_y) plane is a circle of radius $\mathbf{q}_{\perp c}$ and the maximum excursions along $\mathbf{q}_z$ axis are $\pm \mathbf{q}_{zc}$. Integration of the above equation first with respect to $\mathbf{q}_\perp$ yields

$$J_1(\omega) = \frac{3kTS^2}{8\pi^2\omega} \sum_\alpha \frac{1}{K_\alpha} \int_0^{q_{zc}} dq_z \left\{ \arctan\left[\frac{K_\alpha q_{\perp c}^2[1 - (q_z^2/q_{zc}^2)] + K_3 q_z^2}{\eta_\alpha \omega}\right] - \arctan\left[\frac{K_3 q_z^2}{q_{zc}^2}\right] \right\} \tag{1.76}$$

Defining

$$A_\alpha^2 = \frac{K_\alpha q_{\perp c}^2}{\eta_\alpha \omega}; \quad B_\alpha^2 = \frac{K_3 q_{zc}^2}{\eta_\alpha \omega}; \quad D_\alpha = | B_\alpha^2 - A_\alpha^2 | \tag{1.77a}$$

The final expression for $J_1(\omega)$ can be written as

$$J_1(\omega) = \frac{3kTS^2}{8\pi\sqrt{2}\omega}\sum_\alpha \frac{1}{K_\alpha}\left[\frac{\eta_\alpha}{K_3}\right]^{1/2}\left\{\frac{1}{2\pi}ln\frac{B_\alpha^2 - B_\alpha\sqrt{2}+1}{B_\alpha^2+B_\alpha\sqrt{2}+1} + \frac{1}{\pi}(arctan(B_\alpha\sqrt{2}-1)\right.$$

$$+\frac{1}{\pi}arctan(B_\alpha\sqrt{2}+1)+\frac{B_\alpha\sqrt{2}/2\pi}{\sqrt{2D(\sqrt{1+A_\alpha^4}\mp A_\alpha^2)}}ln\left[\frac{\sqrt{1+A_\alpha^4}\pm\sqrt{2D(\sqrt{1+A_\alpha^4}\mp A_\alpha^2)}+D}{\sqrt{1+A_\alpha^4}\mp\sqrt{2D(\sqrt{1+A_\alpha^4}\mp A_\alpha^2)}+D}\right]$$

$$\mp\frac{B_\alpha\sqrt{2}/\pi}{\sqrt{2D(\sqrt{1+a_\alpha^4}\pm A_\alpha^2)}}\times\left[arctan\frac{\sqrt{2D}-\sqrt{\sqrt{1+A_\alpha^4}\mp A_\alpha^2}}{\sqrt{\sqrt{1+A_\alpha^4}\pm A_\alpha^2}}\right.$$

$$\left.\left.+arctan\frac{\sqrt{2D}+\sqrt{\sqrt{1+A_\alpha^4}\mp A_\alpha^2}}{\sqrt{\sqrt{1+A_\alpha^4}\pm A_\alpha^2}}\right]\right\} \qquad (1.77b)$$

The expression for the one constant approximation can be recovered from the above equation since the ellipsoid of integration reduces to a sphere and $A_\alpha \rightarrow B_\alpha$ i.e., $D \rightarrow 0$ for the isotropic nature of elastic constants. The principle difference between this expression and that of Blinc (1976) obtained with cylindrical volume of integration is in the cutoff region (Vold and Vold, 1988). The contribution from ellipsoidal volume of integration is smaller than the Blinc's expression ; the maximum ratio (i.e., $J_1(\text{cylindrical})/J_1(\text{ellipsoidal})$) of 1.5 is obtained when $B_\alpha^2 \rightarrow 0$. This limit is rarely reached in typical range of NMR frequencies. The frequency dependence of $J_1(\omega)$ as a function of the three elastic constants for different combinations is shown in Fig 1.3. . Here a variation of K_3 between 1 $\times 12^{-10}$ and 1 x 10^{-2} dyne with other parameters chosen as S = 1, T = 298.2 K, $\eta_1 = \eta_2$ = 0.5 poise, K_1 = K_2 = 10^{-6} dyne and cutoff wavelength, $\lambda_{zc} = 2\pi/q_{zc}$ and $\lambda_{\perp c} = 2\pi/q_{\perp c}$ of 30 A resulted in a cutoff frequency of 140 MHz. The plot can be roughly divided into three regions (the region in between the vertical lines is typically covered by conventional NMR experiments). The solid line in the figure corresponds to the isotropic case K_1 = K_2 = K_3 and represents the well known $\omega^{-1/2}$ behavior for frequency far below the cutoff frequency. For Larmor frequency well above the cutoff frequency ω_c, the absolute value of J_1 is small and drops off as ω^{-2}. The different conditions for the frequency dependence of $J_1(\omega)$ above and below the director mode cutoff frequencies, **for different combinations of the visco-elastic coefficients is given in Table. 1.1.**

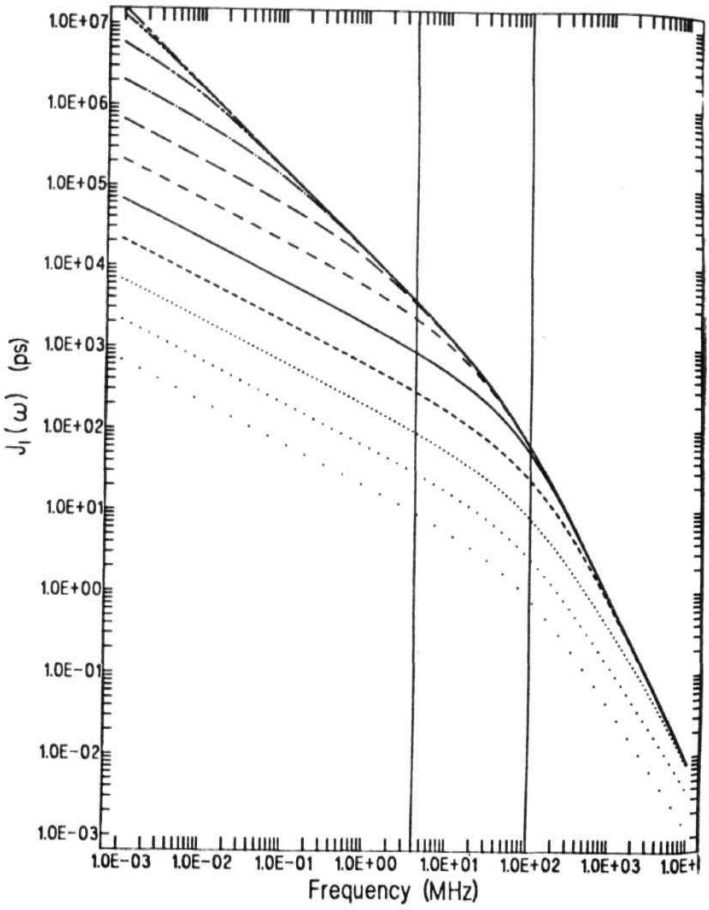

Fig. 1.3 Variation of spectral densities $J_1(\omega)$ with Larmor frequencies, for different distortion coefficients K_1,K_2 and K_3 (Vold & Vold, 1989). The region in between the vertical lines is the region typically covered by conventional NMR.

Table 1.1 : Frequency dependence of $J(\omega)$ **below and above the director mode cutoff**

		$\omega \ll \omega_{\alpha c}, \omega_{zc}$	$\omega_{zc} < \omega < \omega_{\alpha c}$	$\omega \gg \omega_{\alpha c}, \omega_{zc}$
$K_1 = K_2 = K_3$		$\omega^{-1/2}$		ω^{-2}
	$K_3 = 0$	ω^{-1}		ω^{-2}
	$K_3 \ll K_1, K_2$	$\omega^{-1/2}$	ω^{-1}	ω^{-2}
	$K_3 \sim K_1, K_2$	$\omega^{-1/2}$		ω^{-2}
	$K_3 \gg K_1, K_2$	$\omega^{-1/2}$		$\omega^{-3/2}$
$K_3 \ll K_1, K_2$	$K_3 \gg K_1, K_2$	$\omega^{-1/2}$		ω^{-2}
	$K_3 \ll K_1, K_2$	$\omega^{-1/2}$		$\omega^{-3/2}$

Two distinct limiting cases can be observed from Fig. 1.3

Case (i) : $\omega \ll \omega_c$

In the region where $\omega \ll \omega_c$ the frequency dependence of $J_1(\omega)$ is seen to vary from -1 to -1/2 as the value of K_3 changes from $K_3 \ll K_1, K_2$ to $K_3 \gg K_1, K_2$ respectively. This case is similar to the 2d case as invoked by Marquese et al. (1984) to explain the frequency dependence of lipid bilayers.

Case (ii) : $\omega \gg \omega_c$

In this case, $J_1(\omega)$ varies from ω^{-2} to $\omega^{-3/2}$ as K_3 is varied from $K_3 \ll K_1, K_2$ to $K_3 \gg K_1, K_2$.

The situation where $K_3 \ll K_1, K_2$ is equivalent to pseudo 2d systems in which the bend elastic term, K_3 does not contribute to the free energy and hence the relaxation mechanism for such systems results in a ω^{-1} dependence of $J_1(\omega)$ at low frequencies. Thus depending on the particular combination of elastic constants and viscosities, some what steeper frequency dependence than $\omega^{-1/2}$ can occur - especially as the Larmor frequency approaches ω_c.

Often the cutoff frequencies for nematic liquid crystals occur in a broadened frequency range (1 - 100 MHz). Accordingly, the spectral density measured over a limited frequency range may show a frequency dependence between $\omega^{-1/2}$ and ω^{-1} or $\omega^{-3/2}$ This treatment though seems to be the most complete and recent, does not take into account the possible coupling of the fluctuations and individual molecular reorientations (Freed, 1977 ; Zientara and Freed, 1983 ; Gertner and Lindenberg, 1991)

Self diffusion

The usual macroscopic description of diffusion through the random flights used for isotropic liquids with an average diffusion coefficient ($D = < r^2 > /6r$, where $< r^2 >$ is the mean square flight distance of the molecule and τ is the mean time between each flight) is not sufficient to describe the diffusion in liquid crystals since, the ordering in these systems leads to anisotropy in diffusion coefficients, $D_{||}$ (diffusion coefficient along the director) and $D_{\perp}$ (diffusion coefficient along a direction perpendicular to

the director). Zumer and Vilfan (1978) have extended Torrey's theory for isotropic liquids (discussed in section 1.2.1) to anisotropic medium by taking into account the anisotropy of molecular diffusion, the cylindrical shape of the molecule and the specific distribution of spins along the long molecular axis to obtain the relaxation rate for self diffusion. Following the notation of Torrey, the random correlation functions which on Fourier transform give the spectral densities are given by

$$F^{\alpha}[\mathbf{r}_{ij}(t)] = F^{\alpha}_{\xi}[\mathbf{r}(t)] \tag{1.78}$$

where

$$F^{\alpha}_{\xi}(\mathbf{r}) = \frac{e^{i\alpha\phi}}{[\rho^2 + (z+\xi)^2]^{5/2}} \times \{\rho(z+\xi)\}, \quad \alpha = 1 \tag{1.79}$$

Here $\xi = \xi_j - \xi_i$, ξ_j and ξ_i are the vectors from the molecular centers to the j^{th} and i^{th} spins. ρ, z and ϕ are the cylindrical cordinates of r, the distance between the centres of nearest neighbor molecules.

The anisotropic diffusion tensor, given by

$$\begin{pmatrix} D_{\perp} & 0 & 0 \\ 0 & D_{\perp} & 0 \\ 0 & 0 & D_{\parallel} \end{pmatrix} \tag{1.80}$$

can be written in terms of the components of $D^{\bullet}$, the diffusion coefficient of a perfectly ordered mesophase (Blinc et al. 1974). The anisotropic diffusion constant describes the solution of the diffusive motion i.e.,

$$\frac{1}{4\pi(D_{\perp}^2 D_{\parallel}^2 t^3)^{1/2}} \exp\left(-\frac{z^2}{4D_{\parallel}t} - \frac{\rho^2}{4D_{\perp}t}\right) \tag{1.81}$$

Here $D_{\parallel}$ and $D\pm$ are the diffusion coefficients in the directions parallel and perpendicular to the director, $\mathbf{n}_o$.

A proper choice of $p_1(\mathbf{r})$ (explained in 1.2.1) is

$$p_1(\mathbf{r}) = \frac{1}{4\pi D_\perp \tau}\left[\rho^2 + \frac{D_\parallel}{D_\perp} z^2\right]^{-1/2} \times exp\left\{-\left[\frac{z^2}{D_\parallel \tau} + \frac{\rho^2}{D_\perp \tau}\right]^{1/2}\right\} \tag{1.82}$$

and the corresponding Fourier transform

$$A(\mathbf{q}) = (1 + D_\perp \tau q_\perp^2 + D_\parallel \tau\, q_\parallel^2)^{-1} \tag{1.83}$$

where r is the mean time in between flights which gives the mean square jump length $< \mathbf{r}^2(t) >= (4D_\perp^\circ + 2D_\parallel^\circ)t$. The effective diffusion constants are given by

$$D_\perp^\circ = \frac{< r_\perp^2 >}{4\tau_\perp} \tag{1.84a}$$

and

$$D_\parallel^\circ = \frac{< r_\parallel^2 >}{2\tau_\parallel} \tag{1.84b}$$

Here $D_\perp^\circ$ and $D_\parallel^\circ$ are the macroscopic self diffusion constants of the perfectly aligned liquid crystalline phase. Substituting eq. (1.84) in eqn. (1.83), A(q) can be obtained. Considering the static pair correlation function (which partly correlates the final positions of the two molecules) to be of a simple square well function, (Zumer and Vilfan, 1978) i.e.,

$$g(p,z) = 1 \;;\; |z| < l \text{ and } p > d \text{ or } |z| > l \tag{1.85}$$
$$= 0 \;;\; p < d \text{ and } |z| < l$$

and the spins to be distributed uniformly along the long molecular axis, the relaxation rate can be obtained as (Zumer and Vilfan, 1978)

$$T_1^{-1} = \frac{9}{8}\gamma^4\hbar^2\frac{n\tau}{d^3}Q\left[\omega\tau,\ \frac{<r_\perp^2>}{a^2},\ \frac{D_\parallel^\circ}{D_\perp^\circ}\right] \qquad \textbf{(1.86)}$$

The function Q in the above equation is dimensionless and can be obtained numerically. The variation of Q as a function of ω (in the frequency range $UJT = 0$ to $UJT = 10$), when $l = 25\mathring{A}$, d = 5A, //d = 5 is given in Fig.1.4, for three different values of $< r_\perp^2 > /d^2$ viz., 1, 0.1 and 0.01. The value of $D_\parallel^\circ/D_\perp^\circ$ is taken from different experimental data as two (Yun and Frederickson, 1970 ; Kruger and Spiesecke, 1973 ; Zupancic et al. 1974) and does not differ much for different nematic compounds. The main features observed are

(i) When $UJT \rightarrow 0$, the ratio $< r_\perp^2 > /d^2$ increases from 0.01 to 1 and hence the relaxation rate due to self diffusion increases.

(ii) For low values of $\omega\tau$, $T_1^{-1} \propto$ constant $- (\omega\tau)^{1/2}$ and in the high frequency limit, $T_1^{-1} \propto \omega^{-2}$ andare similar to the isotropic case. This is also clear from the Fig.1.5 , where the ratio R of $T_{1iso}^{-1}/T_{1aniso}^{-1}$ is plotted as a function of UJT when $D_{iso} = D_\perp^\circ, r_{iso} —$ d and r is equal in both the cases. It is observed that R is equal to a constant (1.4) as the frequency is increased till $UJT \sim 0.1$. This constant region is followed by a small increase in R until it reaches a marginally higher contant value in the high frequency region. The change in the value of R can be minimized to 5% by a suitable choice of D. Thus the Torrey's expression of isotropic diffusion itself, reduced by a factor of 1.4, can explain the relaxation due to *SD* in nematic phase in the frequency region of the present work i.e.,

$$(T_1^{-1})_{SD} = \frac{1}{1.4}(T_1^{-1})_{Torrey} \qquad \textbf{(1.87)}$$

where $(T_1^{-1})_{Torrey}$ is given by eqn(1.34)

Reorientations :

At frequencies above 10^6 Hz which is in the range of conventional NMR frequency, molecular rotations also form a major part of the relaxation spectrum and are to be

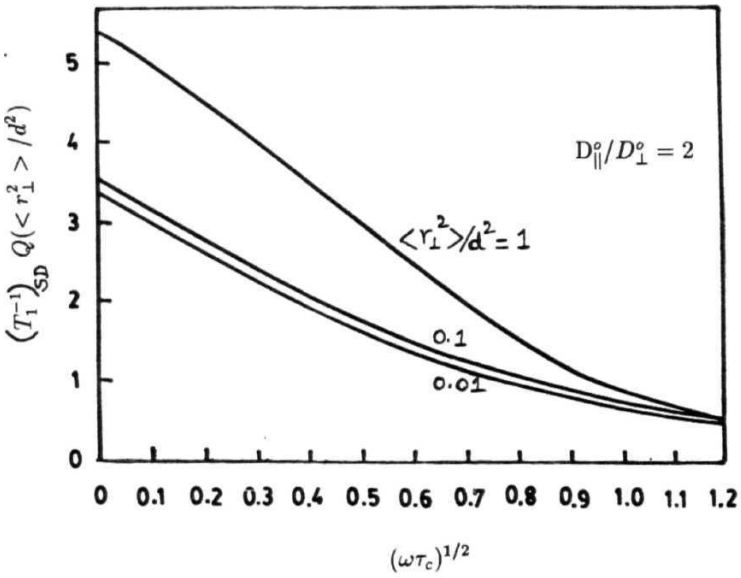

Fig. 1.4 Frequency dependence of $Q \propto (T_1^{-1})_{SD}$, for three different jump lengths in the nematic phase (Zumer et al. 1978).

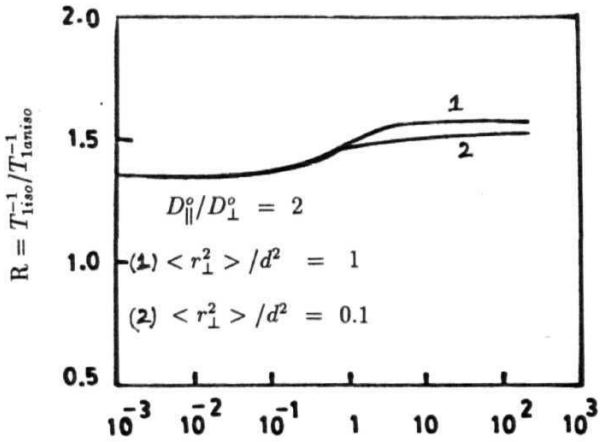

Fig. 1.5 Frequency dependence of the ratio $R = (T_1^{-1})_{iso}/(T_1^{-1})_{aniso}$ in the nematic phase (Zumer et al. 1978).

considered. The anisotropic nature of the molecules results in three different types of rotational motions (Blinc et al., 1978) viz., (a) fast reorientations around long axis (b) reorientations about short axis and (c) the reorientations of the end chains. Thus the theory for T_1 relaxation due to rotations should in principle include the effect of all the above rotational reorientations i.e., relaxation by diffusion jumps of ellipsoid like molecules about their long and short axes and relaxation by the reorientaions of CH_2 and CH_3 groups.

The different correlation times of interest are τ_l and τ_s for rotations of the entire molecules about their long and short axes respectively and τ_{CH_2} and τ_{CH_3} for rotations of CH_2 and CH_3 groups. There are evidences from dielectric experiments (Rondelz and Mircea-Roussel, 1974 ; Agarval and Price, 1974) and neutron scattering experiments (Janik et al., 1973, 1974) that the molecules in nematic phase rotate much faster about long axis with time scales well outside the normal NMR frequency range and hence these rotations do not contribute to relaxation. In other words, only τ_s is of major significance. Since the rotations of CH_2 and CH_3 occur in parallel with fast rotations of molecules about long axis, it follows that even these do not effect the relaxation rate. The relaxation rate for rotation about the short molecular axis is written in the BPP form (Bloembergan et al. 1948) as

$$\left(\frac{1}{T_1}\right)_{RS} = \epsilon C' \left(\frac{\tau_s}{1+(\omega\tau_s)^2} + \frac{4\tau_s}{1+(4\omega^2\tau_s^2)}\right) \qquad \textbf{(1.88)}$$

where t measures the anisotropy of local reorientations around short axis. The constant C for a molecule consisting of aliphatic groups in the core and aromatic groups in the end chains is given by

$$C' = \frac{9}{8}\gamma^4\hbar^2\frac{1}{15}\sum_k U_k(3l_k^2-1)^2/r_k^6 \qquad \textbf{(1.89)}$$

where U_k stands for the ratio of protons belonging to k^{th} group to the total number of protons in the molecules. l_ks are cosinesof angle between internuclear vector r_k of k^{th} group and the long axis.

1.2.4 Nematic - smectic-A transition (T > *TAN)*

The important feature of smectic phase which distinguishes it from nematic phase is its stratification (Fig. 1.1). The molecules are arranged in layers with correlations in their positions (and hence an additional ordering apart from the orientational ordering). Since the correlation between the molecules in each layer dominates the correlation between adjacent layers, the layers are free to slide over each other. Depending on the degree of positional ordering and symmetry properties, smectics have been classified into different categories. The molecular arrangement in different smectic phases is explained below.

S_A: This is an uniaxial phase, with molecules within each layer aligned perpendicular to the layer normal but uncorrelated with respect to the centers of mass. The thickness of each layer is of the order of molecular length (Fig. 1.1).

S_C: This is an optically biaxial phase, with the molecules in each layer having a uniform tilt with respect to the layer normal (de Gennes, 1974) and fluid like within each layer (Fig. 1.1). Thus, the thickness of each layer is less than the molecular length. Tilt angles up to 45° are observed.

S_B: This phase in addition to the layered structure is characterized by a hexagonal crystalline order within each layer (Fig. 1.1). The thickness of each layer is of the order of molecular length (de Gennes, **1974).**

Similarly, there are other ordered smectics like *SD,* S_E, S_F, S_G **etc.,** with varying degrees of positional order of the molecules within the layers. Smectic-A being the least ordered in all the smectics is the first mesophase to form (if present), as the nematic phase is cooled.

As the smectic-A phase is approached from say a nematic phase, local smectic clusters (cybotactic groups) form and breakup. This results in pretransitional smectic fluctuations and hence exclusion of the bend and twist deformations. That is, the elastic constants K_2 and K_3 diverge as the system goes from nematic to smectic-A phase (Brochard, 1973). Following de Gennes (1972, 1974) and McMillan **(1971, 1972**

and 1973) for a fixed orientation of the director, the free energy density near T_{AN} can be written in terms of the smectic order parameter, ψ as

$$F_s = \alpha \mid \psi \mid^2 + \beta \mid \psi \mid^4 + \frac{1}{2M_v}\left[\frac{\partial \psi}{\partial z}\right]^2 + \frac{1}{2M_T}\left[\left(\frac{\partial \psi}{\partial x}\right)^2 + \left(\frac{\partial \psi}{\partial y}\right)^2\right] \tag{1.90}$$

where ψ is given by

$$\psi = \mid \psi \mid e^{i\phi} \tag{1.91}$$

ϕ is the phase factor which gives the position of the layers and $|\psi|$ is the amplitude of wave vector which denotes the degree of layering. M_T and M_v are the components of mass tensors (Brochard, 1973). Symmetry conditions ensure the presence of terms with even powers of ψ only. The coefficient β is always *+ve* and at a certain temperature T^*, which is a second order point, $\alpha = 0$. The renormalised elastic coefficients (due to the divergence of K_2 and K_3) are given by

$$K_2 \rightarrow \tilde{K}_2 = K_2 + \delta K_2 \tag{1.92a}$$

$$K_3 \rightarrow \tilde{K}_3 = K_3 + \delta K_3 \tag{1.926}$$

where δK_2 and δK_3 are the critical parts of the elastic constants given by (Brochard, 1973)

$$\delta K_2 = \frac{\pi}{6}\left[\frac{kT}{M_T d^2}\right]\left[\frac{M_v}{A_s(T)}\right]^{1/2} \propto \xi \tag{1.93a}$$

$$\delta K_3 = \frac{\pi}{6}\left[\frac{kT}{d^2}\right]\left[\frac{1}{M_v A_s(T)}\right]^{1/2} \propto \xi \tag{1.936}$$

Here ξ is the coherence length, q = $2\pi/d$ is the length of the smectic layers. The term $A_s(T)$ is given by

$$A_s(T) = [T - T_{AN}]^{\nu} \qquad \textbf{(1.94a)}$$

where *TAN* is the nematic-Smectic A transition temperature. The increase in the bend and twist elastic coefficients is only partly compensated by the increase in some of the viscosity coefficients ; eqns. (1.93a) and (1.93b) together with eqn. (1.71) thus predict a significant decrease in the contibutions to the relaxation rate from nematic order fluctuations near N — S_A transition. Hence smectic flucu tat ions alone are responsible for any change in T_1 at T_{AN}.

$$\text{i.e.,} \qquad T_1^{-1} \propto [T - T_{AN}]^n \qquad (1.94b)$$

where *n* critically depends on the value of the exponent *v*.

1.2.5 ($T < T_{AN}$):

Deep inside the smectic phase, in addition to the order director fluctuations of the nematic director, smectic wave undulations, fluctuations due to adjacent smectic C phase and self diffusion mediate the relaxation processes (Blinc et al., 1975). Thus the free energy of the system is written as a summation of the free energies due to all the above contributions i.e.,

$$F = F_n + F_s + F_c + F_d \qquad (1.95)$$

where F_s is the free energy due to smectic layering, F_n is the free energy due to nematic ordering, F_c is the free energy due to the formation of adjasent S_c phase and F_d is the free energy due to self diffusion (SD).

Order director fluctuations :

Due to the large increase in the twist and bend elastic constants, the contribution to T_1^{-1} from 'nematic' order fluctuations reduces considerably in S_A phase. Below

T_{AN}, assuming **the coherence** length (amplitude of the smectic wave) to be constant, and only the phase angle ϕ to vary, the gradient in the expression for free energy can be written as (de Gennes, 1972)

$$F_s = \frac{\psi_o^2}{2M_v}\left[\frac{\partial\phi}{\partial z}\right]^2 + \frac{\psi_o^2}{2M_T}\left[\left(\frac{\partial\phi}{\partial x}\right)^2 + \left(\frac{\partial\phi}{\partial y}\right)^2\right] \tag{1.96}$$

The gradient terms $\frac{\partial\phi}{\partial x}$ and $\frac{\partial\phi}{\partial y}$ represent the tilt of the layers with respect to the director. In case the orientation of the director is not fixed, considering the relative tilt between the layers and the director, the free energy can be written as

$$F_s = \alpha \mid \psi \mid^2 + \beta \mid \psi \mid^4 + \frac{1}{2M_v}\left[\frac{\partial\phi}{\partial z}\right]^2 + \frac{1}{2M_T}[\nabla_T\psi + iq_s\delta\mathbf{n}.\psi]^2 \tag{1.97}$$

where ∇_T is the gradient operator in the plane of the layers. The term *6n* stands for the fluctuating part of the nematic director n. The total free energy due to collective fluctuations is thus obtained as $F_s + F_n$, where F_n is the total free energy due to fluctuations in the nematic director given by **eqn.** (1.58). In S_A phase, $<\mid \phi \mid> = \psi_o = (-\alpha/\beta)^{1/2}$. Assuming $\mid \psi \mid$ to be spatially uniform,

$$F_s = F_o + \frac{1}{2}\left\{-\frac{\alpha^2}{F} + B_s\left[\frac{\partial u}{\partial z}\right]^2 + D_s\left[\left(n_x + \frac{\partial u}{\partial x}\right)^2 + \left(n_y + \frac{\partial u}{\partial y}\right)^2\right]\right\} \tag{1.98}$$

where $B_s = (\psi_o^2 q_s^2)/M_v = K_1/d^2$ and $D_s = (\psi_o^2 q_s^2)/M_T$ represent the restoring forces for fluctuations in the phase ψ and for fluctuations of the molecular orientation respectively. V, the layer displacement is related to ϕ as $\mid \phi \mid^2 = q^2 \mid u \mid^2$. Introducing the Fourier transforms of $\delta\mathbf{n}$ and using the equipartition theorem, as in the case of nematic phase, the amplitude of mean square fluctuations of the director are obtained as

$$<\mid \delta\mathbf{n}_1(\mathbf{q}) \mid^2> = \frac{kT}{V}\left\{K_1 q_\perp^2 + K_3 q_z^2 + B_s\left(\frac{q_z}{q_\perp}\right)^2\left[1 + \frac{B_s}{D_s}\left(\frac{q_z}{q_\perp}\right)^2\right]^{-1}\right\}^{-1} \tag{1.99a}$$

$$<|\delta n_2(\mathbf{q})|^2> = \frac{kT}{V}\left\{K_2 q_\perp^2 + K_3 q_z^2 + D_s\right\}^{-1} \tag{1.996}$$

where $q\pm = (q_x^2 + q_y^2)^{1/2}$ and q_z are the components of deformation wave vector q in the directions perpendicular and parallel to the smectic layers respectively. The corresponding dispersion relations for these collective modes in S_A phase are given by (Schaetzing and Lister, 1979)

$$\tau_1(\mathbf{q}) = \eta_1\left\{K_1 q_\perp^2 + K_3 q_z^2 + B_s(q_z/q_\perp)^2\left[1 + \frac{B_s}{D_s}(q_z/q_\perp)^2\right]^{-1}\right\}^{-1} \tag{1.100a}$$

$$\tau_2(\mathbf{q}) = \eta_2\left\{K_2 q_\perp^2 + K_3 q_z^2 + D_s\right\}^{-1} \tag{1.1006}$$

Here η_1 and η_2 are two effective viscosity coefficients which are considered to be independent of q. The elastic constant *B,* is about ten times larger than D_s in the smectic-A phase. As the nematic phase is approached, the disappearance of layered structure results in B_s and D_s tending to zero and hence the mean square amplitude of fluctuations given by eqns. (1.99a) and (1.99b) result in the expression for mean square amplitude for the nematic phase. Substituting the relavant parameters and integrating over the q modes from zero to upper cutoff wave vector $q_{max} = q_s$, which is given by inverse dimension of one molecule, the spectral density is obtained as (Vilfan et a]., 1987)

$$J_1(\omega) = \frac{1}{2}\frac{S^2 kT r^{-6}}{\sqrt{2\pi}} D_s^{-1/2}\left[\eta_1 K_1^{-3/2} Y + \eta_2 K_3^{-1/2} K_2^{-1}\left\{1 - \left(1 + \frac{\omega_2}{\omega_{s2}^2}\right)^{1/2}\right\}^{-1/2}\right]$$

where

$$Y = \int_0^1 x^{-1}\left[x^2 + (1 - x_2)\frac{D_s}{B_s}\right]^{1/2} \times \left(1 - x^2 + K_3\frac{x^2}{K_1}\right)^{-3/2} \times \left[1 + \left\{1 + \frac{\omega^2}{\omega_{s1}^2}\left(1 - \frac{(1-x^2)D_s}{B_s x^2}\right)^2\right\}^{1/2}\right]^{-1/2} \tag{1.1016}$$

Here $\omega_{s\alpha} = D_s/\eta_\alpha (\alpha = 1,2)$ are the characteristic upper cut off frequencies in the directions perpendicular to the director. The relaxation rate due to ODF modes is now obtained as

$$T_{1ODF}^{-1} = \frac{9}{8}\gamma^4\hbar^2 J_1(\omega) \qquad \textbf{(1.102)}$$

Since the contribution from $J_2(\omega)$ is insignificant, it is neglected (Pincus, 1969 ; Vilfan et al. 1987 ; Vold and Vold, 1989).

The frequency and angular dependence of $(T_1^{-1})_{ODF}$ depends on the relative values of ω_{s1}, ω_{s2} and ω ; and on the ratio of the elastic constants K_3/K_1 and D_s/B_s. The contributions to the spectral density from the two normal modes, given by the term containing $Y(\alpha = 1)$ and by the second term (for a = 2) in eqn. (1.101) are plotted in Fig. 1.6 for specific values of $D_s/B_s = 0.1, \eta_1 = \eta_2$ and $K_1 = K_2 = K_3$. Also represented in the figure is the variation of the sum of the modes. Two limiting cases may be discussed in this context.

Case(i): $\omega \gg \omega_{s1} = \omega_{s2} = \omega_s$,

The angular and frequency dependence of $J_1(\omega)$ is the same as in the nematic phase i.e., $J_1(\omega) \propto \omega^{-1/2}$. However, the value of T_1 should be much longer than in the nematic phase in view of the increase in the elastic constants K_2 and A3.

Case(ii): $\omega \ll \omega_{s1} = \omega_{s2} = \omega_s$;

In this case, the relaxation rate is effected by the smectic order fluctuations and results in a levelling off of the dispersion curve (Vilfan et al. 1987), i.e., T_1 is independent of frequency and proportional to the smectic order parameter $| \psi_o |$. The term due to the mode for a = 1, increases slightly with decreasing ω while the second term approaches a constant value. The transition from nematic like behavior to the leveling off occurs close to $\omega \sim \omega_s$ depending on the value of K_3/K_1 and D_s/B_s (Vilfan et al, 1987). For a typical smectic phase, the value of ω_s is estimated to be $10^6 s^{-1}$ indicating the region in which the change over occurs is close to about 1 MHz. Thus not only the $\omega^{1/2}$ dispersion law but also the low frequency deviations from it

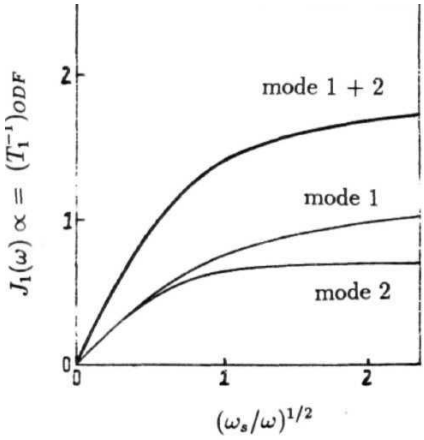

Fig. 1.6 Frequency dependence of the transverse modes of $J_1(\omega)$ ($\alpha = 1,2$) and their sum (Vilfan et al. 1987) for $D/B_e = 0.1$; $k_1 = k_2 = k_3 = k$ & $\eta_1 = \eta_2 = \eta$.

can be explained in principle by nematic director fluctuations in the smectic phase and the coupling between nematic and smectic order. Comparing the variation of $(T_1^{-1})_{OD}$ in S_A phase with that of nematic phase (Zupancic et al. 1976), where the summation over q includes terms with wave vectors larger than $q_{min} \sim 2\pi/\lambda_{max}$ and the critical frequency ω_c at which the levelling off occurs is given by $(Kq_{min}^2)/\eta = (K(2\pi)^2)/\eta\lambda_{max}^2$ is very interesting. From Fig. 1.7, it can be seen that though the dispersion curves look similar, ω_c is several orders of magnitude smaller than ω_s as the ratio $\omega_s/\omega_c \sim (\lambda_{max}/d)^2$.

Considering the wave vector dependence of η_2 (deGennes, 1974) the frequency dispersion of $J_1(\omega)$ due to the mode $\alpha = 2$, is found to be the same for different values of η_2 (Vilfan et al., 1987). However the problem of wave vector dependence of all the viscosity coefficients in S_A phase is still not solved completely. As explained earlier, a modification of the above expression for spectral density by considering an ellipsoidal volume of integration instead of cylindrical volume used by Blinc (1976) is done by Vold and Vold (1988) to include the variation in the elastic and viscosity coefficients, which is usually the case in the smectic phase due to the smectic fluctuations.

Smectic wave undulations

Another possible mechanism contributing to T_1 in the smectic phase is the contribution of the smectic wave undulations (when the interlayer distance is constant and the director is normal to the layers). The relation between the local displacement of the layer in a direction normal to the layer $(u_z(x,y))$ and the fluctuations in the director $(\delta\mathbf{n}(\mathbf{r},t))$ are given by

$$\delta n_x = -\frac{\partial u_z}{\partial x} \quad ; \quad \delta n_y = -\frac{\partial u_z}{\partial y} \tag{1.103}$$

In addition, the modes which are restricted to the *xy* plane i.e., $q_z = 0$ are purely diffusive (Blinc et al. 1975) i.e.,

$$\tau^{-1}(q) = \frac{K_1 q_\perp^2}{\eta} \tag{1.104}$$

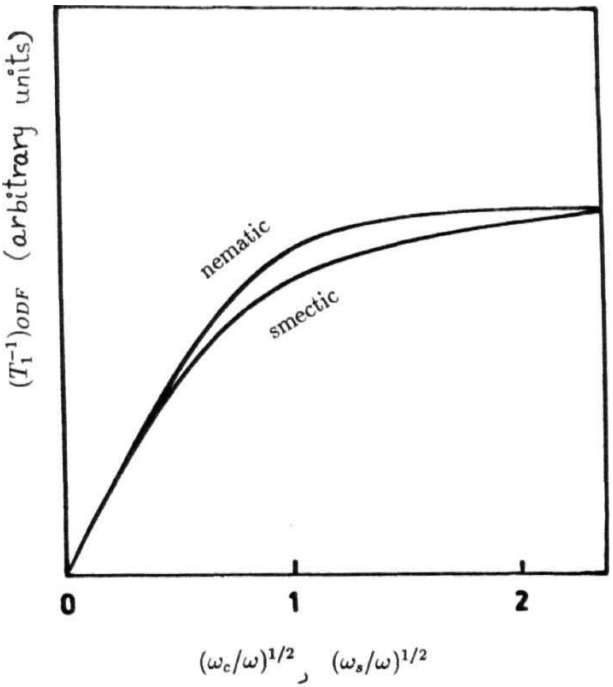

Fig. 1.7 Comparision of the shape of nematic and smectic dispersion curves for (smectic) = ω_c (nematic phase) (Vilfan et al. 1987).

Assuming the coherence length to be independent of $q_\perp$ and using the elastic continuum theory, the expression for spectral density can be obtained as

$$J_h(\omega) = f_h(\Delta) S^2 \frac{kT}{4K_1 \xi} \frac{1}{\omega} \tag{1.105}$$

But in a typical system, $\xi = 1/\lambda q_\perp^2$ where A is a constant of the order of molecula: length. Thus

$$J_h(\omega) = f_h(\Delta) S^2 \frac{kT}{4\pi K_1^2} \lambda\eta \ \ln\ (\omega_c^2 + \omega^2) - 2 \ln\ \omega \tag{1.106}$$

where only the upper cutoff frequency is taken into account (Blinc et al. 1975)

Relaxation due to S_c fluctuations :

A considerable contribution to relaxation rate in the S_A phase may arise from S_c phase fluctuations, if there is an underlying S_c phase. In the smectic-C phase, the preferred direction of the molecular alignment is tilted away from the normal to the layer and hence large fluctuations are expected in the tilt angle near T_{CA}, on approaching from the S_A phase. The tilted state is specified by the magnitude of the tilt angle *0* and the azimuthal direction of the molecular axes ϕ with respect to the smectic plane normals. The order parameter in S_c phase is thus a complex number given by

$$\chi = Sin\theta e^{i\phi} = |\ \chi\ |\ e^{i\phi} = \chi_x + i\chi_y \tag{1.107}$$

which is related to the nematic director as

$$\mathbf{n} = \mathbf{n}_o + \delta\mathbf{n} = (0,0,1)\ +\ (\chi_x, \chi_y, 0) \tag{1.108}$$

The free energy density in the presence of S_c fluctuations can be written as (Blinc et al., 1975)

$$F_c = F_A + \frac{1}{2}A_c(T) \mid \chi \mid^2 + \frac{1}{2}K_1 \left(\frac{\partial \chi_x}{\partial x} + \frac{\partial \chi_y}{\partial y}\right)^2 + \frac{1}{2}K_2 \left(\frac{\partial \chi_x}{\partial y} - \frac{\partial \chi_y}{\partial x}\right)^2$$
$$\frac{1}{2}K_3 \left[\left(\frac{\partial \chi_x}{\partial z}\right)^2 + \left(\frac{\partial \chi_y}{\partial z}\right)^2\right] \qquad (1.109)$$

with $A_c(T) \propto (T - T_{AC})^{\nu}$ and F_A is the smectic-A free energy density in the absence of smectic-C fluctuations. As in the earlier cases, introducing the Fourier components of $\chi_x(\mathbf{r})$ and $\chi_y(\mathbf{r})$ with $K_1 = K_2 = K_3 = A'$ (one constant approximation) and using the equipartition theorem to find the mean square amplitude of thermal fluctuations and the corresponding order parameter relaxation time $\tau^{-1}(\mathbf{q}) = A_c(T)(1 + q^2\xi^2)/\eta$ where $\xi^2 = K/A_c(T)$, the spectral density is obtained as (Blinc et al. 1975)

$$J_h(p\omega) = f_h(\Delta)\, S^2\, \frac{kT\eta^{1/2}}{(2\pi)^2 K^{3/2}}\, \frac{\sin[\frac{1}{2}\tan^{-1}(p\omega/r)]}{\sin[\tan^{-1}(p\omega/r)]}\, \frac{\pi}{(p^2\omega^2 + r^2)^{1/4}} \qquad (1.110)$$

Here $r = (K\xi^2)/\eta$. The above equation is similar to the expression for spectral density due to ODF in nematic phase. This shows that the angular dependence of T_1 due to S_c fluctuations is the same as in the case of director fluctuations in the nematic phase.

In the limiting case, $\omega \gg r$; the frequency dependence of T_1 also is the same as in the nematic phase i.e., $T_1 \propto \sqrt{\omega}$. However when $\omega \ll r, T_1$ is independent of frequency, but critically dependent on the temperature i.e., $T_1 \propto (T - T_{AC})^{\nu}$.

Diffusion assisted **ODF**

Lastly, another important mechanism aiding the relaxation in the smectic phases is the modulation of intra molecular dipolar interactions due to translational self diffusion wherein the long molecular axis is adjusted parallel to the director $\mathbf{n}_o(\mathbf{r}, t)$ which is space dependent (due to order fluctuations) during the process of diffusion. In such a case, an additional factor, taking into account the change in the orientation of a molecule due to diffusion i.e., diffusion assisted ODF is to be included in the auto correlation function **for the** simple nematic case i.e.,

$$< F_h(0)F_h^*(t) >= f_h(\Delta)S^2 \sum_q \sum_{\alpha=1}^{2} <| \delta n_\alpha(\mathbf{q}) |^2> e^{-t/\tau_\alpha(\mathbf{q})} e^{-(D_{\|}q_z^2 + D_\perp \cdot q_\perp^2)t} \quad (1.111)$$

Here $D\backslash\backslash$ and $D_\perp$ stand for the principal values of the diffusion tensor parallel and perpendicular to the nematic director $\mathbf{n}_o$ respectively. Introduction of these additional factors due to diffusion leads to the following substitutions for K_1, K_2 and K_3 to obtain the decay times of the modes i.e.,

$$\frac{\tilde{K}_3}{\eta} \rightarrow \frac{\tilde{K}_3}{\eta + D_{\|}} \; ; \; \frac{K_1}{\eta} \rightarrow \frac{K_1}{\eta + D_\perp} \; ; \; \frac{\tilde{K}_2}{\eta} \rightarrow \frac{\tilde{K}_2}{\eta + D_\perp} \quad (1.112)$$

in expressions for $\tau_\alpha^{-1}(\mathbf{q}); \tau_1^{-1}(\mathbf{q}); \tau_2^{-1}(\mathbf{q}); \tau^{-1}(\mathbf{q})$ for the wave vector dependent relaxation time $\tau(\mathbf{q})$.

In the Isotropic approximation $(K_1 = K_2 = K_3)$, ξ^2/η is replaced by $\xi^2/\eta + (D/A_c(T))$ where $D = \frac{1}{3}(D_{\|} + 2D_\perp)$. Hence the the spectral density term can now be obtained as

$$J_h(p\omega) = f_h(\Delta)\, S^2\, \frac{kT\sqrt{2}}{(2\pi)^2} \sum_{\alpha=1}^{2} \frac{1}{K_{\alpha'}\sqrt{K_3'}} \frac{\pi}{\sqrt{2p\omega}} \int_{-1}^{1} \frac{dx}{(K_3/K_3')x^2 + (K_\alpha/K_\alpha')(1-x^2)} \quad (1.113)$$

In case $K_3/K_3' > K_\alpha/K_\alpha'$, the above expression can be written as

$$J_h(p\omega) = f_h(\Delta)S^2 \frac{kT\sqrt{2}}{(2\pi)^2} \frac{\pi}{\sqrt{p\omega}} \sum_{\alpha=1}^{2} \left[\sqrt{K_3'}K_\alpha \frac{K_3K_\alpha'}{K_3'K_\alpha} - 1\right]^{-1} \times \tan^{-1}\left[\frac{K_3K_\alpha'}{K_3'K_\alpha} - 1\right]^{1/2} \quad (1.114)$$

which is the same as that obtained for the S_A phase. When $D_{\|} < D_\perp$ and $K_3 > K_\alpha$, $(K_3D_\perp)/(K_\alpha D_{\|}) > 1$. Also when $D\pm > K_\alpha/\eta$ i.e., smectic order parameter is negligible, the spectral density is given by

$$J_h(\omega) = f_h(\Delta) S^2 \frac{kT}{4\sqrt{2\omega}} \sum_{\alpha=1}^{2} (\tilde{K}_3 \tilde{K}_\alpha)^{-1/2} \frac{1}{\sqrt{D_\perp}} \qquad (1.115)$$

Thus the diffusion assisted ODF mechanism gives the same angular and frequency dependence to the relaxation rate T_1^{-1} as ordinary ODF mechanism. On the other hand, the temperature dependence of T_1 is essentially determined by the temperature dependence of diffusion coefficient. If the diffusion process is thermally activated, the corresponding $T\backslash$ has a Arrhenius type of temperature dependence.

Self diffusion :

The model for self diffusion in S_A phase is different as compared to nematic phase, due to the layered structure. The system is considered to be constituted by molecules of length / and diameter d $(d/l \ll 1)$, with the spins distributed along the long molecular axis. This approximation is justified, when the rotations of molecules around their long axes are fast. Vilfan and Zumer (1980), have given the theory of T_1 in S_A phases due to translational self diffusion. As the nematic order is close to 1 well inside the S_A phase, it is assumed that the orientational order of the molecular axes is perfect. Similar to the case of isotropic and nematic diffusion, a random, fast, diffusive jump model where the time spent for a jump is much shorter than the average time interval $T\pm$ between two successive jumps, is considered to describe the diffusion. Further the interlayer motion is also described by a thermally activated random jump process, wherein the molecules are assumed to jump only to one of the two adjacent layers, the jump length being equal to the interlayer distance. The time spent for a jump is assumed to be much smaller than $\tau_{\|}$, the average time between two successive inter layer jumps. Considering all the above factors, the spin lattice relaxation rate can be written as (Vilfan and Zumer, 1980)

$$T_1^{-1} = \frac{3}{2}\gamma^4 \hbar^2 I(I+1)\left[J_1(\omega, \Delta) + J_2(2\omega, \Delta)\right] \qquad (1.116)$$

where A is the angle between the director within each layer and the field. As in

the nematic case the spectral density can be written as the Fourier transform of the correlation function for intra molecular dipolar Hamiltonian as

$$J_\alpha(\omega) = \frac{\eta}{16\pi^3} \int Re \left[< F_\xi^{(\alpha)*}(\mathbf{q}) F_\xi^{(\alpha)}(\mathbf{q}) > \right] S_s(\mathbf{q}, \frac{\omega}{2}) \tag{1.117}$$

where $S_s(\mathbf{q}, w)$ is the Fourier transform of the one particle auto correlation function $G_s(\mathbf{r}, t)$. The functions $F_\xi^{(\alpha)}$ (q) which are the auto correlation functions, are different for the interlayer and the intra layer diffusion and are given by eqn. (1.79) (Zumer and Vilfan, 1978 ; Harmon and Muller, 1969). Using the same notation as in the isotropic case, the distribution function $P_1(\mathbf{r})$, and the Fourier transform are given by (Vilfan and Zumer, 1980)

$$P_1(z) = \frac{1}{2} [\delta(z + l) + \delta(z - l)] \tag{1.118a}$$

and

$$A_\perp(\mathbf{q}_\perp) = \frac{1}{1 + D_\perp^o \tau_\perp q_\perp^2} \quad ; \quad A_{\|}(q_{\|}) = cos(q_{\|} l) \tag{1.1186}$$

The static pair correlation function has to be written as a product corresponding to the long range and short range positional order i.e.,

$$g(r) = g_1(\mathbf{r}) g_o(\mathbf{r}) \tag{1.119}$$

where $g_1(\mathbf{r}) = g_1(z)$ and $g_o(\mathbf{r})$ is of the form of a square well (as in the nematic case). Finally, considering a distribution of spins to be uniform along the long molecular axis, the expression for the relaxation rate due to *SD* is obtained as

$$T_1^{-1} = \frac{9}{8} \gamma^4 \hbar^2 \frac{\eta \tau_\perp}{d^3} R \left(\omega \tau_\perp, \frac{< r_\perp^2 >}{d^2}, \frac{D_{\|}}{D_\perp}, \frac{l}{d}, \Delta \right) \tag{1.120}$$

where the function *R* is to be calculated for different parameters by numerically integrating over $q_{\|}$, $q\pm$ and ξ. The frequency dependence of the relaxation rate for l/d

= 5 (a, the closest distance between two spins belonging to adjacent layers being 2) is given in Fig. 1.8. The function *Ji* exhibits a characteristic frequency dependence and depends on the orientation of the sample in the external field. The dispersion curves in Fig. 1.8 are plotted for two extreme orientations A = 0° and A = 90°. Also, the isotropic relaxation rate with the diameter of the spherical molecules being d and $\tau_{iso} = \tau_{\perp}$ is plotted for comparison. From the Fig. 1.8, it is clear that the relaxation rate significantly differs for both the cases at low frequencies ($\omega\tau < 0.3$). The decrease in the relaxation rate with increasing $\omega\tau_{\perp}$ is much steeper for A = 90°. The dispersion curves at low frequencies do not follow the well known expression $J_1(\omega) = C - F\omega^{1/2}$ which is valid for the isotropic and nematic phases. The function *R* calculated for the three different cases, $D_{\parallel}/D_{\perp}$ = 1, 0.3 and 0 shows that *R* increases with slowing down of interlayer diffusion and reaches a maximum value for diffusion within layers (similar to nematic phase). At high frequencies ($\omega\tau_{\perp} > 0.3$), the influence of anisotropy of the jump diffusion on the relaxation disappears and hence the curves for different $D_{\parallel}/D_{\perp}$ fuse into one. Finally, in the frequency range in between $\omega\tau_{\perp}$ = 0.3 and 1, the range which is of practical importance for conventional NMR studies, the frequency dependence of the anisotropic relaxation rate due to diffusion is similar to that of nematic phase with similar molecular dimensions. Thus, Torrey's expression for the relaxation rate (with $\tau_{iso} = \tau_{\perp}$ and d as the diameter of the molecule) diminished by an appropriate factor of 1.4, seems to be a good approximation when the nematic director is parallel to the external field.

Reorientations:

In high temperature smectics, the contribution to relaxation arises from the rotations about the short axes (as explained in the case of nematic phase).

1.2.6 Ordered smectics and solid phase

Ordered smectics are characterized by additional degrees of ordering within each layer. The order director fluctuations are frozen and hence do not contribute to relaxation in these phases. In spite of the high positional order of the molecules, there are fast local motions with large amplitudes (> 2) (Levelut et al. 1981) and molecular self

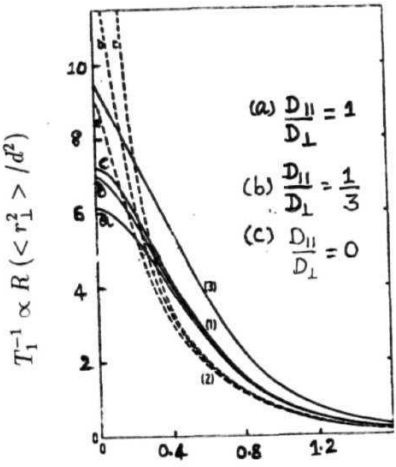

Fig. 1.8 Frequency dependence of $R \propto (T_1^{-1})_{SD}$ for three different ratios of $D_\parallel/D_\perp$ (0, 0.33, 1) for H $\parallel$ n and H $\perp$ n ($< r_\perp^2 > /d^2 = 1$). Torrey's function is

1. H∥n
2. H⊥n
3. Isotropic function

diffusion (which is a slow jump process as in solids) with much weaker dynamical correlations. Hence, self diffusion and reorientations alone mediate the relaxation in these phases.

Self diffusion

The diffusion process is described (Zumer and Vilfan, 1983) by two thermally activated jump processes, interlayer and intralayer with jump length equal to d, similar to the S_A phase. The molecules are represented by rigid cylinders with the nuclei distributed along the long molecular axis. In addition, the possible interlayer ordering (correlations in the layer stacking) is considered in deriving the relaxation rate as (Zumer and Vilfan, 1983)

$$T_1^{-1} = \alpha\tau_\perp \mathbf{P_1}(\omega\tau_\perp, D_\perp/D_\parallel,\ l/d, a/d,\ \Delta) \qquad \textbf{(1.121)}$$

where 06= $(9\gamma^4\hbar^2 n)/8d^3$ measures the strength of the intermolecular dipolar interaction and P_1 is a dimensionless function to be evaluated numerically. The quantity 'a' measures the distance of closest approach between two nuclei belonging to two neighboring molecules lying in two adjacent layers. For typical values of l/d = 5, and a/d= 0.5 ; the dispersion of T\ in crystalline *B* and hexactic *B* phase is similar to the dispersion in S_A phase (eqn. (1.120)) as long as the relative layer motion is not too fast. At higher frequencies, $\omega\tau_\perp$ > 2, the dispersion can be approximated to the Torrey's expression (eqn. 1.34)). Also, the dispersion curves of S_B phases follow the Torrey's well known low frequency dependence, $C_o - C_1\omega^{1/2}$only for A $\neq$ 0, and $\omega\tau_\perp$ < 10^{-2}. In intermediate frequencies corresponding to the usual NMR range ($\omega\tau_\perp$ > 10), the diffusion induced T_1^{-1} has ω^{-2} dependence given by

$$T_1^{-1} = 4\,(C^{(1)} + C^{(2)})\alpha\,\frac{D_\perp}{d^2\omega^2} \qquad (1.122)$$

where $C^{(1)}$ = **0.005 and** $C^{(2)}$ = 0.346.

Reorientations

In the low temperature smectic phases, the rotations around the long axes may become important. In case the director $\mathbf{n}_o$ makes an angle A with the external field, the relaxation rate is given in $\omega\tau_l \ll 1$ limit as

$$(T_1^{-1})_{R,l} = \frac{9}{8}\gamma^4\hbar^2 \sum U_k \frac{(3l^2-1)^2\tau_l}{8r_k^6}(1+3cos^2\Delta) \tag{1.123}$$

Here U_k stands for the relative weight of the proton belonging to the k^{th} group and / for the cosine of the angle between the inter nuclear vector r_k of the k^{th} group and the long molecular axis.

In ordered smectics, rotations around the short molecular axis are known to be frozen (Seliger et al. 1977). The rotations about the long axis are still fast. The main contribution to T_1^{-1} expected in these phases are the isotropic tumbling of the end chains (Blinc et, al. 1978). The relaxation rate due to the isotropic tumbling of end chains is given by a BPP type expression

$$(T_1^{-1})_{RE} = C'' \left[\frac{\tau_{cE}}{(1+\omega^2\tau_{cE}^2)} + \frac{4\tau_{cE}}{(1+4\omega^2\tau_{cE}^2}\right] \tag{1.124}$$

Here the constant C'' represents the relative weights of end chain protons with respect to the total number of protons. Thus T_1 as a function of τ_{cE} shows a minimum at $\omega\tau_{cE} \simeq 0.616$ and at the minimum relaxation rate is given by

$$(T_1^{-1})_{\min} = 1.43\ \frac{C''}{\omega} \tag{1.125}$$

Since all the relevant reorientational motions are taking place in the fast motion limit - i.e., $\omega\tau_c \ll 1$ in these mesophases, no frequency dispersion is expected from the reorientations, as far as T_1 behavior in liquid crystals is concerned i.e., for $\omega\tau_{cE} \ll 1$; $(T_1^{-1}) = 5C''\tau_{cE}$. However, strong temperature effects can be inferred, owing to the dependence of T_1 on various $\tau_c's$. For $\omega\tau_c > 1$

$$T_1^{-1} = \frac{2C''}{\omega^2\tau_c} \tag{1.127}$$

Usually, Arrhenius type of temperature depedence is assumed for τ_c since the reorientations are thermally activated i.e.,

$$\tau_c = \tau_o e^{E_a/kT} \tag{1.128}$$

τ_o is the precxponential factor (correlation time at TOO) and E_a is the activation energy associated with the motional process (k is the Boltzmann constant). Thus, a plot of $\ln(T_1)$ vs T will have two straight lines with slopes $-E_a/k$ and E_a/k at higher and lower temperatures respectively.

Thus, the relaxation rate in a liquid crystal in the various mesophases can be written as

$$T_1^{-1} = (T_1^{-1})_R + (T_1^{-1})_{ODF} + (T_1^{-1})_{SD} \tag{1.129}$$

where the three terms have their own temperature and frequency dependences in various mesophases (as explained before). Thus, the data of relaxation times is fitted to the above model numerically in various phases to obtain the contribution from each of the mechanism and the dynamics parameters associated with them.

Section - 3

1.3 *Dipolar relaxation time (T_{1D})*

The dipolar spin lattice relaxation time (T_{1D}) is mainly dominated by the spectral components corresponding to the local fields (kHz region) and hence can probe slower molecular motions. The time evolution of the local dipolar order plays a major role in determining the relative importance of the intermolecular and intramolecular contributions to the nuclear spin lattice relaxation process. In a typical magnetic resonance experiment, the energy associated with the dipolar order arising from the

local fields is much smaller than the Zeeman energy associated with the coupling of the spins to the external field and hence direct observation of dipolar order is impossible. A typical scheme is to take advantage of the large Zeeman order and transform it into observable dipolar order adiabatically. Since entropy of the system does not change during an adiabatic process, the equilibrium magnetization in the Zeeman order ($M_o = CH_o$) now alligns along the local dipolar fields. This technique is called Adiabatic demagnetization in the rotating frame, ADRF (Slichter and Holton, 1961). Here the magnetization is first locked to a rotating field, H_1 which is reduced to zero adiabatically, i.e., $dH_1/dt \ll \gamma H_1^2$, because of which the Zeeman order is now aligned along the dipolar fields. This dipolar order decays to equilibrium value allowed by Curie's law ($M = CH_o/T$) with an exponential time constant, T_{1D}, the dipolar relaxation time. The other technique for measuring the dipolar relaxation time is by the use of phase shifted pulse pair sequence (Jeener and Broekaert, 1967), where the dipolar order is created by the application of two closely spaced pulses separted by a time delay r (90° out of phase). This dipolar order is observed by applying a third pulse (with an arbitrary phase) at a variable time.

The dipolar echo produced in an anisotropic system like liquid crystal is very complicated, since there are different subsets of spins contributing to the NMR signal i.e., spins associated with aromatic rings - giving rise to a pair of peaks at $\omega_o \pm \delta\omega$ - and spins associated with alkyl end chains which give rise to motionally averaged central peak at the Larmor frequency, ω_o in the proton NMR spectrum. The two components of the free induction decay associated with the two spin subsystems have different time derivatives. Since the efficiency of transforming Zeeman to dipolar order is proportional to the derivative of the FID at time τ, it is in principle possible to selectively transfer the order associated with each subsystem, while suppressing the transfer of order associated with the other subsystems, which results in probing several interesting properties of liquid crystals (Dong and Sandmen, 1983).

The orientation dependence (Blinc et al. 1975 ; Dong and Sandmen, 1983) of T_{1D} is particularly useful to study the nature of collective fluctuations in S_A and S_c phases (since the contribution to the fluctuation spectrum at very low frequencies is mainly from ODF). The relaxation rate in the fast motion limit (weak collison limit)

is given by (Van Steenwinkel, 19G9)

$$T_{1D}^{-1} = [C_o J_0(0) + C_1 J_1(\omega) + C_2 J_2(2\omega)] \tag{1.130}$$

C_o, C_1 and C_2 are of the same order of magnitude. The dimensionality in T_1 and T_{1D} can be accounted for by making $C_2 = 0$ in eqn. (1.130) (Dong and Sandmen, 1983) and the relaxation rate for two spins is approximately written as

$$T_{1D}^{-1} = ah(\Delta) + b \tag{1.131a}$$

where

$$h(\Delta) = \frac{C_o}{C_1} f_o(\Delta) + f_1(\Delta) \tag{1.1316}$$

$$f_o(\Delta) = 18(\cos^2 \Delta - \cos^4 \Delta)$$
$$f_1(\Delta) = \frac{1}{2}(1 - \cos^2 \Delta + 4\cos^4 \Delta)$$
$$f_2(\Delta) = 2(1 - \cos^4 \Delta)$$

where A is the angle between the molecular axis in the mesophases and the external field. In the weak collision limit, it can be seen from eqn. (1.130) that $T_{1D} \sim T_1$. At the outset of motional narrowing i.e. $T_2 = \tau_c$ (correlation time of the responsible moleucar motion), T_{1D} shows a minimum (Ailion, 1983).

The onset of ordered Smectic phases, S_B,S_G from high temperature smectics leads to slowing down of ODF and self diffusion (Blinc et al. 1975). In this slow motional regime, the mean time, τ_c between two successive molecular jumps is much longer and the corresponding T_{1D} becomes very small. In the strong collision limit (Slichter and Ailion, 1964) i.e. rigid lattice limit, T_{1D} can be obtained when $H_1 = 0$. Then

$$T_{1D}^{-1} = \frac{2(1-p)}{\tau_c} \tag{1.132}$$

From the value of T_{1D} obtained from the experiments in the ordered smectic phase, the corresponding correlation time, τ_c can be obtained from the above equation. The constant, *p* is a geometric coefficient varying between 0 and 1. Since the precise value of *p* is not known, only an upper bound, $(\tau_c)_{max}$ can be computed by taking *p* as 0 and the corresponding lower limit of diffusion coefficient D_{min} can be calculated.

Chapter 2

INSTRUMENTATION

One of the aims of the work reported in this thesis is to set up an experimental facility to undertake nuclear spin lattice relaxation studies over a wide frequency and temperature range. A conventional pulsed NMR spectrometer operating over 5 to 50 MHz of proton frequencies already exists in the laboratory. In order to carry out measurements below 5 MHz, a field cycling NMR (FCNMR) spectrometer has been fabricated as part of the present work. The details of the instrumentation done are presented in three sections in this chapter. The first section covers the general methodologies involved in pulsed NMR experiments and certain common pulse sequences used for the measurement of different relaxation times. The technique and the design considerations of field cycling experiments are discussed in the second section. The instrumentation carried out for setting up the field cycling spectrometer and the control circuit are also described in this section. Further, the details and specifications of the pulsed NMR spectrometer used to do the experiments in the frequency range of 5 - 50 MHz, along with certain accessories are described in the third section. Finally the fourth section describes the experimental procedure used for spin-lattice relaxation measurements in liquid crystals.

2.1 *Methodology of pulsed NMR experiments*

NMR experiments are generally done either in frequency domain or time domain. In the frequency domain experiments (CW technique), a low power *rf* radiation is applied to the sample in a high dc magnetic field. Either the frequency of *rf* or the strength of the dc field is slowly swept through resonance. On the other hand, in a time domain experiment (pulse technique), the response of the spin system excited by intense bursts of high powered resonant *rf* magnetic fields for short durations is monitored. While, the CW method deals with the study of absorption and dispersion spectra, $F(\omega)$, the pulsed irradiation method deals with the study of time correlation of a specific dynamic quantitiy f(t) sensitive to the detection system. The two methods are related by Fourier transformation (FT) given by

$$f(t) = \frac{1}{2\pi} \int_{-\infty}^{\infty} F(\omega) \exp(-i\omega t) dt \tag{2.1}$$

and inversely

$$F(\omega) = \int_{-\infty}^{\infty} f(t) \exp(i\omega t) d\omega \tag{2.2}$$

and hence the same spectral information can in principle be obtained from both methods. However, the time domain method, which is the topic of present work, is more efficient regarding the time consumed and also the sensitivity of the signal obtained, since all the spins are excited simultaneously and not sequentially. Another advatange of time domain experiments is that the response of the system is phase coherent, i.e. there is a definite reference point in time (point of excitation) for measurement of all the components of response (Derek Shaw, 1976).

A nuclear magnetic moment μ (arising due to a spin I where μ = 7/), under the influence of an external magnetic field H experiences a torque $\mu \times$ H, which is equal

to the rate of change of angular momentum. The resulting equation of motion of the magnetic moment in a fixed coordinate system xyz (Laboratory frame) is given by

$$\frac{d\boldsymbol{\mu}}{dt} = \gamma\,(\boldsymbol{\mu} \times \mathbf{H}) \tag{2.3}$$

Since $\sum \mu_i$ = M, the total magnetization of the system, the equation of motion for the macroscopically observable total magnetization can be written as

$$\frac{d\mathbf{M}}{dt} = \gamma\,(\mathbf{M} \times \mathbf{H}) \tag{2.4}$$

The application of a perturbing *rf* field, $\mathbf{H}_1(t)$ (with a frequency ω), in a plane perpendicular to H (say along the *x* axis), modifies eqn.(2.4) as

$$\frac{d\mathbf{M}}{dt} = \gamma\,\mathbf{M} \times [\mathbf{H} + \mathbf{H}_1(t)] \tag{2.5}$$

The solution of the above equation is simplified when viewed from a different coordinate system x'yV, which is rotating with respect to the Laboratory frame about some axis, say the *z*-axis, with an angular frequency, same as that of the *rf* field (Slichter, 1978). The equation of motion of the magnetization in this rotating coordinate system is similar to that in the Laboratory frame, with the magnetic field replaced by an effective field, $\mathbf{H}_{eff}$ = [(H + $\boldsymbol{\omega}/\gamma$) + $\mathbf{H}_1(t)$], (Fig. 2.1) i.e.,

$$\frac{\partial \mathbf{M}}{\partial t}\Big|_{rot} = \gamma\,\mathbf{M} \times (\mathbf{H}_{eff}) \tag{2.6}$$

Thus the spins precess about an effective field in the rotating frame, with angular frequency 7 H_{eff}. Chosing H to be along the *z*-axis of the laboratory frame i.e., H = k H_o (where k is an unit vector along *z*-axis), the effective field is modified to $\mathbf{H}_{eff}$ = [(H_o + $\frac{\omega}{\gamma}$)k+ H_1i]. Also choosing the frequency of the rotating frame to be equal to that of the Larmor frequency, i.e., $\omega = \omega_o = -\gamma H_o$, it can be seen that

the effective field in the rotating frame is i//] and hence the magnetization that was initailly parallel to H_o now processes about H_1 in the y'z' plane. If such an *rf* is applied for a time t_w, the angle by which the magnetization precesses is given by

$$\theta = \gamma H_1 t_w \tag{2.7}$$

Thus with an appropriate combination of the intensity and the duration of the rotating field, the magnetization can be rotated by any desired angle. For a given $\mathbf{H_1}$, a pulse applied such that the magnetization is rotated by 180° is called a π pulse and a pulse applied such that the tilt angle 0 = 90° is called a $\pi/2$ pulse.

In practice, the perturbing field $\mathbf{H_1}$ (2), which is an alternating magnetic field can be achieved by the application of a sinusoidal voltage across the sample coil. This results in a linearly polarized field along the axis of the coil which can be considered as consisting of two components counter-rotating about an axis perpendicular to the polarization axis. At resonance, the component rotating in the same sense as the magnetic moment alone is effective in exciting the spin system and the other component rotating in the opposite direction is neglected.

Following the turn off of the excitation field, say a 7r/2 pulse along *x'* axis, the magnetization is rotated into the *y'* direction in the rotating frame, but precesses with Larmor frequency γH_o with respect to the laboratory frame. This precessing magnetization induces an alternating voltage in a pick up coil surrounding the spin system, with its axis perpendicular to the laboratory field. In an actual experiment, the precessing magnetization decays owing to various interactions among the spins which are the objects of NMR study. The interaction between the different nuclei leads to the spins experiencing different fields H = H_o ± A H, where A H is the field due to neighbouring nuclei. This results in the spins precessing with different frequencies and hence leads to a dephasing of the spins in the x'y' plane. Conseqently the magnetization decays exponentially with a time constant T_2, called the spin-spin relaxation time. This signal induced in the pick up coil is a decaying, free precession signal and hence is called the Free Induction Decay signal (FID).

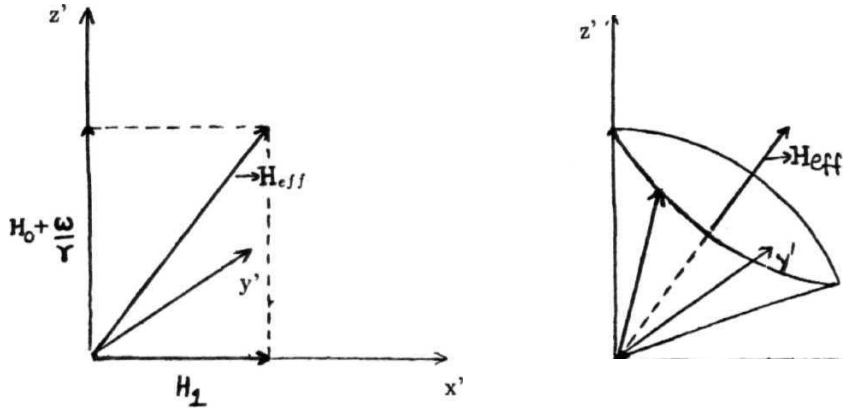

Fig. 2.1 Effective field (H_{eff}) in the rotating frame and motion of the magnetic moment μ around H_{eff}.

An important factor to note at this point is that any in homogeneity in the static magnetic field will result in different spins experiencing different static fields, $H_o = H_o \pm \delta H$. This leads to a further spatial distribution of the resonance frequencies of the spins and consequently a faster dephasing of the spins in the x'y' plane. The time constant associated with this process, T_2^*, is called the apparent spin-spin relaxation time, which is less than T_2.

The decaying magnetization in the x'y' plane, described above, after the removal of H_1, simultaneously evolves to the equilibrium value (parallel to the z' and hence z axis), under the influence of the static field H_o, with a time constant characterised by the interaction of the spins with external degrees of freedom, T_1, called the spin lattice relaxation time. Combining these factors, the equation of motion for the spin system given by eqn. (2.4), can be modified to account for these different relaxation processes as (Bloch, 1946)

$$\frac{dM_z}{dt} = \gamma\,(\mathbf{M} \times \mathbf{H})_z + \frac{M_o - M_z}{T_1} \tag{2.8a}$$

$$\frac{dM_x}{dt} = \gamma\,(\mathbf{M} \times \mathbf{H})_x - \frac{M_x}{T_2} \tag{2.86}$$

$$\frac{dM_y}{dt} = \gamma\,(\mathbf{M} \times \mathbf{H})_y - \frac{M_y}{T_2} \tag{2.8c}$$

The decay of the magnetization in the transverse plane conserves energy in contrast to the magentization decay along the longitudional direction and hence T_2 is different from T\. From Fig. 2.2a, it is clear that the time constant of loss of magnetization in the *xy* plane will never be greater than the time constant of development of magnetization along the *z*-axis i.e., $T_2^* < T_2 < T_1$. If the resonance condition is not satisfied, the magnetization vector still relaxes as e^{-t/T_2}, but simultaneously processes about the *z'* axis with the offset frequency, ω_i. The tip of the vector describes a decaying helix as shown in Fig. 2.2b. The component normally detected by the application of magnetic field along x' axis is the *y'* component of this decaying signal i.e., $M_o e^{-t/T_2} \cos(\omega_i t)$, which on FT yields the Lorentzian signal offset by ω_i from ω_o.

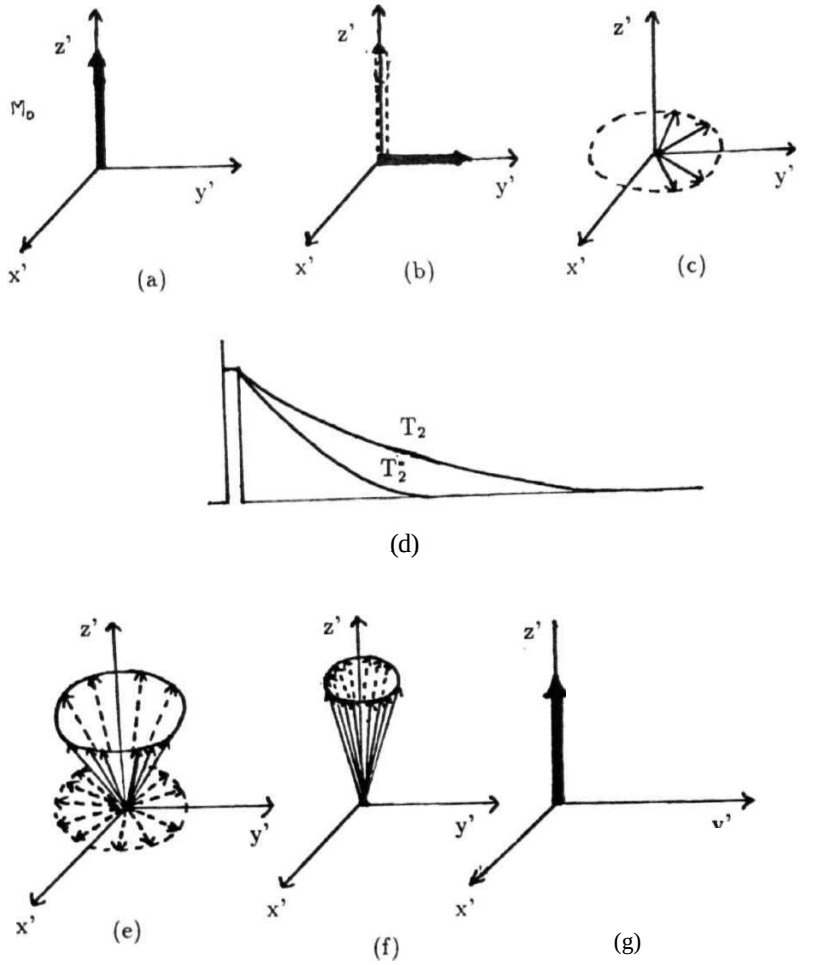

Fig. 2.2a Spin-spin relaxation and spin-lattice relaxation.

(a) Equilibrium magnetization M_o when $H_1 = 0$

(b) Magnetization immediately after $\pi/2$ pulse along x' axis.

(c) Spin-spin relaxation in progress

(d) Free induction decay (i) in the absence and (ii) in the presence of static field inhomogeneity

(e), (f), (g) Spin lattice relaxation in progress.

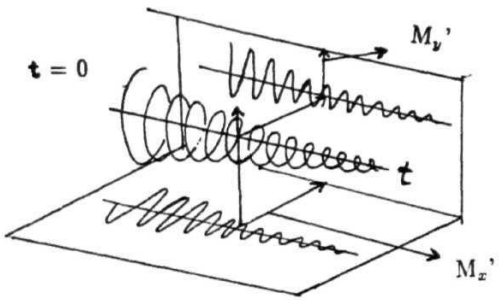

Fig. **2.2b** The off resonance decay and precession of the nuclear magnetization showing the origin of two components

Thus the basic idea of any relaxation time measurement is to disturb the magnetic state from its equilibrium to a given non equilibrium state by an initial pulse (preparation pulse) and then study the evolution of the system back to equilibrium by monitoring the appropriate magnetization component after a variable delay, with another pulse (sampling pulse).

2.1.1 Zeeman Spin-lattice relaxation time (T_1)

During spin lattice relaxation process, the magnetization parallel to the quantizing field (*z*-axis in the present case) evolves. Since the pick up coil is sensitive only to the component of magnetization perpendicular to the *z*-axis, the magnetization that is developed along *z* axis due to T_1 process is detectable only after it is rotated away from the quantizing axis. The different pulse sequences normally used for measuring T_1, their relative merits and demerits are given below.

Saturation recovery sequence ($\pi/2$ — T — $\pi/2$)

This sequence consists of a $\pi/2$ pulse followed by another 7r/2 pulse applied after a variable delay r. The first 7r/2 pulse flips the magnetization into the *xy* plane (magnetization along the z-direction is made zero), which is then allowed to evolve for a time τ and then sampled by the second 7r/2 pulse which tilts whatever magnetization that has developed along the *z*-axis into the xy plane for observation. The amplitude of the FID, *A(T)* at a fixed time from the sampling pulse develops from zero at time τ = 0 to A_o at time τ = oo and satisfies the following equation (Fig. 2.3)

$$A(\tau) = A_o(1 - \exp(-\tau/T_1)) \qquad \textbf{(2.9)}$$

By repeating the experiment for different values of τ and then fitting the data to the above equation, *T*\ is obtained.

Inversion recovery sequence (π - r - 7r/2)

This sequence consists of tilting the equilibrium magnetization into the —*z* direction using an initial π pulse and then monitoring the evolution along z-axis by

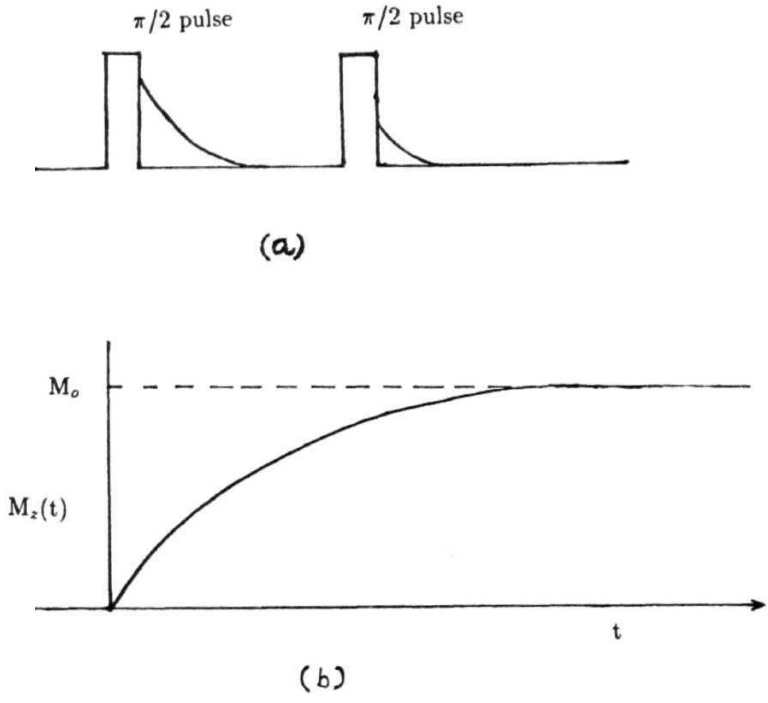

Fig. 2.3a Saturation recovery sequence for T_1 measurements.

Fig. 2.3b Recovery of magnetization in the z-direction with time T.

another sampling 7r/2 pulse after a time r. The preparation (π) pulse inverts the spin population initially and hence the z component of magnetization recovers from $-\mathbf{M_o}$ to $\mathbf{M_o}$. The magnetization recovery follows the equation, (Fig. 2.4)

$$A(t) = A_o(1 - 2\exp(-\tau/T_1)) \tag{2.10}$$

A_o being the amplitude of the FID after a time $T = \infty$. A least square fitting of the data to the above equation will give the spin lattice relaxation time, T_1.

The advantages of this pulse sequence over saturation recovery sequence are

1. T_1 can be roughly estimated by finding the time τ_o for which the magnetization is zero, as $T_1 = \tau_o/\ln 2$.

2. The data has twice the dynamic range ($-M_o$ to M_o) as compared to saturation recovery sequency (0 to M_o), hence increasing the apparant signal to noise ratio.

The disadvantages of this method over the saturation recovery sequence are that this sequence starts with an initial equilibrium magnetization of the spin system in the —z direction and the magnetization has to evolve into the z direction before repeating the sequence for signal averaging. Hence a considerable amount of time ($> 5T_1$) is to be spent for full recovery of the magnetization before the sequence is repeated and this will be time consuming if T_1 is more than a few hundreds of milliseconds.

The spectral width covered by the preparation pulse (π) in this sequence is less compared to that of the *n/2* pulse in saturation recovery sequence for a given transmitter power and hence the saturation recovery sequence yields a better lineshape and intensity for broad lines.

One disadvantage of both these pulse sequences is that, if the preparation pulse width is not exactly set (π or 7r/2), which is often the case, or if H_1 is not homogenous, the initial condition of the magnetizations ($-M_o$ or zero) is not met with, hence leading to reduction in the signal strength.

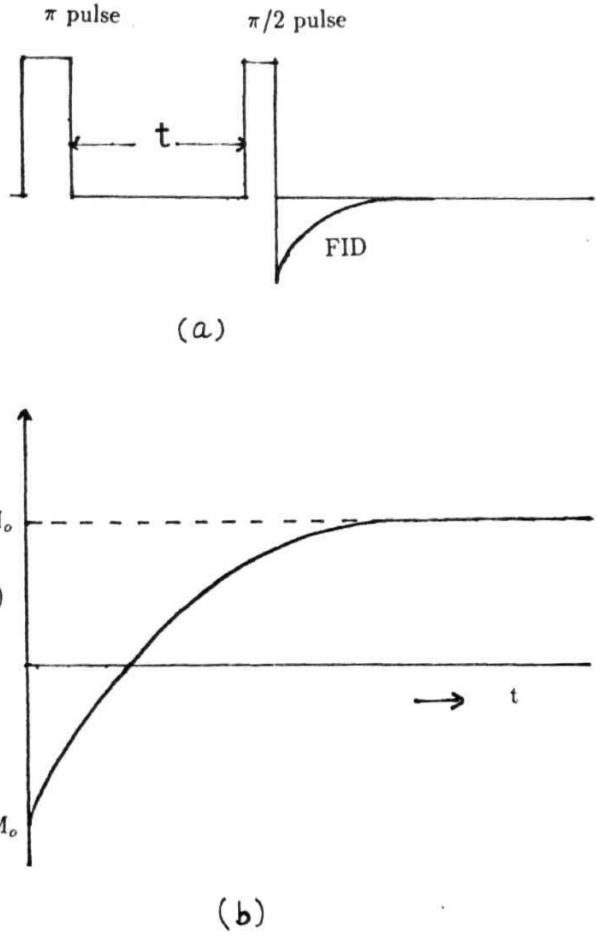

Fig. 2.4a Inversion recovery sequence, for T_1 measurements.

Fig. 2.4b Recovery of magnetization with time r of the sampling pulse.

Saturation burst sequence

A variation of saturation recovery sequence is the saturation burst sequence, where the preparation 7r/2 pulse is replaced by a closely spaced burst (usually 5 to 10) of $\pi/2$ pulses which is followed by a sampling $\pi/2$ pulse after a variable time, r. The spacing between the pulses in the burst is chosen to be greater than T_2, but much less than T_1 (Fig. 2.5). The advantage of using this sequence is that the burst ensures the zeroing of magnetization, enen if the pulse width is not exactly set to 7r/2 or if H_1 is slightly inhomogeneous. The evolution of the magnetization after the preparation pulse is given by eqn. (2.9). The other advantage of this sequence over the inverstion recovery sequence is that the tedious waiting time (> $5T_1$) for long T_1 measurements is eliminated as there is no need for allowing the magnetization to recover fully before the sequence is repeated. In the actual experiments, the first pulse of the next burst can be used as the sampling pulse.

2.1.2 Slow frequency processes

The relaxation process where the magnetization is allowed to evolve under the influence of $\mathbf{H_1}$ in the rotating frame instead of the Zeeman field, is termed as the spin lattice relaxation in the rotating frame, with the corresponding time constant referred to as spin lattice relaxation time in the rotating frame, $T_{1\rho}$. Similarly, if the magnetization is allowed to decay under the influence of the local dipolar fields, $\mathbf{H}_{loc}$ ($\mathbf{H}_{loc} \gg \mathbf{H}_o$), the corresponding relaxation time is known as the dipolar spin lattice relaxation time, T_{1D}. Both T_{1D} and $T_{1\rho}$ sample low frequencies compared to T_1 and hence can give information about slow dynamics of the system under consideration. The different *rf* pulse sequences necessary for the measurement of the above discussed relaxation times are described below.

Spin lattice relaxation time in the rotating frame ($T_{1\rho}$) :

The methodology for the measurement of $T_{1\rho}$ involves locking the spin system to a small *rf* field, H_1, in the rotating frame and observing the magnetization as it evolves from the initial equilibrium value corresponding to H_o to the final equilibrium value corresponding to H_1 (Fig. 2.6).

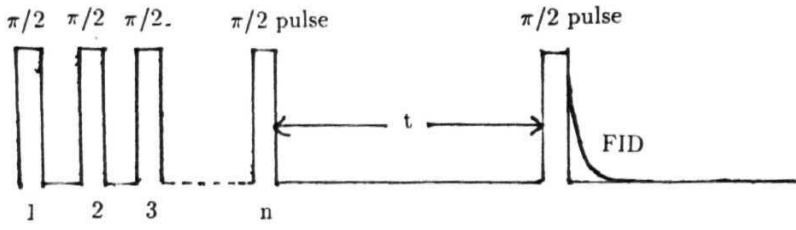

(a)

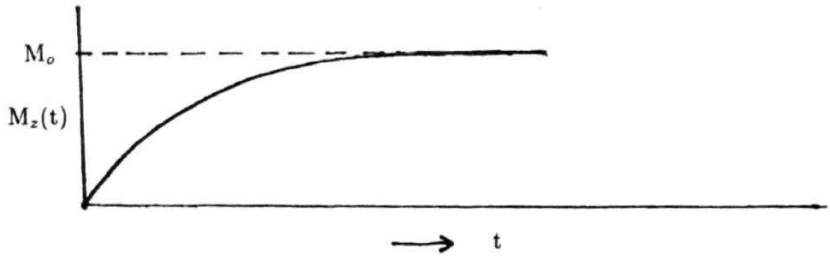

(b)

Fig. 2.5a Saturation burst sequence for T_1 measurements.

Fig. 2.5b Recovery of magnetization with time r of the sampling pulse.

The first 7r/2 pulse flips **the** magnetization from z-axis into the **x'y'** plane. The **second** 90" phase shifted pulse, applied immediately after the first pulse of variable width, locks the spin system to H\ since the *rf* field and the magnetization are in the same direction in the rotating frame (Hartmann and Hahn, 1962). Now the magnetization evolving in the presence of the rotating frame magnetic field is given by

$$A(T) = A_o \exp(-\tau/T_{1\rho}) \qquad \textbf{(2.11)}$$

where r is the variable time for which the locking field is applied. Here $A(\tau)$ corresponds to the amplitude of the FID after an evolution time r. By fitting the experimental data (amplitude of the FID as a function of τ) to the above equation, $T_{1\rho}$ can be calculated.

Dipolar relaxation time (T_{1D}) :

The low frequency motions corresponding to the local dipolar fields can be analyzed by measuring the dipolar spin lattice relaxation time, T_{1D} which is achieved by transferring the **Zeeman** order to the dipolar order and measuring the decay of magnetization in the presence of dipolar fields as the system evolves. Two techniques can be used for this purpose (a) adiabatic demagnetization in the rotating frame (ADRF) (**Slichter and** Holton 1961 ; **Fukushima and** Roeder, 1981; Ailion, 1983) and (b) Jeener Broekaert phase shifted pulse sequence (1967). The first technique consists of following a spin locking pulse by an adiabatic demagnetization - **remagnetization** cycle of the *rf* field, while the second technique consists of creating the dipolar order by a pair of phase shifted *rf* pulses and then monitoring the decrease of the dipolar order by a third pulse. Though ADRF is an efficient method which enables 100% transfer of Zeeman order to dipolar order the **Jeener-Broekaert** sequence is used in the present work, due to the convenience in measuring short T_{1D}s and also due to the ease with which this sequence can be implemented.

Jeener Broekaert *sequence* **(7r/2)o-t** $-(\pi/4)_{90}-\tau-(\pi/4)$

In this technique suggested by Jeener and Broekaert (1967), a state of dipolar

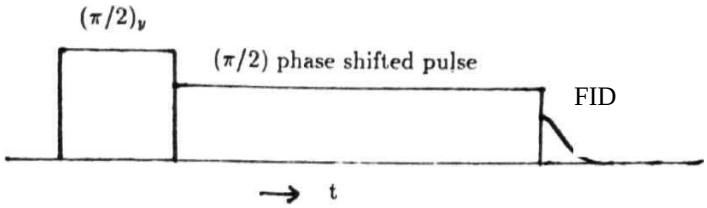

Fig. 2.6 Pulse sequence for $T_{1\rho}$ measurement.

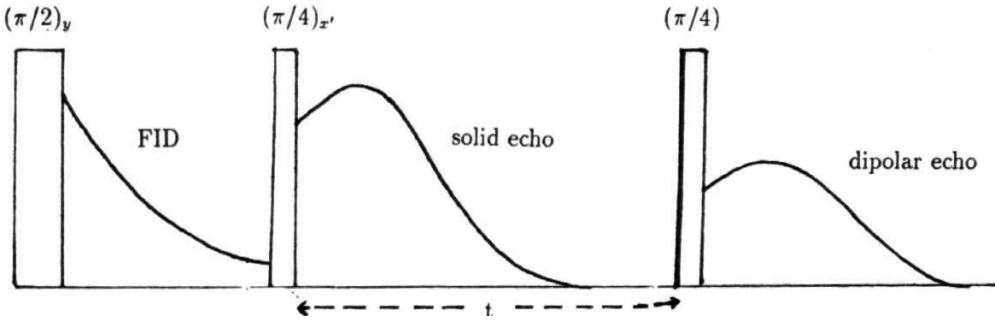

Fig. 2.7 Jeenar-Broekaert (three pulse) sequence for T_{1D} measurement.

order is created by the application of two closely spaced *rf* pulses which are 90° out of phase (Fig. 2.7). The first $\pi/2$ pulse tilts the magnetization into the *xy* plane. The magnetization decays under the influence of the local dipolar fields after the second $\pi/4$ pulse. This decay is then observed by applying a third pulse after an evolution time r, which transfers the remaining dipolar order to Zeeman order. Since the dipolar order is not aligned about any preferential direction, the condition on the phase of the third pulse is not stringent and it can have any phase. An echo (called dipolar echo) is obtained after the third pulse which is a measure of the remaining dipolar order. The decay of amplitude of the dipolar echo i.e., *A(T)* as a function of the delay between the second and third pulses is given by

$$A(\tau) = A_o \exp(-\tau/T_{1D}) \tag{2.12}$$

where **r** is the variable time between the second and the third (sampling) pulse. The third pulse is followed by an FID which is 90° out of phase with the dipolar echo, while the second pulse is followed by the solid echo. Hence for detecting the dipolar echo alone, it is ensured that the reference signal to the phase sensitive detector (in the reciever) is 90° out of phase with respect to the FID. In actual experiment, the reference phase to the receiver is adjusted to maximize the FID following the first pulse and the third pulse is set to be 90° out of phase with respect to the first pulse. Also to maximize the echo, it is necessary to place the second pulse at the steepest part of the FID after the first pulse. The efficiency of this sequence in setting up the dipolar order is maximum (56%) when the second and third pulses are $\pi/4$.

Both $T_{1\rho}$ and T_{1D} measurements can give valuable information about molecular dynamics at very low frequencies (typically upto 100 kHz) where it is not possible to do conventional Zeeman relaxation measurements due to very poor signal to noise ratio. While T_{1D} samples motions corresponding to dipolar fields (around 10 kHz and less), $T_{1\rho}$ can sample molecular dynamics around 100 kHz (limited by maximum possible locking field strength H_1). This restriction is due to the maximum available *rf* power as well as *rf* heating of the sample due to the application of high powered *rf* for longer times. Hence, there exists a considerable gap between the lower limit of

accessible frequency in conventional NMR and high frequency limit of $T_{1\rho}$ technique, which extends to about two orders of magnitude in frequency. Further information on the molecular dynamics in this frquency range necessitates a more versatile technique. In this regard, Field cycling NMR (FCNMR) technique (Anderson and Redfield 1959 ; Kimmich and Bachus 1982 ; Noack, 1986) is more efficient and suited as it facilitates T_1 measurements down to 0 Hz. The details of the FCNMR technique along with the design considerations are explained below.

Section - 2

2.2 *Field cycling NMR*

Low frequency T_1 studies are capable of giving insight into the slow molecular processes. Particularly such studies are extremely useful in liquid crystals where collective fluctuations aassociated with the director are mostly limited to the frequency region below 1 MHz. But conventional NMR technique can be used only at frequencies above a few MHz (typically 5 MHz). Below this frequency, signal to noise ratio becomes unacceptable, since the NMR induction signal is proportional to $(H_o)^{3/2}$ (the energy levels at equilibrium are more evenly populated as the Zeeman field (and hence frequency) is decreased). On the other hand, an FCNMR spectrometer makes it possible to extend the scope of field dependant measurements to almost zero Larmor frequency, while allowing for the convenience of high frequency signal detection. Further, using the FCNMR technique, any frequency dependant study between a given minimum and maximum obtainable frequencies can be easily done without having have to tune the spectrometer independently at each frequency (as the frequency where the signal is detected is not altered in this technique). Another important application of FCNMR is the zero field or low field NMR relaxation **(Das and Hahn 1958 ; Hebel and** Slichter 1959 ; Masuda **and** Redfield, 1962, **1964 ; Refield, 1963, 1967 ; Slusher and Hahn,** 1968 ; Edmonds, 1981) where the Zeeman energy **and consequently** line broadening caused by the distribution **of molecular orientations due to the Zeeman field vanish thus enhancing the spectral resolution.**

Apart from just lowering the intensity of the fields (and hence induction B_o), field cycling may as well include evolution periods with higher field intensity than the detection field, - or even changing the direction of the field - , and hence this technique offers capabilities which go far beyond the original intentions. Cycling of the orientation at high speed facilitates the angular dependant relaxation and diffusion measurements in liquid crystals with relative ease compared to other cumbersome methods of field rotation. Apart from frequency dispersion studies over a wide frequency range, FCNMR spectrometer can be used in (i) certain level crossing experiments (Hecke and Janssens, 1978 ; Coppen et al. 1983 ; Prager et al. 1983) (ii) detection of weak and low frequency resonance signals (Schweikert, 1990) (iii) cross relaxation spectroscopy (Solomon, 1955 ; Solomon and Bloembergen, 1956 ; Seliger et al. 1976 ; Koenig et al. 1978 ; Vilfan et al. 1980 ; Winter and Kimmich, 1982a,b ; Blinc et al. 1983) and (iv) certain 2d experiments (Dolinsek et al. 1992). Some of the manifold applications of FC were illustrated by Kimmich (1980). The details of the fabricated FCNMR spectrometer taken up as part of the present work are given in this section. The FCNMR spectrometer has been tested and standardized. However, it could not be utilized for actual measurements on the five liquid crystals on which detailed high frequency dispersion study of spin relaxation has been taken up by the author, owing to the limitation on time in completing this project.

2.2.1 Technique

Field cycling technique involves the sample being kept at different Zeeman fields (or magnetic induction) during different times of a relaxation experiment. In other words, the induction is modulated periodically in strength (also direction in case of angular dependent measurements). The nuclear spins are polarized and detected at a sufficiently high field to yield a satisfactory signal to noise ratio *(S/N)*. But between the polarization and detection periods, the field (evolution field) is varied from the selected high value to an adjustable lower field. Thus, though the signal is detected at a sufficiently higher field, the properties characteristic of the spins for frequencies between the minimum and maximum can be conveniently studied at a single detection frequency. Comparison of the sensitivity of the induced signal in

the induction coil during an FC experiment with a conventional NMR experiment at low fields (corresponding to evolution fields), clearly shows the signal enhancement in the former case (Noack, 1986). The simplest cycle involving the different periods and times is shown in Fig. 2.8. The polarization field B_{OP} corresponding to the polarization period t_P is made as high as possible with moderate requirements on homogeneity. B_{OE} is the variable evolution field ($0 < B_{OE} < B_{OP} - B_{OD}$) and B_{OD} is the detection field (t_D is the detection period) which is again made as high as possible with better homogeneity for signal detection. 'T' is the total period of the cycle which is repeated many times during the course of the relaxation time measurements. The transit times t_{OFF} ($B_{OP} \rightarrow$ *BOE)* and t_{ON} ($B_{OE} \rightarrow$ *BOD)* are the times of switching the field OFF and ON respectively. The main conditions to be satisfied by these transit times is that on one hand they should be fast compared to the relaxation times of the spin system under study (to avoid losses of the magnetization) and on the other hand, they should be slow enough such that the Fourier spectrum of the time varying magnetic fields do not contain components in the vicinity of the Larmor frequency. Finally, the cycle has to be synchronized with appropriate intervals of the *rf* irradiation ($H_1(t)$) common to the conventional NMR to prepare the system into an initial non-equilibrium state or to detect the induced signal.

2.2.2 Magnet

Conventionally the desired cycle can be obtained by two methods. The first is by mechanical movement of the sample between the chosen magnetic fields (Pound, 1951; Schumacher, 1958; Abragam and Proctor, 1958 ; Pershan, 1960 ; Johnson and Goldberg 1966 ; Jones et al. 1968 ; Blinc et al. 1976 ; Edmonds, 1977). The other method involves electronic switching wherein the field cycling is achieved by varying the current through an inductive load (magnet) (Packard and Varian, 1954; Bloom and Mansir, 1954). Mechanical cycling can be performed with simple apparatus and also there is no limit on the obtainable polarization and detection field levels. But the switching intervals are limited due to the mechanical movement of the sample. On the other hand, electronic switching results in much faster intervals and is also more suited for automation though the experimental realization for higher fields is

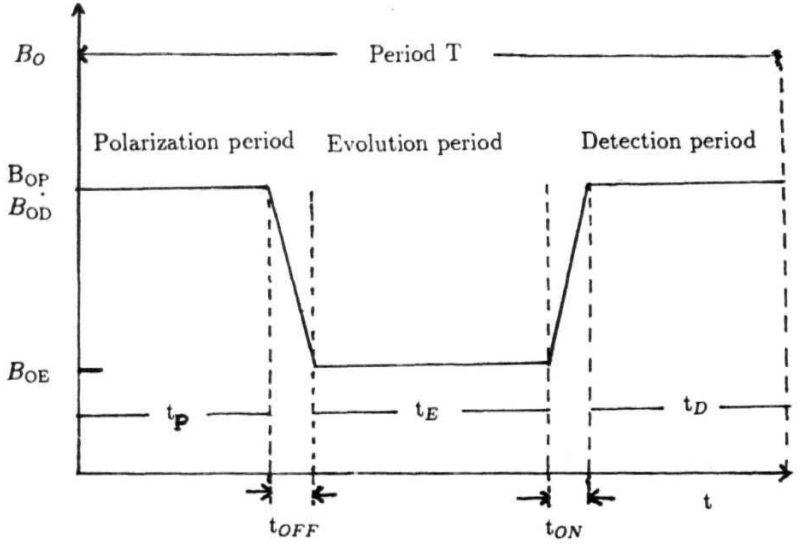

Fig. 2.8 Typical field cycle, with polarization, evolution and detection periods separated by the transit intervals t_{ON} and t_{OFF}.

more involved. In the present case, electronic switching is chosen.

From the simple understanding of the behavior of an inductive load, the maximization of the induction and its rate of variation impose contradicting restrictions. Hence optimization of both these parameters necessitates the critical consideration of the relations between B_o and dB/dt.

Optimization of B_o and dB_o/dt

Due to the large number of parameters involved, an empirical approach (involving standard formulae on the magnetic field for different geomerties) is usually adopted during the construction of an FCNMR magnet. Of the various geometries for the design of the coil available in the literature (Redfield et al. 1968 ; Kimmich and Noack, 1970; Brown and Koenig, 1977; Wolfel, 1978 ; Graf,1980 ; Voigt and Kimmich, 1980 ; Rommel et al, 1986), the Helmholtz ring pair and cylindrical geometries are well known (Fig. 2.9) . The Helmholtz ring pair arrangement, though has an advantage of well understood mathematics and a convenient radial access to the center, is limited by the marked reduction in the induction at the center of the coil compared to that near the windings. Further good homogeneity is limited to a relatively small area around the center. In this respect, cylindrical coils are found to be superior to Helmholtz ring pairs as regards to many specifications like maximum induction, homogeneity and total field volume since, for a given volume, cylindrical geometry provides a better B_o/I ratio. However the inconvenience of having only axial access to the field (at the center) is a disadvantage to be accepted with the above advantages. Due to the above reasons, in the present case a cylindrical geometry is chosen.

The induction along the axis of a long solenoid of length /, radius r and number of turns *n* in a medium of permeability μ is given by

$$\mathbf{B}_o = \mu \mathbf{H}_o = \mu \frac{n}{l} \left[1 + \left(\frac{r}{l} \right)^2 \right]^{-1/2} I \qquad (2.13)$$

where I is the current through the coil. The rate of change of current through the coil, dI/dt, for an applied voltage 'U' is given by Faraday's law of induction as

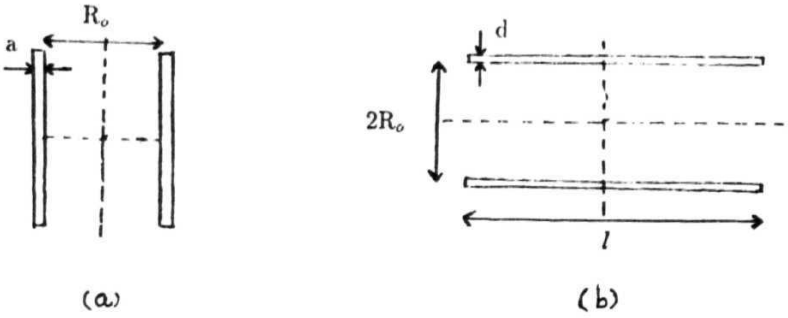

Fig. 2.9 The two well known geometries for the design of a coil
(a) Helmholtz ring pair ($a \ll R_o$)
(b) Cylindrical geometry (Solenoid) ($d \ll R_o \ll 1$)

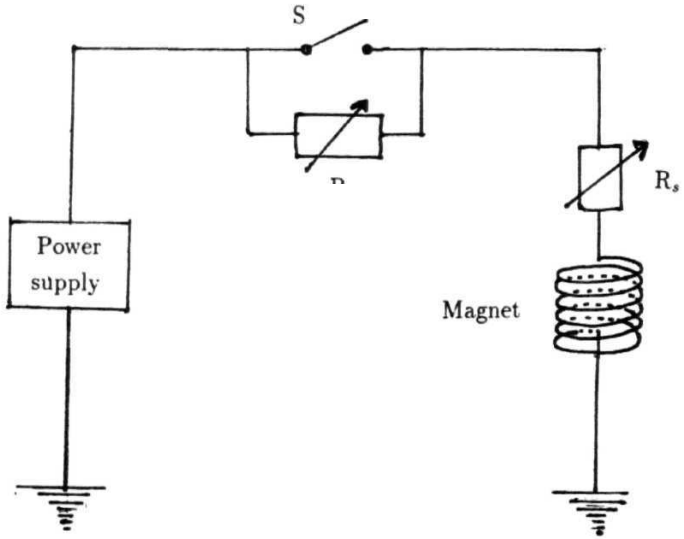

Fig. 2.10 A simple concept of electronic switch for cycling between two current levels I_{min} (corresponding to *BOB)* and I_{max} (corresponding to B_{OP} and B_{OD}).

$$\frac{dI}{dt} = \frac{U - I}{L} R_s \tag{2.14}$$

where R_s is the series resistance and L is the inductance of the coil, given by

$$L = \frac{\mu n^2 \pi r^2}{l} \tag{2.15}$$

The above equations clearly indicate that B_o and dB/dt cannot be optimized independently since maximization of one decreases the other. Thus, a compromise has to be found between them for efficient switching. Eqn. (2.13) and eqn. (2.14) can be rewritten in terms of the volume V of the coil and inductance L as

$$\mathbf{B}_o \,|_{\max} = \sqrt{\frac{\mu L}{V}} I \tag{2.16a}$$

$$\frac{d\mathbf{B}}{dt} \,|_{\max} = \sqrt{\frac{\mu}{VL}} U \tag{2.166}$$

From the above equations

$$(\mathbf{B_o})_{\max} \times \left(\frac{d\mathbf{B}}{dt}\right)_{\max} \sim \mu/V \tag{2.17}$$

which clearly shows that simultaneous maximization of B_o and dB/dt depends on the effective volume V of the coil and the permeability μ of the core material used and is independent of other quantities.

Field switch

The simplest realization of the electronic switch is given in Fig. 2.10, which facilitates the switching between two different states. The power supply generates two current levels in the coil of inductance L and series resistance R_s, through the switch S and an adjustable parallel resistance R_p. The sum $R_p + R_s$ determines the lower level of current, I_{min}, while R_s determines the upper level of the current, I_{max}.

Initially, when the switch S is closed, a voltage 'U_o' applied to the coil increases the current (I) exponentially with a time constant $\tau_{on} = L/R$, i.e.,

$$U_o - L\frac{dI}{dt} = IR_s \tag{2.18}$$

Similarly, when the switch S is open, the voltage across the coil decreases with a time constant $\tau_{off} = L/(R_s + R_p)$ i.e.,

$$U_o - L\frac{dI}{dt} = I(R_s + R_p) \tag{2.19}$$

From the above two equations, it is clear that the transit times are shorter for larger values of R_s and R_p and smaller values of L. The increase in the value of R_s and R_p are limited by the facts that

1. increase in R_s beyond a point reults in an enormous increase of supply voltage (for a given maximum current).
2. increase in R_p fails to suppress the excessive voltages induced due to the sudden decrease in the current during turn OFF.

However, from the turn ON and turn OFF characteristics, it is clear that though the equilibrium state is reached faster for higher values of R_s and R_p, the fastest rate of increase or decrease of current are independent of R_s and R_p, since

$$\frac{dI}{dt}\Big|_{max} = \left|\frac{U_o}{L}\right| \tag{2.20}$$

In fact, the slope U_o/L for the characteristics is maintained longer for smaller values of R_s and R_p (linear characteristics in Fig. **2.11a** and Fig. **2.11b**). In other words, the limit $R, \rightarrow 0$ (**cryomagnet** limit) results in better transit times than a normal conducting coil. The current through the coil during the transits is given by

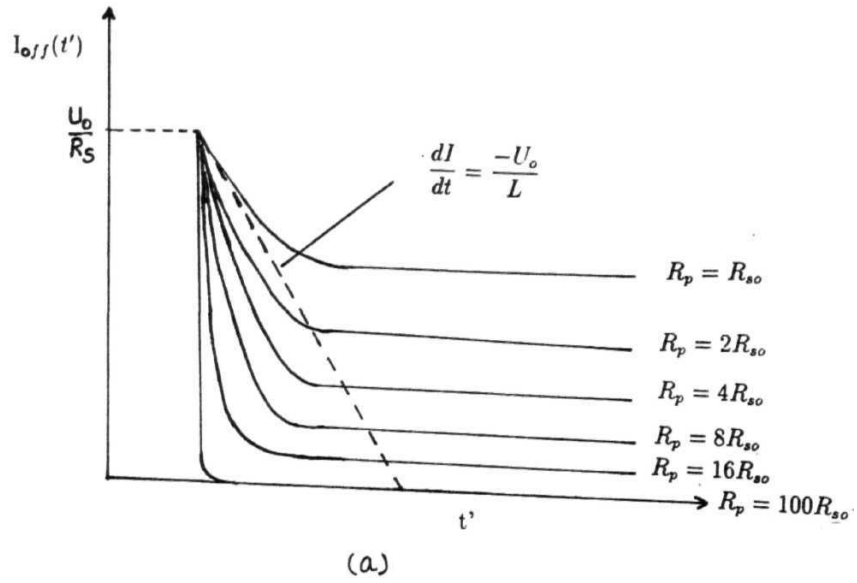

Fig. **2.11a** Turn OFF characteristics for different values of R_p and τ_{off}. R_p is given in terms of arbitrary value R_{so}

Fig. **2.11b** Turn ON characteristics for different values of R_s and τ_{on} The linear increase **dI/dt** = *Vo/L* represents the $R_s \to 0$ limit. R_s is given in terms of arbitrary value of R_{so} (MOACH, 1986)

$$I_{ON}(t'') = I_{\min} + \left(\frac{U_o}{R_s} - I_{\min}\right)\left(1 - e^{-R_s t''/L}\right) \quad \textbf{(2.21a)}$$

$$I_{OFF}(t') = I_{\min} + \left(\frac{U_o}{R_s} - I_{\min}\right)\left(e^{-(R_s+R_p)t'/L}\right) \quad \textbf{(2.216)}$$

Another alternative to reduce the transit times is to reduce the inductance of the coil as evident from eqn. (2.20) i.e., by replacing iron core magnets of larger inductance by air core magnets of small inductance, compatible with other requirements on the cycle like satisfactory induction fields.

Energy storage principle

Another important factor which results in a marked improvement in the transit times is the increase in the voltage across the coil during the transits (eqn. (2.20)). This can be acheived using energy storage principle (Redfield et al. 1968) which is explained below. During major portions of the cycle (i.e. during the low evolution and transit periods) the full power from the supply, $P_o = I_o U_o$ is not dissipated in the circuit elements. If this redundant energy E_{red} can be transferred by a storage device to the turn ON period where it becomes useful and acceptable by the switching circuit, instead of increasing the supply voltage, the switching times can be reduced. The simplest way to achieve this, is by charging a powerful capacitor C by means of E_{red} and then to take advantage of the voltage generated on C during the transits, to reduce them.

The current characteristics given in eqn. (2.21). are now modified to

$$I_{ON}(t'') = I_{\min} + \left(\frac{U_+}{R_s} - I_{\min}\right)\left(1 - e^{-R_s t''/L}\right) \quad \textbf{(2.22a)}$$

$$I_{OFF}(t') = I_{\min} + \left(\frac{U_+}{R_s} - I_{\min}\right)\left(e^{-(R_s+R_p)t'/L}\right) \quad \textbf{(2.226)}$$

where $U_+ = U_o + U_c$. Fig. 2.12 shows the improvement in the turn ON transits acheived using the energy storage principle.

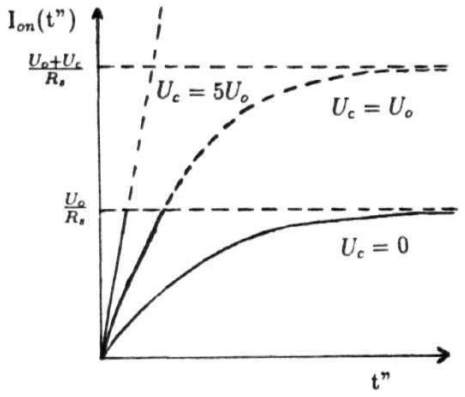

Fig. 2.12 Turn ON characteristics after incorporating energy storage principle for different values of U_c. (Noach, 1986)

Magnetization during the transits

Unlike in conventional NMR, where the magnetization (under the influence of a constant Zeeman field) at different stages is perturbed by a small field H_1, in FCNMR, the Zeeman field itself is modulated and hence the effects of this modulation on the magnetization also is to be considered (since the behavior of spins in **the** evolution period **necessarily** depends on the behavior during the other periods of the cycle and especially during transits). Considering the equilibrium value of the magnetization to be M_o and the spin lattice relaxation time, T_1 to be field dependent, the Bloch equation for **the** magnetization parallel to the external field, M_z can be written as

$$\frac{d\boldsymbol{M}_z}{dt} = \gamma\,[\boldsymbol{M}\,(t) \times \boldsymbol{B}_o]_z - \frac{1}{T_1(\boldsymbol{B}_o)}\,[M_z(t) - M_o(\boldsymbol{B}_o)] \tag{2.23}$$

Let the equilibrium values of M_z in the polarization, evolution and detection periods be M_{OP}, M_{OE} and *MOD* with the corresponding spin lattice relaxation times T_{1P}, T_{1E} and T_{1D} respectively. The condition on the transit times is that the switching is fast compared to the relaxation times i.e.,

$$t_{off} + t_{on} \ll T_1(\boldsymbol{B}_o)_{\min} \tag{2.24}$$

but slow enough compared to the Larmor frequency ω_o so that the magnitude and **the** angle between *M(t)* and $B_o(t)$ is preserved.

The above two conditions ensure that there is no change of magnetization during the transits and hence the field after the transits is constant and parallel to the applied field **just** before the transits i.e.,

$$M_z\ (\boldsymbol{B}_{OP} \rightarrow \boldsymbol{B}_{OE}) = \textit{constant} = MOP \tag{2.25a}$$

$$M_z\ (\boldsymbol{B}_{OE} \rightarrow \boldsymbol{B}OD) = \textit{constant} = MOE \tag{2.256}$$

The development of the manetization in the different regimes of the cycle are summarized in Table 2.1 (Fig. 2.13). Thus FC measurements enable the measurement

Table 2.1 : Variation of the magnetization M (t) during the different regimes of an ideal Field cycle.

Polarization (P)	$M_z(t) = M_{0D} = M_{0P}$ $(t < t_P)$
Transit (P → E)	$M_z(t) = M_z(t_P) = M_{0P}$ = constant
Evolution (E)	$M_z(t) = M_{0P} - (M_{0P} - M_{0E}) [1 - \exp(-[t-t_p]/T_{1E})]$ $(t_p < t < t_E)$
Transit (E → D)	$M_z(t) = M_z(t_E)$ = constant
Detection (D)	$M_z(t) = M_z(t_E) + (M_{0D} - M_z(t_E))[1 - \exp(-[t-t_E+t_p]/T_{1D}$ $(t_p+t_E < t < t_p+t_E+t_D)$

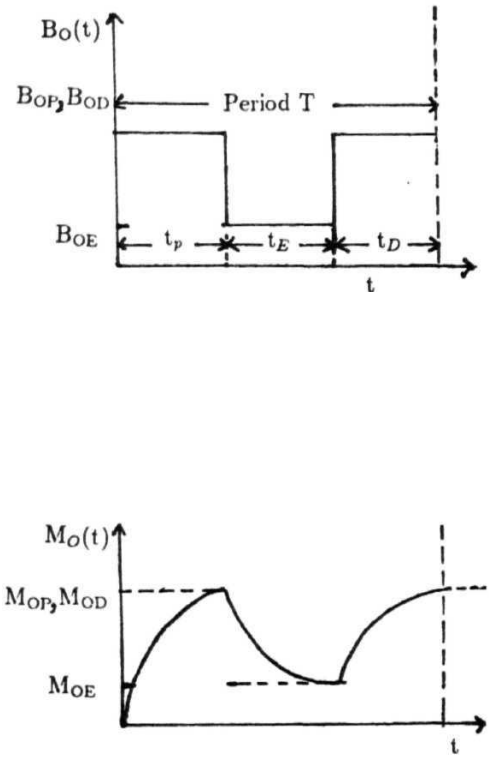

Fig. 2.13 Variation of $M_z(t)$ during a typical field cycle (the switching times t_{OFF} and t_{ON} are neglected).

of $M_z(t)$ as a function of the magnitude of the evolution field B_{OE}. Though most FC experiments are concerned with longitudinal relaxation processes, any other NMR quantities which follow general Bloch type relations like diffusion constant, cross relaxation rate etc., are also measurable through standard NMR procedures with suitable B_o cycles.

To summarize, the requirements and demands for optimization of FC spectrometer are

1. The transit times must be fast compared to relaxation times but slow compared to ω_o.
2. The polarization field should be sufficiently high for initial magnetization.
3. The detection field should be sufficiently high and homogenous to ensure good *S/N* ratio.
4. The maximum induction and the rate of change of the induction must be optimised simultaneously.

Lastly, the limit on homogeneity and transit times depends on the type of systems under investigation i.e., liquids have smaller line widths and hence require more homogeneous fields even with poor transit times. On the other hand, solids require enhanced B_o and dB/dt, with a moderate homogeneity since they have larger line widths. Keeping these factors in view, the field cycling magnet and the necessary electronics to control and switch the field are designed, the details of which are given below.

Design considerations

The crucial part of the instrumentation involved in setting up an FCNMR spectrometer is the design and construction of the switchable magnet. Apart from the usual specifications of an NMR magnet like maximum induction, homogeneity and stability etc., an *FC* magnet is characterized by an additional feature i.e., the geometry of the coil which enables fast switching. The highest obtainable field $(B_o)_{max}$

and the fastest rate of change of induction $(dB/dt)_{max}$ characterizing the magnet are interdependent through the coil parameters like inductance, permeability, volume etc., (eqn. (2.16a) and eqn. (2.16b)). Hence the performance of the magnet can not be ascertained by optimizing any single parameter. The obvious choice thus is to maximize both the quantities simultaneously i.e., $(B_o)_{max}$ x $(dB/dt)_{max} \sim \mu/V$, where V is the effective volume enclosed by the coil. Thus, a good *FC* coil should be very small and filled with magnetic material of large permeability (in the regions not occupied by the sample). However, both aspects are bound by mathematical and technical problems which are complicated. For example, the choice of the magnetic material is limited since ferromagnetic materials are completely inadequate due to poor frequency response and hysteresis effects, while ferrimagnetic materials are not very promising due to their low $\mu(B_o)$ saturation. Thus, air core magnets seem to be best choice. Similarly, reduction of volume is limited by the technical requirements on the cooling facility and also a minimum size of the sample and cryostat required for temperature variation measurements.

Homogeneity

Suitable refinements to the cylindrical geometry due to finite length of cylindrical coils result in improved homogeneity. For example, uniform induction can be obtained by (i) linearly varying the number of windings per length (Hak, 1936) (ii) adding outer notches (Grossl et al, 1985) (iii) graduating the spacing between the conductor loops (Cesnak and Kabat, 1972) etc. (Fig. 2.14). Considering all the above factors, a cylindrical geometry with outer notches is chosen in the present case for the design of the magnet.

The optimization method of Grossl (1985), with external notches is followed since it has the advantage of providing accurate field values in a considerable volume around the neighborhood of the center of the coil. The geometrical parameters of a general solenoid (Fig. 2.15) are denoted as $\alpha = R_o/R_i, \beta = 1/2R_i$, θ = fc/i*,, $\eta = l_k/l$. $R = \frac{1}{2}(\alpha + 1)R_i$ is the mean radius and C is the layer thickness given by (a - $1)R_i$. The relative axial and radial variables are $x = l_a/l$ and y = R_a/R_i .The procedure consists of optimizing the quantity B x dB/dt for a given peak input power. The solutions

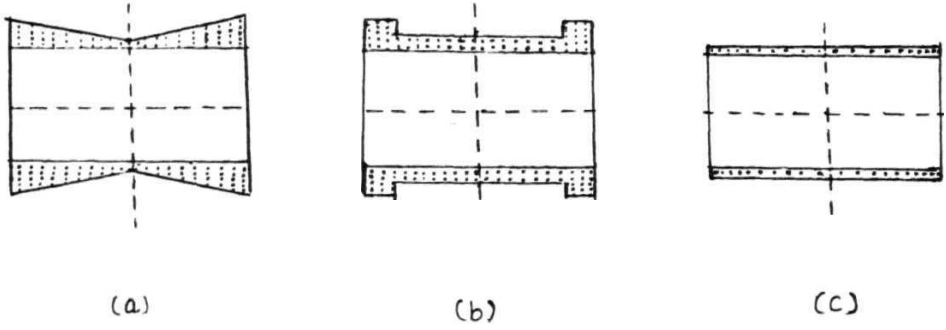

Fig. 2.14 Variations in the cylindrical geometry to improve the homogeneity of the field

(a) Linear variation of the number windings per length

(b) Addition of outer notches

(b) Graduating the spacing between the conductor loops

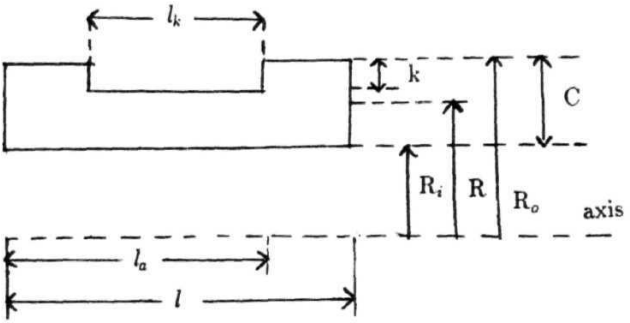

Fig. 2.15 The different geometrical parameters of a solenoid to be optimized for homogeneity(ftub'ssL et al. 1985).

of the elliptic integrals obtained (Grossl et al., 1985) result in the switching time, r being proportional to the square of the flux density. This optimization procedure leads to the different parameters of the coil as given in Table. 2.2. The final design of the magnet is given in Fig. 2.16a. The maximum magnetic field obtained in the present case is 1.2 kG with a stability of 1 in 10^5 in an hour. The requirement of a low ohmic and low inductive magnet is satisfied by winding the coil with copper wire of appropriate dimensions.

The large currents through the coil result in a large power dissipation which necessiates critical cooling requirements. Compressed air, liquid nitrogen, water and oil are convenient cooling agents to remove the heat from the coil, each with its own advantages and disadvantages. Air is not very effective though it is easy to handle. Liquid nitrogen is very effective but is expensive and difficult to regulate. Though water is effective, necesary measures to avoid corrosion by electrolyis are required. Oil is more effective than water but requires a more closed cooling arrangement than water. Considering all the above factors, in the present case, the magnet is enclosed in a closed oil bath which is cooled with chilled running water (Fig. 2.16b).

Construction details

The basic circuit used to control and switch the current through the magnet based on the energy storage principle (Noack,1986) is shown in Fig. 2.17. Here semiconductor devices such as metal oxide semiconductor field-effect transistors (MOSFET's) are used to control electric currents, since they combine the advantages of bipolar transistors as well as switching components like Gate turn off (GTO) thyristors. The GTO is used to switch the capacitor in and out of the magnet circuit during transits. Here the specifications of the current source determine the maximum induction obtained while the specification of the switching devices (GTO and MOSFET's) limit the maximum switching times of the cycle. The use of the energy storage principle and the most recent switching devices to overcome the high voltage surges makes the circuit more versatile.

N_1 is the main power supply (180V/25, APLAB make, No. 7146S), which provides the maximum current needed during the polarization period. The decoupling diodes

Table 2.2 : Specifications of the magnet coil.

1.	Geometry	Cylinder with outer notches
2.	material	Copper wire
3.	Total No. of windings	2552
4.	Number of windings in notches	352
4.	Coil length	22 cm
5.	Diameter of the bore	5 cm
6.	Inductance	66 mH
7.	Max. induction	0.15T
8.	Homogeneity	1 in 10^5
9.	Maximum current	10 A
11.	Cooling agent	oil
12.	Transit times	5 msec.

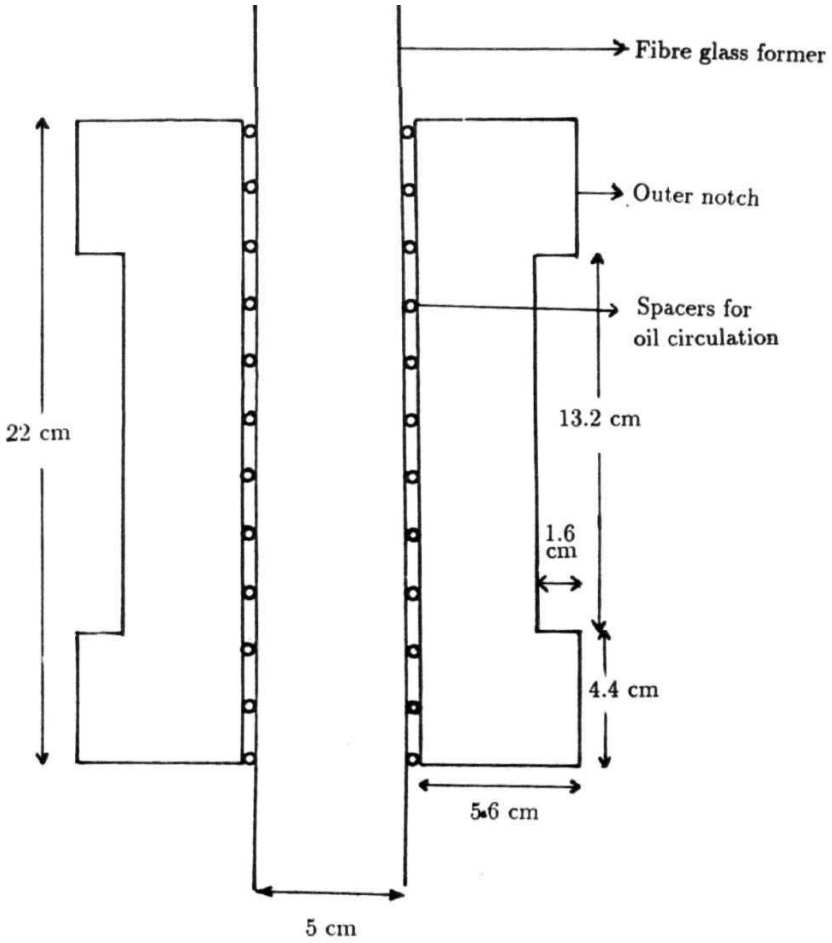

Fig. 2.16a Optimized dimensions of the magnet.

Total No. of windings	= 2552
No. of windings in the notch	= 352
Inductance of the coil	= 66mH
Resistance of the coil	= 7 ohms

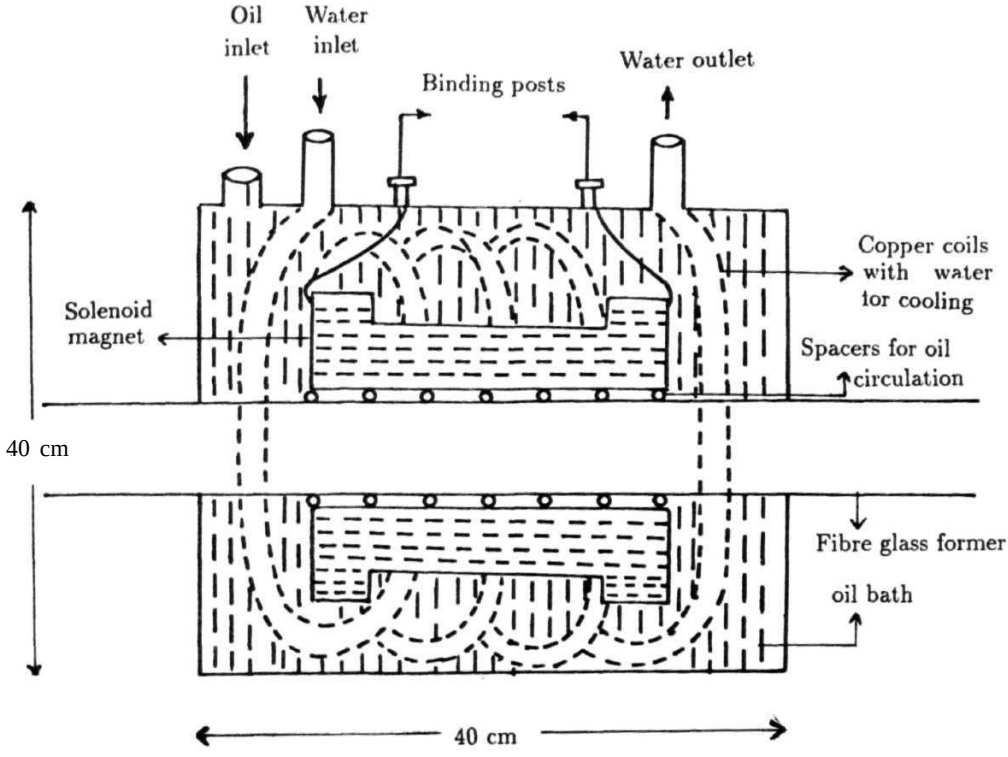

Fig. 2.16b Cooling arrangement for the coils.

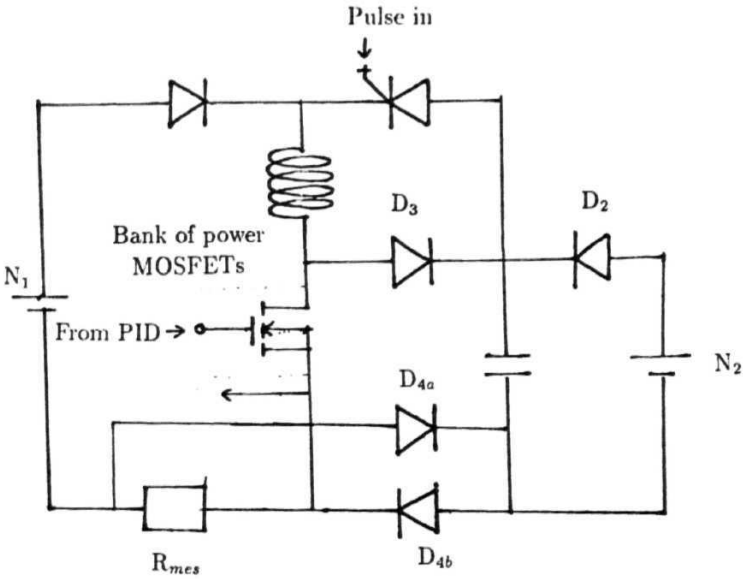

Fig. 2.17 Electronic field switch with power **MOSFET's,** GTO and energy storage principle.

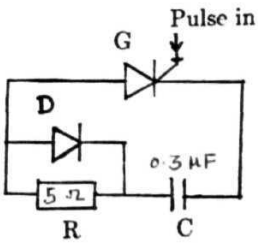

Fig. 2.18 RCD snubber network to protect the GTO from high voltages.

D_1 (BY 127, 20 of them in parallel) decouples the coil from the mains during the transit times. The action of the storage capacitor, C (three capacitors in parallel, each 3000μ F/ 300V) is enhanced by precharging with the help of an additional power supply N_2 with negligible current demand (1200V/lAmp, APLAB make, 7323), so as to provide extra driving power for the transits. The charging diode D_2 allows the charging of the capacitor C and also decouples the coil from the source N_2 during the transits. The free wheel diode D_3 (Nihon inter elect. corp. model no. 45MLA), provides a path for current during the turn off interval, where the energy of the coil is transferred to the capacitor. The transistor arm *T* consists of 20 MOSFETs (IBRFPG 40) which enables the control of the fields. The GTO thyristor G (Model No. 358RGA100 of Nihon Interelec. Corpn.) used during turn ON period is protected against excessive voltages or current transients using a snubber network (Fig. 2.18) consisting of a combination of a resistor R, a capacitor *C*\ and a diode D. The working of the circuit during different time intervals is broadly explained below (Fig. 2.19).

1. During high or low field periods the coil current is regulated at any chosen value, by the MOSFET control circuit (Fig. 2.19a).

2. During the transit from high to low fields (turn off of the field), the signal corresponding to the required low field is given to the MOSFET control circuit, resulting in the reduction of the current and also generation of large voltage at the coil. The energy storage condenser *C* is precharged by N_2 and is further charged with the coil voltage to a higher voltage U_c, during this period. If the precharged voltage is close to U_c, the capacitor charges quickly to the maximum value resulting in a faster decay of the current through the coil (Fig. 2.19b)

3. As soon as the applied lower current level (the required evolution period) is reached, the MOSFET transistors control the field and hence a steady evolution field is obtained (Fig. 2.19c). Thus the operation in both the high and low fields is indistinguishable, as regards the operation of the control circuit.

4. During the transit from the low evolution field to the detection period, the high voltage U_c from the condenser is fed back to the coil, through the ignition of

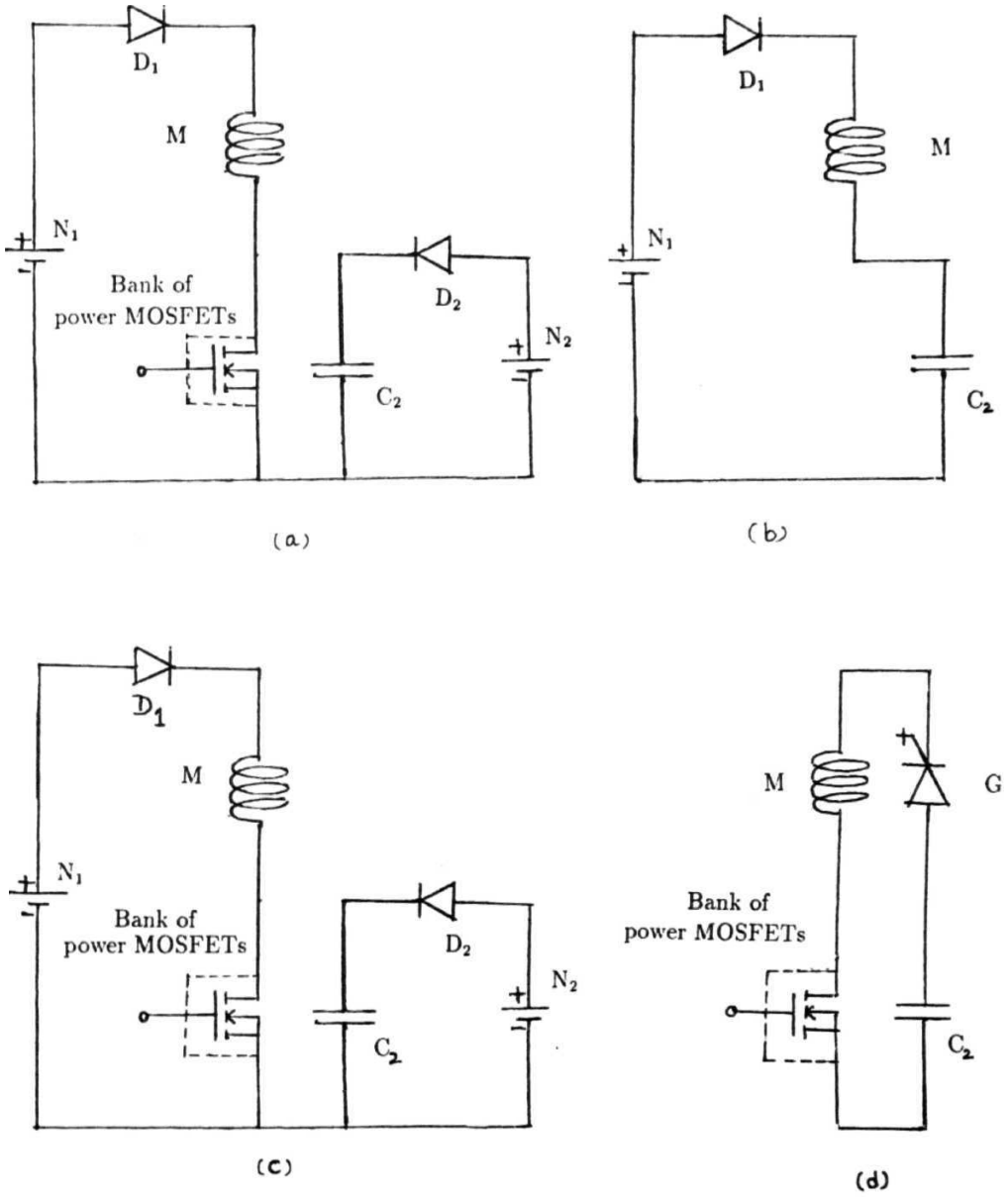

Fig. 2.19 Current paths during different field levels and transits.

(a) High field (**Polarization** and detection field)

(b) Transit high to low

(c) Low field (Evolution field)

(d) Transit low to **high.**

the GTO thyristor *G* (by applying suitable pulses to its gate). The current through the coil, thus increases from the low value to that corresponding to the detection field (Fig. 2.19d).

5. Finally, when the detection field is reached, the GTO is swithced OFF (by applying a suitable pulse at its gate) and the MOSFET transistors are switched ON to regulate the field, resulting in the initial condition. In the present case, the operation is simplified by making the polarization and detection field levels equal. This cycle is repeated at regular intervals depending on the relaxation times of the system under investigation. The details of the control circuit using MOSFETs, the switching circuit using GTO and the current regulating circuit are given below.

Control circuit

If the maximum and minimum realizable Larmor frequencies i.e., polarization (or detection) and evolution fields are to be achieved with the same control circuit, a regulation of more than 1 in 10^5 is required. In other words, if a stable magnetic field (either high or low) is to be achieved as soon as the cycling is done, the voltage levels to be applied to the gates of the MOSFET's during the different phases of the cylcle are to be very stable. A drift free and modulation free regulation circuit serves the purpose (Schweikert, 1990). The block diagram of the control circuit is given in Fig. 2.20. In the present case, a fast, noiseless operational amplifier (OP27) which results in a minimum offset voltage of $1\mu V$ and a drift of 0.01 μV/degree is used to achieve high current stability and fast response times.

The input current levels to the control circuit are obtained through a stable 1.5 V dry cell. To facilitate a variation in the input level, the output from the dry cell is given through a variable resistor. Any fluctuations or variations in the coil current are to be fed back to the controller in the right sense (opposite sign, in the present case) with respect to the reference, so that the variations are annuled, resulting in a stable signal at the output of the control circuit. The feedback input to the controller is given from a measuring resistor R_{mes}, which is in the path of the coil current, and is sensitive to the changes in the coil current. The most important part of the

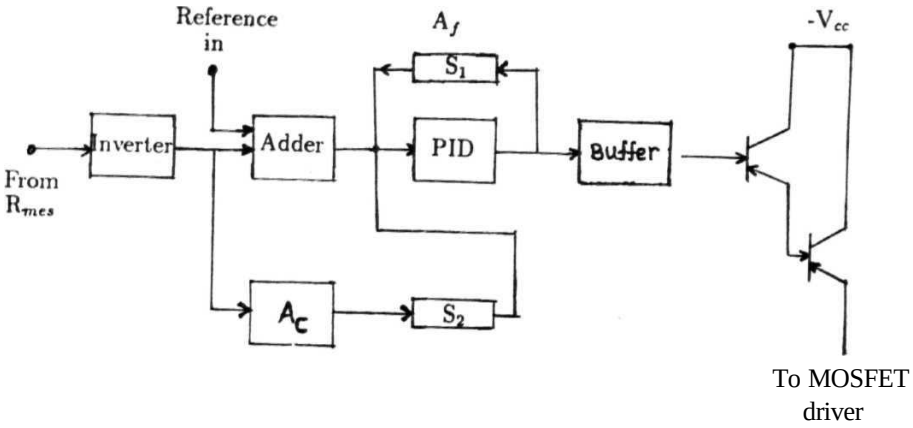

Fig. 2.20 Block diagram of the control circuit

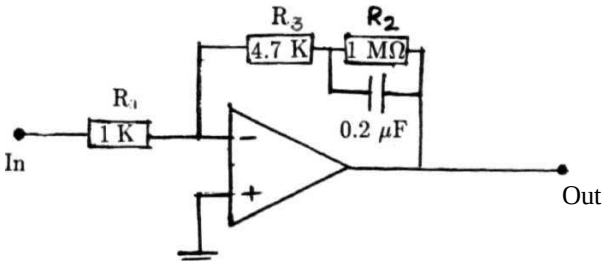

Fig. 2.21 Pole zero pair amplifier

controller circuit is a pole zero pair amplifier circuit (Fig. 2.21). The typical response characteristics of the pole zero circuit are shown in Fig. 2.22. The low frequency part I_1 is responsible for the stability with the drift compensated input. The second part I_2 coupled with the high frequency region adjusts the control parameter to a high frequency limit. The third part p allows the controller to work in the proportional region (regulation). The pole and the zero of the circuit are given by

$$f_p = -\frac{1}{R_2 C_2} \tag{2.26a}$$

$$f_z = \frac{R_3 R_2 C_2}{R_3 + R_2} \tag{2.266}$$

The dc gain of this amplifier is given by

$$A_o = \frac{R_2 + R_3}{R_1} \tag{2.26c}$$

In the present case, the gain is chosen to be 1000. The pole and zero of the circuit are adjusted by trial and error method to obtain high stability during the polarization and detection periods (f_p = 5 Hz and $f_z \backsimeq$ 1 kHz).

The input current levels corresponding to the different evolution periods are obtained from a pulse programmer, which provides the control signal for the cycles, the driving signal for the *rf* pulses, triggering pulse for the recording of the relaxation time measurements and finally a trigger pulse to two switches during the transits.

However, due to the finite time constant of the pole zero circuit, the change of the current from one value to the other (switching) results in overmodulation of the current level. In other words, a completely false output signal results before the current stabilizes at the required new value (Fig. 2.23). Due to this overmodulation, the voltage at the gates of the MOSFET's has the correct value only after a time $t = t_o + t_s$. In an FC experiment, where the field is periodically varied, correction of such periodic over modulations is compulsory to obtain stable currents through the magnet.

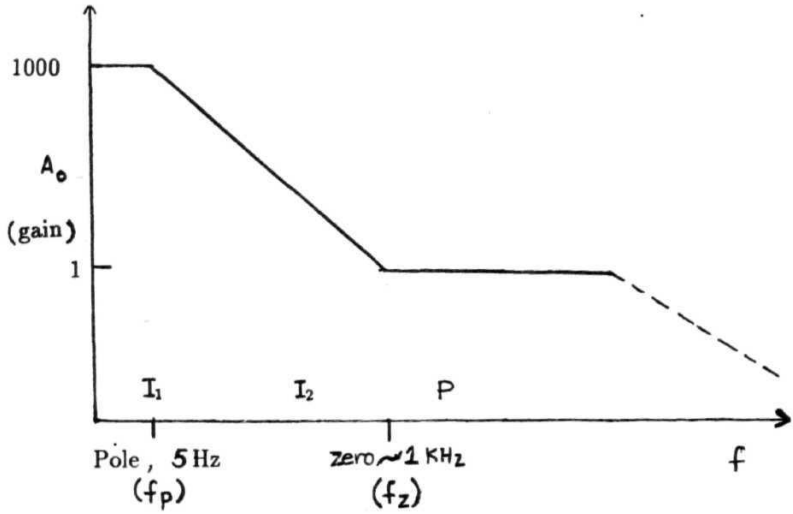

Fig. 2.22 Frequency characteristics of Pole zero pair amplifier

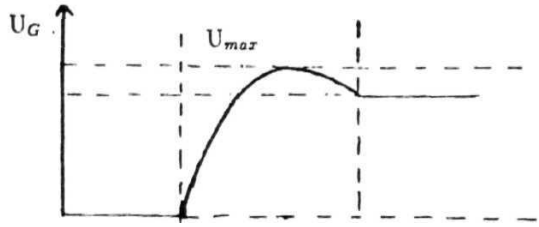

(a)

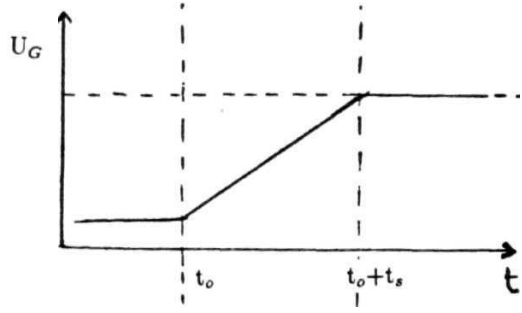

(b)

Fig. 2.23a Over modulation of the MOSFET gate voltage due to finite time constant of the Pole. zero pour amplifier.

Fig. 2.23b MOSFET gate voltage & Magnet current after overmodulation correction

A simple but logical option to correct the overmodulated voltage at the MOSFET gate is to disable the pole zero amplifier during the transits. This is acheived by enabling a strong negative feedback arm A_f (by switching ON the electronic switch S_1 in Fig. 2.20). This reduces the gain of the pole zero amplifier drastically during the transits (resulting in a simple inverter). However, this leads to a change of input voltage and hence the output voltage. Thus this voltage has to be compensated to obtain the required evolution field. This is done by enabling the compensating arm A_c by switching ON the electronic switch S_2 in Fig. 2.20. The compensating signal is obtained through an oppositely directed feedback signal from R_{mes} and amplified appropriately. The compensating amplifier C_A has a variable gain in. order to vary the evoltuion field. Two n-channel MOSFET's (IBRFPG40) are used for the switching purposes in Fig. 2.24. The required pulses to the gates of the switches are obtained from the pulse programmer described in section 2.2.3 (Fig. 2.24). Thus the circuit works as a simple proportional amplifier with a strong negative feedback during the transits and the evoltuion period. However is acts like a full fledged pole zero circuit resulting in a stable output signal immediately after the field is changed to the detection level.

After the turn ON i.e., in the detection period, the switches S_1 and S_2 are open and the circuit now works as a controller with good stability. The pulses with variable levels from the pole zero amplifier are buffered before being fed to the gates of the controlling MOSFET's. The Darlington pair (Fig. 2.20) provides enough current to drive the large number of MOSFETs.

With **the** correction for overmodulation and reduction in the turn ON time due to the induction of the magnet, the other possible sources for the drift of the magnetic field are the oscillations of the magnetic coils due to the vibrations of the cooling arrangement around the coil and fluctuations in the temperature of the coil due to the main current. These deviations can be corrected by correcting the coil current, the required signal being obtained from the temperature measurement system of the magnet. In the present arrangement, the drift due to these two sources is found to be negligible and hence no such precautions are needed. It is found that the magnetic field has high stability of 1 in 10^5 in an hour.

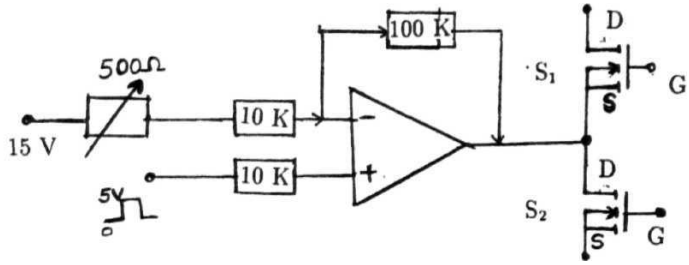

Fig. 2.24 Configurations of the switches S_1 and S_2(MOSFET's) to compensate the overmodulation.

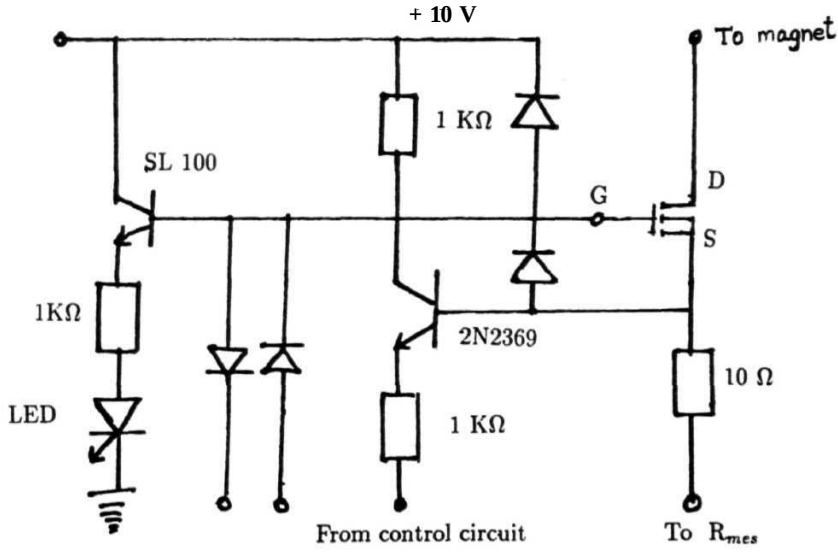

Fig. 2.25 MOSFET gate driver

The power MOSFETs used in the circuit are solid state devices, the current through them being controlled by applying appropriate signals at the gates. The constant current characteristics of the MOSFET is used in regulating the current. However the MOSFET has to withstand the large amounts of current during the cycle, and hence a large number of them (in the present case 20 are found to be adequate) are connected in parallel. Unless the cutoff frequencies and input capacities of all the MOSFETS match, they tend towards oscillations during the transits. This complication due to the parallel connection can be eliminated by decoupling the individual gates and is acheived by driving each MOSFET independently using a seperate driver circuit (Fig. 2.25). This arrangement of gate driver circuit partially linearizes the voltage-current characteristics. The LEDs in each of the gate driver help in visualising the function of each gate driver and hence any problem in the MOSFET circuit can be localized and detected easily.

Since the feedback signal to the controller is given from the measuring resistor, it is necessary that the resistor measures the current through the magnet without any error. Several positions can be chosen in the circuit for placing R_{mes} (Fig. 2.26) depending on the relative merits and demerits. Positions *a* and 6 do not hold the ON, OFF current correctly and are at a high variable potential to the ground. Hence a direct and precise transmission of the signal to the control circuit is not possible. Positions *c* and *d* are directly in the magnet power supply lines and hence measure the current without any error but they are at a higher potential with respect to the ground. The positions e. and / are at easily operating positions but at e, the driving current for the MOSFET driver falsifies the data apart from improper OFF current measurement. Hence the position e has the most favorable characteristics and is chosen for positioning the measuring resistor. This circuit is modifed slightly to hold the input current properly (Fig. 2.17).

The choice of the value of R_{mes} is also very critical. On one hand, it must be large enough so that the voltage drop from the control signal is large enough (i.e., even minute changes in the control signal should result in perceptible voltage drop across R_{mes} for better resolution). On the other hand, R_{mes} should be small enough so that the power loss and hence the heat dissipated should be small to ensure a stable

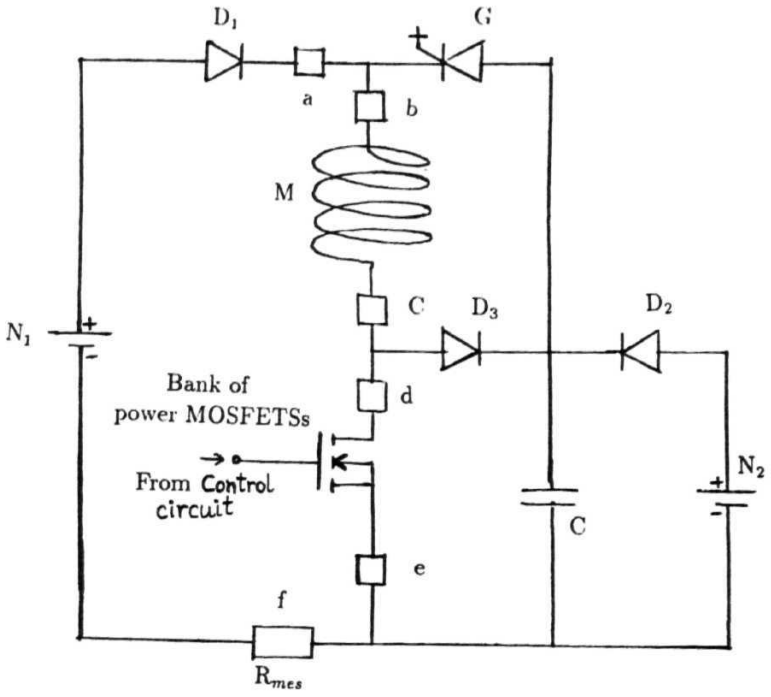

Fig. 2.26 Several possible positions for the measuring resistor (R_{mes})

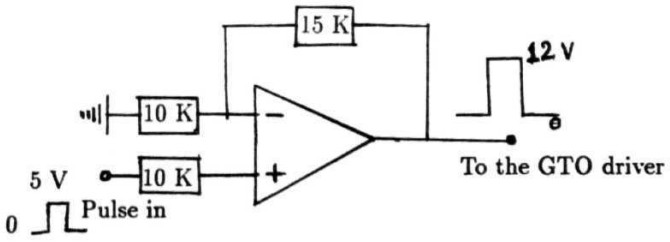

Fig. 2.2.7 Pulses to the **GTO** driver.

operation. In the present case, 150 mΩ resistor satisfies the above requirements since it results in a maximum voltage drop of ~1V (corresponding to the polarization and the detection period) and a maximum power dissipation of only 7 Watts across R_{mes}

Switching circuit

Apart from the overmodulation correction, the turn ON time of the magnet, as explained earlier can be reduced by increasing the voltage at the coil (by the use of energy storage capacitor) through the switching of a GTO thyristor. The details of this switching circuit are given below.

The GTO thyristor used to impress high voltages across the magnet during turn ON period is Model No. 358RGA100 of Nihon interelect. corpn. . Unlike in ordinary thyristors, which can be triggered ON with the help of a signal at the gate but can be switched OFF only by breaking the anode circuit, a GTO can be controlled through a trigger pulse given at the gate. The trigger and quenching pulses needed for the control of the thyristor are obtained through a commercial gate driving circuit GK2AN. The input pulses to this gate driver are obtained from the pulse programmer (Fig. 2.27). The GTO is protected from the dangerous high voltages developed during switch OFF and switch ON through the use of an external protection circuit shown in Fig. 2.18 (Snubber network). The values of the components in this circuit are R = 5Ω ; C = 0.3 μF. The diode used in the snubber network is 20MLA with 0.1 μF capacitor connected across it.

Due to the large voltages developed and high currents flowing in the circuit, a large power is dissipated in different parts of the circuit and hence necessitates cooling arrangements. The MOSFETs, GTO thyristor, free wheel diode, decoupling diodes and the measuring resistor, *Rmes* are mounted on a thick aluminium sheet cooled by circulating chilled water.

2.2.3 3.5 MHz Pulsed NMR Spectrometer

The details of the fixed frequency (3.5 MHz) spectrometer **fabricated as part of the FCNMR** spectrometer is described **in** this section. The block **diagram of the spectrometer is given in Fig. 2.28. It** consists of (1) a **transmitter (2) a matching network**

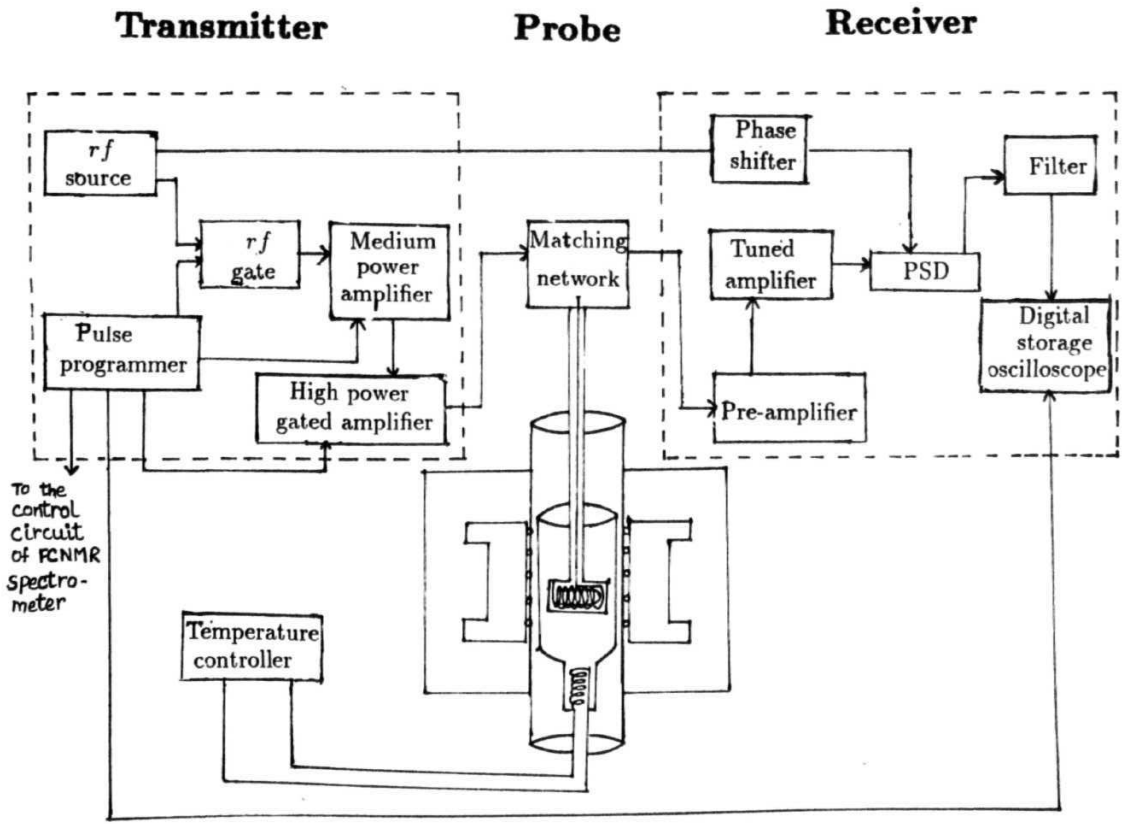

Fig. 2.28 Block diagram of the pulsed NMR spectrometer

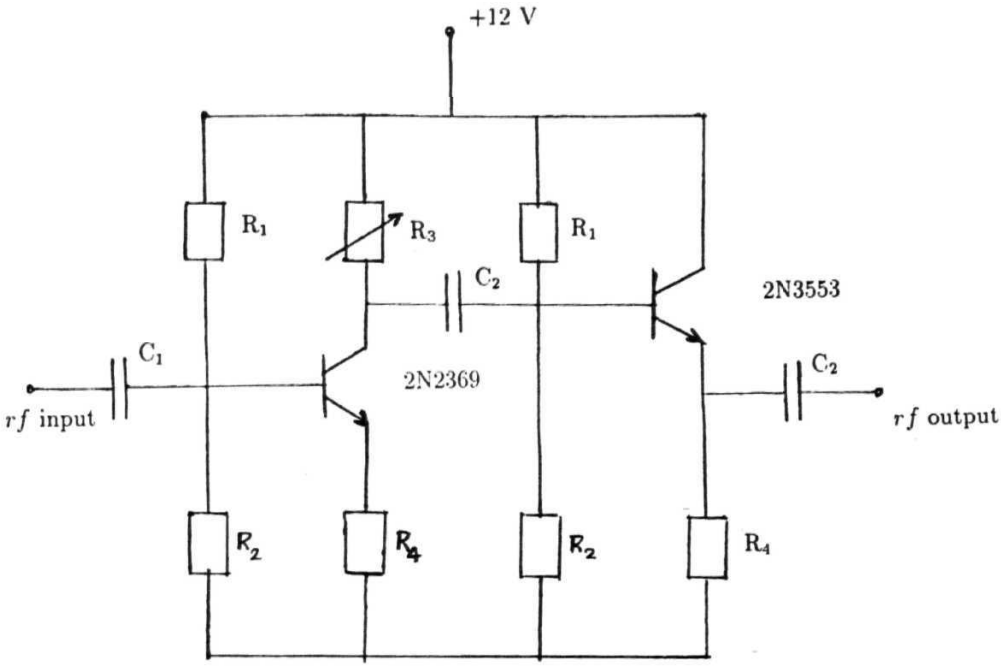

Fig. 2.29 *rf* amplifier using *2N2369*

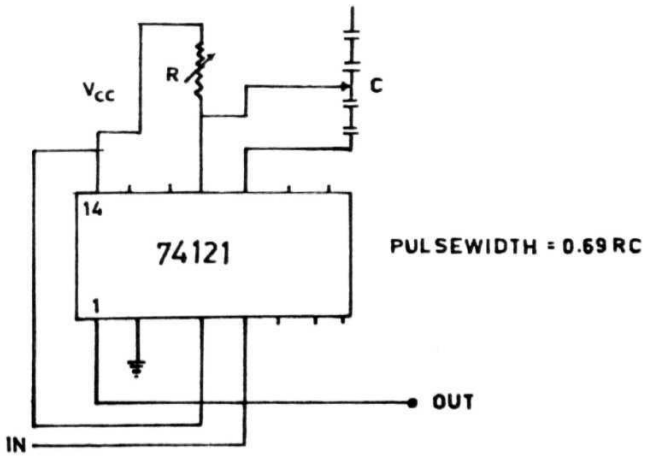

Fig. 2.30 Pulse generator using *IC74121*

(probe) and (3) a receiver. The ideal requirements of these three parts with their subunits is described below. The transmitter should be capable of providing strong *rf* pulses (typically in the range of a few hundreds of watts with sharp rising and falling edges) of short duration (1-100 μsec). The ON/OFF ratio of the *rf* pulses should be very large so as to ensure that there is no leakage of *rf* voltage into the receiver during the transmitter OFF time. The *rf* field (H_1) provided by the transmitter should be as homogeneous as possible over the sample volume. The power from the transmitter should be efficiently transferred to the system (sample coil) by an impedance matching network. This matching network along with the sample coil is termed as the probe.

The signal induced in the sample coil after the transmitter pulse is very small (typically in μV), and hence it should be amplified by the reciever to a few hundreds of times, and then demodulated to recover the decaying pattern. Apart from this, the reciever should be capable of withstanding overload voltages and also recover fast from these overload voltages (due to leakages during pulse ON periods). The recovery time (dead time) of the receiver (from overloading) should be as small as possible to ensure that the signal is not lost during the dead time of the receiver. Also the reciever should be capable of detecting only the carrier wave in order to increase the signal strength. The various units mentioned above are described in detail below.

Transmitter

The transmitter essentially consists of an *rf* source, a pulse programmer capable of generating the required pulse sequences, a pulsed *rf* mixer, a medium power amplifier and a gated high power amplifier.

rf source

The *rf* source used is a commercial unit (Kikusui, Model No. 4100) capable of generating *rf* of high spectral purity from 0.1 kHz to 110 MHz with a stability of about 1 in 10^9 s. This is further amplified using 2N2369 transistors to a required level of about *3V* peak to peak (Fig. 2.29). The *rf* thus obtained is power divided into two parts, the first part is used for pulse modulation and the other is used as reference (through a phase shifter) for the phase sensitive detector.

Pulse programmer

The required pulses and the pulse sequence for the field switching with necessary delays are obtained through a commercial four channel digital delay generator DG (EG&G make, Model No. 9650) and a home made pulse generator. IC74121 (Fig. 2.30) is used to obtain the *rf* pulse, which is triggered by DG. Pulse outputs are also available for triggering the oscilloscope and the gated high power amplifier. Complicated *rf* pulse sequences (for example two pulse or three pulse sequences) can also be generated using a combination of home made pulse generators and delay generators as explained latter (Fig. 2.42 and Fig. 2.43).

rf gate

The pulse modulation of *rf* is achieved using a quad two input NAND gate ($74LS00$) connected as shown in Fig. 2.31, with a good *rf* suppression ratio ($> 100dB$) during the OFF time of the pulse. The rise and fall times obtained are very sharp (10 nsec typically). The *rf* suppression during the pulse OFF periods can be further improved by increasing the number of gates.

Medium rf power amplifier

The fluctuation spectrum of the different mechanisms mediated through the dipolar interaction in solids results in considerable increase of line width and hence results in very short FIDs. As explained earlier, the inhomogeneity in the Zeeman magnetic field leads to a further shortening of T_2 to T_2^*. In order to excite all the spins equally in such a broadened spectrum, the pulse width should be as small as possible. Normally pulsed *rf* in the range of a few *KW* is needed to get a $\pi/2$ pulse width of about 2-3 μsec for proton. This is achieved in two stages. The gated *rf* obtained from the NAND gates is amplified to 20 Vpp using a gated medium power amplifier which subsequently is used to drive a gated high power amplifier to get the required pulsed *rf* power.

The medium power amplifier is built using a power transistor 2N3553 (Shenoy, 1978) (Fig. 2.31). The - 5 Vdc and the TTL pulses at the base of the transistor provide the necessary biasing and ensure that the transistor is OFF during the pulse OFF period. On the other hand, during the pulse ON period, the transistor is forward

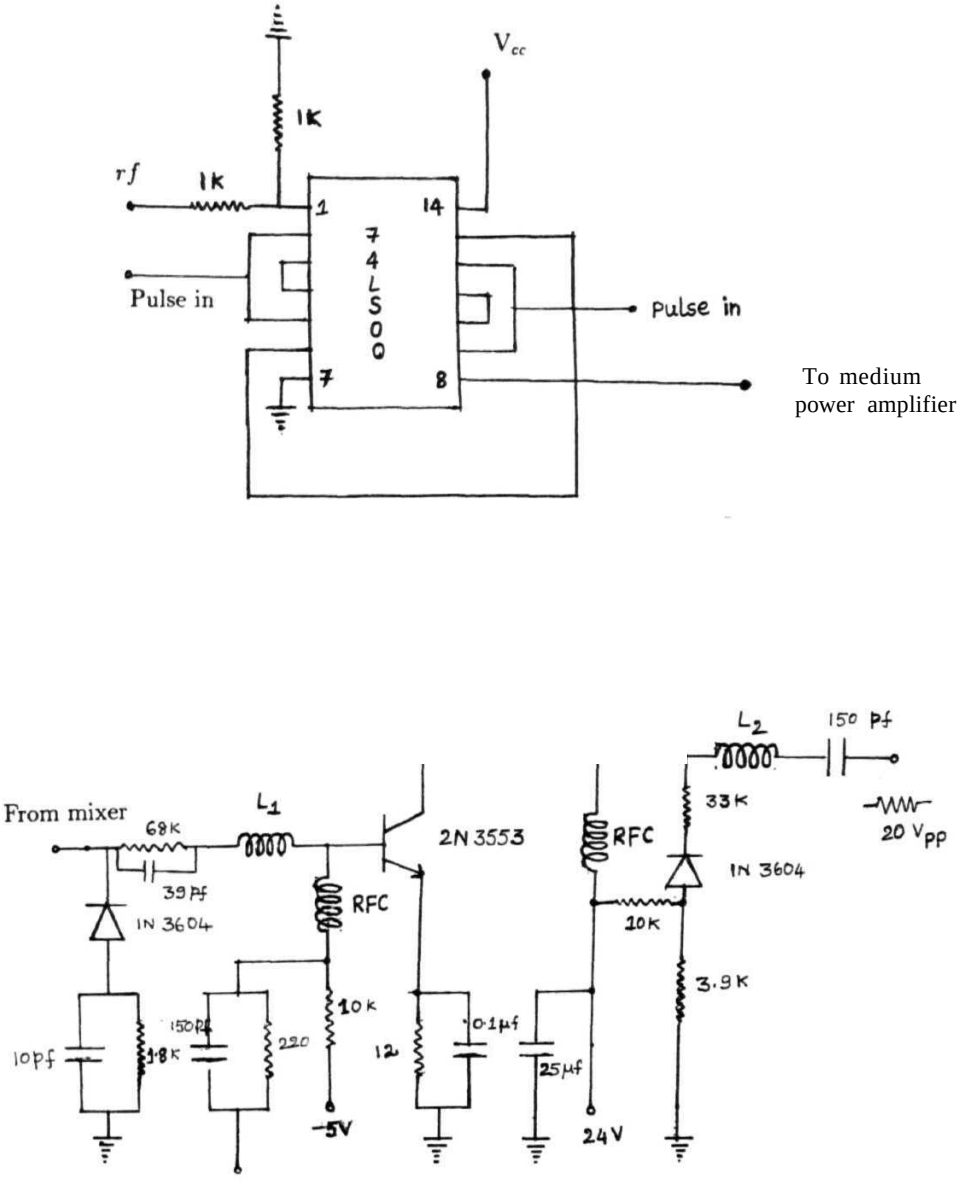

Fig. 2.31 Mixer or *rf* gate and medium power amplifier.

biased, thereby forcing the input pulsed *rf* to be amplified by β = 10 times the input current. The additional gating provided by the pulses synchronous with the pulsed r/, further suppresses the *rf* leakage during the OFF period. The inductors L_1 and L_2 are adjusted to match the input and output impedances to the previous and following stages respectively. The *rf* chokes are adjusted to obtain the necessary gain during the ON period. A peak voltage of 20V is obtained at the output of this medium power amplifier (typical input of about 200 mV of pulsed *rf).*

Gated rf high power amplifier

This amplifier is constructed using 3E29 dual tetrode tubes operating in push pull configuration (Lowe and Tarr, 1968) and is gated with a 0 to - 150 V pulse amplifier. The 0 to - 150 V synchronous, gating pulses and the input pulsed rf are given to the tubes through a wide band input transformer (model NH0900B of North Hills make). This is capable of amplifying pulsed *rf* with negligible rise and fall times, the 3 dB bandwidth being 5 to 30 MHz. The rise and fall times of the final pulsed *rf* from the power amplifier are determined by the rise and fall times of the grid pulses (typically < 50 nsec). The circuits of the gated pulse amplifier and the tube amplifier (Fig. 2.32) are discussed individually below.

High power amplification and good ON/OFF ratio is accomplished by biasing the grids of the dual tetrodes with 0 V during pulse ON period and —150V during the pulse OFF period. The working of the pulse amplifier can be understood as follows. During the pulse OFF period, the transistor T_1 is OFF, resulting in -150V at the bases of T_2, T_3 and T_4. Since both the pnp transistors T_2 and T_3 are conducting and the npn transistor, T_4 is not conducting, -150V appears at the grids of the tubes. Thus, during the pulse OFF period, no amplification is done resulting in an improved ON/OFF ratio. During the pulse ON period, T_1 conducts making the voltage at the base of T_2, T_3 and T_4 0 V from -150 V. Thus T_2 and T_3 are OFF and T_4 is ON resulting in 0V at the grids of the tubes. The output of the amplifier is taken through another wide band transformer (North Hills NH1703BA). Since the plates of the tetrodes are at about 800V, very high amplification ($\sim$ 10) of the input pulsed *rf* is achieved during the pulse ON period.

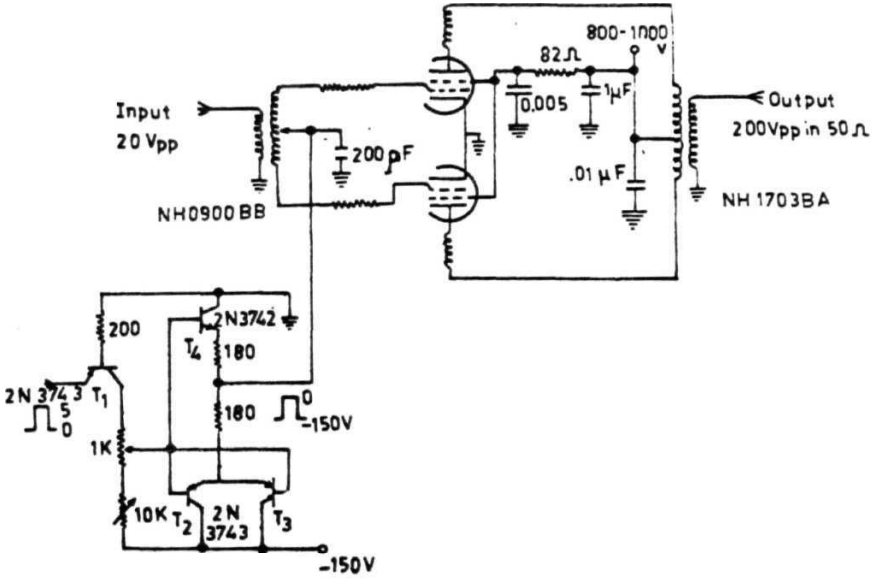

Fig. 2.32 High power gated amplifier.

Matching network

The most important part of a pulsed NMR spectrometer is the coupling system (probe) which couples the power from the transmitter to the sample coil during pulse ON period and converts the precession magnetization into a detectable signal at the input of the receiver immediately following the pulse. The matching network should be capable of coupling the sample coil to the transmitter during pulse ON period and should also couple the sample coil to the reciever during the pulse OFF period. It should also decouple the reciever from the transmitter during the pulse ON period. The important considerations during the construction of the probe are given below. The size of H_1 and hence the $\pi/2$ pulse width is determined by the transmitter coil and the final *S/N* ratio is determined by the sensitivity of the receiver coil. One crucial factor in the design of the size of the sample is that since $H_1 \propto (V)^{-1/2}$, where *V* is the effective volume of the sample, a probe built for a larger sample will have smaller H_1 for the same power. Also since signal to noise ratio *(S/N)* $\propto (f)^{1/2}$, where / is the filling factor of the coil, it is necessary that the probe should have a filling factor close to unity. Finally, the receiver coil in the probe should not give rise to spurious signals (for example, from the mechanical oscillations of the inadequately secured *rf* coil or generation of acoustic waves and signals which interfere with the actual signal).

The above factors can be satisfied by using tunable circuits consisting of LCR networks. Either crossed coil method (Bloch et al., 1946), where separate transmitter and receiver coils are used or single coil method (Clark and McNeil, 1973 ; Ailion, 19S3), where a single coil is used for both the transmitter and the receiver can be used for this purpose. The single coil arrangement is simpler and has advantages over the crossed coil probe, like, the coil can be tightly wound around the sample and hence has maximum power efficiency. Since the coil is common to both the transmitter and the receiver, care should be taken to protect the receiver from leakage of *rf* pulses from the transmitter, i.e., the probe should isolate the receiver from the transmitter. This can be achieved by using crossed diodes and A/4 transmission lines which appear as short circuit to high voltages and open circuit to the small signals.

Two matching circuits available in the literature are used in the present studies and their relative merits are discussed below. Both the circuits are single coil circuits which are easier to handle and also efficient compared to the crossed coil probe as explained earlier.

Series *resonant circuit*

This matching network (Clark and McNeil, 1973) consists of three resonant circuits ; L_1C_1, L_2C_2 and L_3C_3, each tuned independently at the Larmor frequency (Fig. 2.33). The crossed diodes (D_1) at the input act as a short circuit to the high power *rf* pulses (during pulse ON period) and as a open circuit to the small signal voltages (during pulse OFF period). The series combination, L_2C_2 represents a low impedance path in parallel with that of *L3C3* so that the entire transmitter voltage is dropped across L_2 and very little voltage is fed into the receiver during the pulse ON period. Also, since the diode pair (D_2) represents short circuit to ground, voltage at *E* is dropped across L_3 before reaching the receiver. After the transmitter pulse, the diode pair D_1 effectively disconnects it from *E* and D_2 acts as an open circuit to the low voltage induced resonant signals, thereby forcing the signal into the receiver through *L3C3.* Hence, L_2C_2 and *L3C3* represent a composite series circuit tuned at the Larmor frequency. The FID is received at F (a high impedance point to ground). The tuned input receiver circuit *{L3C3)* provides good coupling of L_2 to the receiver and hence increases the 5/N. Thus the circuit ensures an efficient transfer of power from the transmitter to the sample coil and also good protection of the receiver from destructive overloads.

Tuning

The three resonant circuits are to be tuned independently such that maximum transmitter power is transferred to the sample coil. The tuning should also ensure a good coupling between the sample coil and receiver. This is achieved using the following procedure.

1. Initially, the switch S_1 is closed and L_1C_1 is tuned to maximize the amplitude of the pulsed *rf* at A by tuning *C*\.

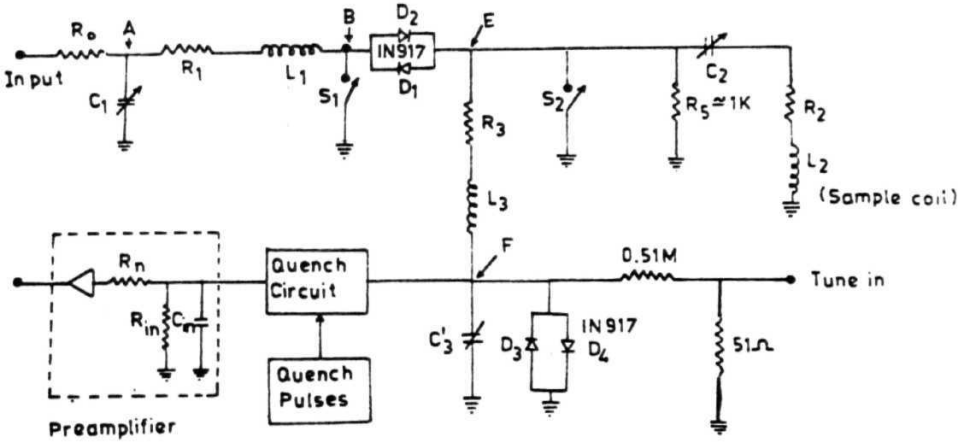

Fig. 2.33 Series resonant matching network.

2. The pair L_3C_3 is tuned by closing S_2 and giving a low level *rf* at the tune input and then maximizing the voltage at *F* by tuning C_3.

3. Finally, the tank circuit L_2C_2 is tuned by opening the switches S_1 and S_2. The pulsed *rf* from the transmitter is given at the input and the voltage across L_2 is maximized by tuning C_2. However, some final adjustments are to be made by observing the signal to optimize the pulse width and signal strength.

The values of the different components and capacitors are chosen following the procedure of Clark and McNeil (1973). Typical values of the various components at 3.5 MHz for R_o = 50ft (the output impedance of the circuit) are $L_1 = L_3 = 0.45\mu H$; $L_2 = 0.9\mu$H. A sample coil of radius $1cm$ with 17 turns is found to be the proper choice for optimum signal strength. The major precaution to be taken in the process of designing the probe is to avoid using cables of A/4 length or its multiples from the transmitter to the sample coil since they act as open circuit to the high powered transmitter pulses at the designed frequency. The bandwidth of this circuit is about 2 MHz.

Parallel resonant circuit :

The second circuit (Ailion, 1983), given in Fig. 2.34, consists of a single resonant tank circuit *(L\C\),* in series with a capacitor C_2. The crossed diodes at the input of the circuit allow the high power *rf* voltages to pass through the sample coil, while acting as open circuit to the small signals induced in the coil. The diodes at the output of the circuit allow any *rf* power leaked into the ground, thus protecting the receiver from the *rf* pulses, while acting as open circuit to the small NMR signals thereby forcing them to go entirely into the receiver. These crossed diodes also remove low level noise and other transients originating in the transmitter and hence improve the *S/N* ratio of the system. In addition, presence of quarter wave network before the diode pair offers a high impedance for transmitter pulses thus protecting the receiver from overload further. The input and output impedances of the tuned coil is chosen to be equal to 50ft. C_2 is chosen to be as small as possible in order to minimize the degradation of *L/C* ratio and in turn the quality factor *Q* of the circuit. The conditions for tuning the **circulit** are given by

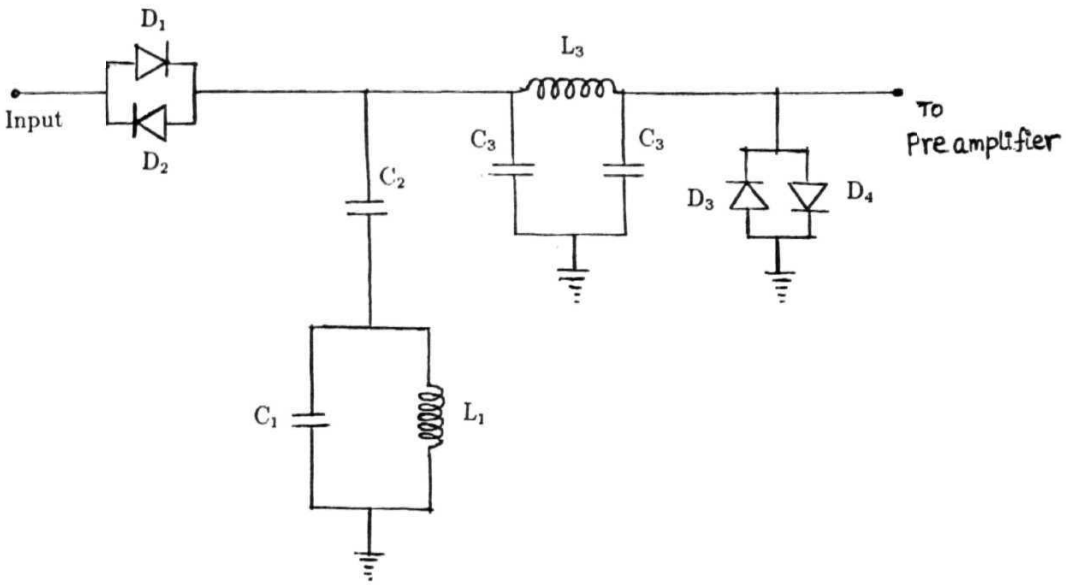

Fig. 2.34 Parallel resonant matching network.

$$\omega(C_1 + C_2) = \omega L \quad \textbf{(2.27a)}$$

$$C_2 = (RQ\omega^3 L)^{-1/2} \quad \textbf{(2.276)}$$

$$L_3\omega = 1/C_3\omega = 50\Omega \quad \textbf{(2.27c)}$$

Here Q is the quality factor of the coil which is made as large as possible to optimize S/N ratio and power transfer efficiency. On the other hand very large Q would result in a long ringing time and hence a long system recovery time of the receiver, following the turn OFF of the rf. Hence for broad signals, it is advantageous to reduce Q at the cost of a lower S/N ratio. L is determined from eqn. (2.27b) and C_1 from eqn. (2.27a). Typical values of the components at 3.5 MHz are Q = 100, C_2 = 150p/, C_1 - 900p/, the coil L_1 has 21 turns with an inductance of 2.3 μH, C_3 = 900p/ and finally the coil L_3 has 21 turns with an inductance of μH.

Tuning

The tuning of the circuit is done by tuning the tank circuit for maximum power at the coil. Fine tuning can be done further by observing the ringing pattern after the pulse. The Q of the circuit is optimized to reduce the ringing time sufficiently. The A/4 circuit acts as an impedance transformer network. When shorted at one end, the A/4 line transmits the low voltage signals at the designed frequency and hence attenuate all other frequencies (equivalent to a selective filter). In the present case this line consists of an inductor, L_3 and two capacitors, C_3 (connected as a π section) wherein the active elements are chosen to offer an impedance of 50 Ohms (as in eqn. (2.27c)) at the designed frequency i.e., $L_3\omega = 1/C_3\omega = 50\Omega$. The signal strength is maximized at each frequency by tuning the capacitors C_3. The tuning of this probe is relatively easier compared to the Clark's circuit since there is only a single capacitor to be tuned. Also for a given geometry of the sample coil, the parallel resonant probe offers a much higher Q and hence better sensitivity. However the high Q of the parallel resonance circuit results in an increase in the recovery time of the reciever and hence it is advantageous to use Clark's probe for broad signals (and hence short FID's).

Receiver

The reciever consists of a fast recovery preamplifier, a tuned amplifier, a phase sensitive detector, a filter and finally a signal averager for signal acquisition and averaging purposes. The details of these subunits are given below.

Fast recovery pre-amplifier :

The NMR signal from the probe is very weak (typically a few μV) and hence has to be amplified by a few orders of magnitude before detection. Hence the reciever should have a gain of about 10^5. But, despite the many precautions taken, the receiver is always overloaded by the large *rf* pulses from the transmitter resulting in two problems, the dead time of the receiver and the baseline shift after the detection due to asymmetry of saturation together with *ac* coupling. A fast recovery pre-amplifier (Ramadan et al., 1974) is used to overcome these problems.

The amplifier (Fig. 2.35) possesses high sensitivity and short recovery time besides a large band width. The diodes D_1 and D_2 protect the input of the receiver from large *rf* pulses. Diodes D_3 and D_4 in the feed back circuit limit the high voltage *rf* pulses to the reciever to approximately $\pm 0.5V$. The *dc* level of the feedback circuit is adjusted by a variable resistor R_1 such that the positive and negative limit of the *rf* pulses are symmetric about the baseline. The amplifier has a gain of 10 and a bandwidth from 1 kHz to 15 MHz. The recovery of the system is about $5\mu S$ with this amplifier.

MOSFET tuned amplifier :

The signal from the pre-amplifier is further amplified using a low distortion and a stable gain MOSFET amplifier which is stagger tuned (Landee et al. 1957) around the Larmor frequency, ω_o. The amplifier consists of three identical stages followed by a source follower (Fig. 2.36). The first three stages are made of *n*-channel insulated gate FET with a gain of 20 dB each. A source follower using a JFET after the third stage provides the impedance matching and the final output is taken through a broadband transformer (North Hlls 0900BB). The high input impedance of the MOSFETs ensures a low noise figure and negligibly small distortions of the amplified signal. In the stagger tuned mode the last stage is tuned to the frequency f_o whereas

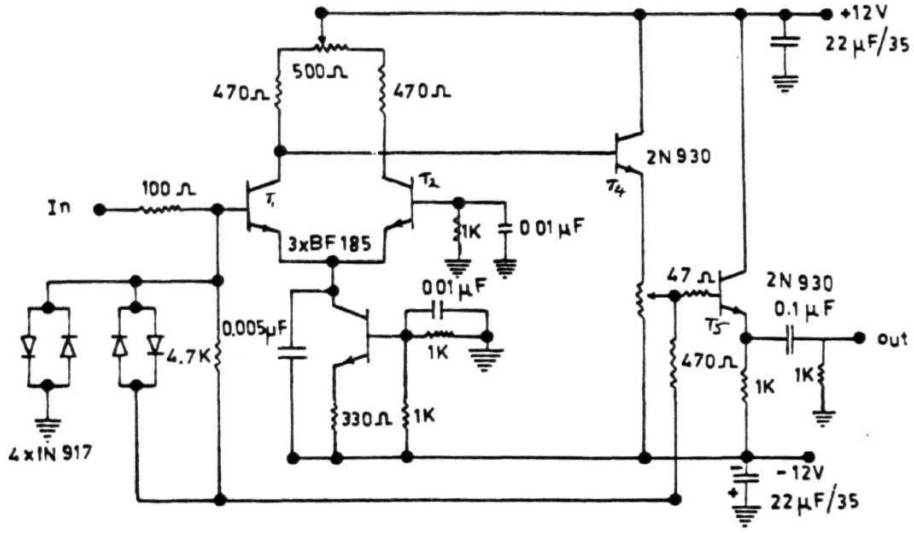

Fig. 2.35 Fast recovery pre-amplifier.

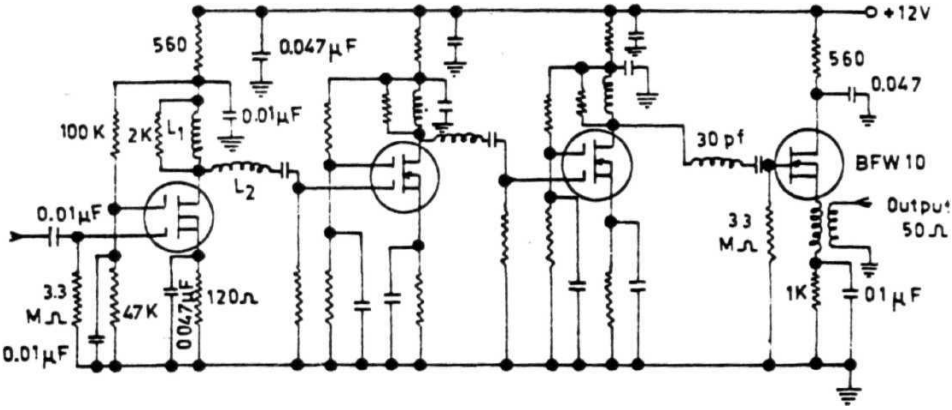

Fig. 2.36 MOSFET tuned amplifier.

the first two stages are detuned symmetrically on either side of f_o. The staggered tuning is done to achieve a band width of 2 MHz so as to allow the FID signals of short duration. The *Q* value of the last stage is chosen to be equal to half of that of the symmetrically detuned stages. The interstage coupling is done using series tuned *LC* circuits between each stage which effectively block out any low frequency transient and allow the *rf* signal without any attenuation.

Phase sensitive detector and phase shifter :

The signal from the probe often consists of all frequency components, apart from the frequency of interest, and hence has to be demodulated before signal averaging. This can be done either using diode detection or phase sensitive detection. A phase sensitive detector (PSD) has many advantages over a diode detector. A PSD has a smaller bandwidth than a diode detector and hence a better *S/N* ratio (Farrar and Becker, 1971). Since PSD is sensitive to the phase of the signal, the phase information is retained. Finally, it discriminates heavily against signals which do not have the same phase as the reference signal and hence can be used in signal averaging experiments when the *S/N* ratio is larger than one (Stejskal, 1963).

The phase sensitive detector used in the present case is a double balanced mixer (Hewlett Packard make, model 10534A). The signal (of frequency /) is applied at the LO port while the reference (of frequency f_o) is fed into the *rf* port (Fig. 2.37). The detected output which is proportional to $(f_o + /)$ and the difference of the frequencies of two inputs $(f_o — /)$ is taken out from the IF port. Thus when the frequency of the reference is same as the signal, an output corresponding to zero (i.e., *dc)* is obtained. The signal strength is further maximized by adjusting the phase difference between the two inputs.

If the reference signal given at the *rf* port is $A_1 \mathrm{Sin}\omega t$ and the signal at LO port, $A_2\mathrm{Sin}(\omega t + \phi)$, ϕ being the difference in phase between the two inputs, then the output signal at the IF port is $A_1A_2\mathrm{Cos}\phi$. When the phase difference is zero, maximum output will be obtained. The reference signal is given from the *rf* source through an adjustable phase shifter for maximising the signal strength. An electronically tunable phase shifter (Merrimac make) is ued for this purpose, where the phase of the output

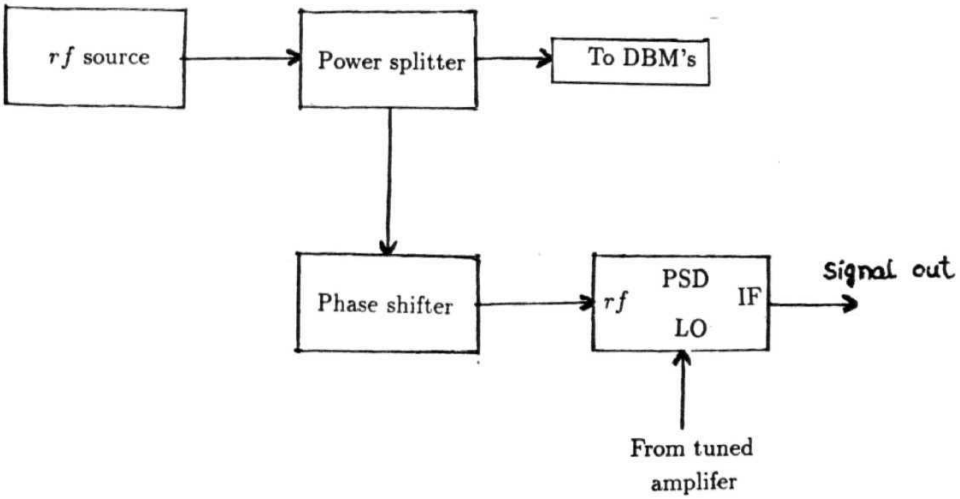

Fig. 2.37 Arrangement of phase sensitive detector with the phase shifter.

with respect to the input can be varied from 0 - 2π by using a variable dc voltage from 0 to 30 V. The arrangement of the PSD along with the phase shifter is given in Fig. 2.37.

Filter and signal averager :

The detected output signal has along with the dc, a component at $2f_0$ and other noise components which can be filtered using a low pass (< 2 MHz) filter made using *RC* network. The filtered output is then given to a digital storage oscilloscope (Tektronix 2230) for signal averaging purposes.

Temperature controller :

A home built, temperature controller is used for temperature variation measurements covering all the mesophases. The details of this temperature controller (Chiu et al., 1979) which works in the range of 85 to 400 K with a stability of 0.1 K (Fig. 2.46) are given in section 2.3.

Various subunits of the spectrometer described above require different regulated power supplies, which are home built through the use of bridge rectifier, filter and three pin regulator (78*XX* series for positive and 79*XX* series for negative supplies). The pulsed *rf* spectrometer built thus is standardized at 3.5 MHz by observing the Nitrogen NQR signal from $NaNO_2$ with a typical unaveraged *S/N* of about 3 to 4 and a 7r/2 pulse width of about 10μsec. This *rf* spectrometer is to be coupled with the magnet so that the field switching and the *rf* pulses are synchronised.

2.2.4 Synchronization of FC magnet and *rf* spectrometer

The switching cycle for the solenoid magnet and *rf* pulses in the 3.5 MHz spectometer are to be synchronised in order to perform the NMR relaxation time measurements (the methodology involved is discussed in section 2.2.6). The typical timing diagram of input pulses to the different components in the controller circuit of the magnet during a cycle are given in Fig. 2.38. As explained earlier, a four channel digital delay generator is used to generate the necessary input pulses (Fig. 2.39). The delay of channel A is set to zero. The delay of B is adjusted to provide the evolution period

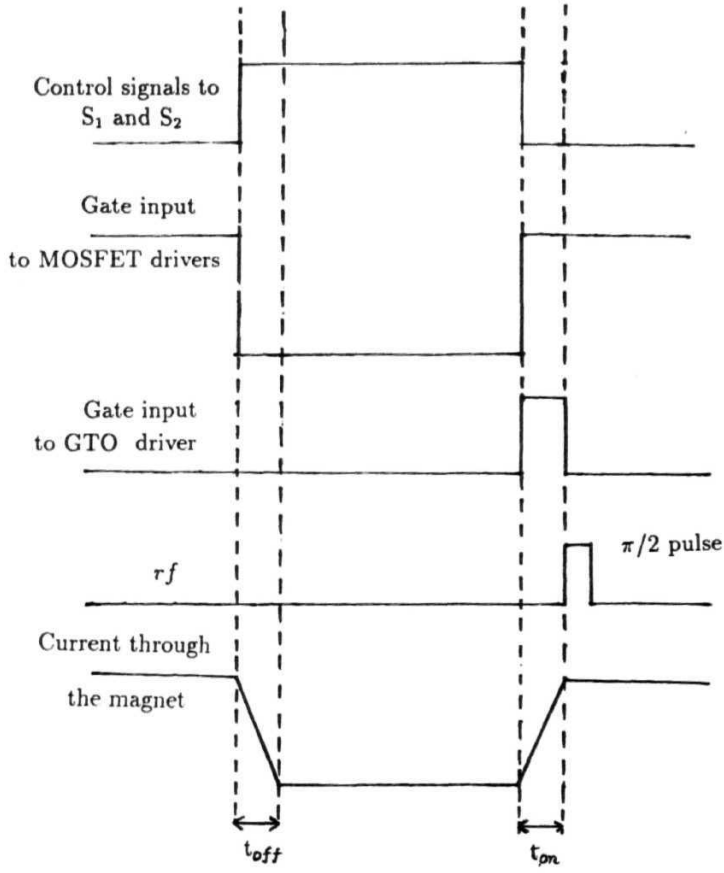

Fig. 2.38 Timing diagram of the various pulses to the different subunits during a typical T_1 measurement using field cycling.

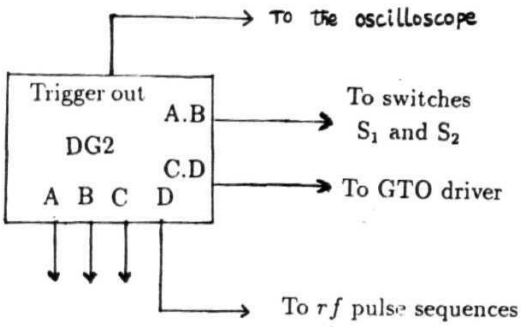

Fig. 2.3d Pulse programmer with different pulse generators and digital delay generators to get the required field cycle and *rf* pulse sequences.

(t_E). The gated output A.B provides the necessary input pulse to the switches S_1 and S_2 (Fig. 2.39). The pole-zero pair amplifier is disabled during the entire period of t_E by closing the switch *S*\ and the necessary signal to obtain the appropriate evolution period is obtained by closing the switch S_2 with the help of A.B signal (Fig. 2.39). Further, the delay of channel C is made equal to the delay of B and the delay D is adjusted to be the sum of the delay B and t_{ON} so that the gate output CD provides the necessary pulse to switch ON the GTO during the t_{ON} period. The trigger pulse at the channel D is synchronous with the edge of t_{ON} and hence it can be used to trigger the pulse programmer in the *rf* spectrometer. In case where a single 7r/2 pulse is sufficient following the field cycle, the trigger output of D can be directly used to generate the *n/2* pulse. The FCNMR spectrometer is automated by interfacing the delay generator and the siganl averager (digital storage oscilloscope) to a PC/AT through IEEE 488 parallel port. The details of the automation are given in section. 2.3.2.

Specifications of the spectrometer

The specifications of the spectrometer described so far are summarized below. The estimated errors in the measurement of T_1 using this spectrometer are generally within 5% and within 10% for T_{1D} measurements.

1.	Operating frequency range	0 kHz to 3.5 MHz
2.	Polarization and detection frequency	3.5 MHz to 5 MHz
3.	Maximum OFF time	1 msec
4.	Maximum turn ON time	25 msec
5.	Field stability	1 in 10^5
6.	Field homogeneity	: 1 in 10^{-5}
7.	Bandwidth	2 MHz at a given frequency
8.	Pulsed *rf* power	upto 1 kV (peak to peak) into 50 Ohms
9.	Typical $\pi/2$ pulse width	2 - 3 μ sec for proton
10.	ON/OFF ratio of *rf* pulse	100 dB
11.	Transmitter isolation	60 dB minimum
12.	Recovery time	15 μ sec (typical)
13.	Interface bus with *PC*	GPIB
14.	Temperature range	77 K to 400 K (with 0.05 K stability over one hour).

2.2.5 Methodology of FCNMR

The methodology of the experiments using *FC* can be approximated to that of the conventional NMR, by taking into account the Zeeman field modulation and the transit times.

Longitudinal relaxation time **(T_1)**

The methodology adopted to measure the longitudinal relaxation using *FC* is similar to that with constant Zeeman field apart from application of adequate B_o cycle. The usual method of disturbing the spin system to a known non-equilibrium value is through the B_o cycle itself *(Bop* $\rightarrow B_{OE}$) and is combined with a $B_1(t)$ sequence to sample the evolving magnetization or the spin temperature belonging to the evolution period i.e.,

$$M_z(t_E) = M_z(t_E = 0) - (M_z(t_E = 0) - M_{OE})[1 - \exp(-t_E/T_{1E})] \qquad (2.28)$$

During the polarization period *(tp* is sufficiently long), M_z increases to an equilibrium value M_{OP}. Following the downward switch to a selected level of B_{OE}, the magnetization $M_z(t)$ relaxes in the evolution period with a time constant T_{1E} towards the new lower equilibrium value M_{OE}. The system is allowed to evolve in the evolution period for a time r before the sampling *n/2* is applied immediately after the upward switch. The sampling pulse flips the $M_z(t_D = 0)$, into the plane perpendicular to B_{OD}. This transverse magnetization $M_\perp(t_D = 0)$ i.e., M_z (t = t_E), now relaxes under the influence of *BOD* with Larmor frequency ω_o giving rise to the familiar FID in the sample coil wound around the sample. The initial height of the FID, U_{sig} (t_D = 0) decays proportional to the magnitude of M_z at t — t_E i.e., the height of the FID obtained decays exponentially with a time constant T_{1E} as a function of the evolution period time, t_E.

Thus the relaxation time T_{1E} (corresponding to the evoluation period) at the selected field strength is measured directly from the envelope of $U_{sig}(t)$ obtained by cycling with different durations of t_E. The T_{1E} corresponding to the other values of

the evolution periods B_{OE} is obtained by readjusting the *BOE* switch amplitude and repeating the above procedure without additional changes. The correlations between the various quantities involved in the cycle ($B_o(t)$, $M_z(t)$,$B_1(t)$and $U_{sig}(t)$) are shown in Fig. 2.40. The total time *T* needed to get a single FID signal is determined by the duration of *BOP* i.e., *top* — $10T_{1P}$. The sampling pulse and the induction signal are in the reference frame rotating with the Larmor frequency and hence are designated by B'(t) and $U'_{sig}(t)$. The T_1 experiment using FC is very much simplified compared to the conventional T_1 experiment at constant Zeeman field, since *Bop* $\rightarrow B_{OE}$ transit already generates the non equilibrium magnetization, without the use of a separate preparation pulse (π or $\pi/2$). Even the anisotropy studies of T_{1E} can be obtained very easily by splitting the evolution field into components parallel to the z and x axes without any significant modification of the scheme, except for high levels of B_{OE}, where the transit fails to deviate the magnetization from equilibrium at t_E — 0 and hence necessitating a π or a $\pi/2$ preparation pulse.

One crucial point to remember during FC experiments is to make *BOD* homogeneous, otherwise T_2^* will be very short making it difficult to detect the full FID due to instrument dead times. This can be overcome to some extent by using a spin echo sequence *(n/2 — τ — π)* where r is small compared to spin spin relaxation time. The echo amplitude and area of echo vary as $M(t_E)$ and hence allow one to determine T_{1E} without the resolution problem involved in an FID.

Transverse relaxation time (T_2)

Similar to the spin lattice relaxation, the methodology used to determine the transverse relaxation using *FC* is same as that with constant Zeeman field. Nevertheless their applications are limited to only liquid like systems with long T_2^* ($T_2 \simeq T_1$) due to the time scales involved.

The transverse nuclear magnetization $M_\perp$ following a $\pi/2$ pulse is given by the familiar Bloch equation

$$\frac{dM_\perp}{dt} = \gamma [M(t) \times B_o] - \frac{M_\perp(t)}{T_2} \qquad \textbf{(2.29)}$$

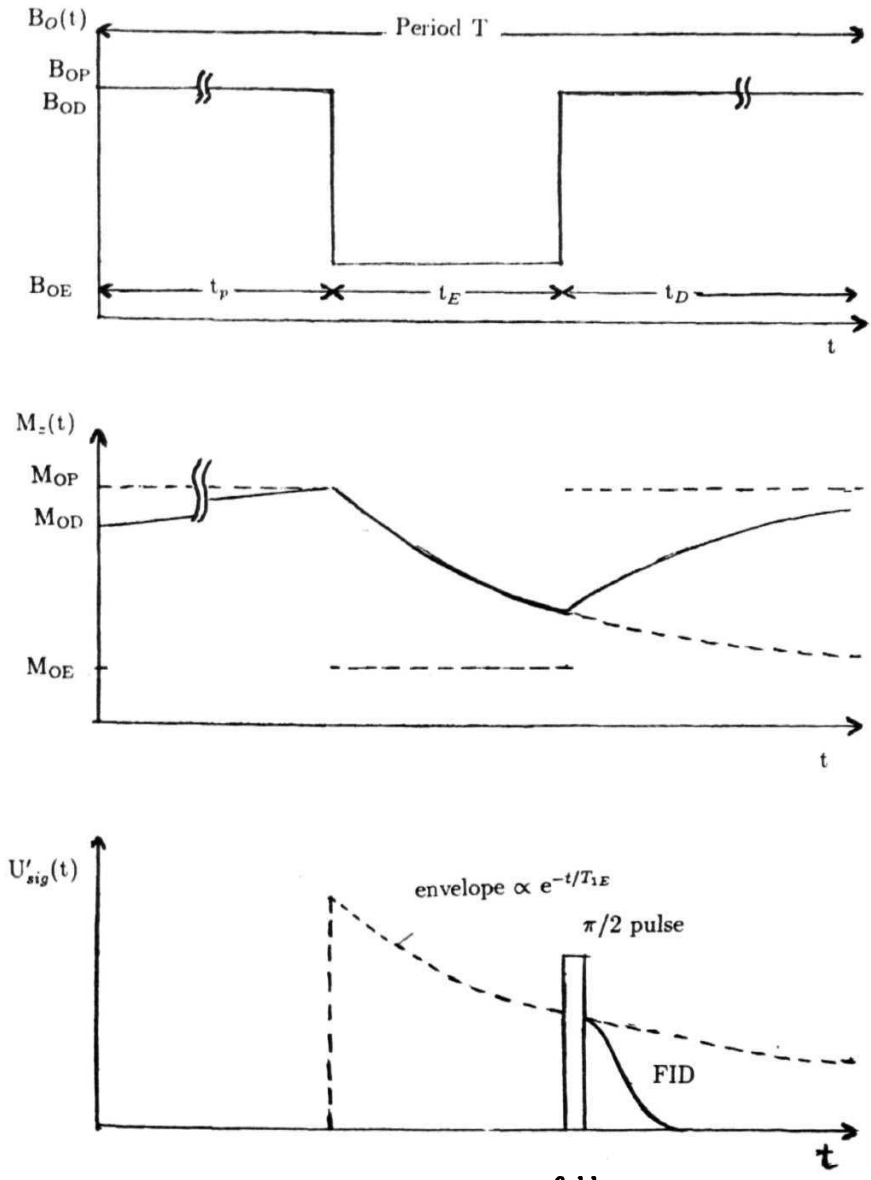

Fig. 2.40 Simple *FC* scheme to measure the **field** dependence of the longitudinal relaxation time T_{1E}. The sign (') refers to the quantities in the rotating frame

(a) **Zeeman** field cycle $B_o(t)$

(b) Longitudinal magnetization $M_z(t)$

(c) rf pulse and recovery of magnetization in the z direction.

The relaxation time T_{2E} in the evolution period may in principle be measured from the FID, created by a *n/2* pulse in polarization period, and sampled as a function of the time, t_E. However, the inhomogeneities in the *dc* field necessitates measurements through spin echo techniques. A typical spin echo sequence $(\pi/2 - T - \pi)$ compatible with B_o cycles is (Carr-Purcell) given in Fig. 2.41. Shortly before the end of polarization period, M_{OP} is flipped into the *xy* plane by the 7r/2 pulse. The subsequent field switch changes the relaxation time from T_{2P} to T_{2E}. The π pulse which refocuses the dephasing spins is applied in the middle of the evolution period with a spacing of *At* = $t_E/2$. Since the available techniques do not allow change of $B_1(t)$ sufficiently fast to the evolution period, it must be cycled to the *Bop* level during the π pulse. The inhomogeneously distributed magnetization in the transverse direction is rephased resulting in a spin echo at t_E = 2At. The pulses and transits must be positioned in such a way that the echo maximum occurs immediately after switching to *BOD* in order to avoid any mixing with T_{2D}. The height of the signal obtained from the echo at t_D = 0 will be proportional to *M*± at *t* = t_E and the signal envelope as a function of t_E yields T_{2E}. The full relaxation dispersion can be obtained by repeating for other *BOE* levels. As mentioned for *T*\ processes, the value of t_{OFF} and t_{ON} set a lower bound to the accessible T_2 range.

Section - 3

2.3 *High field pulsed NMR*

A variable frequency, home made pulsed NMR spectrometer (Venu,1986) is available in the laboratory. The details of this spectrometer, which has been used for the relaxation measurement at high frequencies (> 3 MHz) are briefly described in this section. The various subunits of this spectrometer are similar to that of the *FC* spectrometer described in section 2 except for a few modifications. The magnet used is manufactured by Bruker Spectrospin (Model BE25) and is energized using a power supply (Bruker, Model No. B-MN 155/45 A6). The pole caps are 10" in diameter and the pole gap is adjustable upto 4". The magnet has a stability of 1 in 10^6 with

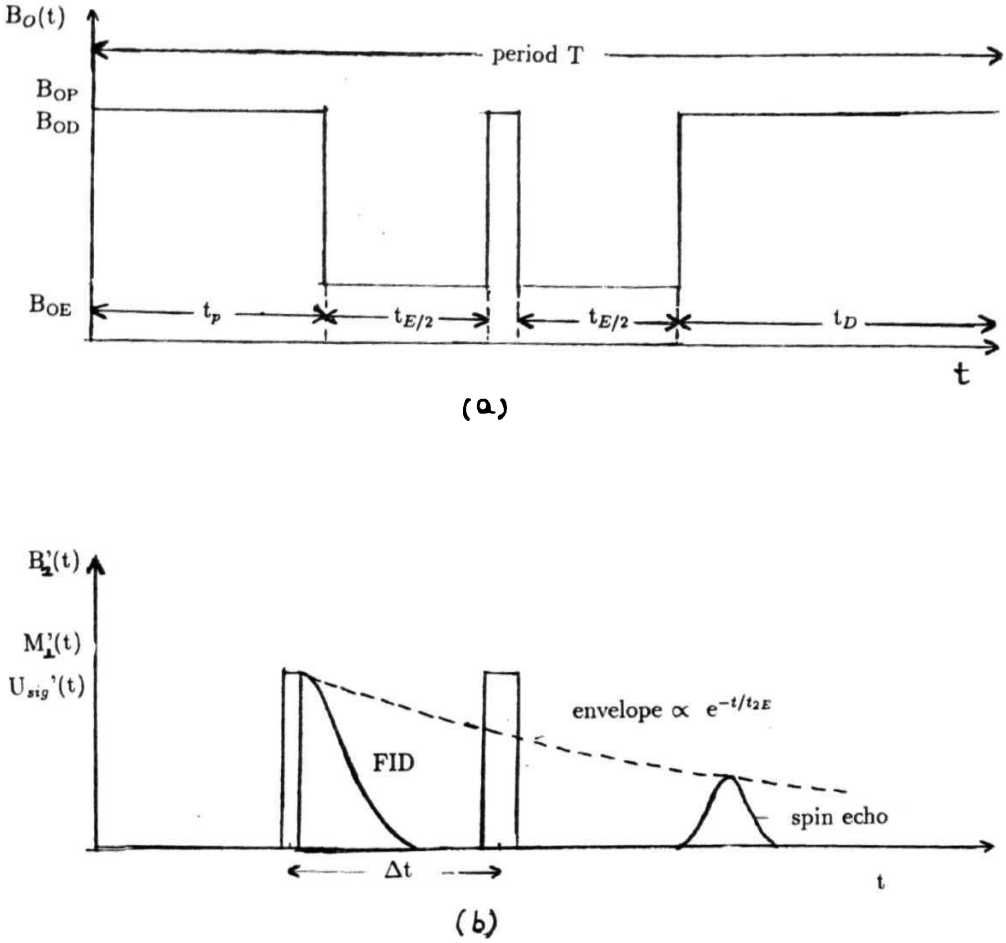

Fig. 2.41 Simple *FC* scheme to measure the **field** dependence of the transverse relaxation time T_{2E}. The sign (') refers to the quantities in the rotating frame

(a) **Zeeman** field cycle $B_o(t)$
(b) rf pulse and recovery of the magnetization in the transverse direction.

a very good homogeneity over about $1 cm^3$. A maximum magnetic field of about 1.2 T with a long term stability can be obtained with good cooling arrangements.

2.3.1 Spectrometer

The pulses of required widths with necessary delays between them are obtained from two commercial pulse generators (BNC, model 8010) in conjunction with a commercial delay generator (BNC, model 7010) (Fig. 2.42). The three pulse sequence for dipolar echo is obtained with the above three units and a home made pulse generator using IC74121 (Fig. 2.43). A commercial synthesizer capable of giving *rf* from 0.1 kHz to 110 MHz with a stability of 1 in 10^8 is used (Wavetek, Model No. 2500A) to get the required rf. Pulse modulation is done using double balanced mixers with a current driving circuit as described below.

Pulse modulation

Mixer

Pulse modulation of the *rf* with very high ON/OFF ratio is achieved using double balanced mixers (Mini Circuits, Model No. SRA-3H). It consists of three ports IF, LO and *RF* perfectly isolated from each other. The circuit diagram of a typical double balanced mixer (DBM) is shown in Fig. 2.44 and the working of the circuit is explained below. If the diodes D_1 and D_2 are matched and the transformers T_1 and T_2 are symmetrical, the voltage at A is equal to the voltage at the center tap of T_1 i.e., ground. Similarly if D_3 and D_4 are matched, the voltage at *B* is equal to ground. Thus the secondary ends of the Transformer T_2 are at ground potential and hence LO port is isolated from both *rf* and IF ports. Now looking from *rf* port, since all the diodes are matched, the voltage at *C* is equal to the voltage at *D* i.e., ground. Hence no *rf* voltage appears at the LO port. Due to symmetry, the voltage at IF port is same as that at *C* and *D* i.e., zero. Thus there is no *rf* output at IF port and hence all the three ports are isolated.

With the pulses applied at the IF port and an *rf* signal at the *rf* port, the current at the IF port rises suddenly during the pulse ON period. This turns on the diodes and hence the *rf* appears at the LO port. When the transmitter pulse is OFF, as

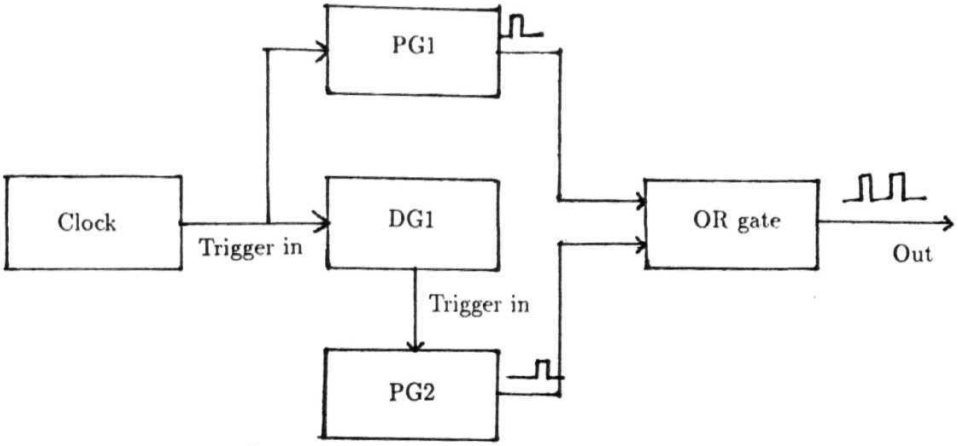

(a)

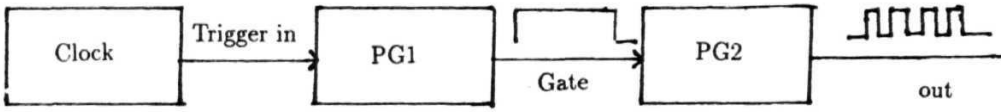

(b)

Fig. 2.12 Pulse programmer for generating different pulse sequences
(a) Arrangement for two pulse sequence
(b) Arrangement for saturation burst sequence.

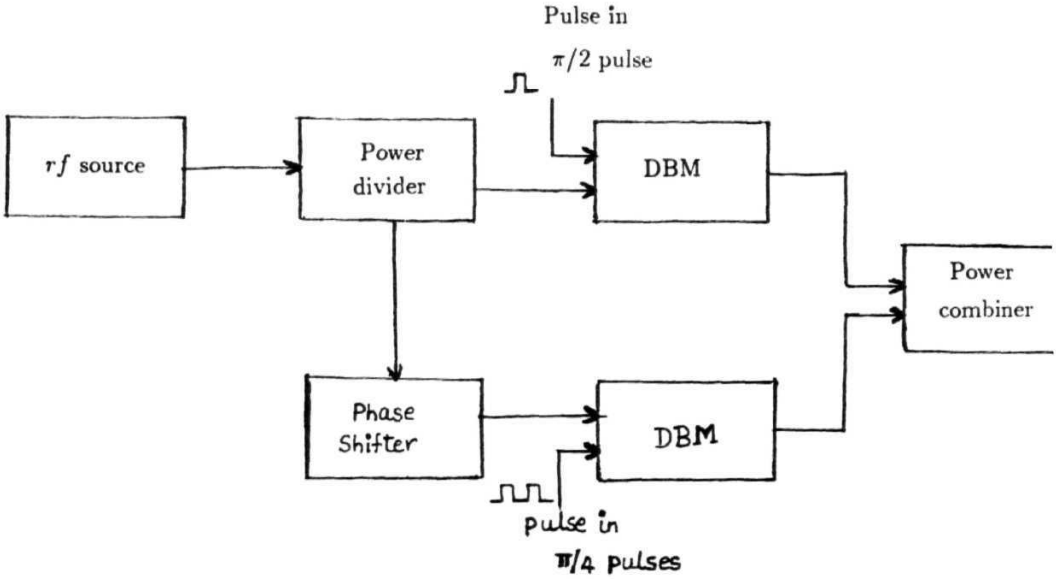

Fig. 2.43 Arrangement for Jeener Broekaert three pulse sequence for T_{1D} measurements.

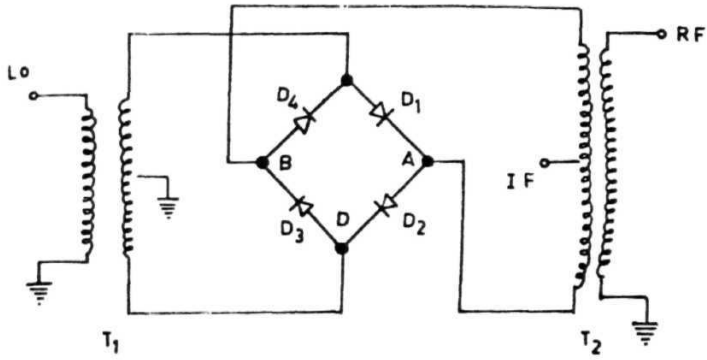

Fig. 2.44 Double Balance Mixer (DBM).

explained above, the IF and *rf* port are isolated resulting in a pulse modulated *rf* with negligible rise and fall times (less than 0.1μ sec).

Practically as the frequency of operation is increased, isolation tends to fall off at the rate of 5 dB/octave. As the current through the IF port is varied, the balance between LO and *RF* will be altered. Since the IF port response extends from *dc* to some high frequency, very fast switching is practical. Assumptions for balance are based on transformer symmetry and diodes being equal. Diode junction capacity differences and transformer winding mismatch leads to imbalance in the bridge and subsequent drop in isolation.

Addition of one more DBM in series, results in a better ON/OFF ratio and hence a better *S/N* at the cost of higher insertion loss (Fig. 2.45a). Better isolation can be achieved using a current driving circuit (McLachlan, 1982) to drive the DBMs (Fig. 2.45b). This circuit enables the adjustment of the amplitude of the pulsed *rf* over a ten fold range by varying the gating pulse current from about 1 to 30 mA. The working of the circuit is briefly described below. The transistors (Q_1 and Q_2) are independent current drivers and have their collector currents adjusted by the $1K\Omega$ trimpot. When the transmitter pulses are OFF, the collector currents switch ON the transistors Q_4 and Q_5 respectively and hence no pulses appear at the IF inputs of the DBMs. During the pulse ON period Q_3 and Q_4 are ON and the collector currents of Q_1 and Q_2 are steered to the IF ports of the corresponding DBMs. Since the transistors used (BC 558) are PNP transistors, inverted TTL pulses are given at the inputs. This circuit has two driving channels and hence different phase shifted pulses can be pulse modulated simultaneously.

The pulsed *rf* from the mixers is initially amplified to a nominal level of 30 V_{pp}, using a commercial medium power amplifier (ENI make, model $350L$), which is used to drive a subsequent high power gated tube amplifier. The matching network used is either a parallel or series resonant circuit described in section - 2. The receiver used is a broad band receiver (Matec, model No. 625) with a narrow band double tuned preamplifier (Matec make, model No. 252) along with a phase sensitive detector, filter and a signal averager, the functioning of which are explained earlier. The temperature

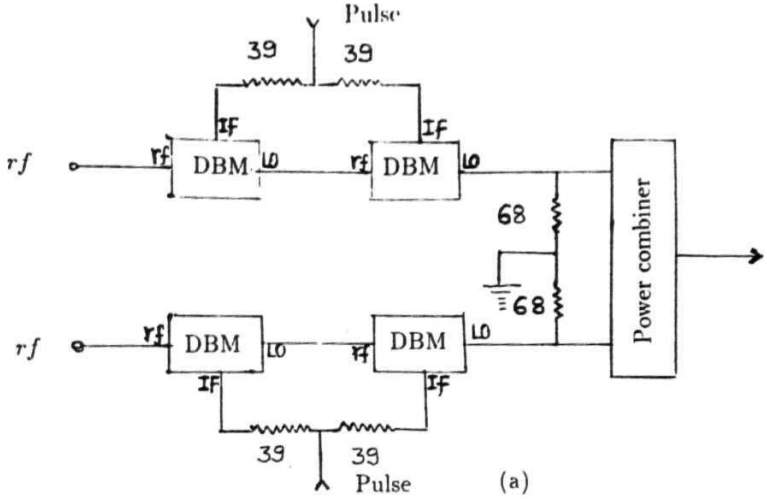

Fig. 2.45a Arrangement of DBM's in series for enhanced ON/OFF ratio

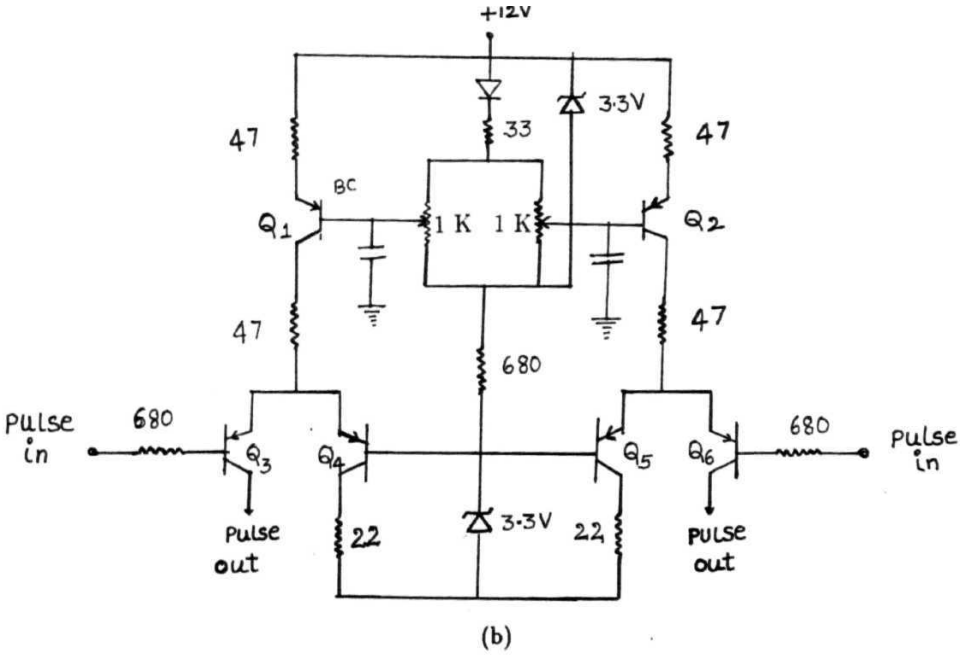

Fig.2.45b Current driving circuit to drive the DBM's.

controller used is similar to that of the *FC* spectrometer.

Temperature controller

To enable the temperature variation measurements covering all the mesophases of the liquid crystals, a temperature variation facility is used. Since the orientation ordering of the molecules in *LC* is sensitive to the temperature, maintaining the sample at a particular temperature during the course of the measurement is an essential factor. Various temperature controller circuits are available in the literature. For the present purpose, a slight modification of the circuit (Chiu et al., 1979) is used which works in the range of 85 K to 400 K with a stability of 0.1 A'. Dry air is used for temperatures above room temperature while Liquid Nitrogen vapor is used for low temperatures.

The circuit mainly consists of an error amplifier (A) which gets a reference signal through a 10 turn calibrated helipot and the sensed voltage from the sample (Fig. 2.46). The difference is amplified and buffered before being fed to the heater through power transistors (2N 3055 in parallel). The temperature required is set by adjusting the helipot which is calibrated to give 1 mV for each turn. The polarity of the reference voltage is so chosen that the output of the error amplifier is positive whenever the sensor temperature is less than the set temperature. The precise measurement of the sample temperature and the reference temperature is obtained using two different thermocouples (Copper-Constantan).

The working of the circuit is explained briefly below. When the reference voltage is more than the sensor voltage, a positive voltage appears at the output of the error amplifier, thereby turning ON the power transistors. Thus current flows through the heater and the temperature of the sensor (sample) rises. The increase in the sensor voltage decreases the error at the input of the error amplifier, thus making the output of the error amplifier less positive and less current through the heater. This happens until the sensor emf is more than the reference voltage. Now the heater is turned OFF. This turning ON and OFF of the heater happens quite a number of times until an equilibrium temperature is reached, thus maintaining the sample temperature constant.

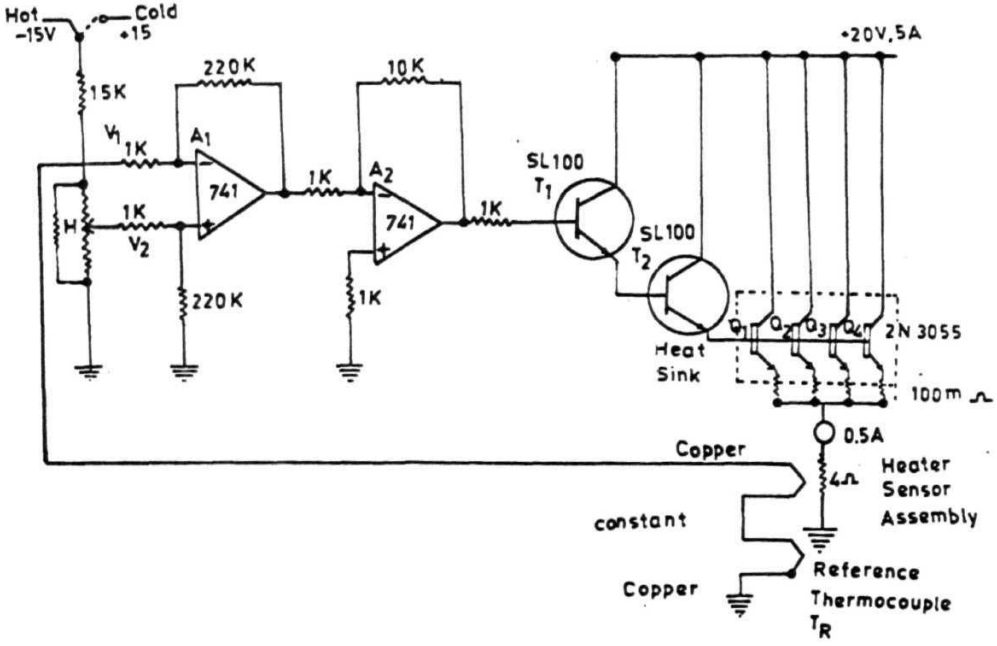

Fig. 2.46 Temperature controller.

The sample is placed in a copper can and is kept inside a double walled evacuated ($10^{-5}T$) glass cryostat (Fig. 2.47) which is used to minimize the heat losses. The heater coil is placed in the path of the air or liquid nitrogen vapors for homogeneous temperature variation of the sample. Since the stability of the sample temperature is crucial, a few precautions are to be followed. A low thermal mass inside the cryostat enables the sample to reach the required temperature quickly but reducing the stability since any fluctuations at the heater are immediately felt by the sample. An increase in thermal mass, although improves the stability, will take very long time to reach the required temperature. Hence the thermal mass of the sample has to be optimized. Apart from this, the rate of gas flow, position of the sensor, position of the heater coil also play an important role in the process of attaining stabilized temperature. All these factors are optimized by trial and error methods to obtain temperature stability of $0.1K$ within an acceptable time of 30 to 45 mts, typical time taken for a given T_1 experiment.

2.3.2 Automation of the spectrometer

The high frequency pulsed NMR spectrometer and the FC spectrometer described earlier are connected to PC/AT's through IEEE 488 interface bus for automatic controlling of the spectometer for data transfer. The parameters to be changed during the course of the experiment are the delays from the digital delay degenerators. The signals to be processed for measuring the relevant relaxation time are acquired and averaged by the digital storage oscilloscope (through automation).

The necessary programs for this purpose are written in BASIC language and are executed through an assembly level program after suitable conversion. These programs differ depending on the pulse sequence required, but in general have a 'declaration block' which defines the different devices on the IEEE bus. Each device has a primary address. A given string of data can be transferred to different devices (talkers and listeners) by executing specific subroutine calls. In a typical program, for the measurement of T_1 using 'saturation burst' sequence, the clock provides the repetition rate r (Fig. 2.42), while the pulse generator PG1 produces the gating pulse

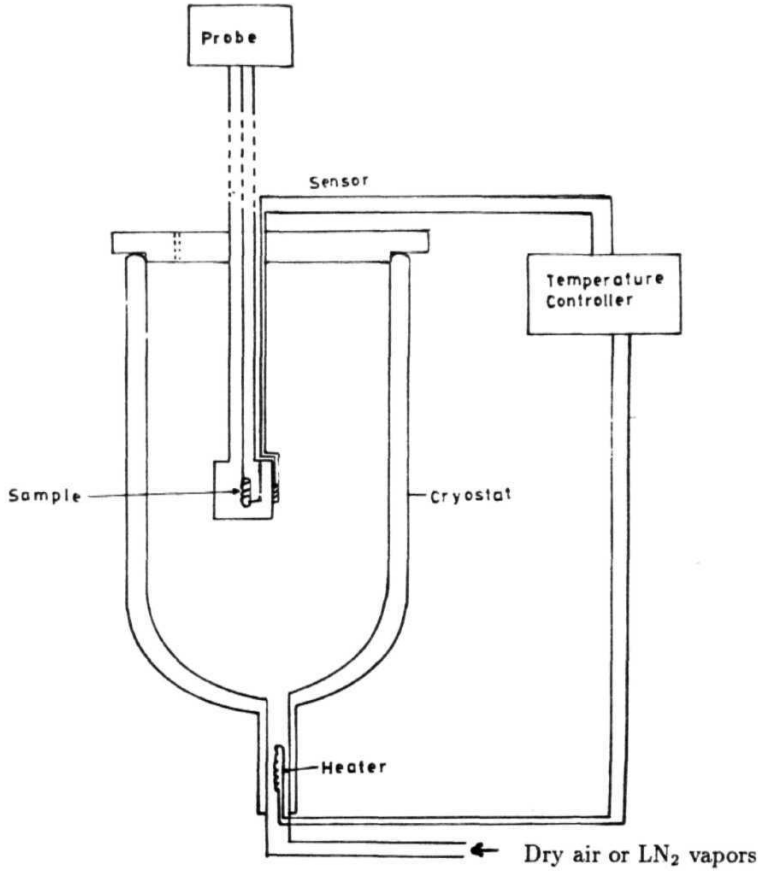

Fig.2.47 Sample assembly with temperature variation facility.

(which essentially determines the number of pulses in the burst). The delay between any two pulses in a single burst is determined by the second pulse generator PG2. The signal averager is programed to perform the required number of averages for a given delay with specified weightages and to display the data and waveforms before repeating for other delays. The PC is programed to control the pulse programmer, clock and the signal averager by proper handshaking procedures. The algorithm used for the above procedure is given in Fig. 2.48.

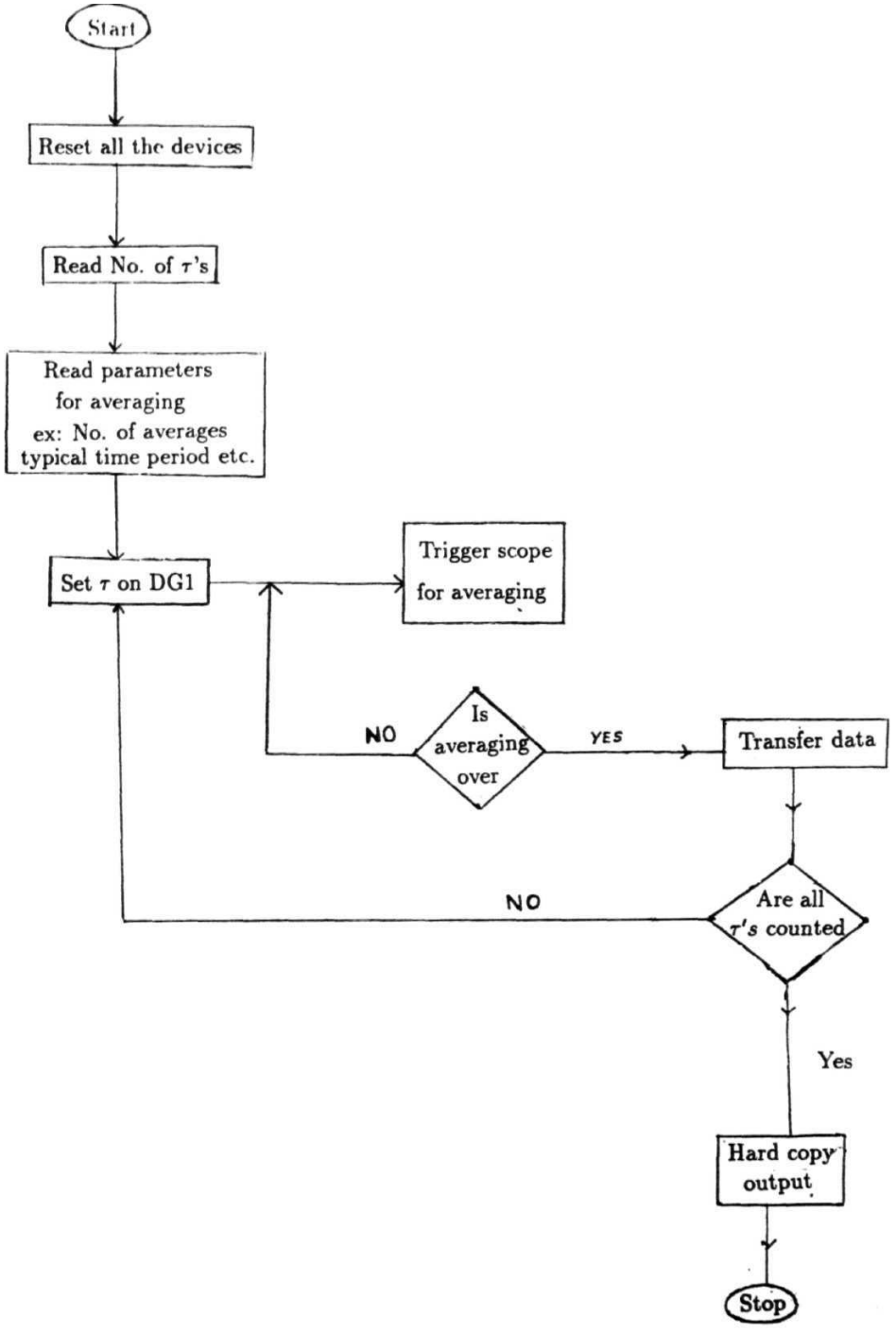

Fig. 2.48 The algorithm for a typical automated T_1 measurement using saturation bunt sequence.

Specifications of the high frequency NMR spectrometer

1. Operating frequency range : 3 to 50 MHz
2. Bandwidth : 2 MHz at a given frequency
3. Pulsed *rf* power : up to $1kV$ (peak to peak) into 50 Ohms
4. Typical 7r/2 pulse width : 2 - 3 μ sec for proton
5. Pulse sequences used : Two pulse sequence
6. Recovery time : $20\mu S$ maximum
7. *rf* gain after detection : $100dB$
8. ON/OFF ratio of *rf* pulse : $100dB$
9. Transmitter isolation : 60 dB minimum
10. Temperature range : 77 K to 400 K (with 0.1 K stability over one hour).
11. Interface bus with PC : GPIB

2.4 *Experimental details*

The work reported in this thesis involves proton spin lattice relaxation measurements done as a function of frequency (a;) in the range of 5 to 50 MHz and temperature covering all the mesophases in a few liquid crystals. These measurements are carried out using the high *rf* frequency spectrometer described in the earlier section. The spectrometer is tuned to obtain the best possible signal using a standard sample (viz., water with a paramagnetic impurity) at each frequency with an unaveraged *S/N* of 50 at the maximum frequency and an *S/N* of about 15 at the minimum frequency. This variation in *S/N* as a function of frequency accounts for the variable scatter obtained as a function of frequency. Inversion recovery and saturation burst sequence are used for the *T* measurements, while Jeenar-Broekaert three pulse sequence is used for T_{1D} measurements. The signal in the isotropic phase (I) is usually very narrow (a long FID) due to the averaging of the dipolar interaction and hence only inversion recovery sequence is used for T_1 measurement. On the other hand, **FID** is short in the nematic phase ($\sim 100\mu$ sec) and hence saturation burst is used, whenever *T* is above 100 msec. The maximum error in the measurement of T_1 is estimated to be about 5% and about 10% for T_{1D} measurements.

The liquid crystalline samples are obtained from Frinton Laboratories (USA) and used without further purification. The transtion temperatures of the systems studied are obtained from differential scanning caloriemetry (DSC) and are found to be agreeing with the literature to within 1° C. The isotropic to nematic phase and nematic to smectic phase transitions are also confirmed by observing the change in the length of the FID at these transitions. The FID begins to shorten near the T_{NI} (isotropic to nematic transition) as the temperature is decreased from isotropic phase and finally collapses to a very short FID (broad line) at the transition.

The samples are sealed in 6 mm diameter glass tubes at about 10^{-5} Torr after removing the dissolved oxygen by freeze-pump-thaw method. The measurements are

made by first heating the system well into the isotropic phase and then cooling to the required temperature in the presence of high fields (about 10 kG) to ensure the proper alignment of the molecules in the mesophase. The temperature variation is done with a home built temperature controller (with a stability of about **0.1** A' over a period of an hour) and the data points are collected in intervals of 2° C in all the mesophases.

Chapter 3

MOLECULAR DYNAMICS IN ALKYLOXY BENZYLIDENE ALKYLANILINES

As explained earlier, liquid Crystals are usually formed by long molecules with a rigid core and flexible end chains. The presence of double bonds in the core leads to an increase in the rigidity and hence stabilization of the mesophases. For example, *n*-alknoic acids with long molecular confirmation, do not exhibit mesophases due to the absence of double bonds in the core (Gray, 1979). Thus mesogenic properties are very sensitive to the molecular structure (even minor changes in the rigidity or flexibility leads to drastic changes on the polymorphism exhibited by these systems). The changes in the end chains are also known to influence the properties of the liquid crystals like even-odd effects (de Jeu et al. 1973 ; Nimtz et al. 1979). Hence, a study of the properties of different systems, by gradually changing the molecular structure (in a homologous series) is very interesting and informative. The typical objectives in undertaking such studies on a homologous series are (i) to investigate the effects of molecular structure on polymorphism (ii) to study changes in the dynamical parameters with changes in the molecular structure, (iii) to test the validity of theoretical models built to explain static/dynamic features of liquid crystals and finally (iv) to search for suitable mesogenic phases for application in technology like liquid crystal displays etc.,. But such systematic studies in the literature are very few.

Of the different homologous series, the families of alkyloxy benzoic acids and Schiff base compounds (*p*-alkyloxy benzylidene *p*-alkylanilines (or no.m, *n* and m varying from 1 to 12), *p*-substituted benzylidene-*p*-alkyl amino cinnamates, *p*-substituted benzyledene-*p*-alkyloxy anilines etc.), have become quite popular due to the ease of preparation and the convenient range of the temperature of the mesophases.

Recent proton NMR studies on a number of compounds belonging to the series *p*-butyloxy benzylidene alkylanilines (4O.m, m = 5, 6, 7, 8 and 9), 60.2 and 6O.Br (Ravindranath, 1991) have revealed quite interesting results regarding the role of different mechanisms in mediating the spin lattice relaxation process. These results have shown that the dynamic processes mediating the spin lattice relaxation in a particular frequency range, like 5 - 50 MHz, need not be the same for all the systems in this family even though the differences in the molecular structure are only in the end chains. The important observations of these studies are that the contribution from order director fluctuations (ODF) extends to higher frequencies as the length of the alkyl chain increases.

In view of the above results, it will be interesting and perhaps necessary to study molecular dynamics in smaller homologues ($m < 5$), in order to arrive at a comprehensive picture regarding the influence of the end chain length on these dynamic processes. Hence, proton magnetic relaxation measurements are done on three compounds belonging to this homologous series (40.4, 40.3 and 40.2) as part of the present work. Dipolar relaxation time (T_{1D}) measurements are also performed on 40.4 to probe low frequency fluctuations. The results are compared with the data available on other nO.m compounds leading to interesting conclusions regarding the role of end chain length on different dynamic processes. The results of these studies are presented in this chapter. A brief review of existing literature on these compounds is provided in the following section.

3.1 *Review on nO.m type compounds*

Alkyloxy benzilidene alkylanilines (nO.m) where n and m vary from 1 to 12 can be obtained by the reaction between aromatic aldehydes and amines (Gray, 1979). The general molecular structure of the compounds is given in Fig. 3.1. Of all the Schiff base compounds, this homologous series is well investigated due to the rich polymorphism exhibited by these systems. The earliest work on these systems (Smith and Gardlund, 1973) reports the transition temperatures among different mesogens belonging to the nO.m series (*n* varying from 1 to 7 and *m* from 4 to 8). Subsequent optical microscopic and X-ray diffraction measurements (Goodby et al., 1980) confirmed these transition temperatures and the presence of S_F, S_B and S_G phases in these compounds. Takahashi et al. (1987) have studied the variation of specific volume with temperature in 5O.m series (m varying from 4 to 14). Density measurements, ultrosonic, caloriemetric measurements and ESR are used extensively to determine the various transition temperatures in the nO.m systems (Lushington et al. 1980 ; Pisipati et al. 1984, 1987 ; Alapati et al. 1988 ; Rannavare et al. 1987, 1988 ; Miechle and Garland, 1983). Magnetic bierfringence studies on 90.4 (Rossenblatt and Ho, 1983), light scattering studies on 60.9 (Mahmood et al. 1985), 60.3 and 90.4 (Potukuchi, 1989 and references therein) are also reported. Neutron scattering measurements are used to study the cooperative nature of molecular motions in ordered smectics (Richardson et al. 1984), while dielectric studies are reported by Nagabhushan et al. (1988).

Apart from the above experiments, nuclear magnetic resonance techniques have also been used to investigate molecular structure and dynamics in a few systems of this homologous series. Information on molecular order is obtained from line width measurements and ESR technique (Frybury et al. 1972 ; Bermann et al. 1974 ; Pushnik et al. 1975, 1976 ; Schimiedel et al. 1980 ; St. Limmer et al. 1984 ; Garland and Stine, 1987). Relaxation measurements over a wide range of frequencies on a few systems have given information on the molecular dynamics and the different

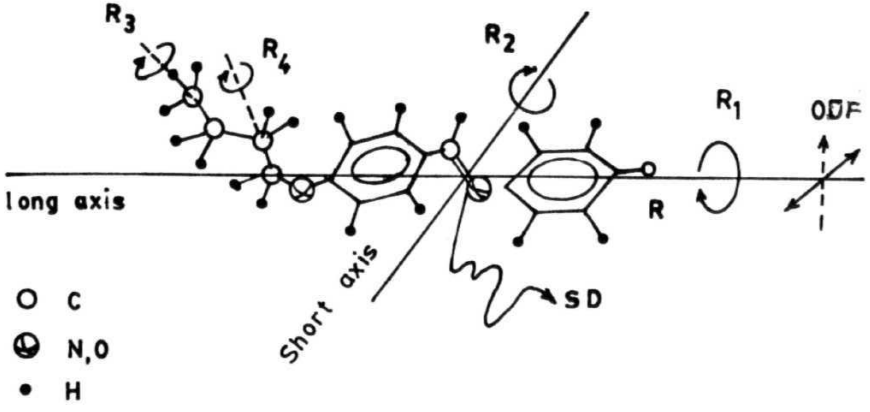

Fig. 3.1 Typical molecular structur of 4O.m systems.

mechanisms mediating the relaxation processes (Dybowski et al. 1971 ; Vilfan et al. 1972 ; Doane et al. 1974 ; Zupancic et al. 1974 ; Blinc et al. 1975 ; Ukleja et al. 1976 ; Graf et al. 1977 ; Wade, 1977 ; Heinze et al. 1978 ; Norida and Segre, 1979 ; Moore et al. 1980 ; Schifferdecker et al. 1981 ; Dong, 1986 ; Vold and Vold, 1989). 10.4 is preliminarily and extensively studied to obtain information about molecular dynamics over a wide range of frequencies (Visintainer et al. 1971 ; Dong et al. 1972 ; Dong et al. 1974a,b ; Blinc et al. 1975 ; Zupancic et al. 1976 ; Ukleja et al. 1976). Low frequency work using field cycling NMR was attempted on 10.4 (Noack, 1986) to investigate the role of ODF modes and their cutoff frequencies.

As explained in the first chapter, the main mechanisms mediating the relaxation processes viz., order director fluctuations (ODF), self-diffusion (SD) and reorientations (R) (Graf et al. 1977, Noack et al. 1988 ; Noack, 1989) have their own distinct frequency, temperature and orientation dependences. Normally, it is difficult to isolate the individual contribution (due to each mechanism) from a T_1 study in a narrow frequency range except in a few fortuitous cases. However, earlier works on a few systems (Owers Bradley et al. 1981 ; Ribeiro, 1987a, 1988 ; Venu et al. 1990 ; Ravindranath et al. 1988, 1990a,b, 1993) reported the identification of the different dynamical processes in a limited frequency range (2 to 80 MHz). Particularly, it is shown that the frequency dependent studies of relaxation times combined with temperature dependent studies can be effectively used to obtain information about these mechanisms. The results of relaxation measurements on 10.4 (Dong et al. 1974a,b ; Blinc et al. 1975 ; Ukleja et al. 1976 ; Graf et al. 1977) revealed that *SD* dominates the relaxation process above 1 MHz and ODF contributions arise below 1 MHz. Similar results on 40.5 and 40.7 (Ravindranath, 1991) have shown self diffusion to be the dominating mechanism above 6 MHz, while, in 40.6 (Venu et al. 1990), ODF contribution was observed till 10 MHz. On the other hand, investigations on 40.8 (Owers Bradely et al. 1981) have shown that ODF mediates T_1 upto 25 MHz with $(T_1^{-1})_{ODF} \propto \omega^{-1/2}$, while in 40.9, ODF along with molecular reorientations mediate the relaxation till 45 MHz. Similar studies on 60.2 (Ravidranath, 1991) and 60.Br (Ribeiro, 1987b) indicate that in 60.2, ODF contributes to relaxation till 40 MHz, whereas, the latter is mediated by SD process down to 5 MHz. Thus, it can be

seen that, whenever the end chain length is large (i.e., in 40.9, 40.8, 60.2 etc.,), ODF seems to be extending upto tens of MHz in nematic and S_A phases, whereas for shorter end chain lengths (i.e., 40.4, 40.5), **ODF** is confined to low frequencies and SD mechanism is responsible for frequency dependence of T_1 above few MHz. It is further observed that the activation energy for reorientations around short axis decreases as the end chain length increases. In this context, it will be interesting to perform similar studies on compounds with even shorter end chains to throw more light on the influence of the end chain length on these dynamic processes. The present investigations are concerned with such studies and the details of the experiments carried out in 40.4, 40.3 and 40.2 are presented below.

Section - 2

3.2 *Butyloxy benzylidene butylanilene (40.4)*

The first system of the series considered in the present work is butyloxy benzilidene butylanilene (40.4). This has a phase sequence given by (Flannery and Hass, 1970)

$$I \underline{\ 75c\ } N \underline{\ 45c\ } S_I \underline{\ 41c\ } S_{II} \underline{\ 7c\ } X$$

S_I phase is a high temperature smectic phase like S_A phase, while *SJJ* phase is an ordered smectic phase. This system has a wide range of nematic phase and a very narrow range of 5/ and 5// phases. The sample is obtained from Frinton Laboratories, USA and used without further purification.

3.2.1 Experimental results

Spin lattice relaxation time measurements are made as a function of frequency (5, 9, 15, 20.1, **39.6** and 50 **MHz)** and temperature covering **the** entire **range of the different** mesophases **(70°C** to **−2°C)** with an average interval **of about 2°C. The data is shown in Fig. 3.2** (Tables **3.1a to** 3.1f), **where** only three frequencies are given for **clarity.**

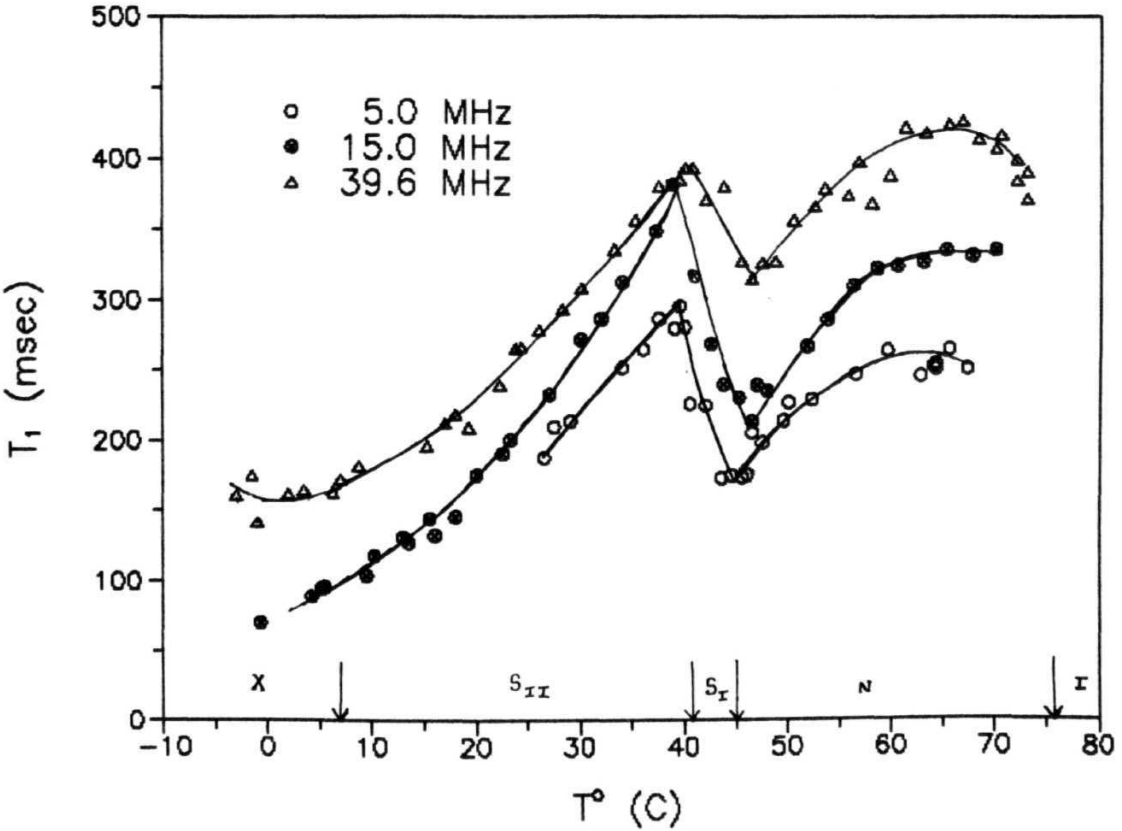

Fig. 3.2 Spin lattice relaxation time T_1, as a function of temperature T at three frequencies in 4O.4. Solid lines are drawn as a guide to the eye The vertical lines denote the transition temperatures.

Table. 3.1b : Variation of spin lattict **relaxation** time (T_1) with temperature <T> at 9 **MHz (40.4)**

T° C	T_1 (msec)	T° C	T_1 (msec)
79.0	233	58.0	**287**
77.0	229	57.5	268
76.0	213	57.0	279
73.0	158	56.0	245
71.8	300	55.0	266
71.5	277	53.8	194
70.0	283	53.0	261
69.5	2 79	**52.5**	246
69.0	**311**	**51.6**	**252**
68.0	270	**51.5**	**256**
67.5	**311**	51.0	**255**
66.8	310	50.5	214
66.5	296	49.8	239
64.8	322	49.5	236
64.6	**321**	49.0	247
63.9	289	48.3	258
62.8	261	47.3	222
62.5	297	46.0	200
61.8	299	46.0	209
61.0	322	45.0	215
60.8	263	44.8	**184**
59.8	323	44.0	258
59.5	305	42.0	**223**
59.5	283	40.0	278

Table. 3.1b : **Variation** of spin **lattice relaxation time** (T_1) with **temperature** (T> at 9 MHz **(40.4)**

T° C	**T.** (msec)	T° C	T_1 (msec)
79.0	233	58.0	**287**
77.0	229	57.5	268
76.0	213	57.0	279
73.0	158	56.0	245
71.8	300	55.0	266
71.5	277	**53.8**	194
70.0	283	33.0	261
69.5	2 79	52.5	246
69.0	311	51.6	**252**
68.0	270	51.5	**256**
67.5	**311**	51.0	**255**
66.8	310	50.5	214
66.5	296	49.8	239
64.8	322	49.5	236
64.6	321	49.0	247
63.9	289	48.3	258
62.8	261	47.3	222
62.5	297	46.0	200
61.8	299	46.0	209
61.0	322	45.0	215
60.8	263	44.8	184
59.8	**323**	44.0	258
59.5	**305**	42.0	**223**
59.5	283	40.0	278

Titbit. 3.1c : Variation of spin lattice relaxation time with temperature <T>at 15 MHz (40.4)

T° C	T_1 (msec)
70-0	335
67.8	331
65.3	335
63.0	327
60.5	324
58.5	322
56.3	310
53.8	286
51.8	267
48.0	235
47.0	239
46.5	213
45.3	230
43.8	239
42.5	268
38.8	381
37.3	348
34.0	312

T° C	T_1 (msec)
32.0	286
30.0	271
27.0	232
23.3	200
22.5	190
20.0	175
18.0	145
16.0	132
15.5	144
13.5	127
13.0	131
10.3	118
9.5	104
5.5	76
5.3	75
4.3	69
-0.7	70

Table. 3.1d : Variation of spin lattice relaxation time (T_1) with temperature <T> at 20 MHz (40.4)

T^{o} C	T_1 (msec)	T° C	T_1 (msec)
68.5	363	44.0	292
65.0	357	43.5	256
62.8	366	43.3	266
61.3	371	42.6	297
60.0	346	41.0	321
57.5	340	40.5	356
56.3	330	39.8	385
54.3	334	37.3	358
52.5	312	34.3	340
48.5	281	27.5	252
46.8	261		

Table. 3.1e : Variation of spin lattlct **relaxation time (T_1) with temperature** <T> **at 30** MHz **(40.4)**

T° C	T_1 (msec)	T° C	T. (msec)
80.0	311	58.0	347
76.0	297	57.5	355
74.8	293	55.3	342
73.8	331	54.0	333
72.0	316	52.8	309
70.3	374	52.2	306
70.3	396	50.5	312
70.0	383	49.5	**288**
70.0	359	49.0	294
69.8	394	**47.8**	311
69.3	369	46.5	324
69.0	391	46.0	313
67.3	381	46.0	**285**
66.5	369	45.0	311
65.0	390	43.8	309
64.8	375	42.0	373
63.6	377	41.5	352
63.6	394	41.5	359
62.0	387	39.5	367
62.0	375	39.0	350
61.0	385	37.5	334
60.0	**363**	29.5	276
59.5	370	24.3	**303**
59.3	355		

Table. 3.1f : Variation of spin lattice **relaxation** time (T_1) with **temperature** <T> at **39.6** MHz <40.4>

T° C	T_1 (msec)	T° C	T_1 (msec)
73-0	390	**40.8**	393
73.0	3/1	40.0	**373**
72.0	384	39.5	384
72.0	399	37.5	380
70.5	416	35.3	356
70.0	407	33.3	335
68.3	414	30.1	308
66.8	427	28.3	293
65.5	424	26.0	278
63.3	**418**	24.3	266
61.3	422	23.8	265
59.8	388	22.3	239
58.0	368	**19.3**	209
56.8	397	**18.0**	218
55.8	374	17.0	212
53.5	379	15.3	196
52.5	366	8.8	182
50.5	356	7.0	172
48.8	327	6.3	163
47.5	326	3.5	164
46.5	315	2.0	162
45.5	327	-1.0	**142**
43.8	380	-1.5	**175**
42.0	370	-3.0	161

T_{1D} measurements are made as a function of temperature in the nematic and smectic phases at 30 MHz (Fig. 3.3) using Jeener Broekaert sequence.

As can be seen from Fig. 3.2, pretransitional effects dominate the spin lattice relaxation process close to the isotropic - nematic transition (T_{NI}) over about 5° C. Beyond this region, T_1 is both frequency and temperature dependent (T_1 decreases with decreasing temperature). The 5/ phase is very narrow and is essentially dominated by pretransitional effects, after which there is a steep increase in T_1 at the smectic-I to smectic-II transition. T_1 is both temperature and frequency dependent in the solid phase also. Further at each frequency, in the solid phase, there is a T_1 minimum which shifts towards lower temperatures as the frequency decreases. T_{1D} decreases with decreasing temperature in the nematic phase. Pretransitional effects in T_{1D} are observed near the smectic-I to smectic-II transition (Table 3.2), before dropping from 3.5 msec to 4 msec in the S_{II} phase. In the 5// phase, T_{1D} decreases further with decreasing temperature.

3.2.2 Analysis and discussion

Nematic phase

The T_1 data in the nematic phase (after the pretransitional effects) is first analyzed to find the dynamic processes responsible for its frequency dispersion (ODF or SD). The preliminary analysis shows that this data at any given temperature varies as $\omega^{1/2}$ (Fig. 3.4) but not as $\omega^{-1/2}$, indicating that SD might be the dominating mechanism in this phase. Assuming reorientations to be present always (giving rise to a frequency independent contribution), the total relaxation rate in this phase is written as

$$T_1^{-1} = A + \frac{1}{1.4}\,(T_1^{-1})_{Torrey} \qquad \textbf{(3.1)}$$

The expression for $(T_1^{-1})_{Torrey}$ is given by eqn. (1.34). Different parameters involved in this expression are as assumed in the **first** chapter. The constant A is due to reorientations around short axis $(T_1^{-1})_{RS}$, given by eqn. (1.88) in the $\omega\tau_s < 1$ limit. The **data at** any given temperature is fitted to the above equation numerically to

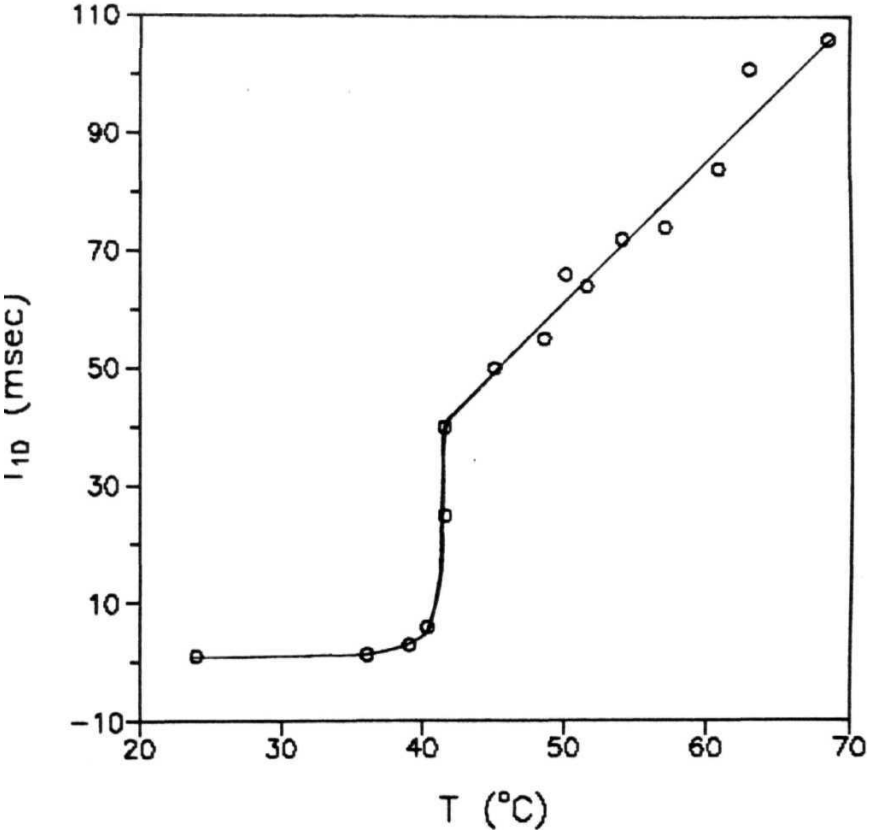

Fig. 3.3 Variation of dipolar relaxation time T_{1D}, as a function of temperature in 40.4. Solid line is drawn as a guide to the eye.

Table 3.2 Variation of dipolar spin lattice relaxation time (T_{1D}) with temperature <T> at 39.6 MHz <40.4>

T° C	T_{1D} (msec)
68.5	106
63.0	100
60.8	84
57.0	74
54.0	72
51.5	64
50.0	66
48.5	55
45.0	50
44.0	35
41.5	25
40.3	6
39.0	3
36.0	2
24.0	1

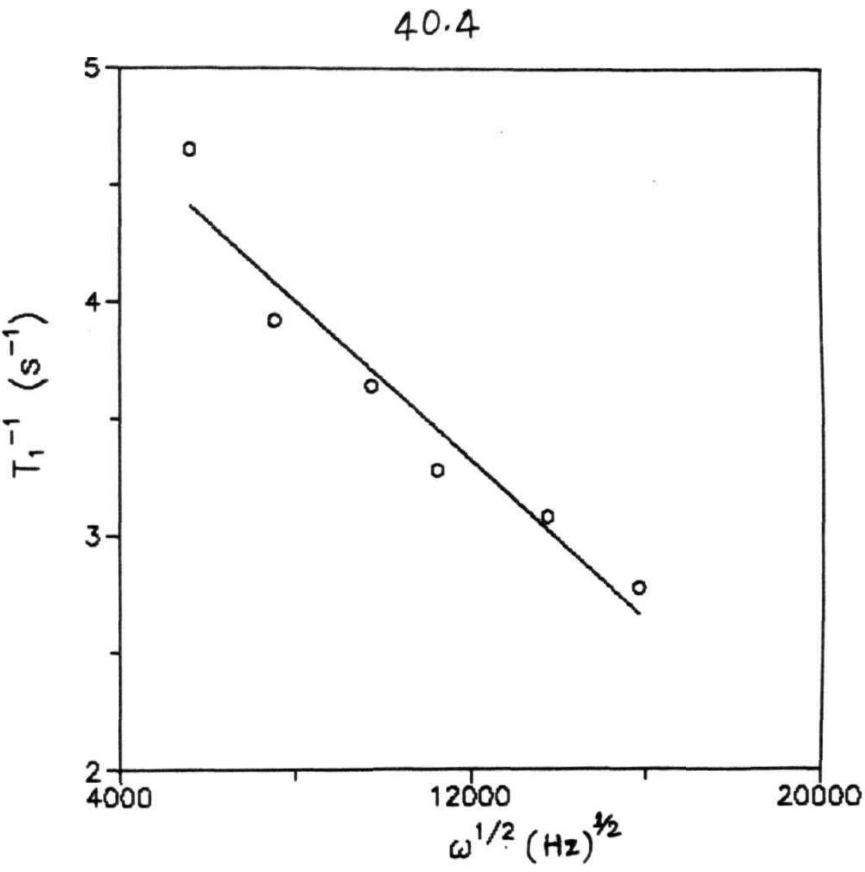

Fig. 3.4 Spin lattice relaxation rate T_1^{-1} as a function of square root of Larmor frequency $(\omega^{1/2})$ at a mid nematic temperature in 40.4. Solid line is the best fit line.

obtain the best fitted value for diffusion coefficient $D\pm$ and $(T_1^{-1})_{RS}$ i.e. A. The variation of $(T_1^{-1})_{RS}$ and $(T_1^{-1})_{SD}$ with frequency obtained from this fit at *52°C* are shown in Fig. 3.5. The relative contributions to the relaxation rate from *R* and *SD* at a mid nematic temperature (52^oC) at 5 MHz are 46% and 54% and are 73% and 27% at 39.6 MHz respectively. Thus the contribution from translational diffusion decreases at higher frequencies. The typical value of diffusion coefficient obtained by this analysis is about $\sim 10^{-7} cm^2/sec$. This procedure is repeated at other temperatures in the nematic phase to obtain the temperature dependence of the diffusion coefficient and $(T_1^{-1})_{RS}$.

While the diffusion coefficient decreases with decreasing temperature (Table. 3.3), the contribution from reorientation increases. The variation of $(T_1^{-1})_{SD}$ and $(T_1^{-1})_{RS}$ with temperature at 5 and 39.6 MHz are given in Fig. 3.6 and Fig. 3.7 respectively (Table 3.4). Assuming both the diffusion and reorientations to be thermally activated, the temperature dependence can be written in Arrhenius form as

$$D_\perp = D_\perp^o \, e^{-E_{aD}/kT} \tag{3.2}$$

and

$$(T_1^{-1})_{RS} = (T_1^{-1})_{RS}^o \, e^{E_{aS}/kT} \tag{3.3}$$

By fitting the temperature dependence of the diffusion coefficient and $(T_1^{-1})_{RS}$ obtained from the above analysis to eqns. (3.2) and (3.3), the activation energy associated with the diffusion process (E_{aD}) and reorientations around short axis (E_{aS}) are found to be 7.9 ± 0.4 (Fig. 3.8) and 8.7 ± 0.4 kCal/mole (Fig. 3.9) respectively.

The narrow 5/ phase is dominated by the pre-transitional effects before T_1 increases at the smectic-I to smectic-II transition and hence no analysis of the data in this phase is attempted.

Smectic II and solid phase

The discontinuous jump in T_1 near the smectic-I to smectic-II transition can be attributed to the sudden slowing down of diffusive motions in ordered S_{II} phase and

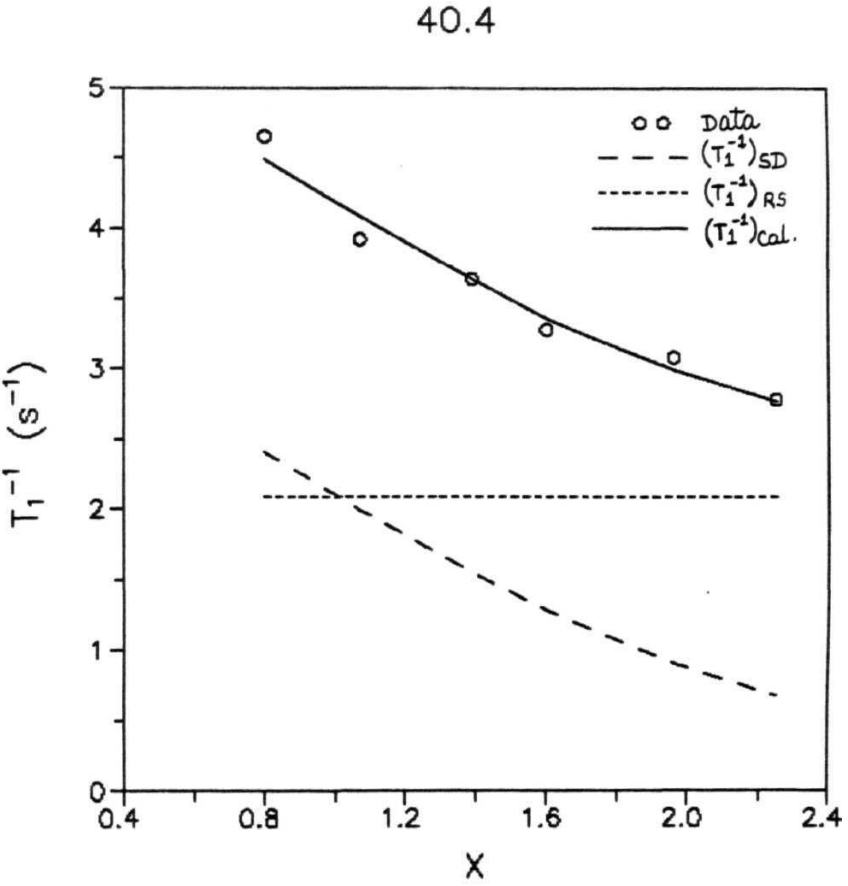

Fig. 3.5 Relative contributions of $(T_1^{-1})_{SD}$ and $(T_1^{-1})_{RS}$ as a function of X in nematic phase (52°C) of 40.4. Solid line is the best fit to the eqn. (3.1). X is a dimensionless quantity $\propto \sqrt{\frac{\omega a^2}{2D}}$

Table 3.3 : Variation of $D_\perp$ with temperature in the nematic phase of 40.4.

T^{o} C	$D_\perp$ <x 1e-7 cm^2/sec)
56.0	1.41
55.0	1.37
54.0	1.32
53.0	1.26
52.0	1.23
51.0	1.21
50.0	1.20
49.0	1.17
48.0	1.14

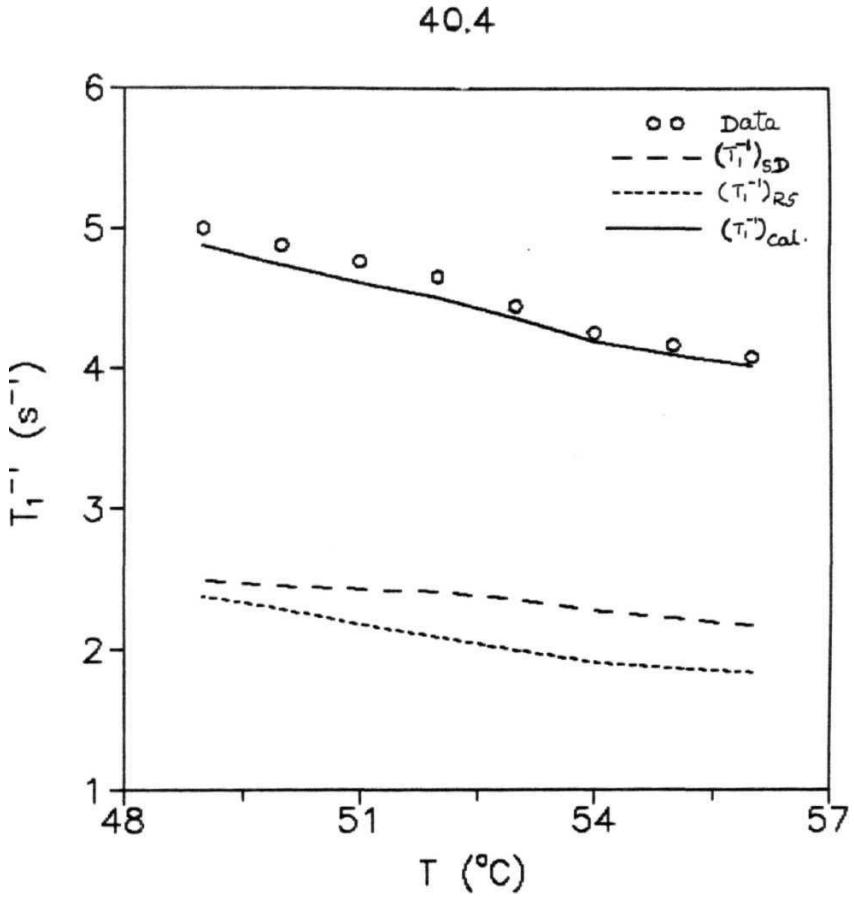

Fig. 3.6 Relative contributions of $(T_1^{-1})_{SD}$ and $(T_1^{-1})_{RS}$ as a function of temperature in the nematic phase at 5 MHz. •.

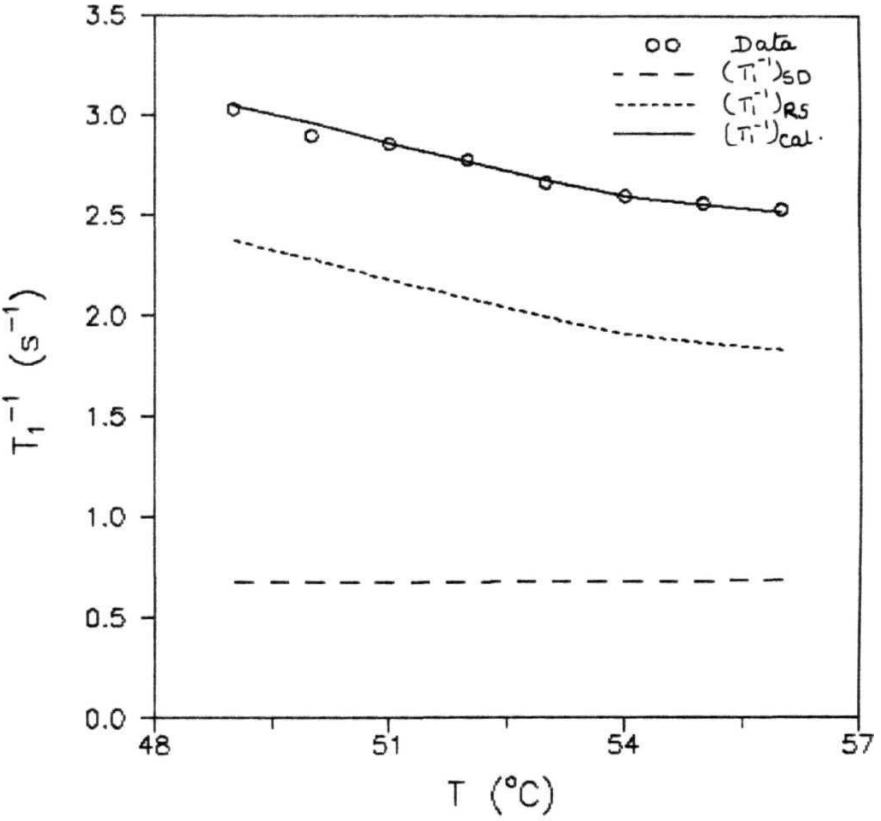

Fig. 3.7 Relative contributions of $(T_1^{-1})_{SD}$ and $(T_1^{-1})_{RS}$ as a function of temperature in the nematic phase at 39.6 MHz. . . . . .

Table 3.4 : Variation of T_{1R}^{-1} and T_{1SD}^{-1} with temperature in the nematic phase of 40.4

T^{o} C	T_{1R}^{-1} (sec^{-1})	T_{1SD}^{-1} (sec^{-1})	
		5 MHz	39.6 MHz
56.0	1.84	2.18	0.69
55.0	1.87	2.22	0.69
54.0	1.91	2.28	0.69
53.0	1.99	2.36	0.68
52.0	2.09	2.41	0.68
51.0	2.18	2.43	0.68
50.0	2.29	2.45	0.68
49.0	2.38	2.49	0.67

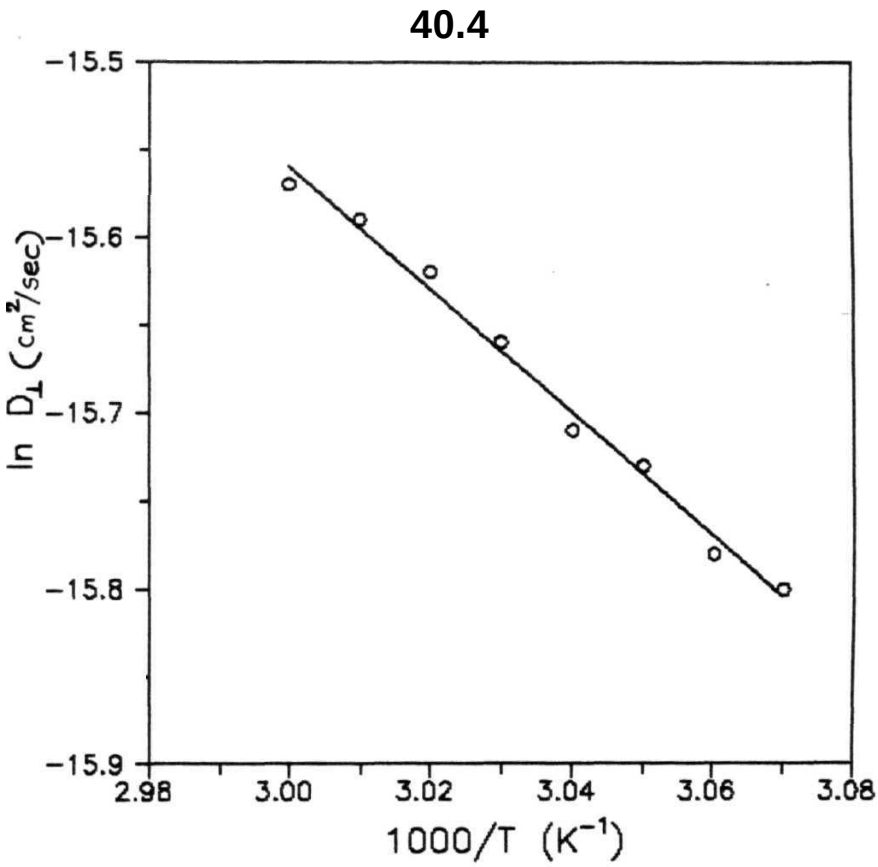

Fig. 3.8 Arrhenius fit of the diffusion coefficient $(D_{\perp})$ in the nematic phase of 40.4 • Solid line is the best fit line

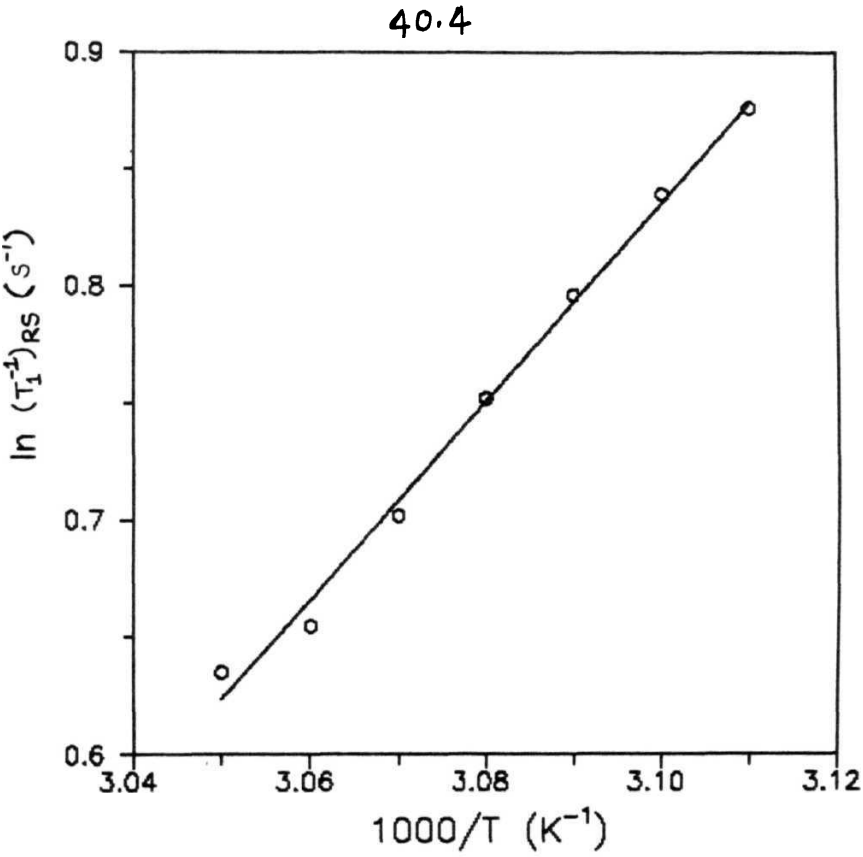

Fig. 3.9 Arrhenius fit of $(T_1^{-1})_{RS}$ in the nematic phase of 40.4 Solid line is the best fit line.

cutoff of ODF effects. In this phase, T_1 is still frequency and temperature dependent with the presence of a T_1 minimum. As discussed in the first chapter, in the ordered smectic and solid phases, C_3 reorientations of CH_3 groups in the end chains contribute to spin relaxation. Further, self diffusion and ordered fluctuations are expected to freeze in these phases. Another possible motion is the C_2 reorientation of the CH_2 groups. However, only the final CH_2 groups might undergo limited angular displacements, and hence do not form a strong source of spin relaxation (Thompson et al. 1977). Hence, the observed T_1 variation in this phase can be essentially attributed to the C_3 motion of CH_3 groups in the end chains. The relaxation rate in this phase can be written as

$$(T_1^{-1})_{RE} = C'' \left[\frac{\tau_{cE}}{1+\omega^2\tau_{cE}^2} + \frac{4\tau_{cE}}{1+4\omega^2\tau_{cE}^2} \right] \tag{3.4}$$

C", as explained in the first chapter depends on the geometry of the molecule under consideration and is given by $(9\gamma^4\hbar^2/10r^6)$ (27/6) (the factor 27/6 arises since only 6 out of 27 protons are present in the methyl groups that contribute to the relaxation). The above equation indicates a minimum at $\omega\tau_{cE}$ = 0.616 given by

$$(T_1^{-1})_{\min} = 1.43 \frac{C''}{\omega_1} \tag{3.5}$$

The T_1 minimum expected from this equation at 33.6 MHz is 91msec, while the experimental value obtained is 155 msec. This discrepancy could be due to dynamic inequivalence in the two methyl groups in the end chains (with different correlation times for the inequivalent groups). Multiplying eqn. (3.4) and eqn. (3.5) by 1/2 (if only one out of the two methyl groups contribute to relaxation) yields a T_1 minimum value of 182 msec, which is close to the experimental value of 155msec (thus confirming the inequivalent CH_3 groups). Assuming Arrhenius type of temperature dependence to the correlation times associated with this dynamics i.e.,

$$\tau_{cCH_3} = \tau_{oCH_3} e^{E_{aCH_3}/kT} \tag{3.6}$$

the activation energy associated with the dynamics of CH_3 can now be calculated by fitting the T_1 data in this phase to eqn. (3.6). Fig. 3.10 shows such a fit at two frequencies (15 and 39.6 MHz) with an activation energy of 7.8 ± 0.4 kCal/mole and a correlation time of τ_{oCH_3} = 1.48 X 10^{-15} s.

Dipolar relaxation

The T_{1D} process which samples the spectral densities at local dipolar fields is generally mediated by ODF. But as explained in 1.2.4, the spectral densities due to ODF are normally temperature independent except when these fluctuations are assisted by self diffusion of the molecules. Hence the observed temperature dependence of T_{1D} in nematic phase (Fig. 3.3) can be explained as due to diffusion assisted ODF. By fitting the temperature dependence of T_{1D} to Arrhenius model (Fig. 3.11), the activation energy associated with the diffusion process is calculated to be 7.6 ± 0.8 kCal/mole. This agrees with the E_{aD} measured from T_1 data. The sudden jump in T_{1D} at the smectic-I to smectic-II transition is attributed to sudden slowing down of diffusion processes in the smectic-II phase resulting in a steep increase in spectral density at frequencies corresponding to the local dipolar fields. T_{1D}^{-1} can be related to the correlation times of slow diffusion mechanisms (τ_D) in the strong collision limit as

$$T_{1D}^{-1} = \frac{2(1-P)}{\tau_D} \tag{0.7}$$

where (1 - *P)* is the geometric factor of the order of unity. The upper limit of the correlation time can be obtained when P = 0 from the above equation as 8 msec. The corresponding lower limit for the translational diffusion can be calculated from eqn. (1.84a) as $10^{-14} cm^2/sec$.

To summarize, the T_1 process in the nematic phase of 40.4 is mediated by self diffusion and reorientation of molecules around short axis. On the other hand, the

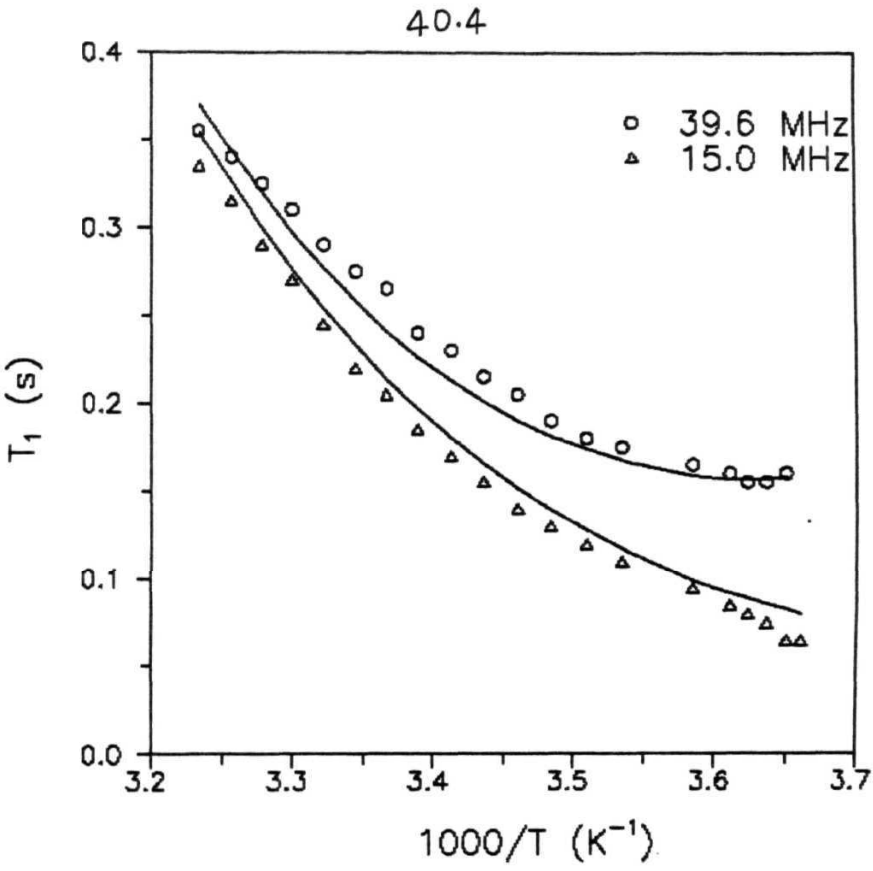

Fig. 3.10 Variation of T_1 with 1000/T in the 5///solid phase of 40.4. Solid line is the best fit line to the BPP expression.

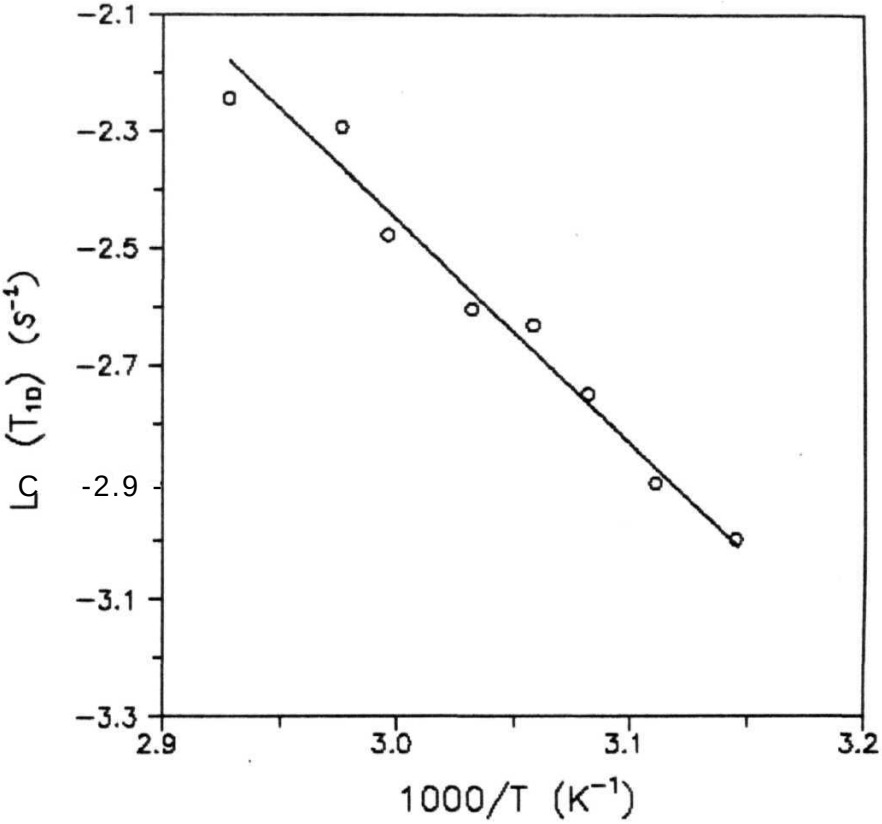

Fig. 3.11 Arrhenius fit of relaxation due to dipolar relaxation in the nematic phase of 40.4. Solid line is the best fit line.

Table. 3.5 : Activation energies associated with the different dynamic processes in 40.4

Relaxation process	dynamic process	Phase	Activationenergy (kCal/mole)
T_1	SD	Nematic	7.9 ± 0.4
	R around short axis		8.7 ± 0.4.
	R around end chains	Solid	7.8 ± 0.4
T_{1D}	SD assisted ODF	Nematic	7.6 ± 0.8

reorientational motions of CH_3 groups dominate the relaxation processes in ordered smectic and solid phases. These methyl groups are found to be dynamically inequivalent giving a BPP like T_1 minimum in the investigated temperature range. The order director fluctuations in the nematic phase as probed by the dipolar relaxation measurements seem to be diffusion assisted. The activation energies associated with the different dynamic processes are summarized in Table. 3.5

Section - 3

3.3 *Butyloxy benzylidene propylaniline (40.3)*

The second system studied in the series of 4O.m is butyloxy benzylidene propylanilene (40.3), with one CH_2 group less compared to 40.4. The system has the following phase sequence (Kei Murase, 1971)

/ 82.5 C *N* 54 C *X*

This system has a single mesophase (nematic) over a range of about 30°C. The compound is obtained from Frinton Laboratories and used without further purification.

3.3.1 Experimental results

Spin-lattice relaxation time measurements are done at 6 frequencies (5, 9, 15, 20, 39.6 and 50 MHz) and in a temperature range of 70° to room temperature, with an average interval of about 2°C (Fig. 3.12) (Tables 3.6a to 3.6f). Only three frequencies are shown in the figure for clarity. Beyond the isotropic - nematic transition temperature in the nematic phase, T_1 is both frequency and temperature dependent. A temperature independent T_1 is observed over about 10°C in the nematic phase near the transition from the isotropic phase.

As the system is further cooled, pre-transitional effects predominate T_1 near the nematic - solid phase transition, before it increases to a higher value at the transition.

Table 3.6a Variation of spin lattice relaxation time (T_1) with temperature <T> at 9 MHz (40.3)

T° C	T_1 (msec)	T° C	T_1 (msec)
76.2	385	55.0	305
74.9	363	54.8	304
72.0	348	53.8	361
69.8	358	53.5	321
69.8	344	51.2	335
69.5	361	49.0	308
68.0	355	46.0	268
67.5	354	45.3	268
67.5	343	44.0	243
67.0	360	44.0	271
65.3	359	41.5	238
64.8	341	41.0	257
63.3	351	39.5	232
63.2	359	38.8	214
62.0	346	37.5	225
61.0	360	36.5	216
60.5	335	34.0	214
60.0	328	31.5	192
59.0	305	30.8	173
59.0	296	29.2	128
57.5	299	28.0	88
57.0	283	24.0	208
56.5	277	22.0	286
55.3	310		

Table 3.6b Variation of spin lattict relaxation time (T_1) with temperature <T> at 15.0 MHz (40.3)

T° C	T (msec)	T° C	T_1 (msec)
74.5	416	51.5	332
73.8	393	50.3	304
71.3	409	48.0	414
69.3	398	47.3	360
68.0	417	46.0	362
64.0	378	43.8	323
62.5	370	41.0	328
60.8	378	36.0	255
59.5	366	34.5	226
57.0	347	29.0	130
56.0	353	28.0	140
54.0	337	23.5	242

Table 3.6c Variation of spin lattice relaxation time (T_1) with temperature (T) at 19.5 MHz (40.3)

T° C	T_1 (msec)	T° C	T_1 (msec)
79.0	380	50.5	341
76.0	415	49.0	317
74.0	411	47.0	312
72.0	450	46.5	387
70.5	445	45.0	377
69.2	430	43.8	351
69.0	447	42.3	352
68.8	460	41.0	319
67.5	469	38.5	284
63.8	455	36.0	261
62.8	419	34.0	221
60.0	396	33.0	226
59.0	365	30.0	185
57.2	398	27.0	165
56.0	371	26.5	200
53.3	367	25.0	624
53.0	366	23.0	600

Table 3.6d Variation of spin lattice relaxation time (T_1) with temperature (T> at 29.8 MHz (40.3)

T° C	T_1 (msec)	T° C	T_1 (msec)
77.0	493	50.5	420
77.0	492	49.8	448
74.8	486	48.5	412
73.5	488	47.0	403
73.0	485	46.0	383
70.0	501	45.5	384
69.0	484	43.8	369
65.8	452	41.0	329
63.0	427	41.0	328
60.5	429	41.0	318
58.5	408	37.5	301
57.3	399	37.0	270
56.8	401	33.5	254
54.0	398	30.8	249
53.3	436	29.5	264
53.0	382	28.0	295
51.3	437		

Table 3.6* Variation of spin lattice relaxation time (T_1) with temperature CT> at 39.6 MHz (40.3)

T^{o} C	T_1 (msec)	T^{o} C	T_1 (msec)
75.0	509	53.0	413
74.3	486	51.0	381
71.0	493	50.0	414
71.0	520	48.8	438
69.5	507	46.5	393
68.5	508	46.5	391
68.3	489	45.0	422
66.0	510	44.8	390
65.5	523	42.0	371
63.3	493	39.5	359
61.3	471	37.5	342
60.0	449	32.8	312
58.5	452	32.0	291
57.5	439	30.3	336
55.8	415	29.5	339
55.5	449	28.5	379
53.3	433	25.8	483

Table 3.6f Variation of spin lattice relaxation time (T_1) with temperature (T> at 50.0 MHz (40.3)

T° C	T_1 (msec)	T° C	T_1 (msec)
78.3	551	50.5	458
73.0	555	50.0	427
72.3	570	48.2	443
69.5	567	46.0	439
67.5	562	45.5	437
65.5	536	41.5	398
64.7	564	38.3	348
64.5	516	36.5	335
62.5	520	35.3	319
58.5	506	32.5	334
57.5	460	30.5	386
54.8	451	30.0	425
53.7	425	28.3	453
51.5	418	27.0	562

The T_1 in this phase is also dependent on temperature (decreases with decreasing temperature) and frequency. The T_1 minima obtained at each frequency becomes sharper and shifts towards the high temperature side as the frequency increases.

3.3.2 Analysis and discussion

Nematic phase

As in the case of 40.4, the frequency dependence of T_1 in 40.3 is also predominantly due to SD mechanism ($(T_1^{-1}) \propto \omega^{1/2}$ as shown in Fig. 3.13). The T_1 data of 40.3 is also fitted to eqn. (3.1) to obtain $(T_1^{-1})_{SD}$ and $(T_1^{-1})_{RS}$ (Fig. 3.14). The corresponding terms in the expression for $(T_1^{-1})_{SD}$ are explained in the first chapter. The relative contributions of SD and R mechanisms to the relaxation rate at a mid nematic temperature ($60°C$) are 58% and 42% respectively at 5 MHz and 32% and 68% respectively at 39.6 MHZ. The frequency dependence is further verified by repeating the above analysis for other temperatures as well. The diffusion coefficient $D\pm$ decreases with temperature (Table. 3.7). A ($i.e.(T_1^{-1})_{RS}$) which is independent of frequency, increases with decreasing temperature (Table. 3.8). The variation $(T_1^{-1})_R$ and $(T_1^{-1})_{SD}$ with temperature at 39.6 MHz is shown in Fig. 3.15 (Table 3.8).

Assuming the diffusion and reorientation processes to be Arrhenius, the diffusion coefficient $D_\perp$ and $(T_1^{-1})_{RS}$ are fitted to eqns. (3.2) and (3.3) respectively from which E_{aD} and E_{aS} are estimated to be 13.4 ± 0.4 kCal/mole and 6.2 ± 0.4 kCal/mole (Fig. 3.16 and Fig. 3.17).

Solid phase

A minimum in T_1 is observed as in the case of 40.4, but at relatively higher temperature at each frequency. This can be attributed to end chain reorientations as in the case of 40.4. Since, these minima are very close to the nematic - solid transition temperature, they may also be influenced by pretransitional effects. This is evident from the minima values which are not proportional to the Larmor frequency (eqn. (1.125)). Further, the shape of the minima is not the same at all frequencies as can be seen from the Fig. 3.12. Perhaps, this could be due to a wide distribution of

40.3

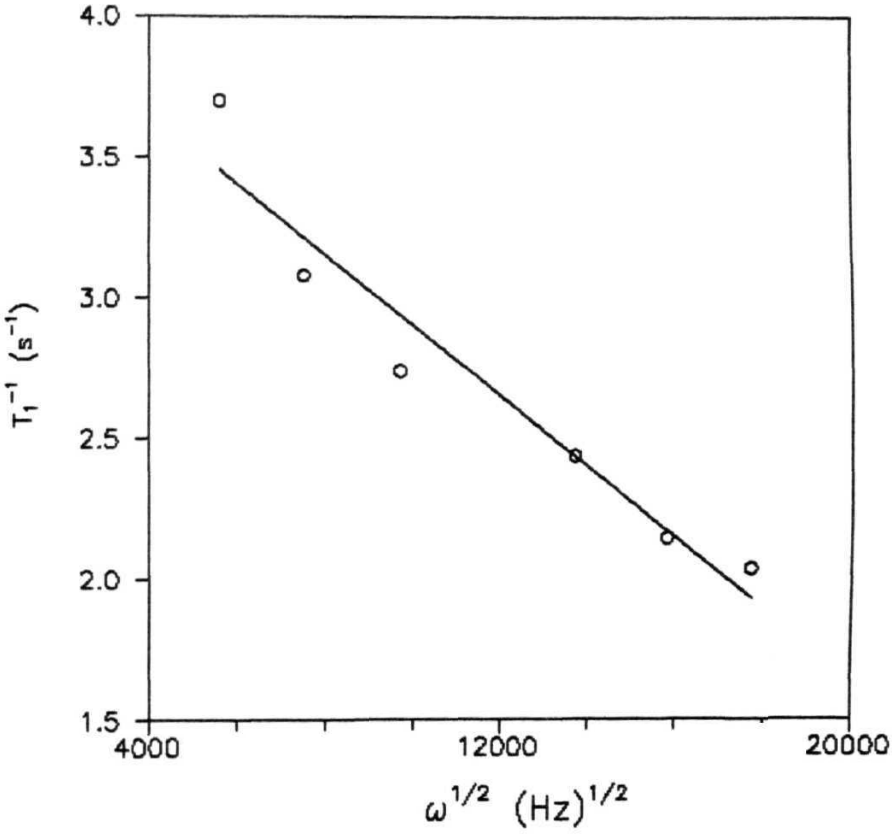

Fig. 3.13 Spin lattice relaxation rate T_1^{-1} as a function of square root of Larmor frequency $(\omega^{1/2})$ at a mid nematic temperature in 40.3. Solid line is the best fit line.

40.3

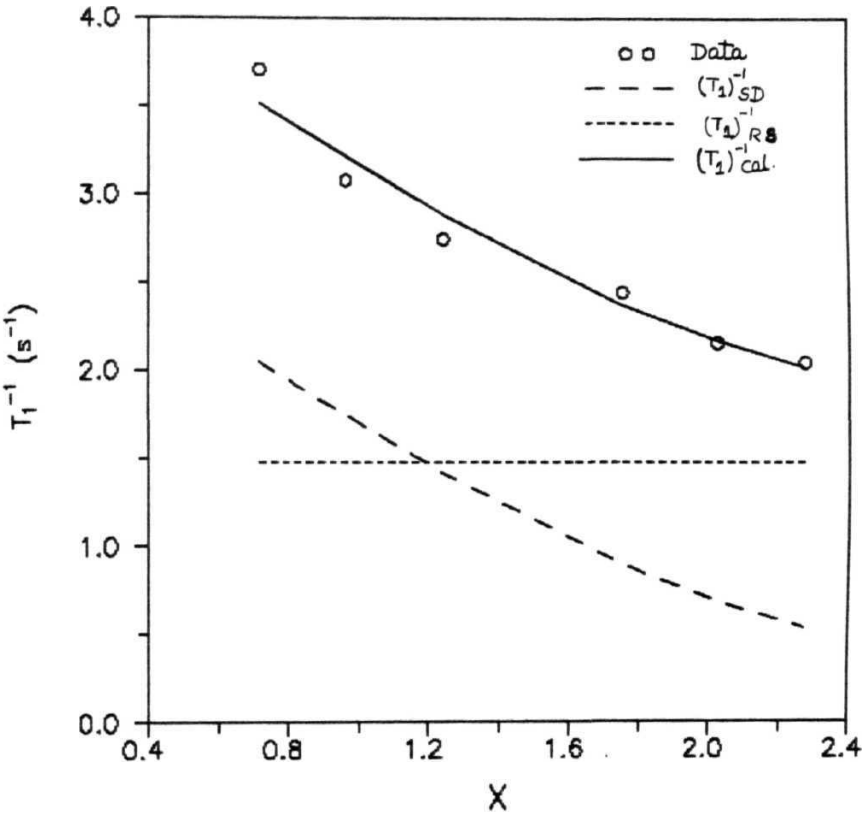

Fig. 3.14 Relative contributions of $(T_1^{-1})_{SD}$ and $(T_1^{-1})_{RS}$ to the relaxation rate in the nematic phase of 4O.3 (60°C)
x is a dimensionless quantity given by $\sqrt{\frac{\omega a^2}{2D}}$

Table 3.7 : Variation of $D_{\perp}$ with temperature in the nematic phase of 40.3.

T^{o} C	$D_{\perp}$ (x 1e-7 cm^{2}/sec)
65.0	1 .71
64.0	1 .74
63.0	1 .68
62.0	1 .66
61 .0	1 .59
60.0	1 .52
59.0	1 .42
58.0	1 .35
57.0	1 .25
56.0	1 .15
55.0	1 .07

Table. 3.8 : Variation of T_{1R}^{-1} and T_{1SD}^{-1} with temperature in the nematic phase of 40.3 (at 39.6 MHz)

T^{o} C	T_{1R}^{-1} (sec^{-1})	T_{1SD}^{-1} (sec^{-1})
65.0	1.29	0.69
64.0	1.33	0.69
63.0	1.36	0.69
62.0	1.40	0.69
61.0	1.44	0.69
60.0	1.47	0.69
59.0	1.51	0.69
58.0	1.57	0.69
57.0	1.62	0.68
56.0	1.66	0.67
55.0	1.74	0.66

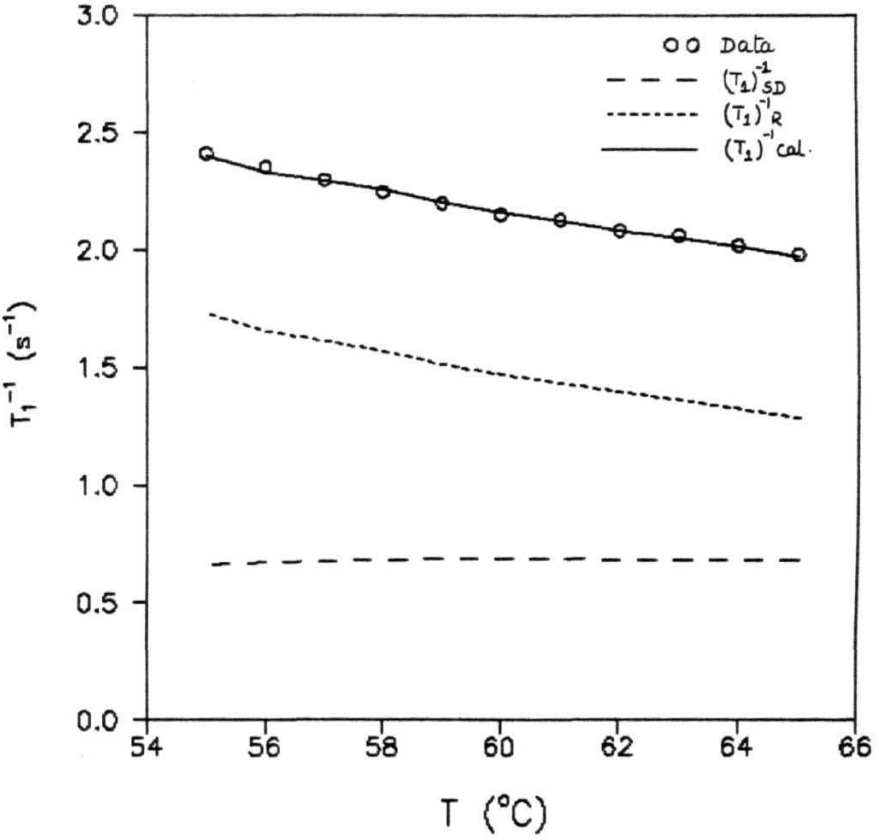

Fig. 3.15 Relative contributions of $(T_1^{-1})_{SD}$ and $(T_1^{-1})_{R}$ a function of temperature in the nematic phase at 39.6 MHz.

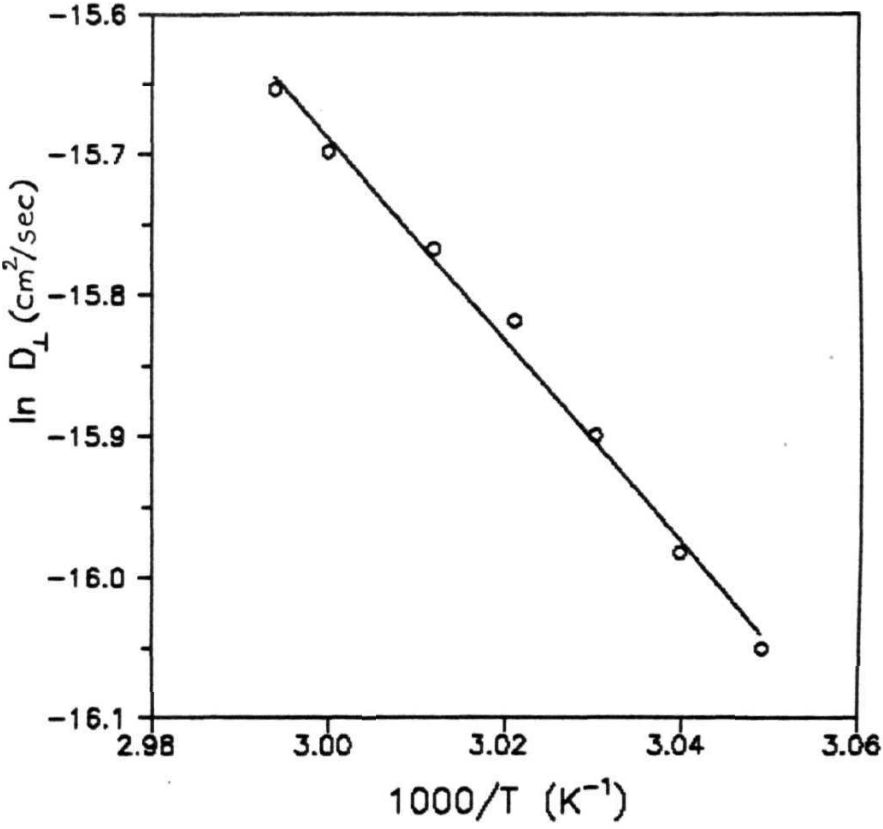

Fig. 3.16 **Arrhenius** plot of the diffusion coefficient *(D±)* in the nematic phase of 40.3. Solid line **is** the best fit **line.** to eqn (3.2)

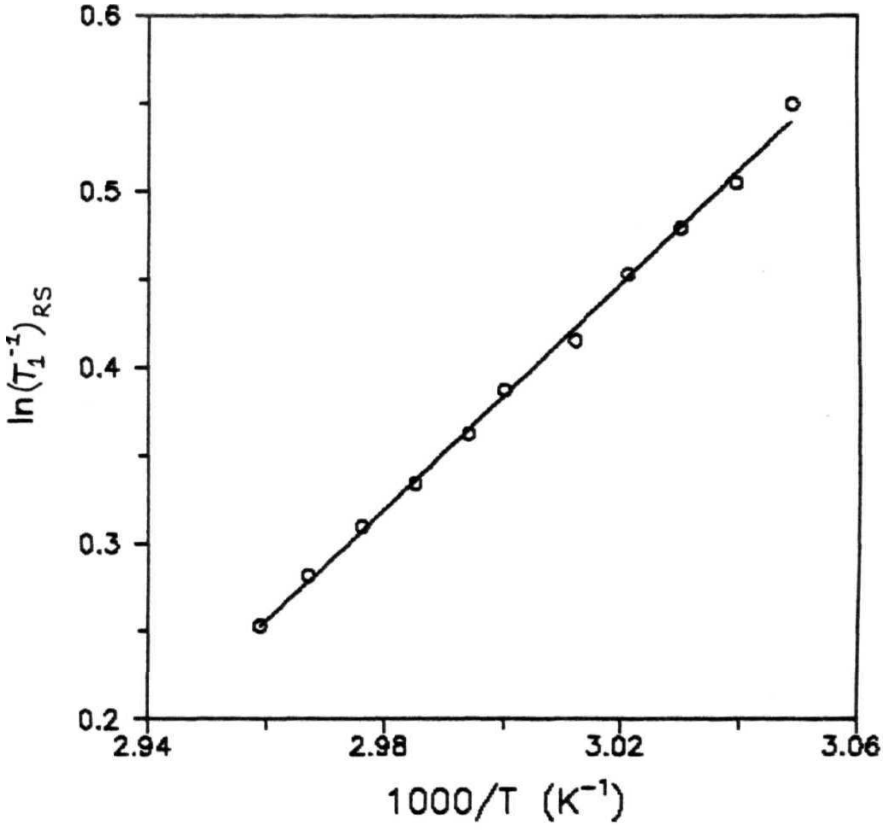

Fig. 3.17 Arrhenius plot of $(T_1^{-1})_{RS}$ in the nematic phase of 40.3. Solid line is the best fit line. to eqn (33).

Table. *3.3* : Activation energies associated with the different dynamic processes in 40.3

Relaxation process	dynamic process	Phase	Activation energy (kCal/mole)
T_1	SD	Nematic	13.4 ± 0.4
	R around short axis		6.2 ± 0.4

corresponding correlation times. Due to these complications, this data has not been used to obtain any dynamic parameters associated with the motions of end chains.

Thus the frequency dispersion and the temperature variation of spin-lattice relaxation time in the nematic phase of 40.3 can be accounted well by self diffusion along with molecular reorientations down to 5 MHz. In the solid phase, the frequency dispersion shows a minimum at each frequency shifting towards low temperature side with decrease in frequency, which can be attributed to contributions from the reorientations of end chains. It may be noted that these minima occur at relatively higher temperatures compared to that in 40.4. The activation energies associated with the different dynamic processes in 40.3, obtained from the above analysis, are summarized in Table. 3.9.

Section - 4

3.4 *Butuloxy benzilidene ethylanilene (4O.2)*

The third system studied in this series is butyloxy benzilidene ethylanilene (40.2). The system has the phase sequence (Kei Murase, 1971).

$$/ \quad \underline{66\,C} \quad N \quad \underline{51.5C} \quad S_{II} \quad \underline{39\ C} \quad X$$

It has a nematic phase over **14.5°C** and an ordered smectic phase *(Sn)* over 9° C. The compound is obtained from Frinton Laboratories, USA and used without further purification.

3.4.1 Experimental results

Spin-lattice relaxation measurements are made in the nematic, smectic - II and solid phases **(70°C** to RT) at an average interval of *2°C* in the frequency range 5 to 50 MHz (5, 9, 15, 19.5, 29.8, 39.6 and 50 MHz) (Tables 3.10a to **3.10f).** The temperature dependence of the T_1 profile in the nematic, smectic and solid phases is illustrated

Table 3.10a Variation of spin lattice relaxation time (T_1) with temperature <T> at 9 MHz (40.2)

T° C	T (msec)	T° C	T (msec)
61.8	220	51.8	341
61.0	315	49.5	301
58.0	246	48.0	286
56.8	277	44.0	245
56.5	255	42.3	241
55.0	212	39.3	196
53.5	227	35.0	96
52.5	253	32.0	87

Table 3.10b **Variation of spin lattice** relaxation **time** (T_1) with **temperature** (T> **at 9 MHz (40.2)**

T° C	T_1 (msec)	T° C	T. (msec)
67.6	216	50.5	326
66.0	219	50.5	264
65.5	203	50.0	344
63.5	**286**	48.5	324
63.2	286	48.5	356
62.3	292	47.5	322
60.5	304	**46.0**	299
59.2	287	**45.3**	311
59.0	319	44.3	301
57.5	**286**	43.0	297
56.6	285	40.8	234
56.3	313	37.9	157
54.5	302	35.4	**86**
54.0	292	35.3	94
53.5	293	34.8	87
53.5	283	33.5	87
52.5	**288**	33.3	71
51.6	274	32.2	96
51.3	270	32.0	94
50.5	264	30.0	97

Table 3.10c Variation of spin lattlct relaxation time (T_1) with temperature <T> at 15 MHz (40.2)

T° C	T_1 (msec)	T° C	T_1 (msec)
63.0	342	48.0	424
62.0	365	47.3	372
59.0	330	44.3	340
58.8	338	42.8	347
56.5	325	41.3	302
54.5	303	39.5	259
53.0	293	39.5	251
51.5	293	39.0	247
51.3	328	37.8	190
50.5	395	36.8	151
49.5	406	34.8	145
48.0	415	32.5	194

Table 3.10d Variation of spin **lattice relaxation time** (T_1) with **temperature** (T> at 19.9 MHz **(40.2)**

T° C	T_1 (msec)	T° C	T. (msec)
62.0	349	46.0	406
62.0	346	45.3	390
60.5	339	43.8	371
59.8	352	42.8	349
58.3	343	39.8	331
55.5	339	37.8	233
54.3	344	37.0	256
53.0	333	36.3	245
52.3	318	36.0	220
52.0	322	35.3	204
51.0	346	34.5	201
51.0	311	32.0	178
50.5	454	30.0	192
49.5	431	30.0	221
49.0	419	27.5	233
48.0	414		

Table 3.10e Variation of spin lattice relaxation time (T_1) with temperature (T) at 29.8 MHz (40.2)

T° C	T_1 (msec)	T° C	T_1 (msec)
65.5	405	46.0	390
63.8	413	44.0	387
58.5	401	43.0	375
59.5	405	41.5	349
57.8	405	40.0	342
54.5	388	37.5	321
51.8	375	36.5	302
50.5	479	35.5	313
50.0	439	32.8	325
49.3	451	30.0	355
47.5	410	28.8	376
47.3	430		

Table 3.10f Variation of spin lattice relaxation time (T_1) with temperature (T> at 90.0 MHz (40.2)

T° C	T. (msec)	T° C	T_1 (msec)
63.8	443	51.8	375
62.3	442	50.0	557
61.3	444	48.5	522
59.8	448	47.5	487
59.5	445	46.5	480
59.0	450	46.3	452
56.5	451	43.3	409
55.5	450	41.5	398
54.8	430	40.0	418
53.8	406	38.0	491
52.8	395	36.0	532
52.0	413	34.3	600

in Fig. 3.18 at three frequencies. In all the cases, T_1 is frequency dependent, but, independent of temperature in the nematic phase with pretransitional effects near the nematic to smectic -II transition. There is a significant discontinuity in T_1 at the transition as indicated by the drastic increase in the T_1 values. There is no change in the variation of T_1 near smectic -II to crystalline transition temperature. As in the case of 40.4 and 40.3, the T_1 in the ordered smectic and the crystalline phase is both frequency and temperature dependent with a minimum at each frequency shifting towards lower temperatures with decreasing frequency.

3.4.2 Analysis and discussion

Nematic phase

The temperature independent data in the nematic phase suggests that SD is not a major contributing mechanism to the relaxation. Hence the data is fitted to a model consisting of order director fluctuations (ODF) and reorientations, i.e.,

$$T_1^{-1} = A + (T_1^{-1})_{ODF} \tag{3.8}$$

The constant term in the above expression denotes the frequency independent contribution from the reorientations around short axes. The data fits to the above model with $(T_1^{-1})_{ODF}$ $B\omega^{-1/2}$. The relative contributions from ODF and R at 5 MHz are 74% and 26% respectively and are 54% and 46% at 29.8 MHz respectively (Fig. 3.19) at $60°C$ in the nematic phase. Thus, ODF contributes to the relaxation in the nematic phase till 50 MHz, the maximum frequency of measurement in these experiments. The analysis is repeated at different temperatures in the nematic phase to obtain the temperature dependences of $(T_1^{-1})_{ODF}$ and $(T_1^{-1})_{RS}$. It is found that both these quantities are temperature independent in the entire nematic phase. The temperature independence of $(T_1^{-1})_{RS}$ in the nematic phase indicates that the activation energy associated with reorientations is very small in this compound.

The jump in T_1 near the nematic to smectic transition indicates the sudden slowing down of molecular motions, due to the onset of translational order within the layers

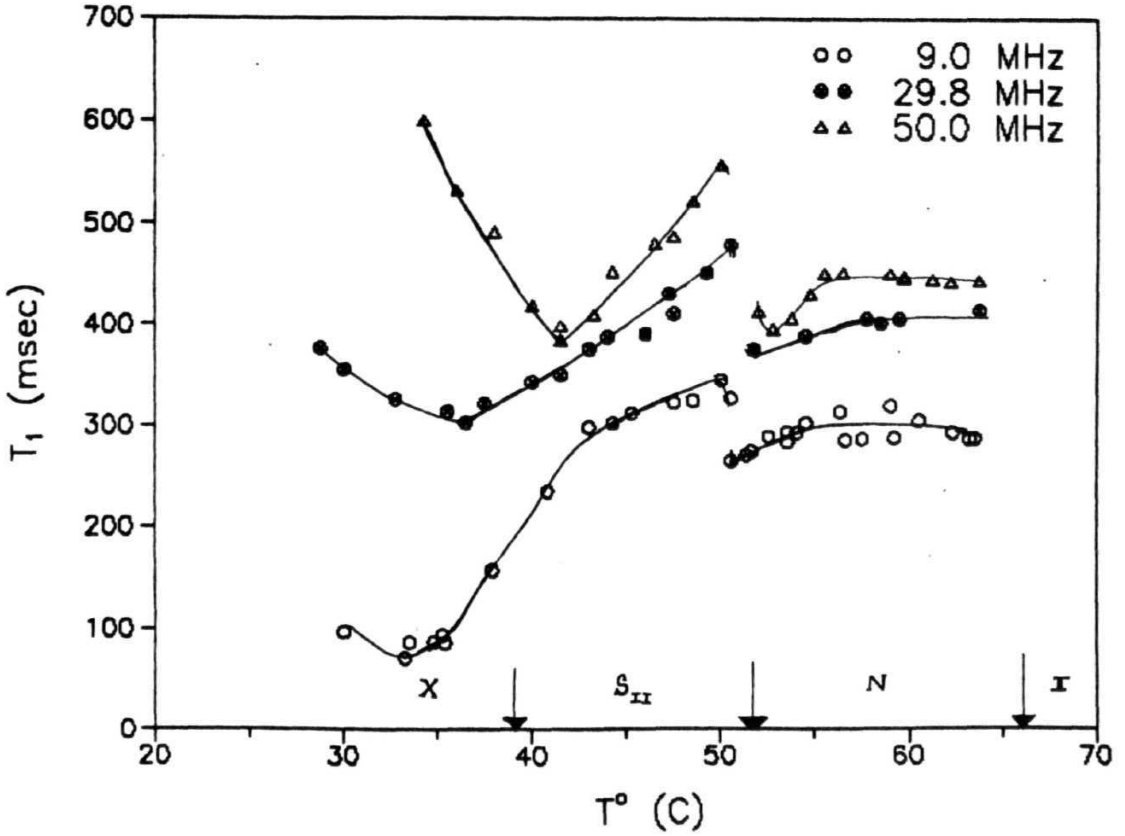

Fig. 3.18 Spin lattice relaxation time T_1, at three frequencies as a function of temperature in 4O.2. Solid lines are drawn as guide to the eye. The vertical lines denote the transition temperatures.

40.2

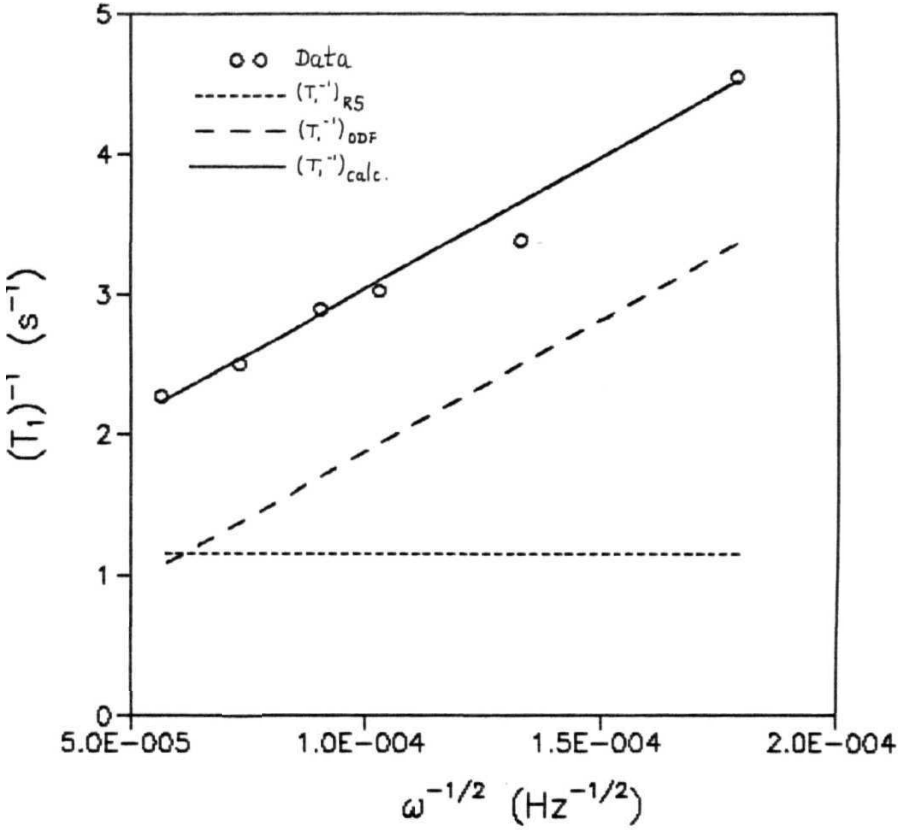

Fig. 3.19 Variation of $(T_1^{-1})_{ODF}$ and $(T_1^{-1})_R$ as a function of $(\omega^{-1/2})$, in the nematic phase of 40.2. (at 60°C)

of smectic phase.

Ordered smectic and solid phase

The observed frequency and temperature dependent T_1 data in the solid phase resemble a BPP type behavior and can be attributed to reorientations of end chains as in 40.4 and 40.3. The T_1 minimum shifts towards lower temperatures with decreasing frequency. Since these minima are very close to the nematic to smectic - II transition temperature, these are predominantly influenced by the pretransitional effects (as seen from the T_1 minima which are not proportional to the Larmor frequency). The variation in the shape of the minima as a function of frequency (Fig. 3.18) suggest wide distribution of correlation times associated with the reorientations of end chains. This does not allow calculation of any meaningful dynamic parameters from this data. But an interesting point to note is, this minimum shifts further to higher temperatures compared to 40.4 and 40.3 at any given frequency.

Thus order director fluctuations along with the molecular reorientations around the short axis are responsible for the spin lattice relaxation in the nematic phase of 40.2. The reorientations are essentially independent of temperature throughout the nematic phase. In the ordered smectic or solid phase, frequency and temperature variation of T_1 are observed with a minimum at each frequency which should be due to the reorientaion of end chains.

Section - 5

3.5 *CONCLUSIONS*

Comparison of the results obtained in the above three compounds with earlier observations show an interesting trend. Earlier studies indicated a shift in the cutoff frequency associated with the collective fluctuations towards higher frequency side as the length of alkyl chain is increased. If this trend were to follow, the T_1 process in compounds with smaller end chains (compounds of the present work i.e. 40.4, 40.3 and 40.2) should have a very low upper cutoff frequency for order director fluc-

tuations and hence their relaxation mechanism must be predominantly due to self diffusion in the frequency range of interest (MHz).

As expected, the relaxation is mediated by self diffusion in 40.4 and 40.3 down to 5 MHz. But interestingly, order director fluctuations dominate the relaxation mechanism in 40.2 upto 50 MHz (highest frequency of study). From these results, it seems that the contribution from ODF extends to higher frequencies, whenever the size of the end chains on either side of the core is considerably different. Table. 3.11 summarizes the molecular weight of the end chains of various nO.m type compounds studied so far (including the present systems). As can be seen, 40.3, 40.4, 40.5 (Ravindranth, 1991), 40.6 (Venu • et al. 1990), 40.7 (Ravindranath et al. 1990a) etc., which have ratio of molecular weights for the end chains on either side of the core less than 1 : 2, exhibit self diffusion as dominating relaxation mechanism down to 5 MHz. This shows that, for compounds with balanced end chains, the cutoff frequency for ODF is well below 5 MHz, confining the ODF contribution to lower frequencies. On the other hand, in compounds like 40.8 (Owers-Bradley 1981) 40.9 (Ravindranth et al. 1993), 40.2 for which the molecular weights on either sides are considerably different, ODF seems to be spreading to higher frequencies. Thus cutoff frequencies for ODF in these compounds seem to be in tens of MHz region.

60.2 and 6O.Br (obtained by replacing the aliphatic chain on one side by Br) also confirm to this picture. 60.2 with highly imbalanced end chains shows ODF contribution upto the highest frequency of study (40 MHz) (Ravindranath, 1991). But, as seen from the Table. 3.11, the end chains of 6O.Br are well balanced and hence it exhibits self diffusion down to 2 MHz, indicating that the ODF contribution is confined to well below 2 MHz. 10.4 (MBBA), on the other hand, has fairly balanced end chainsand exhibits ODF only below 1 MHz.

It will be interesting to examine the factors determining the cutoff frequencies for order director fluctuations. The upper cutoff frequency (for isotropic elastic coefficient) is given by (Vold and Vold, 1988)

$$\omega_c = \frac{K\pi^2}{\lambda_c \eta} \qquad (3.8)$$

Table. 3.11 : Ratio of molecular weight of end chains and its influecne on molecular dynamics in nO.m compounds

Compound	Molecular weight		Ratio	Mediating mechanism
	nO	m		
40.2	73	29	1.00 : 0.40	ODF + R
40.3	73	43	1.00 : 0.60	SD • R
40.4	73	57	1.00 : 0.80	SD • R
40.5	73	71	1.00 : 0.97	SD + R
40.6	73	85	0.86 : 1.00	ODF (< 10 MHz) SD • R <> 10 MHz)
40.7	73	99	0.74 : 1.00	SD + R
40.8	73	113	0.65 : 1.00	ODF + R
40.9	73	127	0.58 : 1.00	ODF • SD + R
60.2	101	29	1.00 : 0.30	ODF + R
60.Br	101	79	1.00 : 0.80	SD + R
10.4	31	57	0.54 : 1.00	SD + R

where λ_c is the lowest wavelength of the order of the molecular dimension. The viscosity 77 is related to the twist viscosity coefficient given by (de Gennes, 1974)

$$\eta_1 = \gamma_1 - \frac{(q_\perp^2 \alpha_3 - q_z^2 \alpha_2)^2}{q_\perp^4 \eta_b + \eta_\perp^2 q_z^2 (\alpha_1 + \alpha_2 + \alpha_4 + \alpha_5) + q_z^4 \eta_c} \tag{3.9}$$

Here α_1, α_2, α_3, α_4 and α_5 are the Leslie coefficients given by $\gamma_1 = \alpha_2 - \alpha_3$ and $\gamma_2 = \alpha_5 - \alpha_6$.

It is clear from eqn. (3.8) that the cutoff frequency decreases whenever the molecular dimensions increase or γ_1 increases or in both the cases. The width of the molecule 'a' remains the same while the length of the molecule increases as the end chain length increases in the present series. This results in a decrease in the cutoff frequency as the end chain length is increased and hence can not be the reason for the appearance of ODF at higher frequencies in homologues with longer end chains. As no information is available regarding the dependence of viscoelastic coefficients of nO.m compounds on the end chain length, their effects on the cutoff frequencies are not known. But, the present results seem to be suggesting that the cutoff frequencies sensitively depend on the details of the end chains, apart from the factors considered in eqn. (3.8).

Another interesting trend that emerges from the present experiments is that though there is no definite trend regarding the variation of e activation energy associated with molecular reorientations, (as the end chain length is varied), the activation energy associated with reorientations around short axes become small as the ODF contribution increases (like in 40.2, 40.6, 40.8, 40.9, 60.2 etc.,). The reorientations that dominate the T_1 process in the nematic phase of these systems are the reorientations around the short axis. It is difficult to distinguish these individual reorientations from ODF in the short wavelength limit (when the wavelength is of the order of the molecular dimensions). If the order fluctuations are extending to higher frequencies (appearance of lower wavelength modes) as in 40.2, 40.8, 40.9, 60.2 etc., it is expected that the individual reorientation motions should become easier. Hence

an increase in the **contribution** from ODF to high **frequencies** should correspond **to** easier reorientations and consequently, a lesser activation energy for reorientations.

Even though there seems to be no systematic dependence of diffusion coefficient on the end chain length, the corresponding activation energies show some interesting trend. Fig. 3.20 shows that the variation of activation energy associated with the self diffusion process in the nematic phase of 4O.m compounds as a function of end chain length. From the above figure, it is clear that the diffusion process seems to be becoming more hindered as the end chain length decreases. This is interesting and contrary to the earlier expectations (Thompson et **al.** 1989) that the diffusion process should become easier as the end chain length is decreased.

Similar comparison can be made about the reorientations of end chains in the ordered smectic/solid phases. Fig. 3.21 shows the variation of corresponding activation energy as a function of end chain length. It can be seem from this figure that the reorientations of end chains become more hindered as the end chain length is decreased. Even though no activation energy could be measured for 40.3 and 40.2, the shift of T_1 minima observed in the solid/ordered smectic phases towards higher temperature side indicates further increase in the corresponding activation energy. Thus, it appears, as the end chain length is reduced from 40.9 to 40.2, the dynamics of the end chains slow down so much that for 40.4 and lower homologues the corresponding minima are seen above 0° C. This shows that possibly the packing of the end chains is increasing as the end chain length is decreased. Even though these observations correspond to ordered smectic/solid phases, they compare qualitatively with that of self diffusion process in nematic phase. Hence, the reason for increase in hindrance for self diffusion and end chain reorientations as the end chain length is reduced seems to be the same viz. better packing of molecules for smaller end chain lengths.

Thus, these results on the whole show that all these dynamic processes viz. **ODF,** self diffusion and individual reorientations are rather sensitively dependent on the details of end chains, even if the structure of the core is the same. Particularly, the results on **ODF** viz. increase in the cutoff frequencies, whenever **the end** chains on

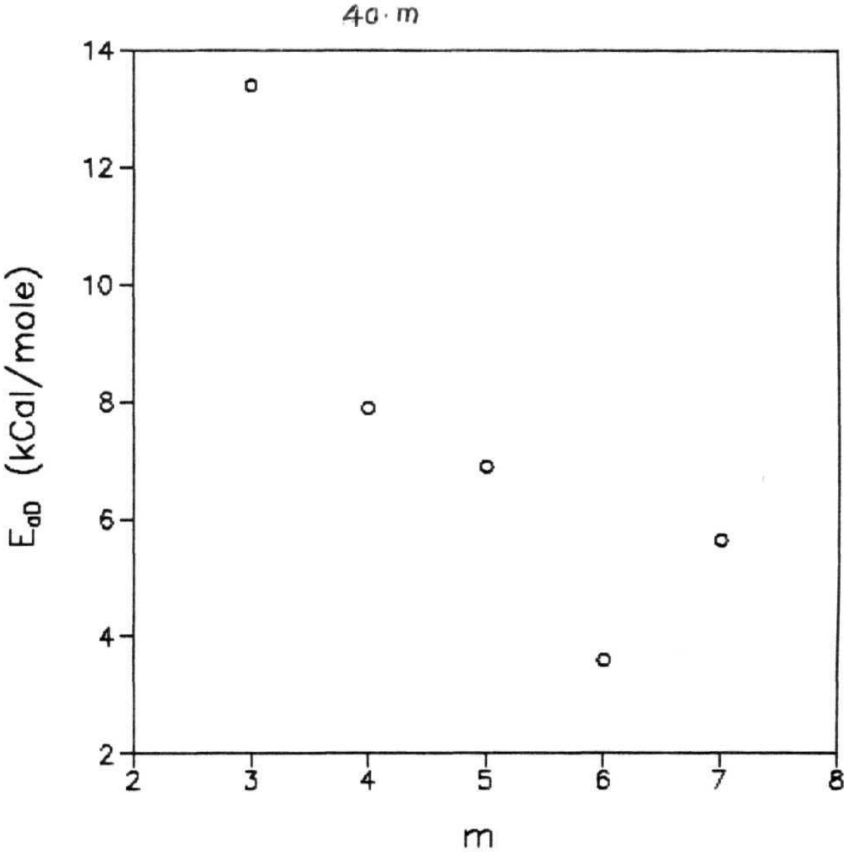

Fig. 3.20 Variation of activation energy associated with the self diffusion (in the nematic phase) as a function of the end chain length in **4O.m** systems.

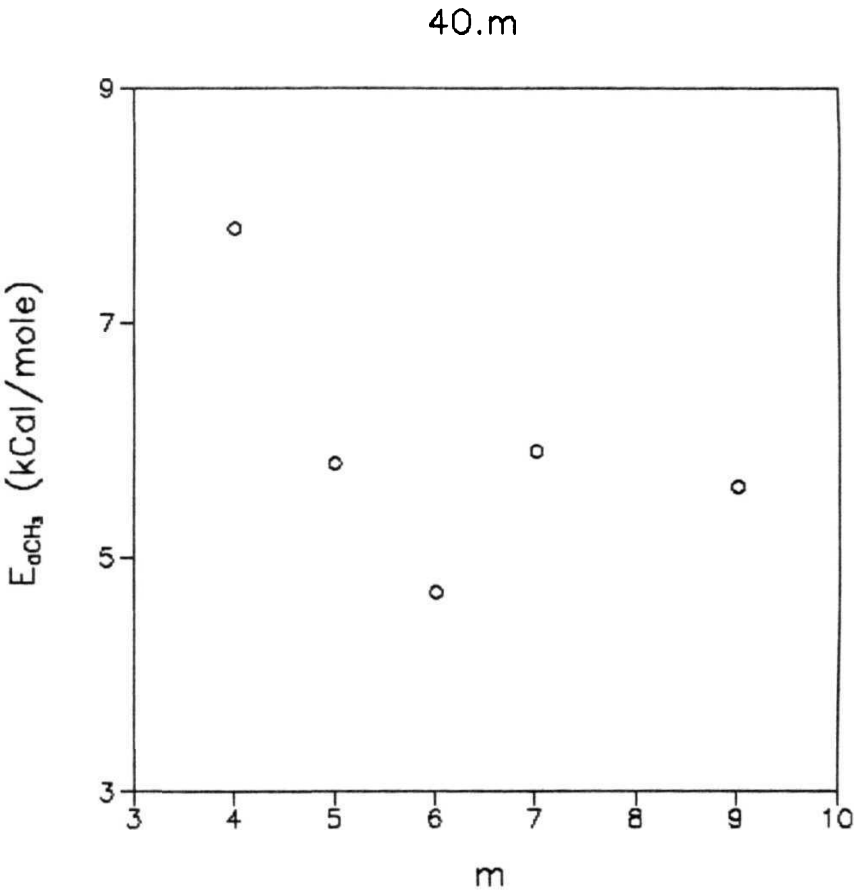

Fig. 3.21 Variation of activation energy associated with CH_3 rotations (in the ordered smectic/solid phases) as a function of end chain length in **40.m** systems.

either sides of the molecules are sufficiently imbalanced. There may also be even odd effect over and above this variation. But the present results are largely qualitative and more quantitative information on the dependence of cutoff frequency associated with ODF will be very interesting from this point of view. Such information can be obtained from low frequency NMR studies.

Chapter 4

MOLECULAR DYNAMICS IN ALKYLOXY BENZOIC ACIDS

Molecules of para-alkyloxy benzoic acids form liquid crystalline mesophases for n (number of carbons in alkyl chains) larger than 3 (Von B. Etenberg et al. 1983). Large percentage of molecules in these compounds form dimers which constitute the basic nematic lattice and less than 10% of the molecules are monomers which are highly mobile. The physical properties and molecular dynamics of this homologous series vary in an interesting manner as a function of molecular structure and hence has been attracting considerable attention (Deloche and Cabane, 1972 ; Marcelja, 1974 ; Thompson et al. 1977 ; Ikeda and Hatakeyama, 1977 ; Thomspson et al. 1989). This chapter presents the results of proton NMR experiments carried out in two liquid crystalline samples belonging to this homologous series. The first section presents a brief review of the earlier studies on these systems. The results and the discussions on two systems, p-heptyloxy benzoic acid and p-nonyloxy benzoic acid are presented in the second and third sections respectively. The final section presents the conclusions arrived at from the present studies.

4.1 *Review on benzoic acids*

The general molecular structure of the systems belonging to this series is given in Fig. 4.1. Earlier works on the members of this series include *X*-ray structural analysis (Bryan et al. 1980), ultra sound absorption studies (Kapustin and Bikova, 1968), dielectric loss studies (Chou and Carr, 1973), IR studies (Ikeda and Hatakeyama, 1977 ; Kirov et al. 1981), Raman studies (Kirov et al. 1981) and DSC measurements (Ikeda and Hatakeyama, 1977 ; Hatakeyama and Ikeda, 1978) apart from NMR relaxation studies (Deloche and Cabane, 1972 ; Thompson and Pintar, 1976 ; Thompson et al. 1977, 1989).

Recent proton magnetic relaxation studies on a number of compounds belonging to this series (Thompson et.al., 1989) were aimed at obtaining information on different dynamical processes contributing to spin relaxation and on the variation in these dynamical parameters as the length of the alkyl chains (and hence molecular mass) is varied. The methodology employed was to measure the spin lattice relaxation time (T_1) as a function of frequency, spin lattice relaxation time in rotating frame ($T_{1\rho}$) as a function of the locking field strength, H\ and dipolar relaxation time, (T_{1D}) in one compound (*p*-decyloxy benzoic acid, pDBA), similar to the methodology adopted in the present case. However, the method of analysis of this data to obtain the contribution to spin lattice relaxation from two important mechanisms viz., order director fluctuations (ODF) and self diffusion (SD) was different from the present analysis. Assuming the contributions from ODF to be mainly from the protons in the core (and hence should be the same for all the other members of the series but for a scaling factor corresponding to the ratio of protons in the core to the total number of molecules), the contribution from ODF is obtained for pDBA (Thompson et al. 1977). These results were utilized to analyse the data of other members of the homologous series to obtain the contribution from SD which was assumed to be frequency independent and same as that of the isotropic case (Miljkovic et al. 1976 ; Thompson et al. 1989). It was found that diffusion slows down as molecular mass

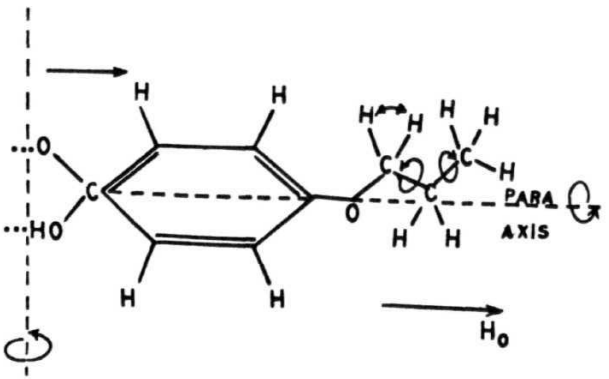

Fig. 4.1 Typical molecular structure of alkyloxy benzoic acids

increases. However, this analysis did not consider the contribution from reorientations which is known to be one of the major mechanisms for relaxation in liquid crystalline mesophases (Blinc et al. 1978).

The results on the systems belonging to 4O.m series, presented in the previous chapter, have clearly shown that contribution from ODF is sensitive to the end chains, the aromatic core being the same in all the systems of this homologous series. In fact, the cutoff frequenceis and the frequency dependence of ODF change in a complicated manner as the length of the end chain is varied. Further, it is well known that molecular reorientations lead to considerable contribution to the relaxation process. Finally, self diffusion (SD) is a frequency dependent mechanism (not a white spectrum), following the Torrey's theory appropriately modified for anisotropic medium. In view of the above, it is necessary to independently study each member of any homologous series by properly accounting for contribution from each dynamic process. The present work aims at proton NMR studies on two benzoic acids viz., *p* - heptyloxy benzoic acid (pHepBA) and *p* - nonyloxy benzoic acid (pNBA). The methodology used is similar to the one adopted for the nO.m type compounds.

Section - 2

4.2 *p - Heptyloxy benzoic acid (pHepBA)*

This system, *p*-heptyloxy benzoic acid (pHepBA), with a molecular structure given in Fig 4.1 has the phase sequence

/ 146*C* *N* 99C 5/ 91*C* *X*

S/ phase is a high temperature smectic phase like S_A phase . The sample is obtained from Frinton Laboratories, USA and used without further purification. The Zeeman spin lattice relaxation measurements are made as a function of temperature covering all the mesophases (150°*C* to *RT)* at five frequencies (6, 10, 20, 30 and 40 MHz). Spin

lattice relaxation measurements at dipolar fields (T_{1D})are also made as a function of temperature at 40 MHz.

4.2.1 Experimental results

The variation of spin lattice relaxation times as a function of temperature at three Larmor frequencies is shown in Fig. 4.2. The data is presented in Tables 4.1a to 4.1e. The general features of the data and values of *T*\ compare well, within the experimental errors, with that of earlier studies (Thompson et al. 1977). T_1 is observed to have frequency dispersion along with temperature dependence in the nematic and 5/ phases, with no observable change of slope at the nematic to 5/ transition. In the S_I phase, pretransitional effects are seen few degrees before the S_I to solid transition temperature and the T_1 increases drastically (from about 300 msec to 12 sec) at the transition to the solid phase. In the solid phase, *T*\ is independent of frequency and decreases with decrease in temperature. The variation of dipolar relaxation time as a function of temperature in all these phases in shown in Fig. 4.3. T_{1D} decreases with decreasing temperature in nematic and 5/ phases before dropping from about 100 msec to 2.5 msec (in about *2°C)* at the 5/ to the solid phase transition (Table. 4.2).

4.2.2 Analysis and Discussion

Nematic Phase

As mentioned above, more than 90% of the molecules in these compounds form dimers, resulting in a rigid core consisting of two benzene rings and aliphatic end chains on either sides. Hence, spin relaxation theory described in the first chapter, meant for long rod like molecules are applicable to the present systems also. The frequency dependence of T_1 in liquid crystals arise due to either ODF or self diffusion, whereas the temperature dependence is due to either self diffusion or reorientations. Through a preliminary analysis, by fitting the frequency dependence of T_1 at a given temperature to $\omega^{1/2}$ type of variation, it is found that SD alone could not account for the observed frequency dependence (Fig. 4.4a), while the data fits fairly well to $\omega^{-1/2}$ variation (Fig. **4.4b).** Thus, neither SD nor ODF alone could account for

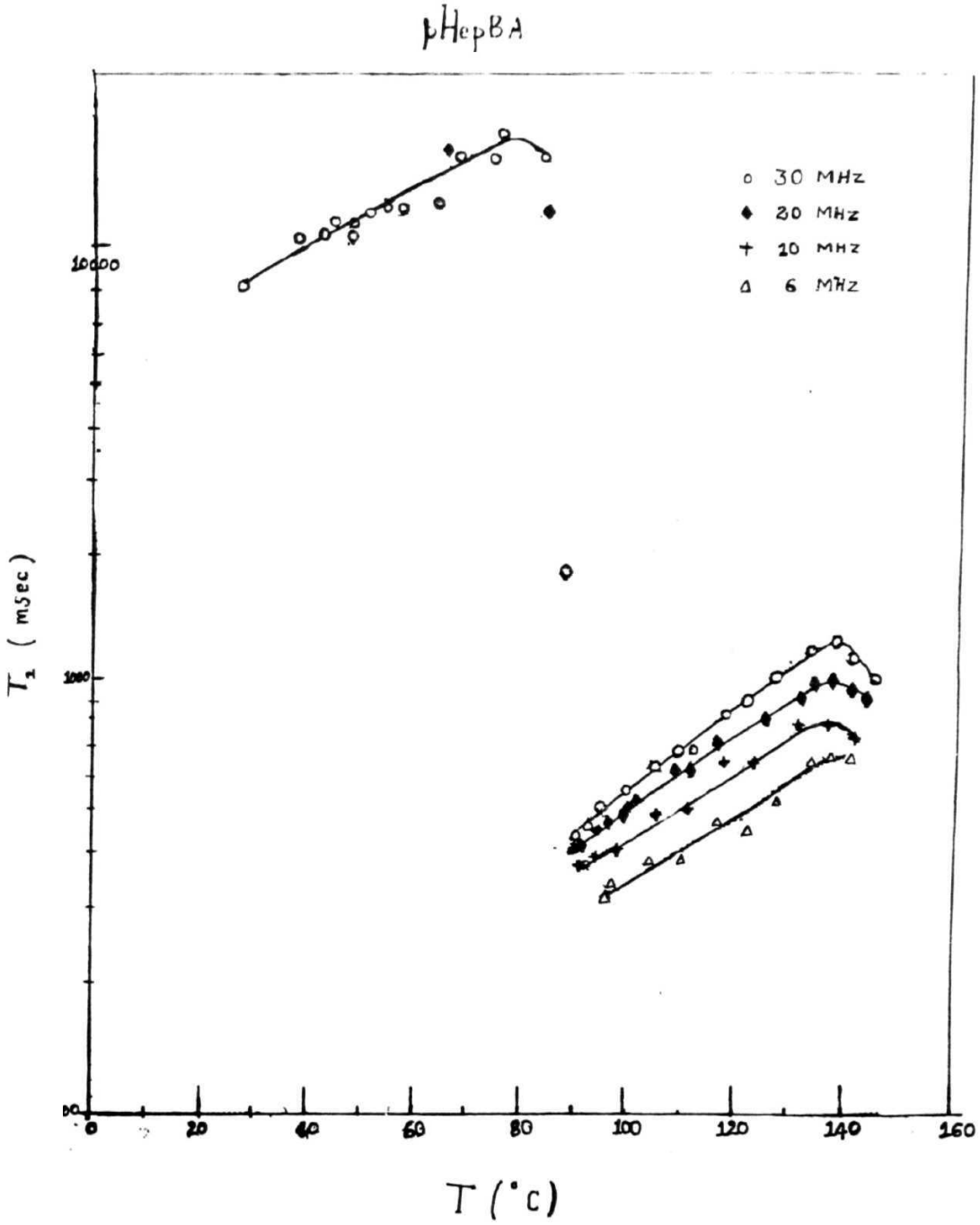

Fig. 4.2 Spin lattice relaxation time T_1, as a function of temperature T at three frequencies in pHepBA. Solid lines are drawn as a guide to the eye The vertical lines denote the traiisition temperatures.

Table 4.1a Variation of spin lattice relaxation time (T_1) with temperature <T> at 6 MHz (pHepBA)

T° C	T_1 (msec)	T° C	T_1 (msec)
143.0	654	122.5	456
141.0	681	110.0	398
138.5	533	104.0	390
137.0	633	96.5	337
137.0	666	95.5	319
134.0	654	91.0	391
132.0	658	90.0	406
128.0	531		

Table 4.1b Variation of spin lattice relaxation time (T_1) with temperature (T) at 10 MHz (pHepBA)

T° C	T_1 (msec)	T° C	T_1 (msec)
155.5	662	111.5	515
150.5	672	105.0	497
143.0	807	98.5	404
142.5	733	94.0	396
137.0	797	91.0	383
130.5	706	89.5	770
123.5	659	81.5	11810
117.5	649		

Table 4.1c Variation of spin lattice relaxation time (T_1) with temperature (T) at 20 MHz (pHepBA)

T° C	T_1 (msec)	T° C	T_1 (msec)
152.5	799	110.5	634
144.0	957	109.0	634
144.0	931	104.5	621
143.0	985	100.0	534
141.0	946	99.0	499
137.5	1014	94.0	484
134.5	996	91.0	424
132.0	923	87.5	1810
125.5	817	79.0	7800
123.0	966	74.5	10980
116.0	749	65.5	17260

Table 4.1d Variation of **spin** lattice relaxation time **(T_1)** with temperature (T) at 30 MHz **(pHepBA)**

T° C	T_1 (msec)	T° C	T_1 (msec)
145.0	1015	88.0	1802
141.0	1137	84.0	12320
139.0	1312	80.0	12830
133.0	1173	80.0	12640
130.0	1037	72.0	12960
127.0	931	64.0	13400
122.0	912	60.0	**11860**
118.0	851	57.0	13200
114.0	849	55.0	12790
111.0	685	51 .0	12520
109.0	627	48.0	**11370**
105.0	658	48.0	10990
101.0	543	44.0	**11600**
100.0	512	43.0	**11130**
99.0	562	39.0	10639
98.0	565	28.0	8237
96.0	492		
95.0	509		
92.0	476		
90.0	445		

Table 4.1e Variation of spin lattice relaxation time (T_1) with temperature (T) at 40 MHz (pHepBA)

T° C	T_1 (msec)	T° C	T_1 (msec)
145.5	1115	113.5	755
138.0	1092	108.0	733
138.0	1141	102.5	612
136.5	1107	96.5	547
132.5	1115	92.0	522
127.5	1029	90.0	7698
127.0	918	77.0	11880
118.5	900		

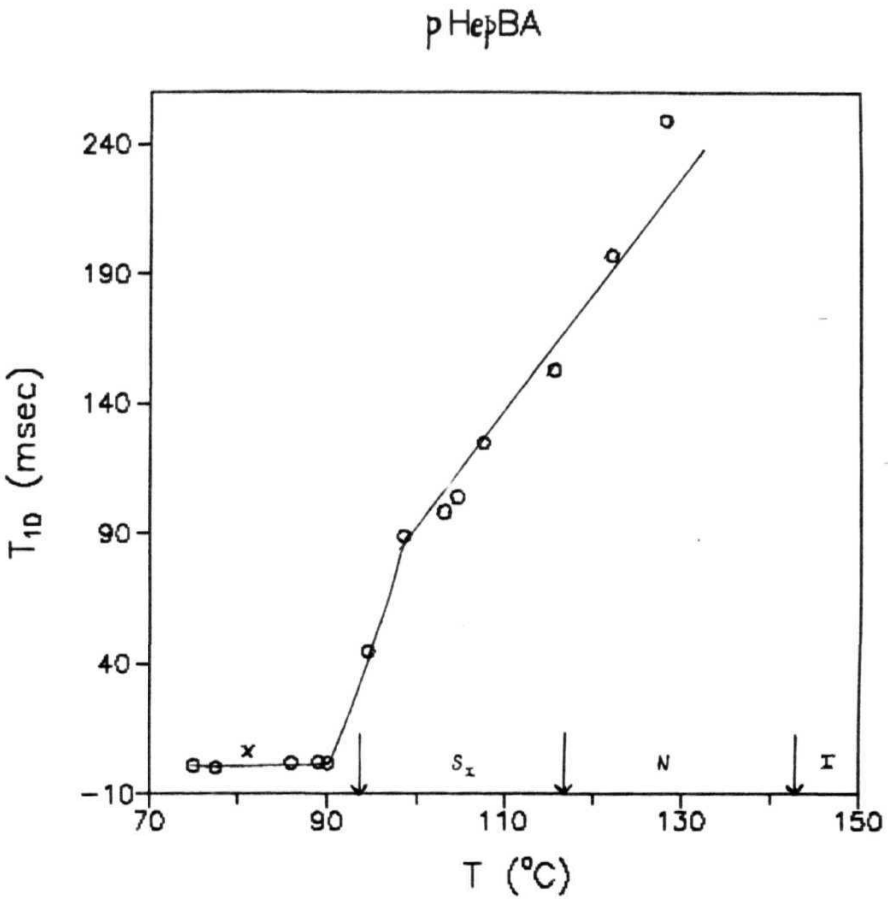

Fig. 4.3 Variation of dipolar relaxation time T_{1D}, as a function of temperature in pHepBA. Solid line is drawn as a guide to the eye.

Table 4.2 Variation of dipolar spin lattice relaxation time (T_{1D}) with temperature (T) at 40 MHz (pHepBA)

T° C	
144.5	184
141.0	229
140.0	205
128.0	249
122.0	197
117.0	140
115.5	153
107.5	125
107.0	98
104.5	104
103.0	98
98.5	89
94.5	45
90.0	2
89.0	2.4
86.0	2.0
77.5	0.2
75.0	1.0

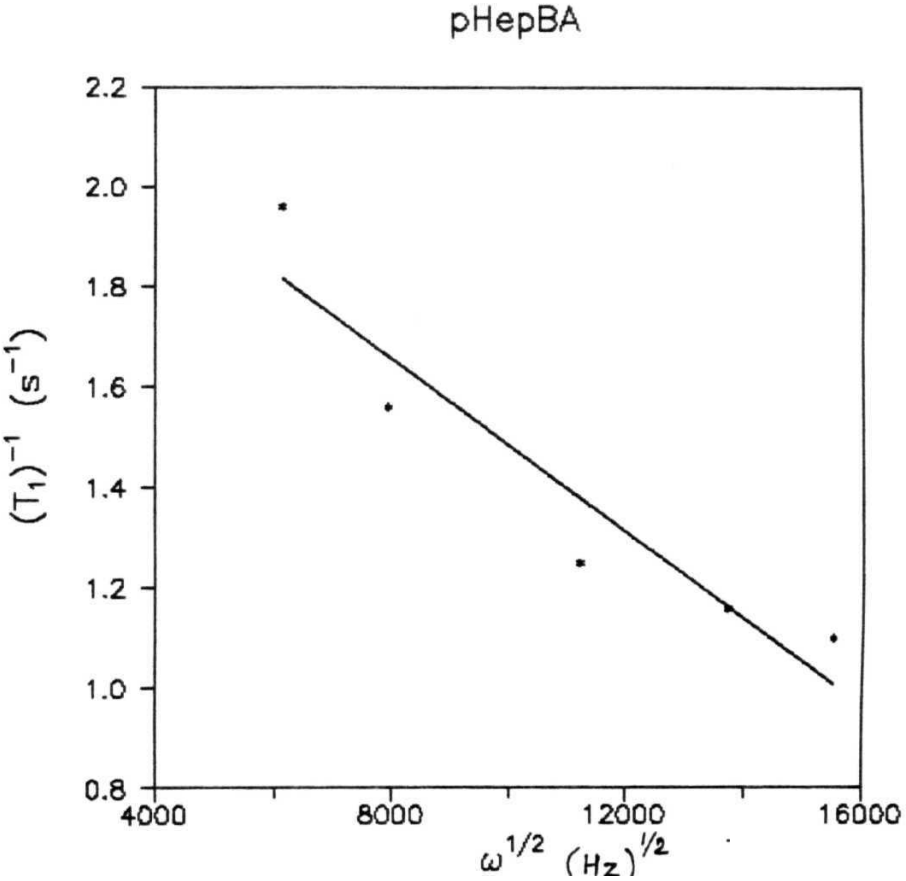

Fig. 4.4a Spin lattice relaxation rate T_1^{-1} as a function of square root of Larmor frequency ($\omega^{1/2}$) at a mid nematic temperature in **pHepBA**. Solid line is the best fit line.

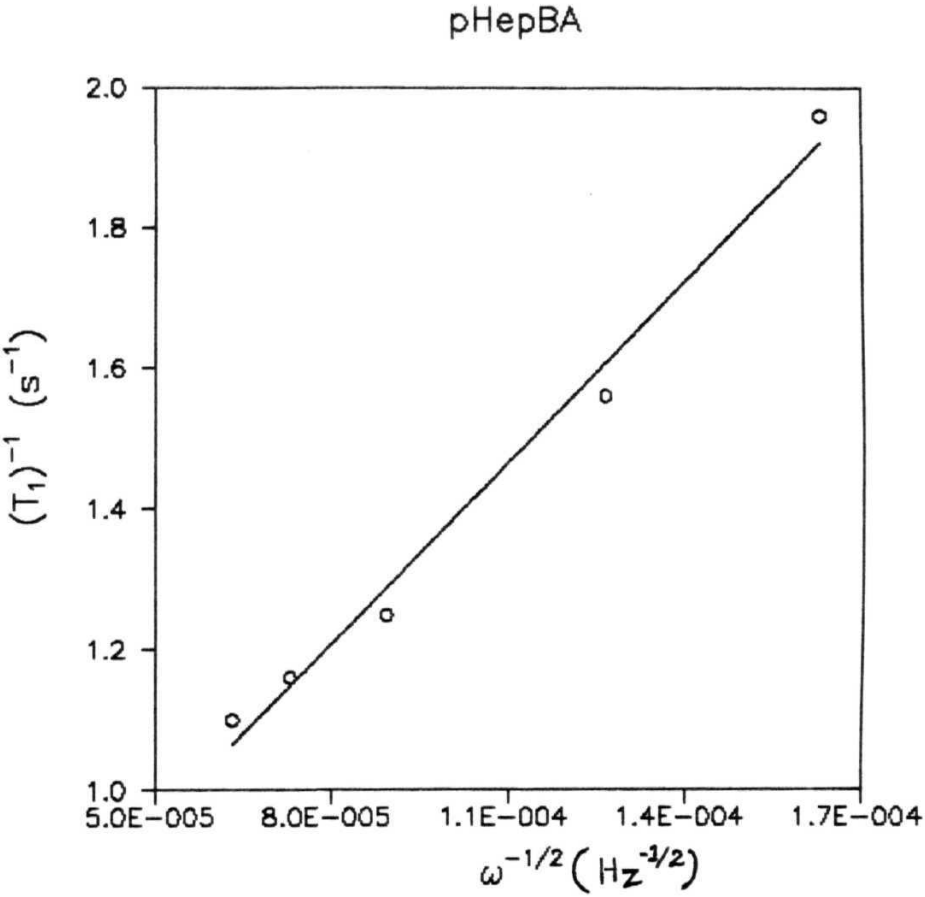

Fig. 4.4b Variation of spin lattice relaxation rate T_1^{-1} as a function of inverse square root of Larmor frequency $(\omega^{-1/2})$ at a mid nematic temperature in pHepBA. Solid line is the best fit line.

the observed frequency dependence completely and hence the total relaxation rate is fitted to a composite model consisting of all the three mechanisms given by

$$T_1^{-1} = (T_1^{-1})_{RS} + (T_1^{-1})_{SD} + (T_1^{-1})_{ODF} \qquad (4.1)$$

Here $(T_1^{-1})_{RS}$ represent the reorientations around short axis in the nematic phase and are given by a frequency independent but frequency dependent term A. Eqn. (4.1) is highly non-linear and hence numerical techniques viz., grid search and gradient search (Bevington, 1969) are used to fit the frequency dependence of the data at a given temperature, to obtain the parameters $(T_1^{-1})_{RS}$, B (in $T_1^{-1}{}_{ODF} = B\omega^{-1/2}$) and $D_\perp$ (the average diffusion coefficient in $(T_1^{-1})_{SD}$). Different initial guess values of these parameters, covering physically meaningful ranges ($T_1^{-1}{}_{RS}$ 0.1 to 10, B = 1 to 1e6, D = 1e-5 to 1e-10) are given as the initial values to the computer program which modifies these parameters to find the minimum root mean square deviation (rmsd), using the above algorithms (details are given in Appendix I). But it is found that the final set of parameters that give minimum rmsd are not the same for all initial sets of parameters, showing that this eqn. (4.1) does not have a unique minimum in the parameter space. However, it is found that one particular minimum, normally the deepest minimum, is obtained for maximum number of combinations of the initial values and hence this set of parameters are taken as the best fit parameters at that temperataure. Such a set of parameters at $120°C$ are $(T_1^{-1})_{RS}$ = 0.294, B = 7.92e3 and $D_\perp$ = 1.17e-6 cm^2/sec. This results in 26%, 24% and 50% contribution to total T_1^{-1} from reorientations, ODF and SD mechanisms. Fig. 4.5a shows the results of this fit.

This procedure is repeated at different temperatures in the nematic phase to find the temperature dependence of these parameters. In this process , the final set of parameters obtained at each temperature are given as initial guess values at next temperature assuming that the values of the parameters may not have shifted too much within this variation of temperature (typically 2 to $3°C$). The temperature variation of $D_\perp$ thus obtained is shown in Fig. 4.5b. As can be seen from this figure, $D_\perp$ exhibits wrong temperature dependence (increases with decreasing temperature).

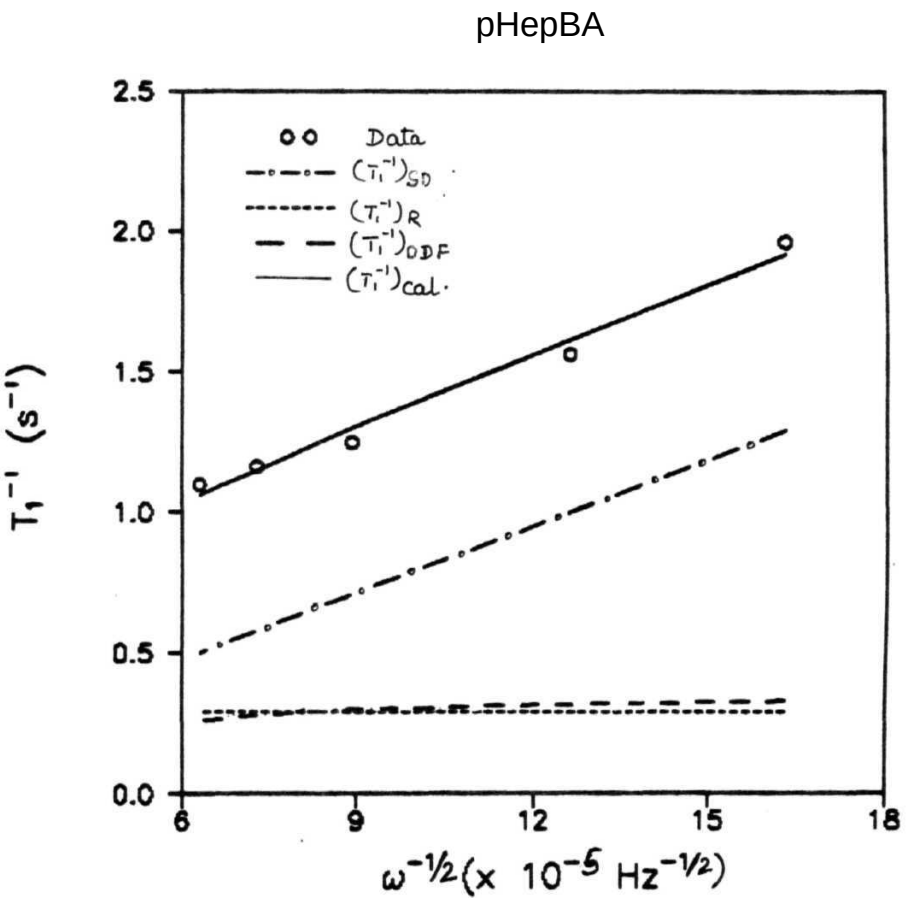

Fig. 4.5a Relative contributions of $(T_1^{-1})_{SD}$, $(T_1^{-1})_{RS}$ and $(T_1^{-1})_{ODF}$ (with a $(\omega^{-1/2})$ dependence) at $120°C$ in the nematic phase of **pHepBA.**

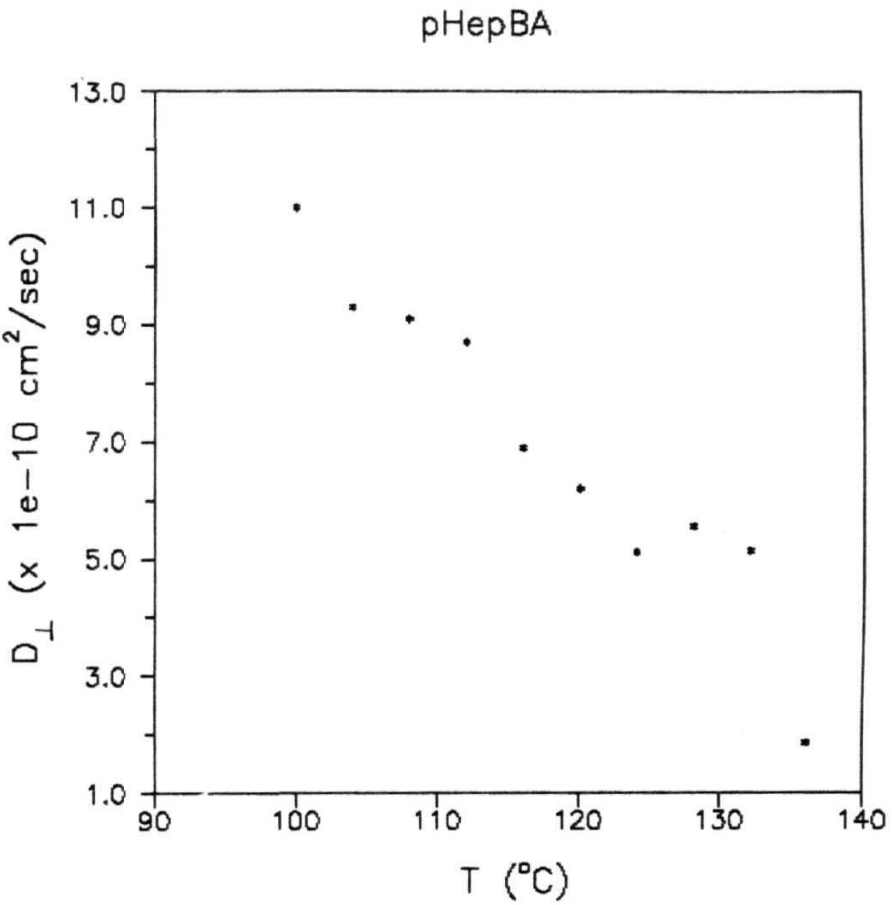

Fig. 4.5b Variation of diffusion coefficient $D_\perp$ as function of temperature in the nematic phase of pHepBA (calculated with the best fit of Fig. 4.5a).

This unphysical variation could be due to some error in the model used. One possibility is, perhaps $(T_1^{-1})_{ODF}$ in eqn. (4.1) is not given by $B\omega^{-1/2}$, but is given by $B\omega^{-1}$.

With this modification in eqn. (4.1), the analysis of the data as explained above, is repeated. The values of parameters thus obtained at 120°C are $(T_1^{-1})_{RS}$ = 0.97 s^{-1} ; B = 3.47e7 and $D_\perp$ = 1.4 x 10^{-10} cm^2/sec (Fig. 4.6a). This results in 47%, 4% and 49% contribution from ODF, SD and reorientations around short axis at 6 MHz and 16%, 0.5% and 83.5% at 30 MHz respectively. This fit as shown in Fig. 4.6a is equally good as in the case of $\omega^{-1/2}$ dispersion for ODF (with an rmsd of 2e-3 and 7.3e-5 for $\omega^{-1/2}$ and ω^{-1} dispersions respectively). As can be seen from this data, the contribution from self diffusion is very small (within experimental error) and hence it can be said that ODF with ω^{-1} behavior essentially determines the frequency disperison of T_1 upto 40 MHz (Fig. 4.6b). Thus, at this stage, it is not possible to choose between these two models. But when this procedure is repeated at different temperatures to obtain the temperature dependence of relevant parameters, it is clear that the model involving ω^{-1} relation to ODF contribution is correct in the present case. This is because the variations of $(T_1^{-1})_{RS}$ (Fig. 4.7 and 4.8) with temperature is physically tenable in this case. By fitting this temperature variaiton of $(T_1^{-1})_{RS}$ to eqn. (3.3), the activation energies associatied with reorientations is found to be 5.6 ± 0.4 kCal/mole (Fig. 4.9). The contribution from SD process is found to be negligible throughout the temperature range of the nematic phase.

Usually ODF is assumed to be a temperature independent mechanism. But the analysis of the present data indicates that the coefficient of $(T_1^{-1})_{ODF}$, B, is strongly temperature dependent, increasing with decreasing temperature (Fig. 4.7 and 4.8). Fitting the coefficient of $(T_1^{-1})_{ODF}$ to an Arrhenius behavior, the activation energy associated with this mechanism is calculated to be 4.8 ± 0.4 kCal/mole (Fig. 4.10). Thus, it can be concluded that the main mechanisms aiding the relaxation in the nematic phase of pHepBA are diffusion assisted ODF (with ω^{-1} type of frequency dependence) and reorientations around short axes.

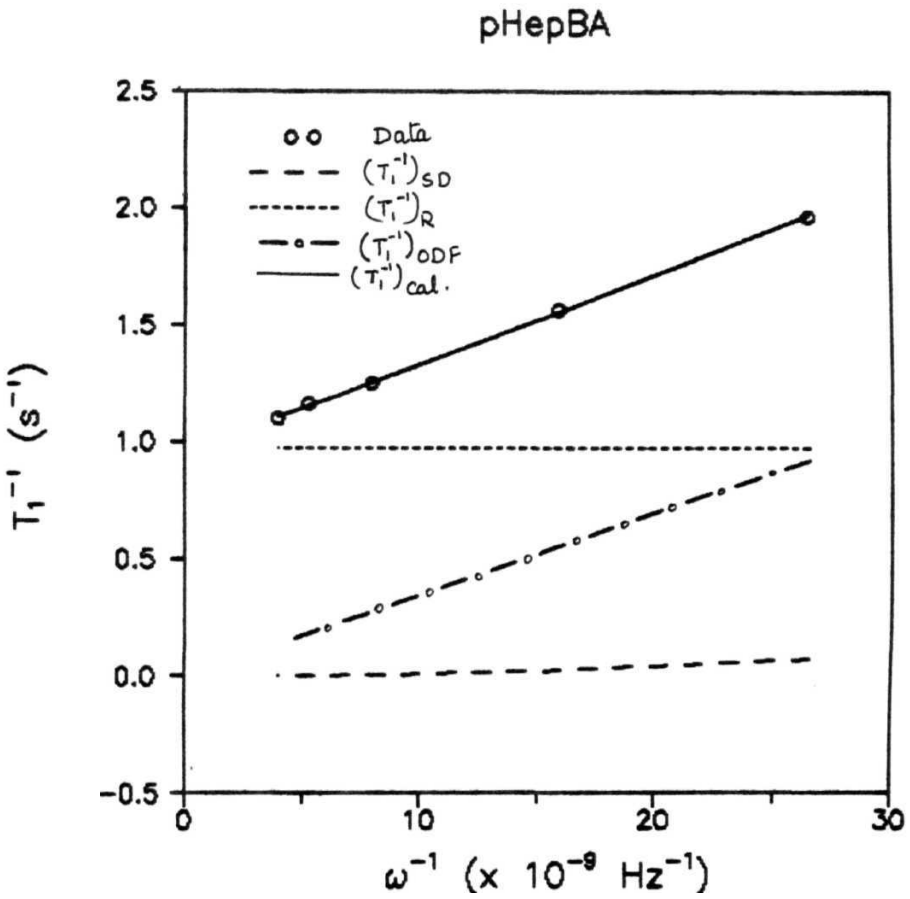

Fig. 4.6a Relative contributions of $(T_1^{-1})_{SD}$, $(T_1^{-1})_R$ and $(T_1^{-1})_{ODF}$ (with a (ω^{-1}) dependence) at $120°C$ in the nematic phase of pHepBA

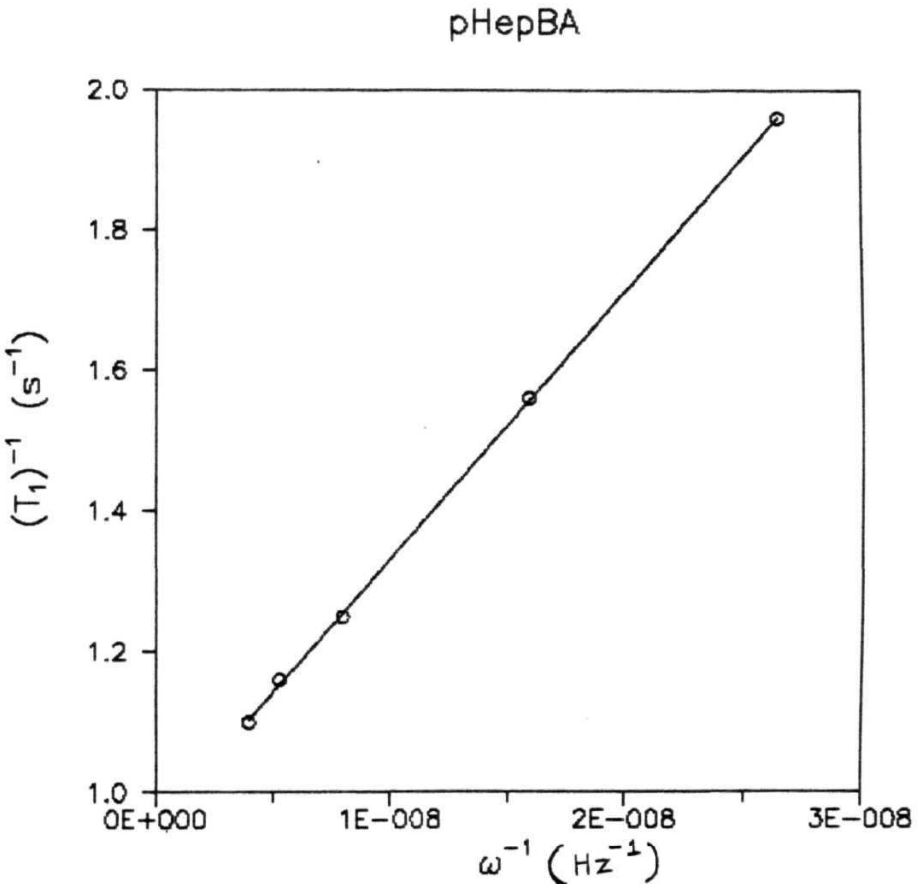

Fig. 4.6b Variation of spin lattice relaxation rate T_1^{-1} as a function of inverse Larmor frequency (ω^{-1}) at a mid nematic temperature in **pHepBA**. Solid line is the best fit line.

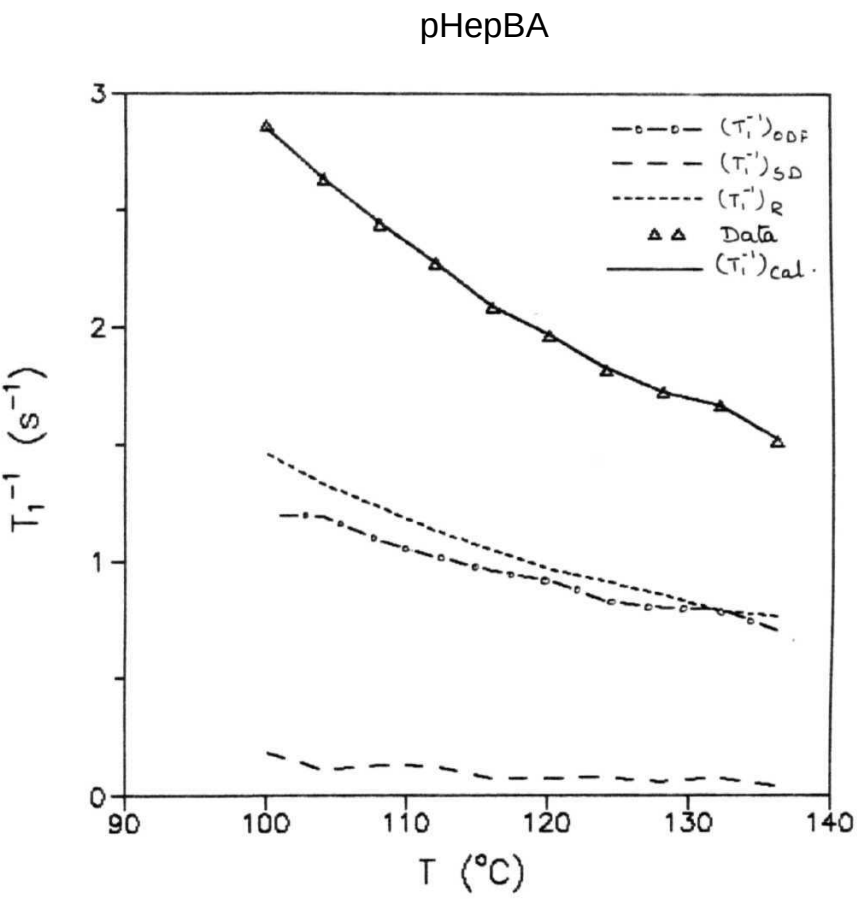

Fig. 4.7 Variation of $(T_1^{-1})_{SD}$ $(T_1^{-1})_{RS}$ and $(T_1^{-1})_{ODF}(\propto \omega^{-1})$ as a function of temperature in the nematic phase at 6 MHz in pHepBA.

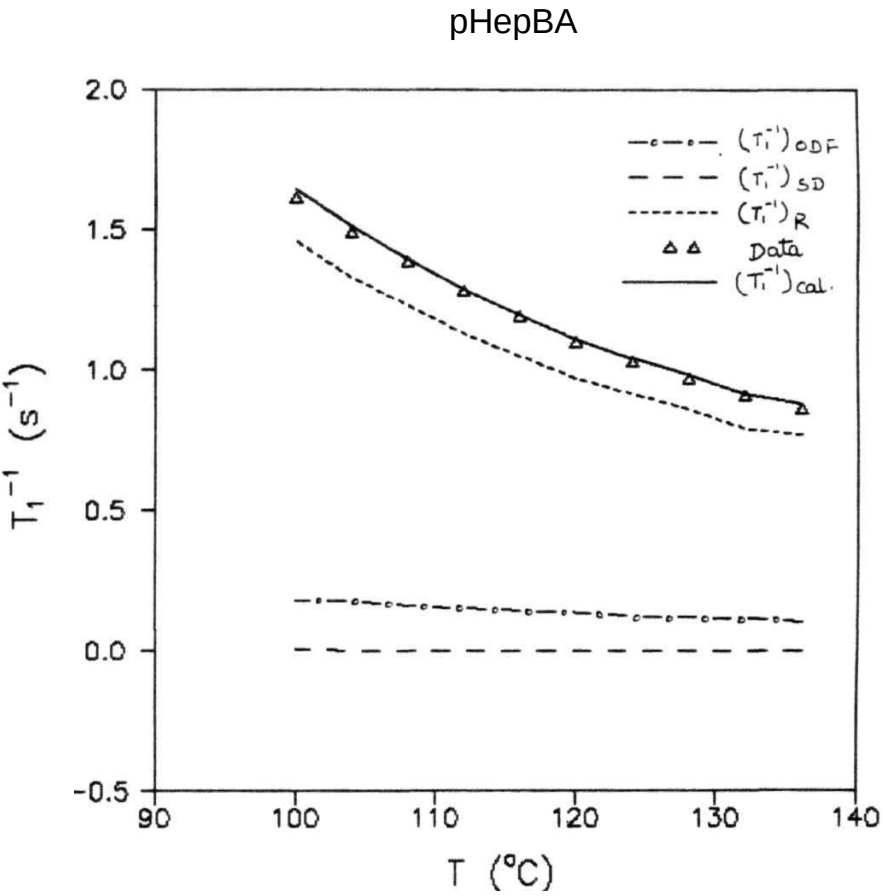

Fig. 4.8 Variation of $(T_1^{-1})_{SI}(T_1^{-1})_{RS}$ and $(T_1^{-1})_{ODF}$ $(\propto \omega^{-1})$as a function of temperature in the nematic phase at 40 MHz in pHepBA.

Table. 4.3 : Variation of $D_{\perp}$ and coefficient B in $\langle T_1^{-1} \rangle_{ODF}$ in the nematic phase of pHepBA

T°C	B x 1e7	$D_{\perp}$ (cm^2/s) x 1e-10
136	2.68	0.83
132	3.01	1 .45
128	3.03	1 .11
124	3.14	1 .46
120	3.47	1 .40
116	3.62	1 .43
112	3.83	2.39
108	4.09	2.41
104	4.50	2.09
100	4.53	3.42

Table 4.4 *t* Variation of $(T_1^{-1})_{ODF}$ and $(T_1^{-1})_R$ with temperature in the nematic phase of pHepBA

T° C	T_{1R}^{-1} (sec^{-1})		
		6 MHz	30 MHz
136	0.77	0.67	0.14
132	0.79	0.80	0.16
128	0.86	0.80	0.16
124	0.92	0.83	0.17
120	0.97	0.92	0.18
116	1 .05	0.96	0.19
112	1 .13	1.02	0.20
108	1 .23	1 .09	0.22
104	1 .33	1 .19	0.24
100	1 .46	1 .20	0.24

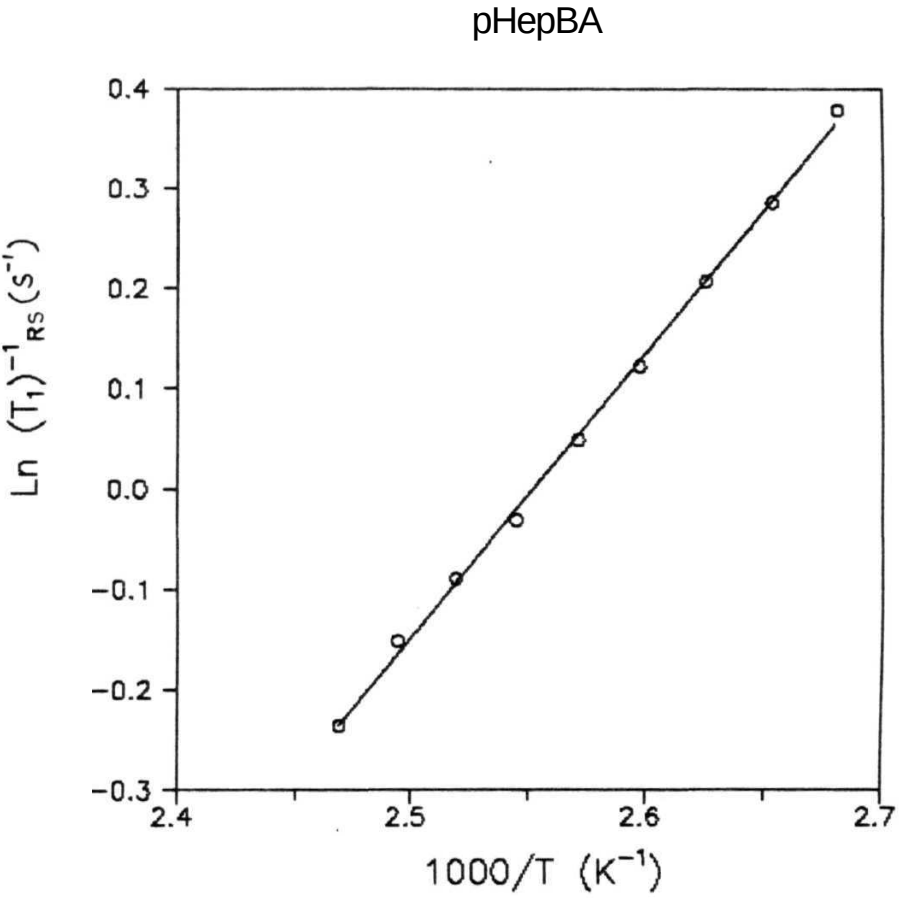

Fig. 4.9 Arrhenius fit of $(T_1^{-1})_{RS}$ in the nematic phase of **pHepBA**. Solid line is the best fit line to eqn. (3.3).

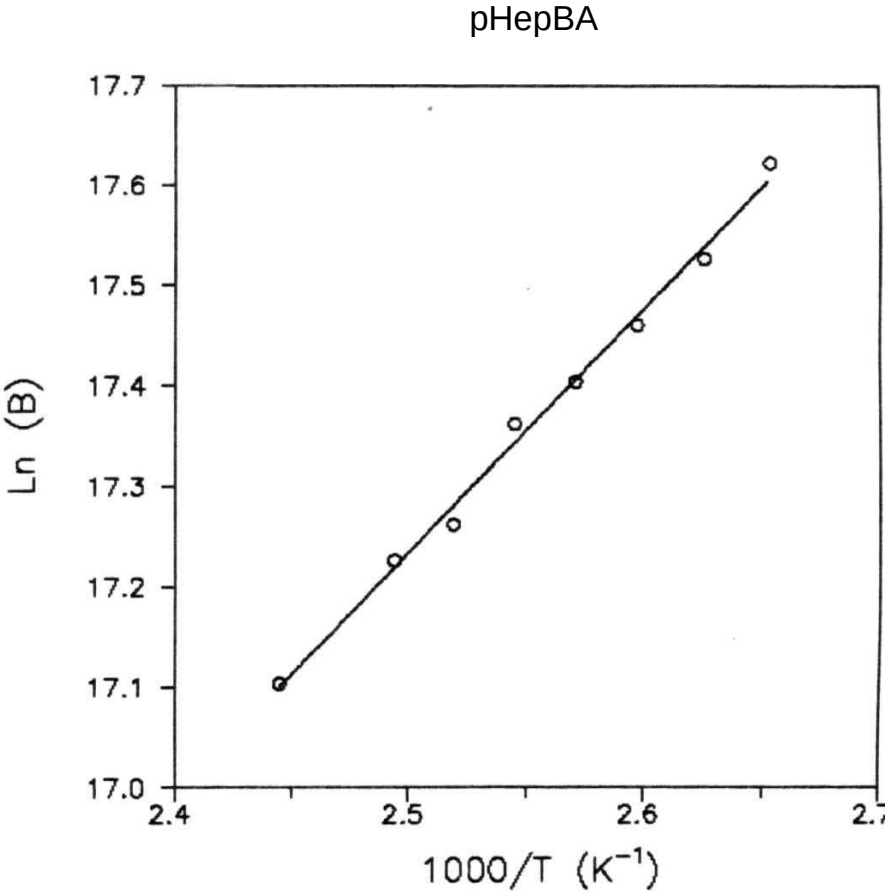

Fig. 4.10 Arrhenius fit of the coefficient B (in $(T_1^{-1})_{ODF}$ $B\omega^{-1}$) in the nematic phase of pHepBA. Solid line is the best fit line,

S/ phase

The data in the 5/ phase also fits well (rmsd = 1.5c — 3, at a mid S/ temperature, $95°C$) to the above model at all temperatures with the accepted temperature dependences of the different dynamic parameters (Fig. 4.11). The relative contributions from ODF, R and SD at $95°C$ are 38%, 50% and 12% at 6 MHz and 13%, 86% and 0.9% at 30 MHz respectively. The typical values of the diffusion coefficient and B (coefficient of $(T_1^{-1})_{ODF}$) are 7.6 x 10^{-10} cm^2/s and 4.76e7 respectively. The contributions from the three mechanisms as a function of temperature at 6 MHz and 30 MHz are given in Fig. 4.12 and Fig 4.13 respectively (Table 4.5 and 4.6). ODF process is found to be diffusion assisted in this phase also. Assuming the temperature dependence of *B* and reorientation term to be Arrhenius type (Fig. 4.14 and Fig. 4.15), the corresponding activation energies are obtained as 4.4 ± 0.4 and 5.7 ± 0.4 kcal/mole. These values are comparable to that of the nematic phase indicating that the dynamic environment in these two phases is similar.

It is interesting to examine the reasons for ω^{-1} dependence of $(T_1^{-1})_{ODF}$ in the present case. As discussed in the first chapter, depending on the relative values of the characteristic cutoff frequencies of ODF and the Larmor frequencies, and the presence of anisotropic elastic coefficinets (Vold and Vold, 1988), the frequency dependence of $(T_1^{-1})_{ODF}$ can be different from $\omega^{-1/2}$. From table. 1.1, it can be seen that the spectral density corresponding to ODF exhibits ω^{-1} dependence for $K_3 \ll (K_1, K_2)$ or $\omega_{zc} < \omega < \omega_{ac}$ or a combination of these two cases. It may also be noted that such a ω^{-1} dependence for $(T_1^{-1})_{ODF}$ is observed in the case of 40.9 also (Ravindranth, 1993) which has a relatively longer end chain as in the present system. Even though it is not possible to clearly identify which of the above reasons are responsible for the ω^{-1} behavior of ODF contribution in the present case, it is possible that as the end chain length increases, ω_{zc} decreases such that the Larmor frequency is in between the cutoff frequencies.

Solid Phase

In the solid phase, the reorient at ions about the short axis and long axis are expected to slow down compared to the isotropic reorientation of CH_3 and CH_2 groups

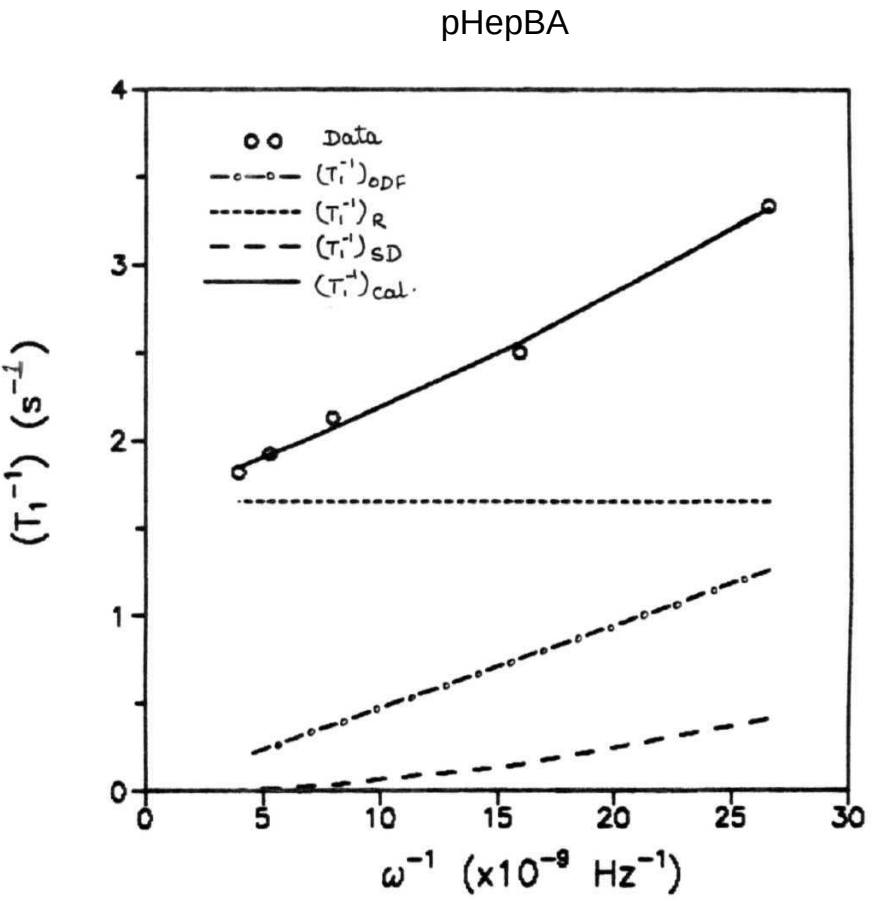

Fig. 4.11 Relative contributions of $(T_1^{-1})_{SI}$ $(T_1^{-1})_{RS}$ and $(T_1^{-1})_{ODF}$ (with a (or^1) dependence) at $95°C$ in the S/ phase of **pHepBA.**

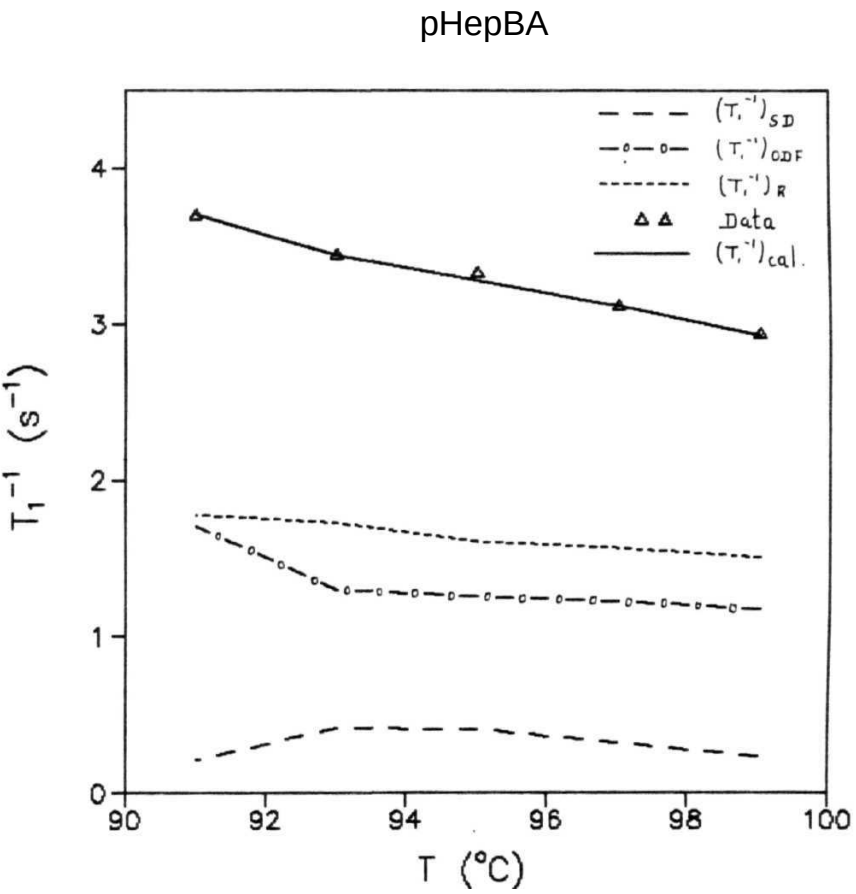

Fig. 4.12 Variation of $(T_1^{-1})_{SD}$, $(T_1^{-1})_{RS}$ and $(T_1^{-1})_{ODF}$ $(\propto \omega^{-1})$ as a function of temperature in the S/ phase (6 MHz) in pHepBA.

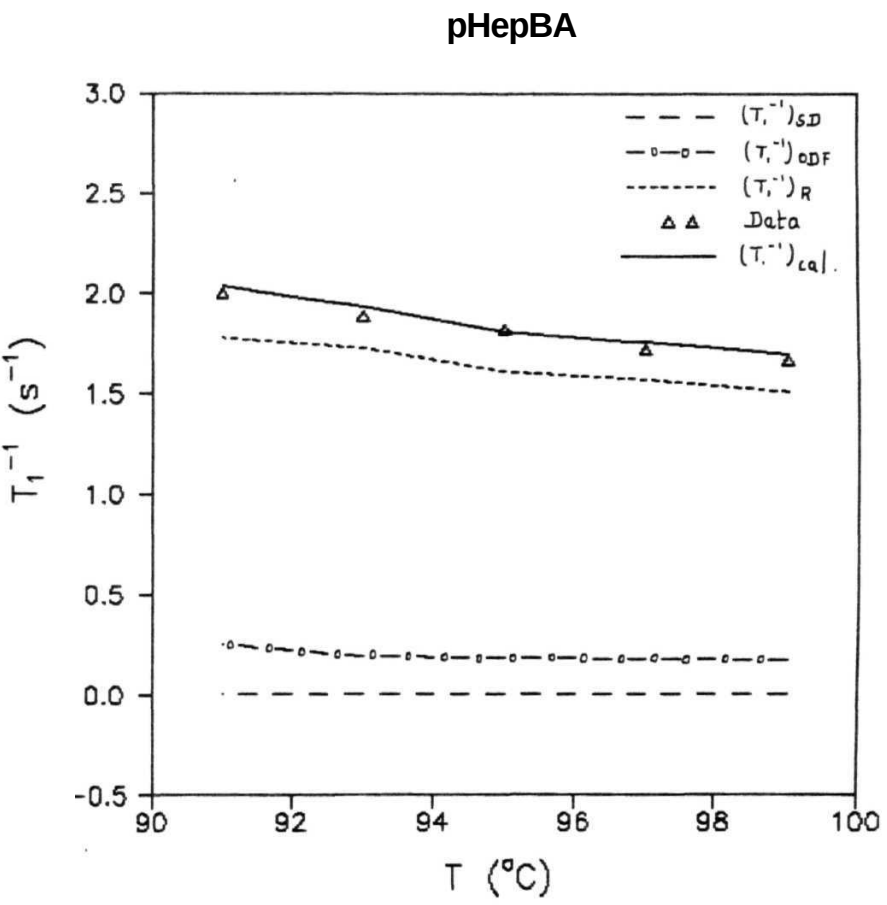

Fig. 4.13 Variation of $(T_1^{-1})_{SD}$ $(T_1^{-1})_{RS}$ and $(T_1^{-1})_{ODF}$ $(\propto \omega^{-1})$ as a function of temperataure in the S/ phase (40 MHz) in pHepBA.

Table. 4.5 : Variation of $D_{\perp}$ and coefficient B in $(T_1^{-1})_{ODF}$ in the smectic-I phase of pHepBA

T°C	B x 1e7	$D_{\perp}$ (cm^2/s) x 1e-10
99	4.44	4.37
97	4.62	6.02
95	4.76	7.60
93	4.90	7.80
91	6.44	3.90

Table 4.6 : Variation of $(T_2^{-1})_R$ and $(T_2^{-1})_{ODF}$ with temperature in the smectic - I phase of pHepBA

T° C			
		6 MHz	30 MHz
99.0	1.52	1.18	0.24
97.0	1.57	1.23	0.25
95.9	1.65	1.26	0.25
93.0	1.73	1.30	0.26
91.0	1.78	1.71	0.34

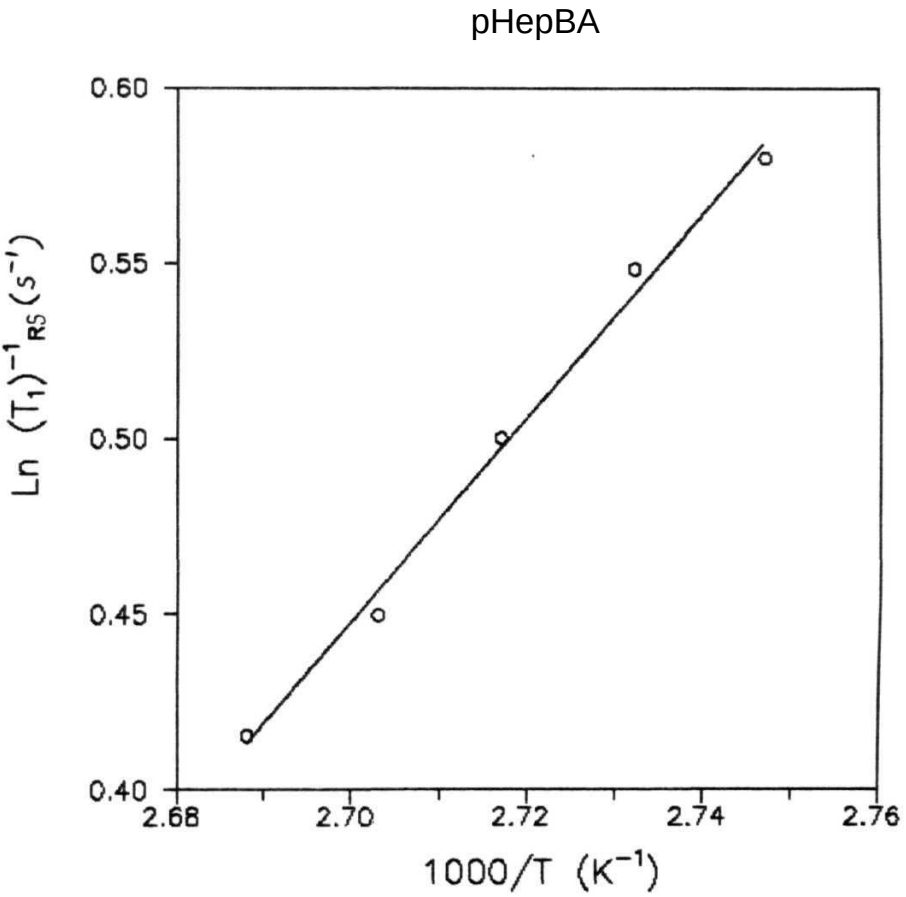

Fig. 4.14 Arrhenius fit of $(T_1^{-1})_{RS}$ in the smectic phase of pHepBA. Solid line is the best fit line to eqn. (3·3)

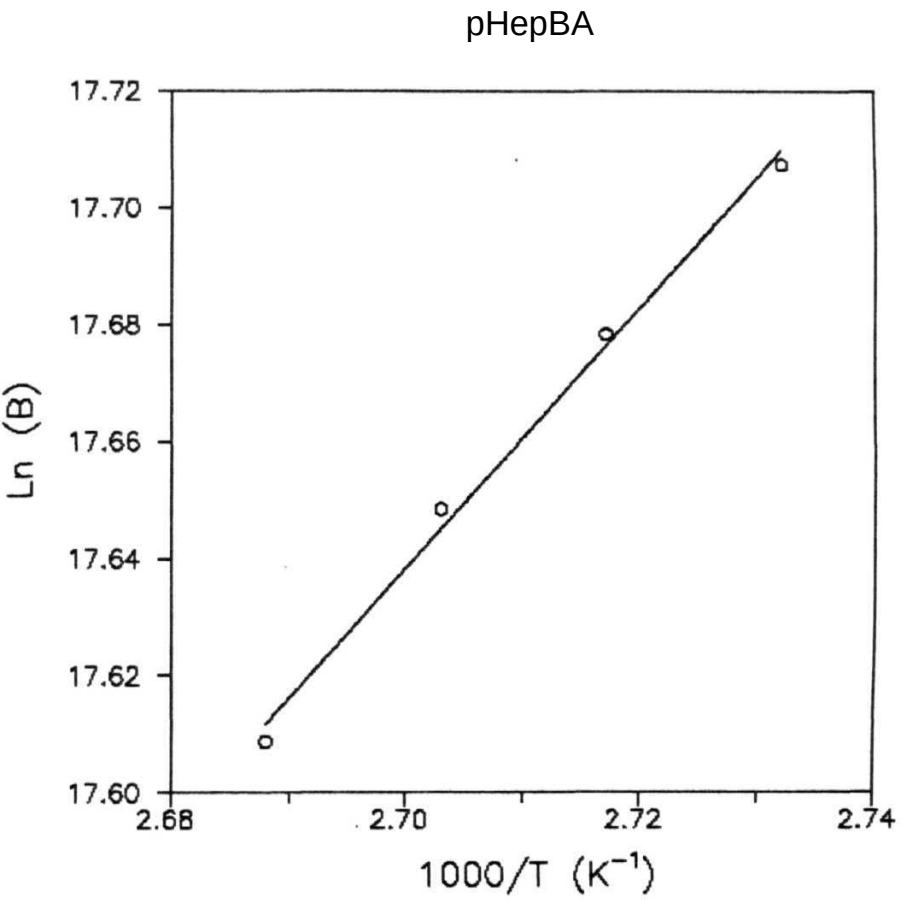

Fig. 4.15 Arrhenius fit of the coefficient B (in $(T_1^{-1})_{ODF}\ B\omega^{-1}$) in the smectic phase of pHepBA. Solid line is the best fit line.

in the end chains. Further, a steep increase in T_1 near the 5/ to solid phase indicates that ODF and diffusion motions have slowed down considerably and hence do not contribute to T_1 in this phase. The frequency independent, temperature dependent relaxation process in the solid phase can thus be accounted by reorientations of the methyl groups alone in the motional narrowing limit i.e., $(\omega\tau \ll 1)$. In $\omega\tau \ll 1$ limit, spin lattice relaxation rate is proportional to the correlation time τ_{CH_3} which exhibits an Arrhenius behavior (eqn. (3.4)). From the slope of the plot of $\ln(T_1^{-1})$ vs $1000/T$ (Fig. 4.16), the corresponding activation energy is obtained as 2.6 ± 0.4 kCal/mole. The activation energies corresponding to different dynamics in the different mesophases are presented in Table 4.7.

Dipolar relaxation T_{1D}

The dipolar relaxation process probes the spectral densities at low frequencies and hence gives information about slow motions. At these frequencies, the relaxation processes are expected to be mediated predominantly by order director fluctuations. From the analysis of T_1 data, it is found that the ODF mechansism is diffusion assisted in nematic and smectic-I phases. T_{1D} is also temperature dependent in these two phases. Pre-transitional effects are observed in the 5/ phase, before T_{1D} drops to a low value of 2.5 msec in the solid phase. This drop as explained before, is due to considerable slowing down of diffusion due to additional ordering in the solid phase. From the expression for T_{1D}^{-1} in the strong collision limit (eqn. (3.7)), the upper limit of the correlation time associated with this slow diffusion is estimated to be 5 msec. The corresponding lower limit of the diffusion coefficient is obtained from eqn. (1.84a) to be $10^{-13}\ cm^2/sec$.

Comparing these results with those of Thompson et.al. (1977), it is seen that $(T_1^{-1})_{ODF}$ obtained from the present analysis of our results is considerably different from that reported by them. $(0.1s^{-1}$ at $130°C$ and 30 MHz as against $0.3s^{-1}$ at 33.8 MHz). This implies that $(T_1^{-1})_{ODF}$ in pHepBA can not be estimated based on that of decyloxy benzoic acid. Further, the present analysis shows that reorientations of the molecules around different axes form a major contribution to the relaxation in the different mesophases. The frequency independent contribution to $(T_1^{-1})_{SD}$ attributed

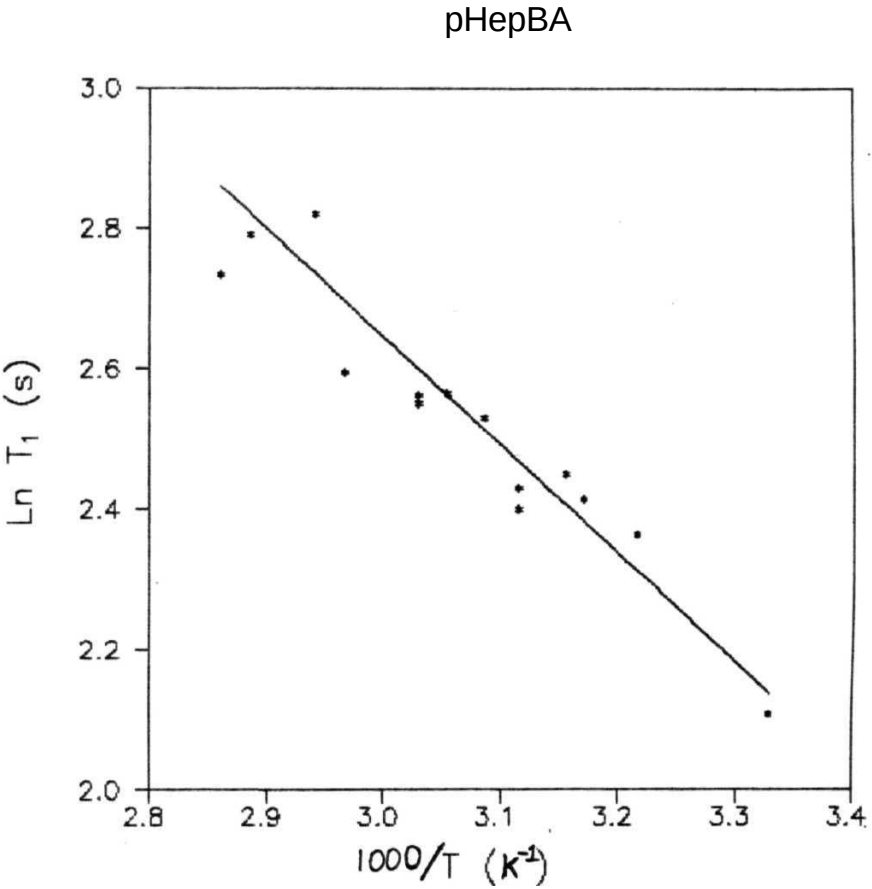

Fig. 4.16 Arrhenius fit of (T_1) in the solid phase of pHepBA. Solid line is the best fit line to eqn. (3.6).

Table. 4.7 : Activation energies associated with the different dynamic processes in pHepBA

Relaxation process	dynamic process	Phase	Activation energy (KCal/mole)
T_1	SD assisted ODF	Nematic	4.8 ± 0.4
	R around shoft axis		5.6 ± 0.4
	SD assisted ODF	S_I	4.4 ± 0.4
	R around short axis		5.7 ± 0.4
	R around end chains	Sol id	2.6 ± 0.4

by Thompson et al. (1977) may be assigned to reorientation mechanisms as the contribution from diffusion is found to be negligible in the present analysis.

From the above discussions, it can be concluded that in pHepBA, diffusion assisted ODF and reorientations are the mechanisms mediating relaxation in the nematic and 5/ phases upto 40 MHz. The frequency dependence of $(T_1^{-1})_{ODF} \propto B\omega^{-1}$ suggest that the Larmor frequency lies in between the two characteristic cutoff frequencies i.e., $\omega_{zc} < \omega < \omega_{ac}$. The T_1 process in the solid phase is mediated by reorientational motions of end chains.

Section - 3

4.3 *p-Nonyloxy benzoic acid (pNBA)*

The second sample investigated in this series is *p*-nonyloxy benzoic acid (pNBA) with *aa* phase sequence

$$/ \quad \underline{143C} \quad N \quad \underline{117C} \quad S_I \quad \underline{94C} \quad X$$

The system exhibits a considerably wide nematic phase with a narrow 5/ phase, which is a high temperature smectic phase. The molecular structure of pNBA is similar to pHepBA with an additional CH_2 group. The sample is obtained from Frinton Laboratories, USA and used without further purification.

4.3.1 Experimental results

Spin lattice relaxation time measurements are done as a function of frequency (3 to 40 MHz) and temperature (T_{NI} to room temperature) with an appropriate interval of $2°C$ (Fig. 4.17). The data are presented in Tables 4.8a to 4.8g. Although measurements are carried out at seven frequencies, the data is presented only for three frequencies for clarity in the above figure. T_{1D} measurements are made as a function of temperature in the nematic and smectic phases at 30 MHz (Fig. 4.18).

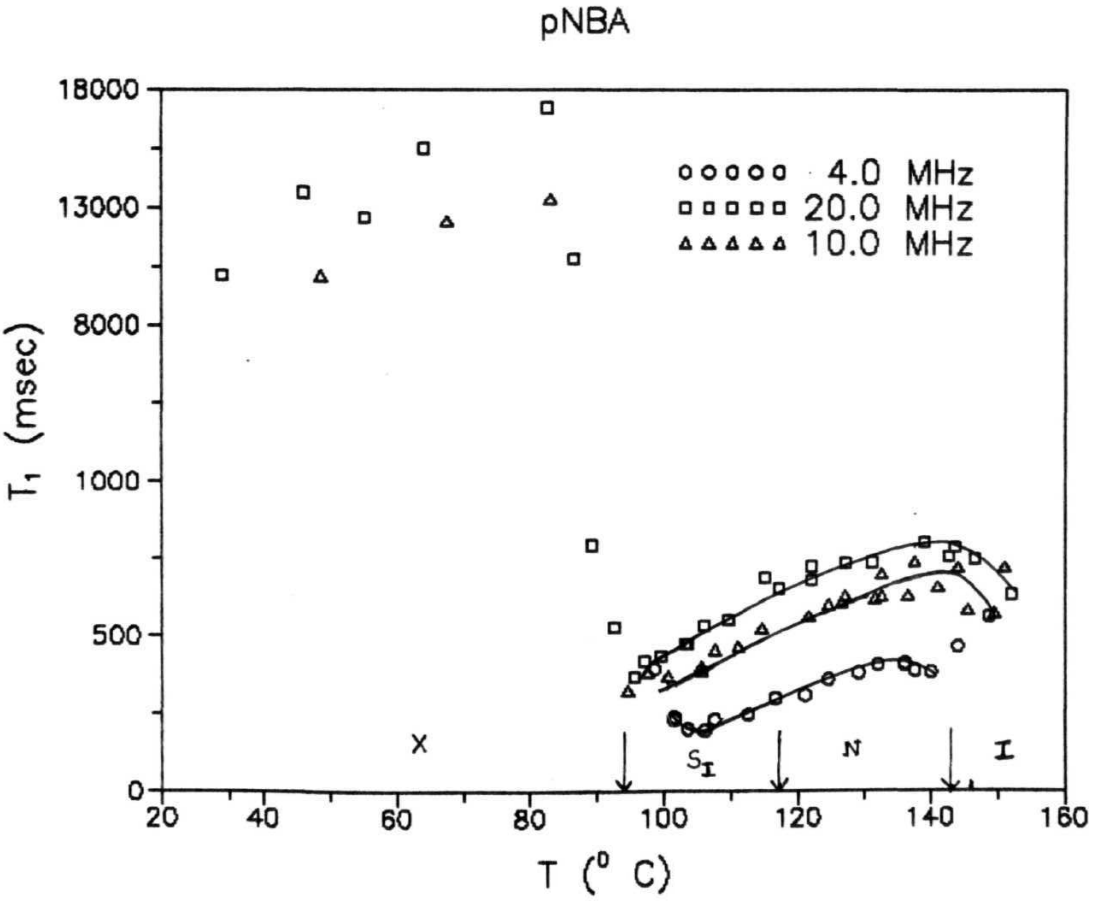

Fig. 4.17 Spin lattice relaxation time T_1, as a function of temperature T at three frequencies in pNBA. Solid lines are drawn as a guide to the eye. The vertical lines denote the transition temperatures.

Table 4.8* Variation of spin **lattice relaxation** time (T_1) with **temperature** <T) at 3 MHz <pNBA>

T° C	T (msec)	T° C	T_1 (msec)
151.5	471	126.0	226
147.5	380	125.0	235
147.5	455	124.5	242
142.0	298	121.0	233
139.0	371	**119.5**	200
138.0	365	109.0	180
135.8	319	106.5	184
135.0	373	105.0	229
134.5	338		

Table 4.8b Variation **of** spin **lattice relaxation** time (T_1) with **temperature** (T) at 4 MHz **(pNBA)**

T° C	T_1 (msec)	T° C	T_1 (msec)
148.8	561	121.0	309
144.0	463	116.5	299
140.0	382	112.5	248
137.5	388	107.5	232
136.0	410	106.0	195
136.0	405	103.5	201
132.0	405	101.5	240
129.0	380	101.0	230
124.5	359	98.5	394

Table 4.8c **Variation of** spin **lattice relaxation** time (T_1) **with temperature** (T) at *6* MHz **(pNBA)**

T° C	T (msec)	T° C	T_1 (msec)
146.5	373	115.5	444
143.0	533	112.5	406
142.0	520	111.O	406
141.0	546	106.0	341
140.0	631	102.0	311
137.0	579	98.0	291
136.0	585	95.5	294
131.0	562	92.0	244
129.0	520	89.0	447
128.0	528	87.5	411
127.0	509	81.5	1299
124.5	492	61.5	1149
119.0	493		

Table 4.8d Variation *oi* spin lattlct **relaxation time** (T_1) **with temperature** <T> at 10 MHz (pNBA)

T° C	T_1 (msec)	T° C	T (msec)
151.0	721	121.5	562
149.5	573	114.5	523
145.5	584	111.0	465
144.0	719	107.5	456
141.0	658	105.5	402
137.5	739	104.5	387
136.5	630	100.5	372
132.5	620	97.5	384
127.0	630	94.5	326
126.5	606	83.0	13351
124.5	600	67.5	12392
131.5	620	48.5	10091

Titbit **4.8e Variation of spin lattice relaxation time (T_1) with temperature (T> at 20 MHz (pNBA)**

T° C	T_1 (msec)	T° C	T_1 (msec)
152.0	632	103.5	472
146.5	747	103.0	472
143.5	786	99.5	434
142.5	754	97.0	420
139.0	800	95.5	369
131.0	737	92.5	527
127.0	735	89.0	792
122.0	725	86.5	10791
122.0	680	82.5	17230
117.0	652	**64.0**	15507
115.0	687	55.0	12561
109.5	551	46.0	13630
106.0	532	29.0	10116

Table 4.8f Variation of spin lattice relaxation time (T_1) with temperature <T> at 30.1 MHz (pNBA)

T° C	T_1 (msec)	T° C	T_1 (msec)
151.5	431	119.5	681
149.0	631	113.0	583
143.5	787	110.0	591
137.0	880	104.0	548
131.0	744	91.5	964
125.5	731		

Table 4.8g Variation of spin lattice relaxation time (T_1) with temperature (T> at 39.8 MHz (pNBA)

T° C	T_1 (msec)	T° C	T_1 (msec)
144.0	713	110.5	566
138.0	844	105.5	568
132.5	775	100.0	485
123.0	675	94.5	430
119.5	634	92.0	410

Pretransitional effects are observed near the isotropic - nematic transition temperature, T_{NI} (Fig. 4.17). Well inside the nematic phase T_1 is both temperature and frequency dependent. The S_I phase is dominated by pre-transitional effects from 5/ to solid phase (over $10°C$ at 4 MHz) and T_1 increases drastically at the phase transition to the solid phase. In the solid phase, T_1 is temperature dependent but frequency independent. T_{1D} decreases with temperature in the nematic phase as shown in fig. 4.18. 5/ phase is dominated by pre-transitional effects before T_{1D} drops from 100 msec to 33 msec in the solid phase (Table. 4.9).

4.3.2 Analysis and discussion

Nematic phase

The frequency dependence of the T_1 data does not fit to the model considering either ODF (with $\omega^{-1/2}$ dependence) or SD (Fig. 4.19a and 4.19b). Thus, the data is fitted to a composite model consisting of both the mechanisms along with frequency independent reorientations. The fit of the data to eq. (4.1) with $(T_1^{-1})_{ODF} \propto \omega^{-1/2}$ at any given temperature is shown in Fig. 4.20a (rmsd = 1e-3). This procedure is repeated at other temperatures to obtain the temperature variation of the different parameters. It is observed that the diffusion coefficient increases with decreasing temperature, which is physically not tenable (Fig. 4.20b). Thus, as in pHepBA, the exponent of ω in $T_1^{-1}{}_{ODF}$ is made -1 and the entire analysis is repeated. Even for this exponent, the results show wrong temperature dependence. Then the exponent is further increased till $T_1^{-1}{}_{RS}$ and the diffusion coefficient have the correct temperature dependences. The frequency and temperature dependence of the data could be accounted properly, only when the exponent of ω is -2.5 i.e., $(T_1^{-1})_{ODF} \propto \omega^{-2.5}$ (Fig. 4.21, rmsd = 1.7e-3). The maximum exponent for ω predicted till now is only -2 (Vold and Vold, 1988). This rather large frequency dependence of $(T_1^{-1})_{ODF}$ could be probably due to yet another mechanism dominant at low frequencies. Taking this into account, the contribution from ODF, *SD* and *R* mechanisms to the total relaxation rate at $130°C$ are found to be 6%, 45% and 49% (10 MHz) and 0.5%, 41.5% and 58% (30 MHz) respectively. The typical values of the diffusion coefficient and the

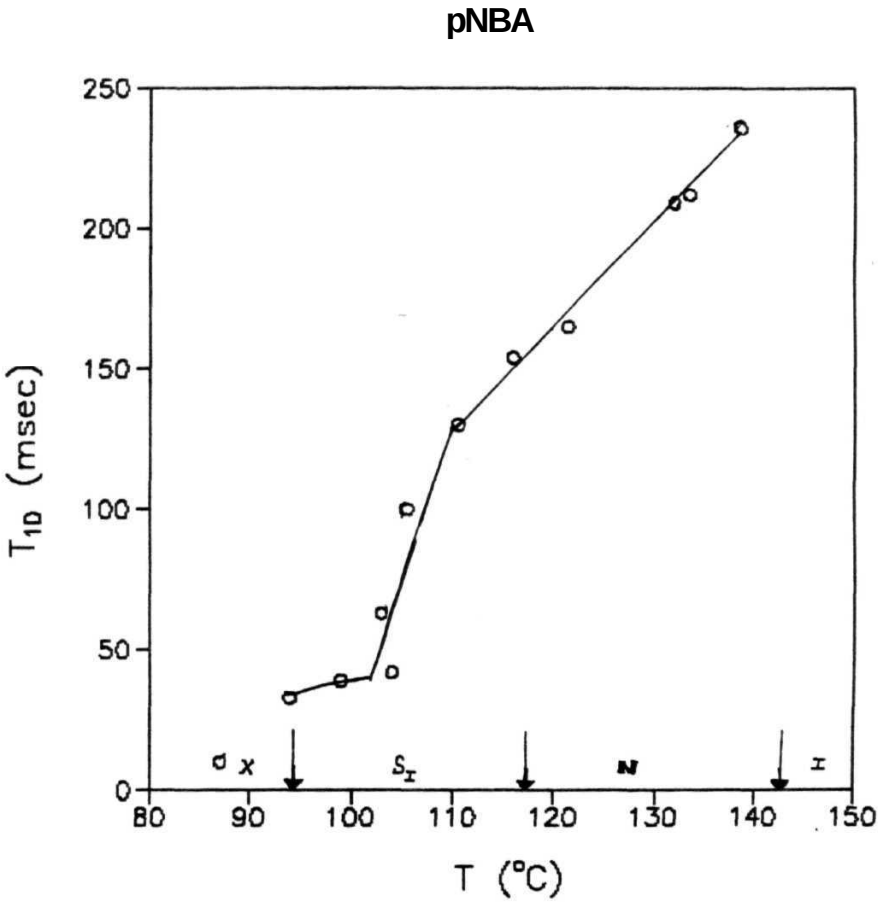

Fig. 4.1 8 Variation of dipolar relaxation time T_{1D}, as a function of temperature in pNBA. Solid line is drawn as a guide to the eye.

Table *4.9* Variation of dipolar spin lattice relaxation time (T_{1D}) with temperature <T> at 30 MHz (pNBA)

T° C	T_{1D} (msec)
144.5	183
140.0	202
138.5	236
133.5	212
132.0	209
121.5	165
116.0	154
110.5	130
105.5	100
104.0	42
103.0	63
99.0	39
94.0	33
87.0	10

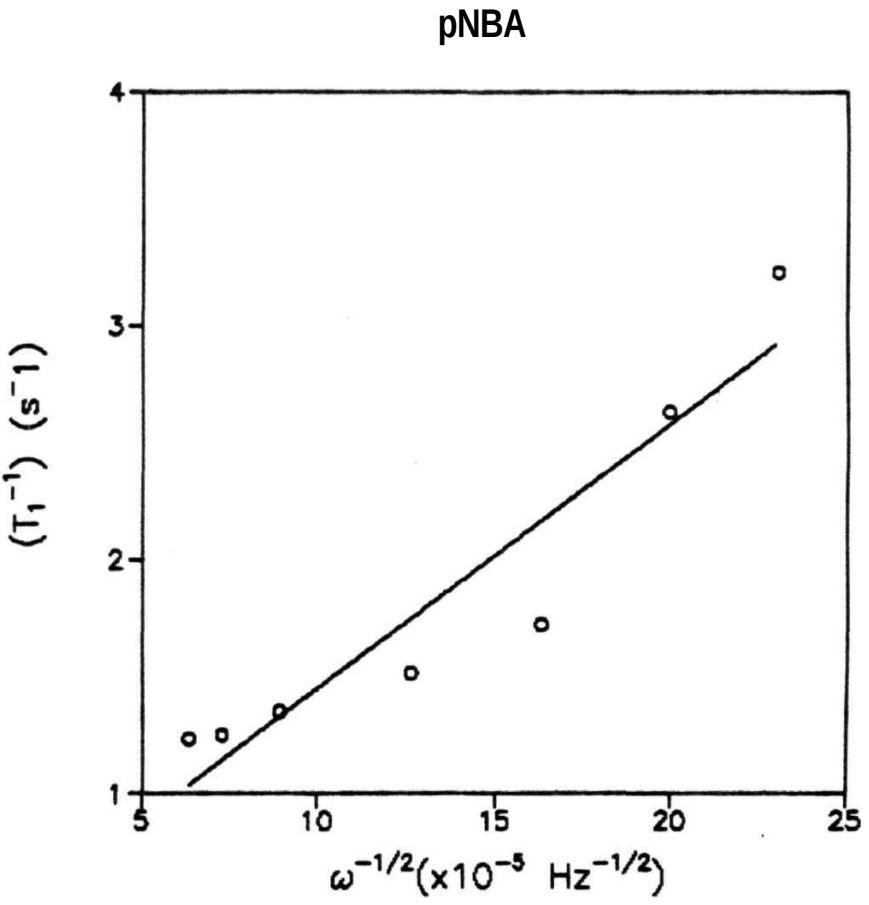

Fig. 4.19a T_1^{-1} as a function of inverse square root of Larmor frequency $(\omega^{-1/2})$ in the nematic phase of pNBA. Solid line is the best fit line

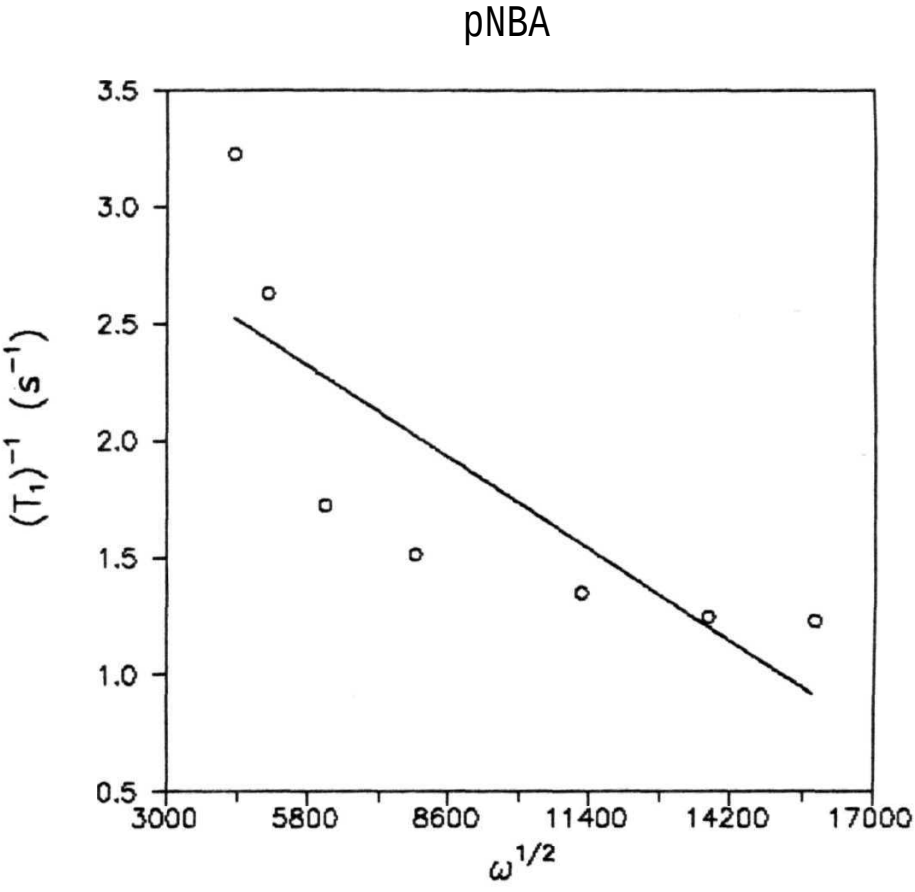

Fig. 4.19b Spin lattice relaxation rate T_1^{-1} as a function of square root of Larmor frequency $(\omega^{1/2})$ at a mid nematic temperature in pNBA Solid line is the best fit line.

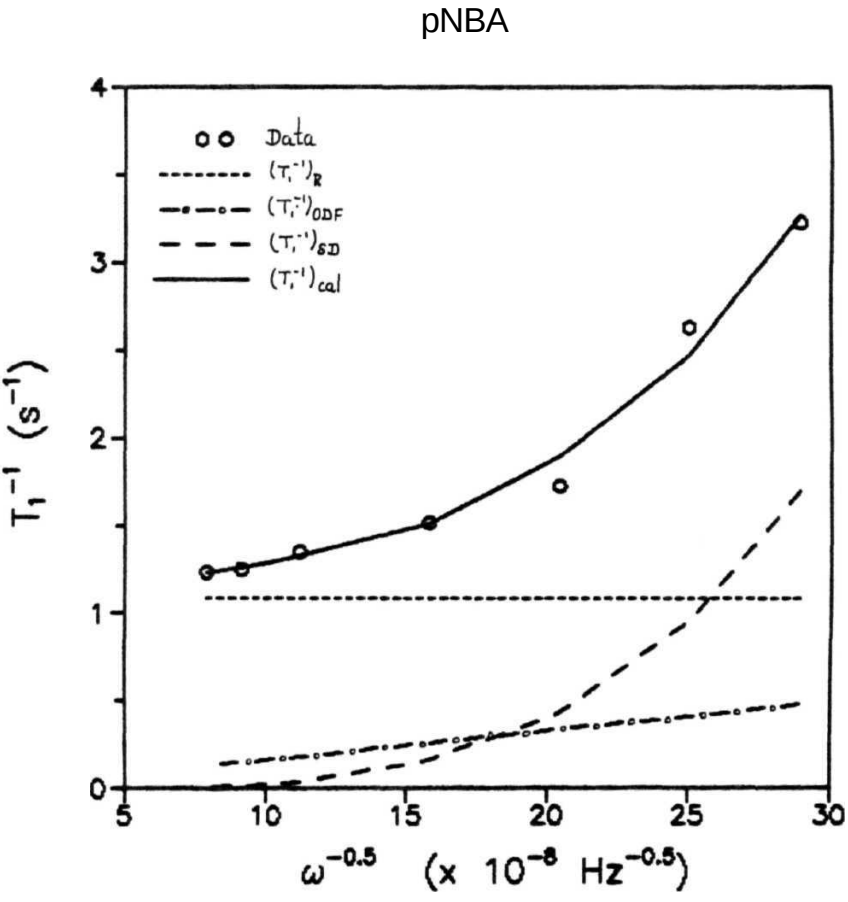

Fig. 4.20a Relative contributions of $(T_1^{-1})_{SD}$, $(T_1^{-1})_{RS}$ and $(T_1^{-1})_{ODF}$ (with a $(\omega^{-1/2})$ dependence) at $130°C$ in the nematic phase of **pNBA**.

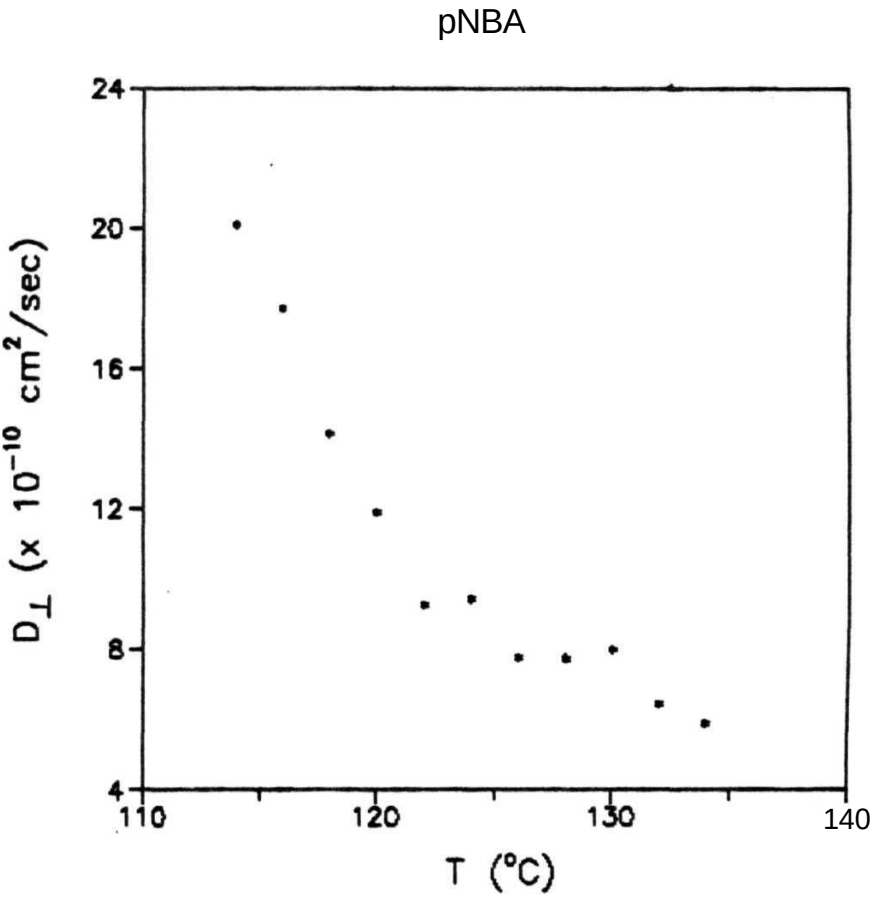

Fig. 4.20b Variation of diffusion coefficient $D_\perp$ as function of temperature in the nematic phase of pNBA (calculated with the best fit of Fig. 4.21a).

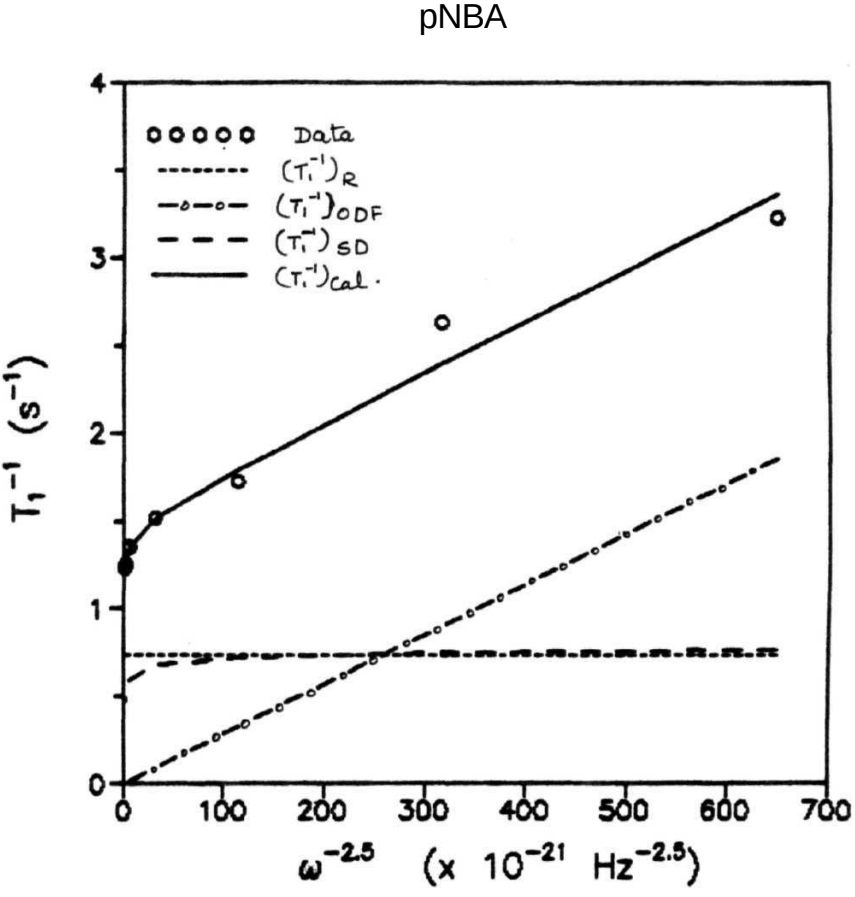

Fig. 4.21 Relative contributions of $(T_1^{-1})_{SD}$ $(T_1^{-1})_R$ and $(T_1^{-1})_{ODF}$ with a $(\omega^{-2.5}$ dependence) at $130°C$ in the nematic phase of **pNBA**

coefficient of $(T_1^{-1})_{ODF}$, are 1 x 10"^{7} cm^2/ sec and 1 x 10^{18} respectively. The variation of the diffusion coefficient $D_\perp$ and B with temperature are given in Table. 4.10. The contributions from the three mechanisms to the relaxation rate as a function of temperature at 10 MHz and 40 MHz are given in Fig. 4.22 and Fig. 4.23 respectively (Table 4.11). Both self diffusion and reorientations around short axes are thermally activated and hence the relevant parameters are fitted to Arrhenius behavior. The activation energy associated with self diffusion and reorientations around short axis (Fig. 4.24 and Fig. 4.25 respectively) are 10.6±0.4 and 4.4 ± 0.4 kCal/mole.

The coefficient associated with $(T_1^{-1})_{ODF}$ is found to be temperature dependent suggesting a diffusion assisted ODF mechanism. The temperature dependence fits to Arrhenius behavior (Fig. 4.26) with an activation energy of 7 ±0.4 kCal/mole.

In the solid phase, T_1 is temperature dependent but independent of frequency, which can be attributed to reorientations of the alkyl chains in the $\omega\tau_c \ll 1$ limit. Thus, fitting the data to an Arrhenius behavior (Fig. 4.27), the actiavation energy associated with these reorientational motions is estimated to be 1.2±0.4 kCal/mole.

Dipolar relaxation time

The decrease in T_1 near the S_I to solid tranition (from about 100 msec to 40 msec) can be attributed to the slowing down of diffusive motions (due to the onset of additional ordering within the layers). This is also seen from the dipolar relaxation data. The sudden drop of T_{1D} at this transition is due to the increase in spectral densities at low frequencuies resulting in an additional path for relaxation. In this case, the dipolar relaxation rate is related to the correlation times of the slow diffusion mechanism (τ_D) given by eqn. (3.7). The upper limit of the correlation time and hence the lower limit of the diffusion coefficient are calculated to be 66 msec and 10^{-14} cm^2/ sec respectively. The mechanism that usually contributes at the low frequencies is ODF and temperature dependence of T_{1D} is in agreement with the observation from T_1 data that the ODF mechanism is assisted by *SD* process. From the temperature dependence of T_{1D} (Fig. 4.28), the activation energy associated with ODF (reorientations around short axis in the appropriate wavelenght limit) is calculated to be 6.4 ± 0.8 kCal/mole. The activation energies associated with the different

Table. 4.10 : Variation of $D_{\perp}$ and coefficient B in $(T_1^{-1})_{ODF}$ in the nematic phase of pNBA

T°C	B x 1e18	$D_{\perp}$ ($cm^2/*$) x 1e-7
136	2.58	4.90
134	2.63	5.00
132	2.77	5.10
130	2.86	5.00
128	2.99	5.04
126	3.07	4.79
124	3.29	4.09
122	3.47	4.04
120	3.64	3.99
118	3.78	3.63
116	3.94	**3.45**
114	4.01	3.10
112	4.30	2.90
110	4.57	2.69
108	4.74	2.37

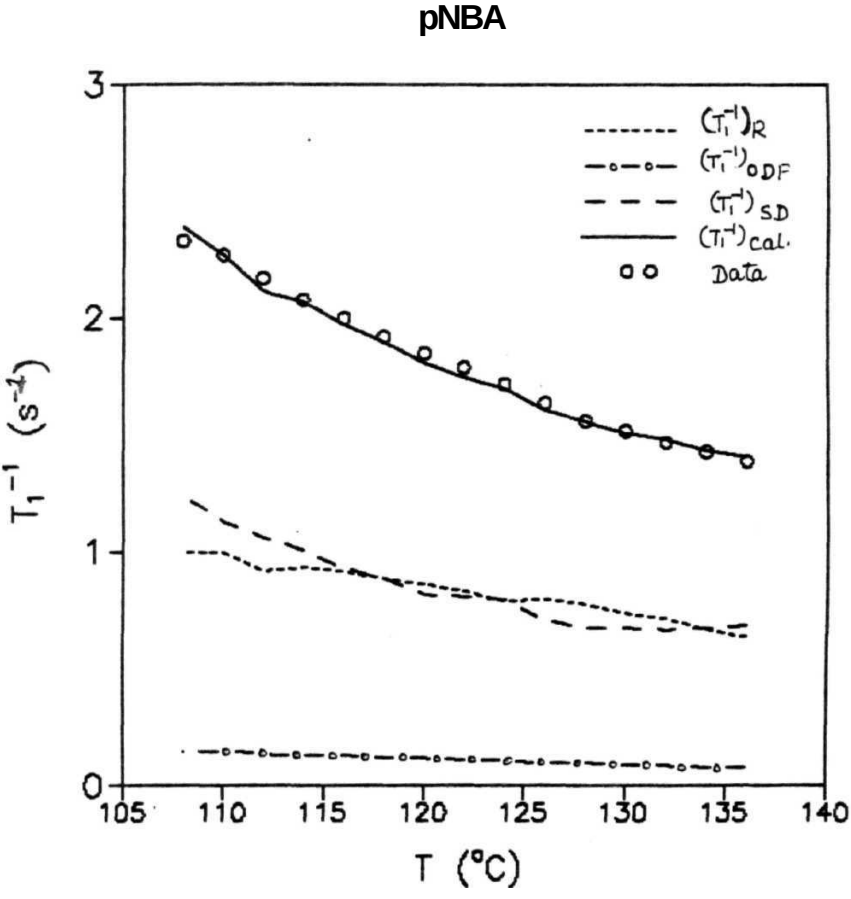

Fig. 4.2Z Variation of $(T_1^{-1})_{SD}$, $(T_1^{-1})_{RS}$ and $(T_1^{-1})_{ODF}(\propto \omega^{-2.5})$ as a function of temperature in the nematic phase at 10 MHz in pNBA.

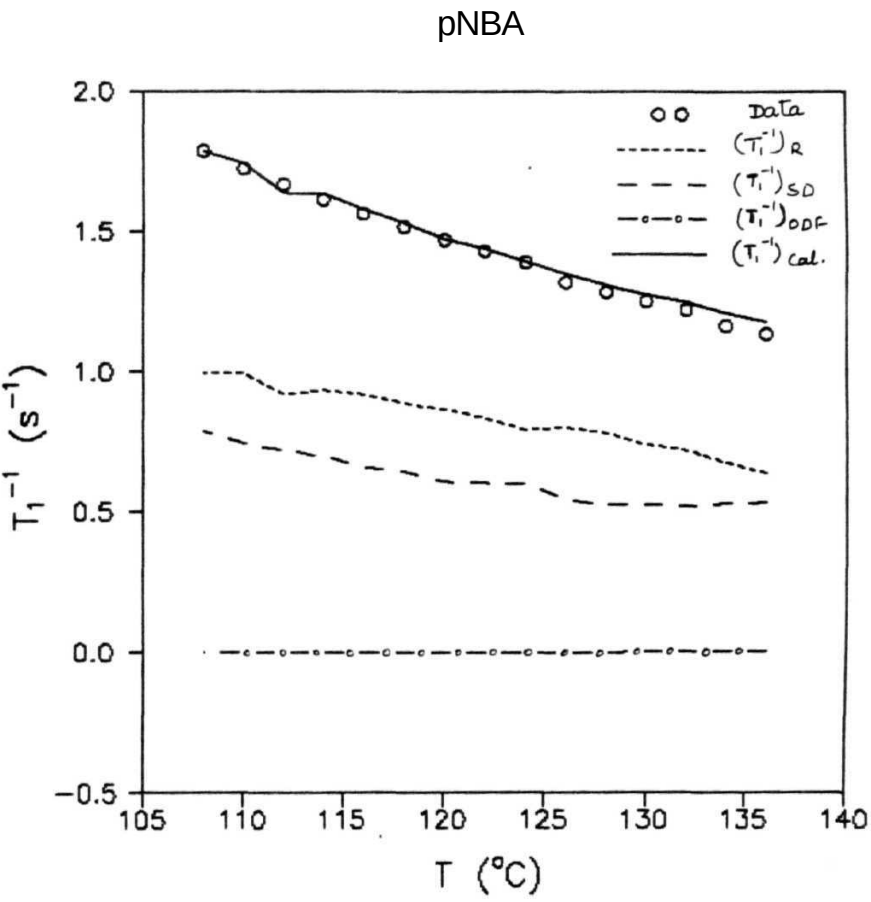

Fig. 4.23 Variation of $(T_1^{-1})_{SI}$ $(T_1^{-1})_{RS}$ and $(T_1^{-1})_{OD}$ $(\propto \omega^{-2.5})$ as a function of temperature in the nematic phase at 40 MHz in pNBA.

Table 4.11 : Variation of $\langle T_1^{-1} \rangle_{ODF}$, $\langle T_1^{-1} \rangle_{SD}$, and $\langle T_1^{-1} \rangle_{RS}$ with temperature in the nematic phase of pNBA

T° C	$\langle T_1^{-1} \rangle_{ODF}$ (s^{-1})		$\langle T_1^{-1} \rangle_{SD}$ (s^{-1})		$\langle T_1^{-1} \rangle_{RS}$ (s^{-1})
	10 MHz	30 MHz	10 MHz	30 MHz	
136	0.08	0.005	0.69	0.54	0.64
134	0.08	0.005	0.68	0.53	0.67
132	0.09	0.006	0.67	0.52	0.72
130	0.09	0.006	0.68	0.53	0.74
128	0.10	0.006	0.68	0.53	0.78
126	0.10	0.007	0.71	0.54	0.80
124	0.11	0.007	0.80	0.60	0.79
122	0.11	0.008	0.81	0.60	0.83
120	0.12	0.008	0.82	0.61	0.87
118	0.12	0.007	0.89	0.64	0.89
116	0.13	0.006	0.93	0.66	0.92
114	0.13	0.006	1.01	0.70	0.93
112	0.14	0.005	1.06	0.72	0.92
110	0.15	0.005	1.13	0.75	1.00

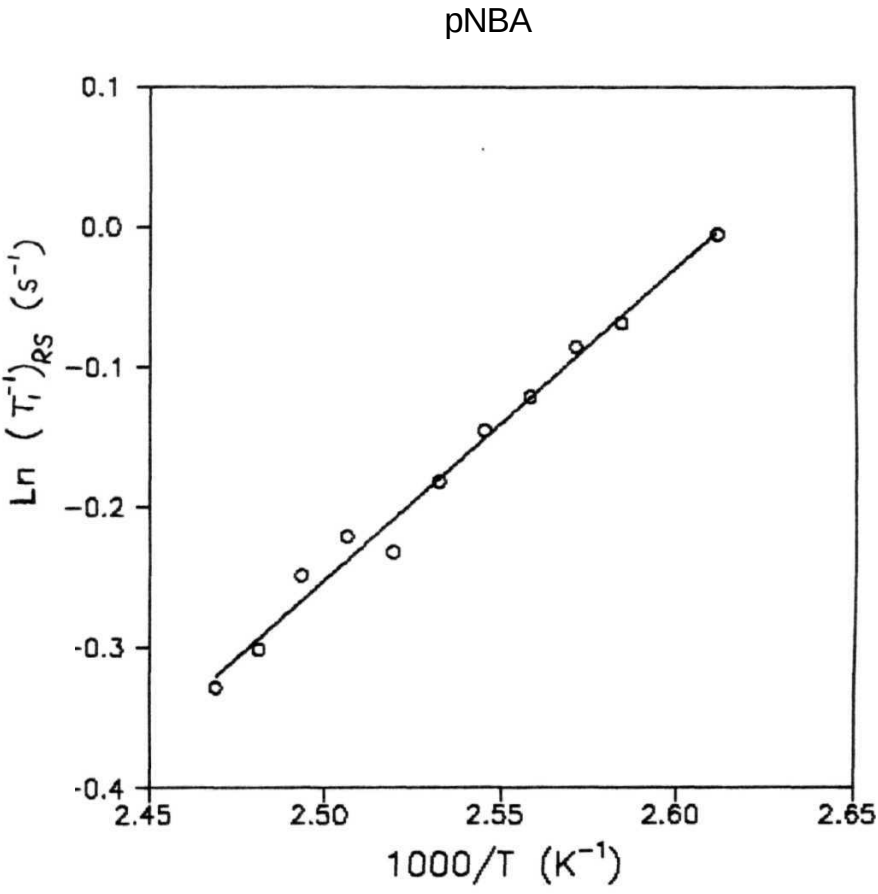

Fig. 4.24 Arrhenius fit of $(T_1^{-1})_{RS}$ in the nematic phase of **pNBA.** Solid line is the best fit line to eqn. (3.3).

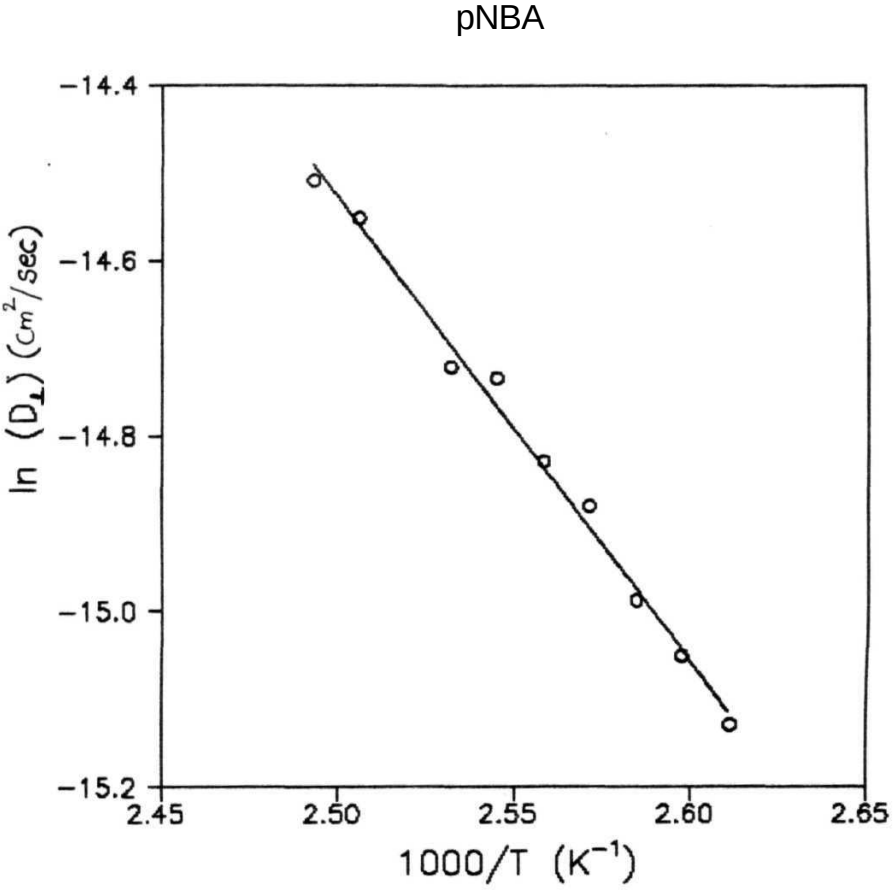

Fig. 4.25 Arrhenius fit of the diffusion coefficient $(D_\perp)$ in the nematic phase of pNBA. Solid line is the best fit line to eqn.(3·2).

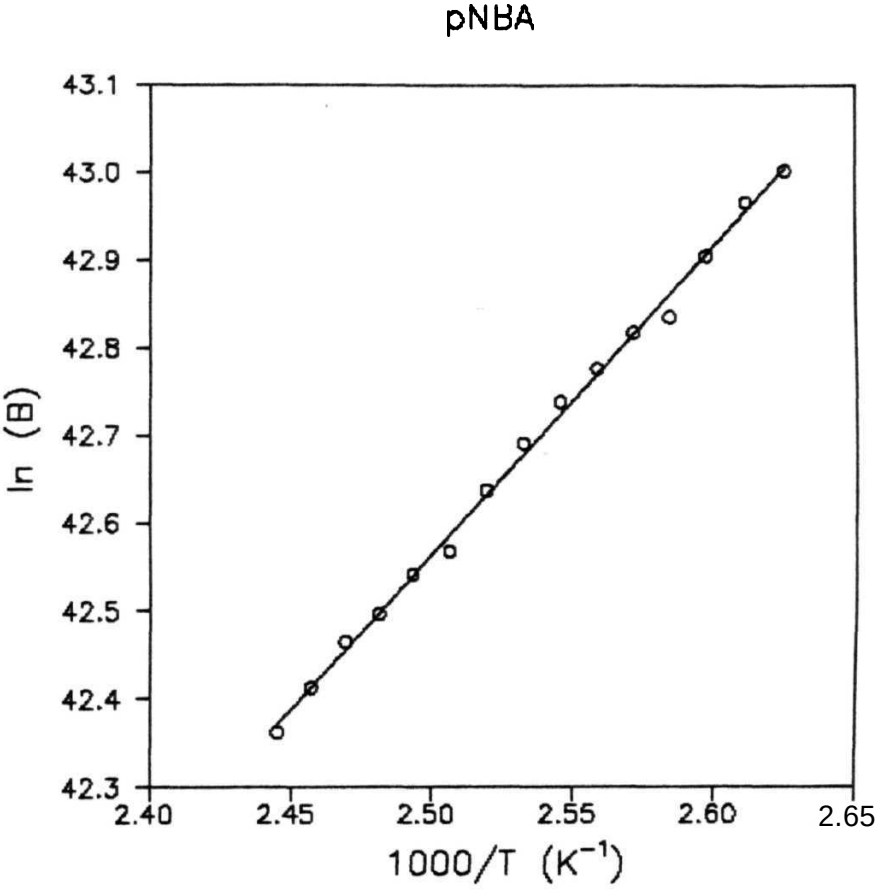

Fig. 4.26 Arrhenius fit of the coefficient B (in $(T_1^{-1})_{ODF}$ $B\omega^{-2.5}$) in the nematic phase of **pNBA.** Solid line is the best fit line

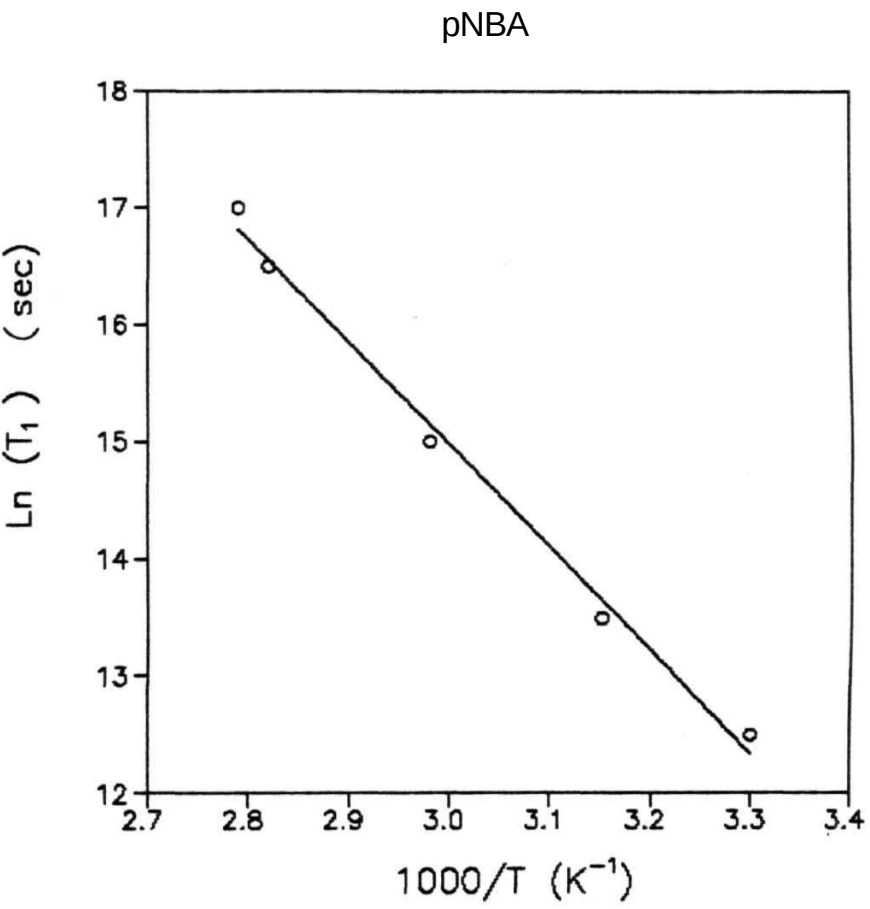

Fig. 4.27 Arrhenius fit of T_1 in the solid phase of pNBA
Solid line is the best fit line to eqn. (3.6).

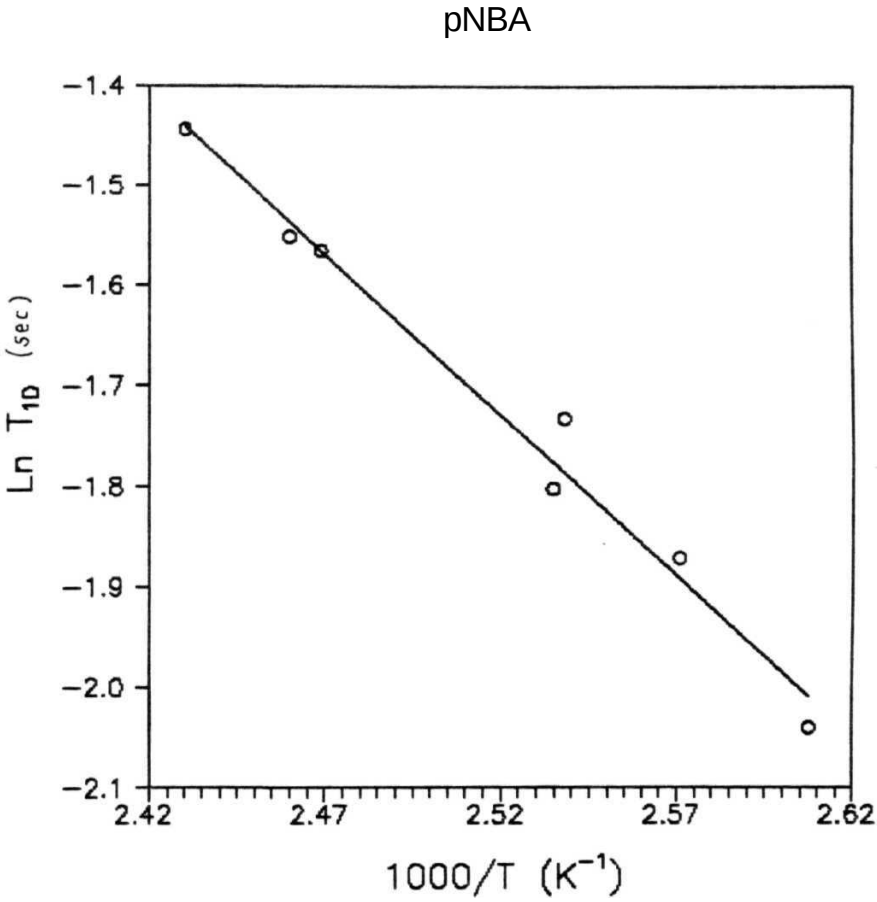

Fig. 4.28 Arrhenius fit of (T_{1D})n the nematic phase of pNBA. Solid line is the best fit line

mechanisms in different mesophases are summarized in Table. 4.12.

Comparison of these results with those of Thompson et al. (1989) show that the $(T_1^{-1})_{ODF}$ obtained in the present analysis is very much different $(0.01s^{-1}$ at $130°C$ and 30 MHz) as compared to that assumed by Thompson et al. $(0.3s^{-1}$ at 33.8 MHz). Also the frequency dependence of ODF contibution in the present case is quite different $(\omega^{-2.5})$ compared to what is proposed by them $(\omega^{-0.5})$. As has been pointed out above, even $\omega^{-0.5}$ dependence fits to the present data, but the temperature dependence of the individual contribution to T_1^{-1} show that this model is not correct. This situation is different from that of nO.m compounds discussed in the earlier chapter, where T_1 data over a relatively narrow frequency region (like 5 to 50 MHz) are sufficient to pin point the mechanism clearly (probably because only either ODF or SD is predominant in determining the frequency dependence of T_1 for 40.4, 40.3 and 40.2). On the other hand, in the present case, frequency dependence does not seem to uniquely decide the correct model to be used. But the present analysis shows that in such situations, the temperature dependence of the data is extremely useful in arriving at the correct model.

Another major difference between the present results and that of Thompson et al. (1989) is in the contribution to T_1 from reorientations in the nematic phase. The present analysis shows that this mechanism has a major contribution to T_1.

4.4 *CONCLUSIONS*

Comparison of the results obtained for the two benzoic acids in the present case with the earlier studies (Thompson et al. 1977, 1989) leads to interesting conclusions. The T_1 data, when analysed independently for both the systems resulted in different contributions to $(T_1^{-1})_{ODF}$. This indicates that the contribution from collective fluctuations should be independently analysed for individual systems and hence can not be taken to be constant for all the members for a homologous series. This agrees well with the observations in the third chapter on nO.m systems. A major outcome of these observations is that the ODF modes depend not only on the details of the

Table. 4.12 : Activation energies associated with the different dynamic processes in pNBA

Relaxation process	Dynamic process	Phase	Activation energy (kCal/mole)
T_1	SD assisted ODF	Nematic	7 ± 0.4
	D		10.6 ± 0.4
	R around short axis		4.4 ± 0.4
	R around end chains	Solid	1.2 ± 0.4
T_{1D}	SD assited OOF	Nematic	6.4 ± 0.8

aromatic core but also are highly sensitive to the changes in aliphatic end chains.

The results on nO.m compounds, as discussed in the third chapter, show that the cutoff frequency for ODF extend to higher frequencies as the end chain on either sides of the core are imbalanced. But, in the present case, the end chains are always balanced as these mesophases are constituted by dimers of the alkyloxy benzoic acid molecules, which have same end chains. This indicates that the ODF are not only dependent on the imbalance of end chains but also on the overall length of the end chains. Thus, these results show that there is a need to examine theoretically the influence of end chains on order director fluctuations.

Another interesting result obtained from the present results is that the frequency dependence of $(T_1^{-1})_{ODF}$ in both the systems differs from the conventional $\omega^{-1/2}$ dependence (ω^{-1} dependence for pHepBA and $\omega^{-2.5}$ dependence of pNBA) indicating that the cutoff frequencies are close to the Larmor frequency under consideration (i.e., the cutoff frequencies are of the order of tens of MHz). This can also be attributed to the strong anistropic nature of the viscoelastic coefficients of the systems. Since no information is available on these coefficients of the present systems, a definite conclusion regarding this aspect is not possible. However, the strong frequency dependence of $\omega^{-2\ 5}$ in case of pNBA could be due to the presence of another possible frequency dependent mechanism mediating the relaxation process.

From Table 4.7 and Table 4.12, it can be seen that the activation energy associated with the reorientations around short axes in pHepBA is marginally more compared to pNBA. This could be due to the reason that these reorientations get restricted (i.e., molecules are closely packed) as the end chain length is decreased. This again is in confirmatiom with the results on 4O.m systems.

Finally, it is observed from the present results that the diffusion mechanism is not a white spectrum as assumed earlier (Thompson et al., 1989) but is dependent on frequency, following the modified theory of Torrey's self diffusion for anisotropic systems. The contribution of self diffusion to the relaxation rate decreases with increase in frequency. Also the contribution from diffusion to the relaxation rate decreases in pHepBA as compared to pNBA. This increase in hinderance for self

diffusion as end chain length is reduced again suggests better packing of molecules for smaller end chain lengths. These results are also in agreement with the results obtained for nO.m systems.

Thus the results presented in this thesis show that all the three dynamic processes, in particular order director fluctuations are intricately dependent on the details of end chains in liquid crystals consisting of long rod like molecules.

REFERENCES

Abragam A and Proctor W G (1954) Phys. Rev. **109,** 1441.

Abragam A (1961) 'The principles of Nuclear magnetism', Clarandon Press, Oxford.

Agarval V and Price A (1974) J. Chem. Soc. Faraday Transact. IV 70, 188.

Ailion D C (1983) 'Methods of Solid State Physics', ed., Mundy J N, Rothman S J, Fluss K H and Sumedskjaer L C (Academic Press), 21, 439.

Alapati P R, Potukuchi D M, Rao N V S, Pisipati V G K M, Paranjpe A S and Rao U R K (1988) Liq. Cryst. 3, 1461.

Anderson A G and Redfield A G (1959) Phys. Rev. **116,** 583.

Bermann A, Gelerinter E, Frybury G C and Brown G M (1974) 'Liquid crystals and ordered fluids', 2, 23.

Bevington P R (1969) 'Data reduction and error analysis for Physical Sciences', McGraw - Hill Book Company.

Blinc R, Hogenboom D L, O'Reilly D E and Peterson E M (1969) Phys. Rev. Lett. 23, 969.

Blinc R, Burgar M, Luzar M, Pirs J, Zupancic I and Zumer S (1974) Phys. Rev. Letts. 33, 1192.

Blinc R, Luzar M, Vilfan M and Berger M (1975) J. Chem. Phys. 63, 3445.

Blinc R (1976) 'NMR basic principles and progress', ed., Pintar, M. M. 13, 97.

Blinc R, Luzar M, Mali M, Osredkar R, Seliger J and Vilfan M (1976) J. Physique Colloque 37, C3-73.

Blinc R, Vilfan M, Luzar M, Seliger J and Zagar V (1978) J. Chem. Phys. 68, 303.

Blinc R, Vilfan M and Seliger J (1983) Bull. Magn. Res. 5, 51.

Bloch F (1946) Phys. Rev. 70, 460.

Bloch F, Hansen W W and Packard M G (1946) Phys. Rev. 70, 474.

Bloembergen N, **Purcell** E M and Pound R V (1948) Phys. Rev. 73, 679.

Bloom A and Mansir D (1954) Phys. Rev. 93, 941.

Brochard F (1973) J. Phys. (Paris), 34, 411.

Brown R D and Koenig S H (1977) IBM Research Rep. RC6712, York town heights.

Bryan R F, Hartley P, Miller R W and Shen M S (1980) **Molec.** Cryst. and Liq. Cryst, 62, 281

Cesnak L and Rabat D (1972) J. Phys.E, 5, 944

Chandrasekhar S (1943) Rev. Mod. Phys. 15, 1

Chiu **U T H,** Griller D, Ingold K V and Knittel P (1979) J. Phys. **E12,** 274.

Chou L S and Carr E F (1973) Phys. Rev. A7 , 1639

Clarke W G and McNeil J A (1973) Rev. Sci. **Instr.** 44, 844.

Coppen P, Van Gerven L, **Clough** S and Horsewill A J (1983) J. Phys. C 16, 567.

Das T P and Hahn E L (1958) Solid State Physics, **Suppl.** 1, Academic Press, New **York**

de Gennes P G (1972) Solid State **Commun.** 10, 1753.

de Gennes P G (1974) The Physics of Liquid Crystals', Clarendon Press, Oxford.

de Jeu W H, Vander Veen J and Goossens W J A (1973) Solid State Commun. **12,** 405

Deloche B and Cabane B (1972) **Mol.** Cryst. Liq. Cryst. 19, 25

Derek Shaw (1976) **'Fourier** Transform NMR spectroscopy', **Elsevier,** Amsterdam.

Doane J W and Johnson D L (1970) Chem. Phys. Lett. 6, 291.

Doane J W, Tarr C E and Nickerson M A (1974) Phys. Rev. Lett. 33, 620.

Dolinsek J, Apih T and Blinc R (1992) J. Phys. ; Cond. Matter 4, 7203.

Dong R Y Forbes W and Pintar M (1972) Mol. Cryst. Liq. Cryst. 16, 213.

Dong R Y, Visintainer J J and Bock E (1974a) Can. J. Phys. 54, 1600.

Dong R Y, Wiszniewska, Tomchuk E and Bock E (1974b) Mole. Cryst. Liq. Cryst. 27, 259.

Dong R Y and Sandmen J (1983) J. Chem. Phys. 78, 4649.

Dong R Y (1986) J. Mag. Res. 66, 422.

Dybowski C, Smith B and Wade Ch (1971), J. Phys. Chem. 75,3834.

Edmonds D T (1977) Phys. Rep. 29, 233

Edmonds D T (1981) Bull. Mag. Res. 3, 53.

Farrar T C and Becker E D (1971) 'Pulse and FT NMR', Academic Press, New York.

Flannery Jr. J B and Haas W (1970) J. Phys. Chem. 74, 3611

Freed J H (1977) J. Chem. Phys. 66, 4183.

Frybury G C, Gelerinter E and Fishel D L (1972) Mole. Cryst. Liq. Cryst. 16, 39.

Fukushima E and Roeder S B W (1981) 'Experimental pulsed NMR - A nuts and bolts approach', Addison - Wesley, Reading, Massachusetts.

Garland C W and Stine K (1987) Proc. of XI Inter. Liq. Cryst. Conf. Berkeley

Gertner B J and Lindenberg K (1991) J. Chem. Phys. 94, 5143.

Ghosh S K (1976) 'Local properties of phase transitions' Ed., Muller K A and Rigamonti A (Course LIX), Inter. School of Phys., 'Enrico Fermi' North Holland, 730.

Ghosh S K, Tettamanti E and Panatta A (1980) Mol. Crys. Liq. Crys. 58, 161.

Goldman M (1970) 'Spin temperature and Nuclear Magnetic Resonance in solids' (Oxford, England) 51

Goodby J W, Gray G W, Leadbetter A L and Mazid M A (1980) 'Liquid Crystals of one and two dimensional order' ed Helfrich W and Heppke G, Springer-verlag, New York

Graf V, Noack F and Stohrer M (1977) Z. Naturforsch. **32a,** 61.

Graf V (1980) Ph.D thesis, Universittat Stuttgart, Germanay.

Gray G W (1979) 'The molecular physics of liquid crystals' Ed. Luckhurst G R and Gray G W, Academic Press

Grossl G, Winter F and Kimmich R (1985) J. Phys. E (Sci. Instr.) **18,** 538.

Hak (1936), Arch. Electrotech. 30, 736.

Hartmann S R and Hahn E L (1962) Phys. Rev. **128,** 2042.

Hatakeyama T and Ikeda M (1978) Mol. Cryst. Liq. Cryst. 45, 275

Harmon J F and Muller B N (1969) Phys. Rev. **182,** 400.

Hebel L C and Slichter C P (1959) Phys. Rev. **113,** 1504.

Hecke Van P and Jannsens G (1978) Phys. Rev. B17,2124.

Heinze E, Grande S and Loshe A (1978) Ann. Phys. 35 145.

Ikeda M and Hatakeyama T (1977) Mol. Cryst. Liq. Cryst. 39, 109

Janik J A, Janik J M, Otnes K, Rosciszewski K and Wrobel S (1973) Liq. Cryst. Ed. Chandrasekhar S, Indian Academy of Science, Bangalore, p253.

Janik J A, Janik J M, Otens K and Rosciszewski K (1974) Physica **77,** 514.

Jones G P, Daycock J T and Roberts T T (1968) J. Phys. E (Sci. Inst.) 2, 630.

Johnson B C and Goldberg W I (1966) Phys. Rev. **145,** 380.

Jeener T and Broekaert P (1967) Phys. Rev. **157,** 232

Kapustin A P and Bykova N T (1968) Sov. phys. cryst. 13, 281

Kei Murase (1971) Bull. Chem. Soc. Jpn. **45,** 1772.

Kimmich R and Noack F (1970) Z. Angew. Phys. 29, 248.

Kimmich R (1980) Bull. Magn. Res. 1, 195.

Kimmich R and Bachus R (1982) Colloid and polymer science, **260,** 911.

Kirov N, Fontana M P, Cavatorta F and Ratajczak M (1981) Mol. Cryst. Liq. Cryst. **75,** 303

Koenig S H, Bryant R G, Hallenga K and Jacob G S (1978) Biochemistry, **17,** 4348.

Kruger G J and Spiesecke H (1973) Z. Naturforsch. **28a,** 964.

Kubo R and Tomita K (1954) J. Phys. Soc. Jpn. 9, 888.

Landau L D and Khalatnikov I M (1954) Dobl. Acad. Nauk. USSR 96, 469

Landee R W, Davis D C and Albereht A P (1957) Elect. designers handbook, Ch-7, 38, McGraw Hill, New York

Levelut A M, Moussa F, Doucet J, Benettar J J, Lambert M and Dorner B (1981) J. Phys. (Paris) **42,** 1651.

Limmer, St. Schiffler J and Findeison M (1984), J. de. Phys. **45,** 1149.

Lowe I J and Tarr C E (1968) J. Phys. E1, 320

Lubensky T (1970) Phys. Rev. A 2, 2497

Luckhurst G R (1988) J. Chem. Soc. Faraday Trans. 84, 861.

Lushington K J, Kasting G B and Garland C W (1980) J. Physique. Lett. **41,** 419

Mahmood R, Khan I, Gooden C, Baldwin C, Hohnson D L and Bewbert M E (1985) Phys. Rev. **A42,** 1286.

Marcelja S (1974) J. Chem. Phys. 60, 3599

Marquese J A, Warner M and Dill K A (1984) J. Chem. Phys. 81, 6404.

Masuda Y and Redfield A G (1962) Phys. Rev. **125,** 159.

Masuda Y and Redfield A G (1964) Phys. Rev. **133A,** 944,

McLachlan (1982) J. Mag. Res. **47,** 490

McMillan W L (1971) Phys. Rev. **A2,** 1238.

McMillan W L (1972) Phys. Rev. A6, 936.

McMillan W L (1973) Phys. Rev. A7, 1673.

Miechle M and Garland C W (1983) Phys. Rev. **A27,** 2624.

Miljkovic L A, Thompson R T, Pintar M M, Blinc R and Zupancic I (1976) Chem. Phys. Lett. 38, 15.

Moore T C, Kubo A L, Mathews R C, Wade C G, Tarr C E and Field M E (1980) J. Mag. Res. 38, 135.

Nagabhushan C, Geetha G Nair, Ratna R (1988) Liq. Cryst. 3, 175.

Nimtz G, Schifferdecker M, Shih I and Mishra S (1979), Solid State Commun. 29, 287.

Noack F (1986) 'NMR field cycling spectroscopy - principles and applications' in Progress in NMR spectroscopy, 18, 171.

Noack F, Notter M and Wess W (1988) Liq. Cryst. 3, 907.

Noack F (1989) : Nato advanced study, Instituite on molecular dynamics of liquid crystals and references therein.

Norrido P L and Segre V (1979) ' The molecular phsyics of liquid crystals', **171,** Ed. Luckhurst G R and Gray G W Academic Press, New York.

Orsay liquid crystal group (1969) J. Chem. Phys. 51, 860

Owers-Bradley J R, Calder I D, Ketterson J B and Halperin W P (1981) Mol. Cryst. Liq. Cryst. 76, 175.

Packard M and Varian R (1954) Phys. Rev. 93, 941.

Pershan P S (1960) Phys. Rev. **117,** 109.

Pincus P (1969) Solid State Commun. 7, 415.

Pisipati V G K M and Rao N V S (1984) Phase Transition, 4, 91.

Pisipati V G K M, Rannavare S B and Freed J H (1987) Mol. Cryst. Liq. Cryst. Lett. 4, 181.

Potukuchi D M (1989) Ph.D thesis (Nagarjuna University, India)

Pound R V (1951) Phys. Rev. 81, 156.

Prager M, Raaen A M and Svare I (1983) J. Phys. **C16,** 181.

Pushnik F, Schara M and Sentjure M (1975) J. Phys. (Paris), 35, 665.

Pushnik F and Schara M (1976) Chem. Phys. Lett. 37, 106.

Ramadan B, Ng T C and Tward E (1974) Rev. Sci. Inst. 45, 1174.

Rannavare S B, Pisipati V G K M and Freed J H (1987) Chem. Phys. Lett. **140,** 225.

Rannavare S B, Pisipati V G K M and Freed J H (1988) Liq. Cryst. 3, 957.

Ravindranath G, Venu K, Sastry V S S and Padmavathi G (1988) Phase Trans. 12, 129.

Ravindranath G, Venu K and Sastry V S S (1990a) Chem. Phys. **140,** 299.

Ravindranath G, Venu K and Sastry V S S (1990b) Z. Phys. B ; Cond. Matter 78, 235.

Ravindranath G (1991) Ph. D thesis, Univ. of Hyderabad, India.

Ravindranath G, Venu K and Sastry V S S (1993) Mol. Cryst. Liq. Cryst. (accepted).

Redfield A G (1963) Phys. Rev. **130,** 589.

Redfield A G (1967) Phys. Rev. **162,** 367.

Redfield A G, Fite W and Bleich H E (1968) Rev. Sci. Inst. 39, 710.

Ribeiro A C (1987a) private communications

Ribeiro A C (1987b) Mol. Cryst. Liq. Cryst. **151,** 261.

Ribeiro A C, Sebestiao P J and Vilfan M (1988) Liq. Cryst. 3, 937.

Richardson R M, Leadbetter A J, Hayter J B, Sterling W G, Gray G W and Tajbakhsh A (1984) J. de. Phys. 45, 1061.

Rommel E, Mischker K, Osswald G, Schweikert K H and Noack F (1986) J. Mag. Res. 70, 219.

Rosenblatt C and Ho J T (1983) J. Phys. **44,** 383.

Rondelz F and Mircea-Roussel A (1974) Mol. Cryst. Liq. Cryst. 28, 173.

Schaetzing R and Lister J D 'Advances in Liquid crystals', (1979) 4, 147, Academic Press.

Schifferdecker M, Aichmann H and Nimtz G (1981) J. Chem. Phys. bf 75,1379.

Schmiedel M, Hillner B, Grande S, Losche A and Limmer St. (1980) J. Mag. Res. **40,** 369.

Schumacher (1958) Phys. Rev. **112,** 837.

Schweikert K H (1990), Ph.D thesis (Universität Stuttgart, Germany)

Seliger J, Orsedkar R, Mali M and Blinc R (1976) J. Chem. Phys. **65,** 2887.

Seliger J, Orsedkar R, Zager V and Blinc R (1977) Phys. Rev. Lett. 38, 411.

Shenoy R K (1978) Ph. D thesis, Indian Institute of Science, India

Slichter C P and Holton W C (1961) Phys. Rev. **122,** 1701.

Slichter C P and Ailion D C (1964) Phys. Rev. **135,** 1099.

Slichter C P (1978) 'Principles of Nuclear Magnetic Resonance', Springer-Verlag, Heidelberg,

Slusher R E and Hahn E L (1968) Phys. Rev. **116,** 332.

Smith G W and Gardlund Z G (1973) J.Chem. Phys. 59, 3214.

Solomon I (1955) Phys. Rev. 99, 559.

Solomon I and Bloembergen N (1956) J. Chem. Phys. **25,** 261.

Stejskal E U (1963) Rev. Sci. Instr. **34,** 971.

Takahashi M, Mita S and Kondo S (1987) Mol. Crys. Liq. Cryst. **147,** 99

Thompson R T and Pintar M M (1976) J. Chem. Phys. **65,** 1787.

Thompson R T, Kydon D W and Pintar M M (1977) J. Chem. Phys. **67,** 5914.

Thompson R T, Kydon D W, Lasic D D and Peemoellar H (1989) Mol. Crys. Liq. Crys. **172,** 151.

Torrey H C (1953) Phys. Rev. 97, 962.

Ukleja P, Pirs J and Doane J W (1976) Phys. Rev. **A14,** 414.

Van Steenwinkel R (1969) Z. Naturforsch **a24,** 1526.

Venu K (1986) Ph. D thesis, Univ. of Hyderabad, India

Venu K, Ravindranath G and Sastry V S S (1990) Liq. Cryst. 80, 299.

Vilfan M, Blinc R and Doane J W (1972), Solid State Commun. 11, 1073.

Vilfan M and Zumer S (1980) Phys. Rev. A21, 672.

Vilfan M, Seliger J, Zagar V and Blinc R (1980) Phys. Lett. 79A, 186.

Vilfan M, Kogoj M, and Blinc R (1987) J. Chem. Phys. 86, 1055.

Visintainer J, Doane J and Fishel D (1971) Mol. Cryst. Liq. Cryst. 13, 69.

Voigt G and Kimmich R (1980) Polymer, 21, 1001.

Vold R R and Vold R L (1988) J. Chem. Phys. 88, 4655.

Vold R R and Vold R L (1989) 'NATO advanced summer school on the Molecular dynamcis of Liquid crystals', Italy.

Von B Etenberg, Pilz W, Reich P and Koswig H D (1983) Z. Phys. Chemie 264, 499.

Wade C G (1977) Ann. Rev. Phys. Chem. 28, 47.

Wangsness R K and Bloch F (1953) Phys. Rev. 89, 728.

Winter F and Kimmich R (1982a) Mol. Phys. 45, 33.

Winter F and Kimmich R (1982b) Biochem Biophys. Acta 719, 292.

Wolf D (1979) 'Spin temperature and nuclear spin lattice relaxation in matter', Clarendon Press, Oxford.

Wolfel W (1978) Ph. D thesis, Univ. Stuttgart, Germany.

Yun C K and Frederickson A G (1970) Mol. Cryst. Liq. Cryst. 12, 73. Stu

Zientara G P and Freed J H (1983) J. Chem. Phys. 79, 3077.

Zumer S and Vilfan M (1978) Phys. Rev. **A17,** 424.

Zumer S and Vilfan M (1983) Phys. Rev. A28, 3070.

Zupancic I, Pirs I, Luzar M, Blinc R and Doane J W (1974) Sol. State Commun. 15, 227.

Zupancic I, Zager V, Rozmarin M, Levstik I, Kogosek F and Blinc R (1976) Sol. State Commun. **18,** 1591.

APPENDIX

Analysis of T_1 data in liquid crystals often requires non-linear curve fitting techniques. For example, when ever the data in a given frequency range has contributions from ODF, SD and molecular reorientations, the total relaxation rate is given by the eqn. (4.1), which is a complicated non-linear function. T_1 data is to be fitted in such a case to this expression to find the prefactors for ODF contribution (B), self diffusion coefficient $(D_\perp)$ and reorientation contribution $((T_1^{-1})_R =$ A). There are a number of non-linear curve fitting techniques that can be used for each purpose, each varying in its power to find the best fit set of parameters, the quickness in which it can arrive at such a best fit etc. The choice of a suitable technique for a given purpose depends on the complexity of the function to be fitted, the amount of the data available and the scatter in the data. There is always a question of uniqueness of this best fit obtained from such methods, particularly if the number of data points are not sufficiently large, if the number of parameters to be determined from the fit are too many and if the scatter in the data is too large. In such cases, arguements based on physical tenability of the resulting parameters are always useful in arriving at the most suitable parameters. In the present case, a combination of two methods based on the algorithms, grid search technique, gradient search technique is used.

Let

$$Y = Y(\{a_j\}, x) \quad (j = 1, 2...M)$$

is a non-linear function involving the parameters, a_j's. x is the experimental variable like frequency in the present case. The corresponding experimental values are $Y_{exp}(x_i)$ (i = 1... N). The function Y can be calculated for a given set of parameters, a_j's at all data points, given by $Y_{cal}(x_i)$. Now the root mean square deviation (rmsd) of these calculated values for the experimental points can be defined as

$$rmsd = \left\{ \frac{1}{N} \sum_{i=1}^{N} [Y_{exp}(x_i) - Y_{cal}(x_i)]^2 \right\}^{1/2} .$$

The analysis is initialized with a primary set of guess values of the parameters (say a_{oj}'s). These parameters are varied subsequently to reduce the rmsd, through numerous iterations. The principle difficulty of these methods is that the parameters obtained are not unique for different sets of initial parameters. Thus the parameter space can have more than one local minimum for the rmsd and hence the space has to be thoroughly searched for a global minimum by giving different initial guess parameters.

The grid search method assumes the parameters to be independent of each other The rmsd is minimized locally for each parameter and the final minimum is obtained by comparison of the minima obtained. The following steps explain this method.

1. Initially one parameter (say a_1) is incremented gradually in small steps δa_1 with a proper sign so that the rmsd decreases.

2. This is repeated till the rmsd does not decrease any more for further variation in the parameter value.

3. The instantaneous value of the parameter a_1 yielding the minimum RMSD is fixed.

4. This procedure is repeated with respect to the other parameters and hence all the parameters are fixed.

5. Then this procedure is repeated starting from the first parameter until the improvement in the rmsd is within a preset range

6. Finally the iterations are repeated with these parameters by decreasing the step size (δa_1) say 1/10th of the initial values and the whole procedure is repeated. This refinement procedure is repeated with respect to all the parameters till the change in rmsd is not more than a minimum tolerance limit which is considerably less than the expected experimental errors.

These parameters yielding the minimum rmsd are taken as the final set of optimized parameters. This method of searching the parameter space is not very efficient

when the number parameters to be determined is very large or when the parameters are interdependent.

The second method used in the present case is the gradient search method, which can be used in the case that the parameters are dependent on each other. The essential features of this method are given below.

1. The parameters are incremented simultaneously by suitable amounts such that the direction of scanning the rmsd in the parameter space is along the gradient of rmsd with respect to the parameters a_j's, Δrmsd (direction of maximum variation).

2. The gradient of rmsd is computed with respect to each parameter and is a vector whose components are equal to the rate at which rmsd increases in that direction.

3. To account for the variation in the dimensions of the different components of the gradient (due to the variation in the dimensions of the parameters), the increment in each parameter is normalized by a factor γ_i i.e.

$$\delta a_j = -\gamma_i a_i$$

Here γ_i is a dimensionless quantity.

4. The direction in which the minimum rmsd is searched is in a direction of steepest descent which is in a direction opposite to the direction of 7 and hence explains the negative sign in the above expression.

However the computation of the minimum using this method becomes less accurate for large step size of the increment and also inefficient for small step size, making this method inaccurate. Hence in the present case a combination of both the methods is used, first the gradient search method is used to locate the approximate minimum and then the grid search method is used for further refinement and hence location of accurate minimum. The typical program used for analysis of the relaxation data using the above non-linear methods is given below.

```
1         a s
5       INPUT  " GIVE THE FILE NAME TO STORE DETAILS OF DATA, PLEASE ",MAD$
6       OPEN MAD* FOR OUTPUT AS #3
10      REM progremme for multiparameter fit of slrt data in liquid crystals
15      REM *******Power of ODF also is taken as a variable parameter*******
20      INPUT  "NUMBER OF FREQUENCIES   = " ;N
30      M=4
40     DIM F1(N),F2(N),F(M),SLRT(N),SLRE(N),R(N>,INA(M),CX<N>,CY(N),FX(N),FY(N)
50      DIM W(N),X(N),A(M),X1(N),SLRC(N),C(N),DMSD(4),DBMSD(4),GAMA(4)
60      A =5E-08
65      KK=0
70      FOR I = 1 TO N
80      READ  W(I),SLRT(I)
90      W(I) = 2 * 22 * W(I)/7
100     SLRE(I) = 1/SLRT(I)
110 C(I ) = (3/250)*((44/7)^5)*( (42.57) ^4)*((1.054591 )^2)/W(I)
120     NEXT I
125     PRINT:PRINT:PRINT
130     PRINT  "         THIS PROGRAMME FITS SLRT DATA TO A FUNCTION AS  "
140     PRINT:PRINT:PRINT
150     PRINT  " SLRT  »  a + (b * w *  (-1)) +(1/1.4)(SLRT)Torrey "
160     PRINT:PRINT:PRINT
170     PRINT  " YOU HAVE TO PROVIDE STARTING VALUES OF a, b, AND d "
175     PRINT:PRINT:PRINT
180     INPUT  " a =  "; A(1)
190     INPUT  " b =  "; A(2)
200     INPUT  " d =  "; A(3)
205     INPUT  " alpha= "; A(4)
210     INPUT "name of the sample please";SA$
215     PRINT #3 ,CHR$(&H10)
220     PRINT #3 ,SA$
225     PRINT #3 ,CHR$(&H10)
235     PRINT #3,CHR$(&H10)
240     GOSUB 800
245     RMSDX=RMSD
250     RMSD1=RMSD
255    PRINT #3,CHR$(&H10) "initial values are: a = ";A(1);" b = ";A(2);" d = ";
A(3);" MSD =";RMSD
260     PRINT:PRINT:PRINT:PRINT "RMSD =";RMSD
270     PRINT:PRINT:PRINT
280     PRINT  "DO YOU WANT TO SEE THE PLOT (y/n)?  "
290     A* = INKEY$:IF A$= "n" THEN GOTO 380
300     IF A* <> "y" THEN GOTO 290
310     GOSUB 4000
380     PRINT "DO YOU WANT TO START GRIDSEARCH OR GRADIENT SEARCH OR NONE (r/a/n
)
390     B$=INKEY$:IF B$="n" THEN GOTO 760
400     IF B$="r" THEN GOTO 415
405     IF B$="a" THEN GOTO 7000
410     GOTO 390
415     SCREEN 0,0,0
420     PRINT:PRINT:PRINT
```

```
430     PRINT "THEN PLEASE PROVIDE INCRIMENTS OF THE PARAMETERS"
440     PRINT:PRINT:PRINT
450     INPUT "         INCRIMENT IN a =";INA(1)
460     INPUT "         INCRIMENT IN b =";INA(2)
470     INPUT "         INCRIMENT IN d =";INA(3)
471     INPUT "          INCRIMENT IN alpha =";INA(4)
472     INPUT"     Number of refinements required = ";MM
473     INPUT"     Reduction factor in iterations = ";NN
474     GOSUB 4000
475    PRINT #3,CHR$(&H10) "incriments are: ina = ";INA(1);" inb = ";INA(2);" i
nc = ";INA(3)
476     PRINT #3,CHR$(&H10) : PRINT #3,CHR$(&H10)
478     PRINT #3,CHR$(&H10) TAB<5> ;"   a ";TAB(20);"   b";TAB(35);"   d ";TAB(5
0);"alpha ";TAB(70)" MSD "
480     PRINT "                        PLEASE WAIT
500     REM PRINT:PRINT:PRINT
520     FOR  J=l TO 4
530     A(J)=A(J)+INA(J)
540     G$=INKEY$: IF G$="s" THEN GOTO 700
550     GOSUB 800
560     RMSD2=RMSD
570     IF RMSD2<RMSD1 THEN GOTO 590
580      INA(J)=-INA(J)
590     A(J)=A(J)+INA(J)
600     GOSUB 800
610     RMSD3=RMSD
620     IF RMSD3 > RMSD2 THEN GOTO 680
625     IF RMSD3 = RMSD2 THEN GOTO 680
630     RMSD1=RMSD2
640     RMSD2=RMSD3
650     GOTO 590
660     P=RMSD3-2*RMSD2+RMSD1
670     Q=(RMSD3-RMSD2)/P+.5
680     A(J)=A(J)-INA(J)
688     RMSD1=RMSD2
690     NEXT J
730     GOSUB 800
735     RMSDY=RMSD
736     IMPR=(RMSDX-RMSDY)/RMSDX
738     GOSUB 4000
746     IF IMPR<.001 THEN GOTO 752
747     RMSDX=RMSDY
750     GOTO 480
752    PRINT #3,CHR$(&H10) TAB(5);A(1) ;TAB(20);A(2);TAB(35);A(3);TAB(50);RMSD
753    PRINT #3,CHR$(&H10) : PRINT #3,CHR$(&H10)
755     PRINT #3,CHR$(&H10)"MSD HAS CONVERGED TO THE REQUIRED ACCURACY"
756    PRINT #3,CHR$(&H10) "NEXT REFINEMENT  IS IN PROGRESS"
757     GOSUB 950
758     GOTO 475
760      SCREEN 0,0,0
765     STOP
770     END
```

```
800     SD=0
805     FOR I=1 TO N
806     X(I)=SQR(W(I)*A*A/A(3))
810     X=X<I>
820     GOSUB 1000
830     F1(I) = F
840     X1(I) = SQR(2) * X(I)
850     X=X1(I)
860     GOSUB 1000
870     F2(I) = F
880     SLRC(I) = A(1)+A(2)*(W(I)^(-A(4)))+(C(I)/1.4)*(F1(I)+F2(I))
890     R(I)=SLRE(I)-SLRC(I)
900     SD=SD+R(I)^2
910     NEXT I
920     RMSD=SD/N
930     RETURN
950     KK=KK+1
955     FOR J = 1 TO 4
960     IF KK=MM THEN GOTO 980
965     INA(J) =INA(J)/NN
970     NEXT J
975     RETURN
980     PRINT #3,CHR$(&H10) "MSD HAS CONVERGED AND REFINEMENT COMPLETE'
985     GOSUB 4000
986     QQ$=INKEY$: IF QQ$ = "q" THEN GOTO 995
990     GOTO 986
995     GOTO 760
1000    REM  program to cal. f
1010    AL=1/12
1050    Q=(AL*X^2)/((1+(AL^2)*(X^4))^(.5))
1060    U=(.5>*<((Q*(1-Q))/AL)^(.5))
1065    V=(.5)*(((Q*(1+Q))/AL)^(.5))
1080    A1=1/((U^2)+(V^2))
1090    A2=(EXP(-2*V))*COS(2*U)
1100    A3=(EXP(-2*V))*SIN(2*U)
1110    A4 = 1-A1   : A5 • 1+A1
1120    F - (2/X^2)*(V*A4+(V*A5+2)*A2+U*A4*A3)
1210    RETURN
2900    DATA
4000    FOR I=1 TO N
4010    CX(I)=SQR(W(I))
4020    FX(I)=CX(I)
4030    CY(I)=SLRE(I)
4040    FY(I)=SLRC<I)
4050    NEXT I
4060    SCREEN 0,0,0
4070    CLS
4080    GOSUB 5000
4090    RETURN
```

```
4845    PRINT:PRINT:PRINT:INPUT  "number of points";N
4850   DIM CX(100),CY(100),FX<100),FY(100),T$(30)
4901    FOR I=1 TO N
4902    READ CX(I)
4903    READ CY(I)
4904    NEXT I
5000    REM variables (calc.) are fx and fy
5010    REM variables (calc.) are fx and fy
5021    PRINT:PRINT
5029    TQ=1
5033    GOTO 5040
5040 X9=CX(1) : X0=CX(1) :Y9=CY(1) :Y0=CY(1)
5050    FOR I= 1 TO N
5060    IF CX(I)>X9 THEN X9=CX(I)
5070    IF CX(I)<X0 THEN X0=CX(I)
5080    IF CY(I)>Y9 THEN Y9=CY(I)
5090    IF CY(I)<Y0 THEN Y0=CY(I)
5100    NEXT
5110    DX=(X9-X0)/10:DY=(Y9-Y0)/10
5120    X9=X9+DX:Y9=Y9+DY
5130    X0=X0-DX:Y0=Y0-DY
5140    IX=570/(X9-X0) : IY=160/(Y9-Y0)
5150    FOR I=1 TO N
5160    CX(I)=50+(CX(I)-X0)*IX
5170    CY(I)=170-(CY(I)-Y0)*IY
5180    NEXT
5290    SCREEN 2
5300    LINE (10,5) - (630,190),,B
5310    LINE (35,170)- (620,170)
5320    LINE (50,10) -(50,185)
5330    XL=107
5340    FOR I= 1 TO 10
5350    LINE (XL,168) - (XL,172)
5360    XL=XL+57
5370    NEXT
5380    YL=10
5390    FOR I=1 TO 10
5400    LINE (48,YL)-(52,YD
5410    YL=YL+16
5420    NEXT
5490    REM TEXT SCREEN 0,0,1,10
5500    XL=107:YK=20
5510    FOR I= 1 TO 4
5520    XC(I)=X0+(XL-50)/IX
5521    XL=XL+65
5522    NEXT
5523    YK=10
5524    FOR I= 4 TO 1 STEP -1
5525    YC(I)=Y0+(170-YK)/IY
5526    YK=YK+40
5527    NEXT
5551    FOR I= 1 TO 4
5552    X1(I)=XC(I)
5553    NEXT
```

```
5560    I=1
5570    XQ(I)=INT(ABS(XC(I)))
5580    X1(I)=XC(I)
5590    L=0:K=0
5600    IF XQ(I)=0 THEN XC(I)=XC(I)*10:L=L+1:XQ(I)=INT(ABS(XC(I))):GOTO 5600
5610    IF XQ(I) > 10 THEN XC(I)=XC(I)/10:K=K+1:XQ(I)=INT(ABS(XC(I))):GOTO 5610
5620    IF L=0 THEN PP=K
5630    IF K=0 THEN PP=-L
5640    IF L=0 AND K=0 THEN PP=0
5650    PP$=STR$(PP)
5652    FOR I= 1 TO 4
5660    X1(I)=X1(I)*(10^(-PP))
5670    X1(I)=(INT(X1(I)*100))/100
5680    NEXT
5701    FOR I= 1 TO 4
5702    Y1(I)=YC(I)
5703    NEXT
5710    I=1
5720    YQ(I)=INT(ABS(YC(I)))
5730    Y1(I)=YC(I)
5740    L=0:K=0
5750    IF YQ(I)=0 THEN YC(I)=YC(I)*10:L=L+1:YQ(I)=INT(ABS(YC(I))):GOTO 5750
5760    IF YQ(I)>10 THEN YC(I)=YC(I)/10:K=K+1:YQ(I)=INT(ABS(YC(I))):GOTO 5760
5770    IF L=0 THEN PP=K
5780    IF K=0 THEN PP=-L
5790    IF L=0 AND K=0 THEN PP=0
5800    PP$=STR$(PP)
5802    FOR I=1 TO 4
5810    Y1(I)=Y1(I)*(10^(-PP))
5820    Y1(I)=(INT(Y1(I)*10))/10
5830    NEXT
5860    QX=87
5870    FOR I= 1 TO 4
5880    X1$(I)=STR$(X1(I))
5900    QX=QX+65
5910    NEXT
5920    QY=126
5930    FOR I= 1 TO 4
5940    Y1$(I)=STR$(Y1(I))
5960    QY=QY-40
5970    NEXT
5980    FOR I= 1 TO N
5990    LINE (CX(I)-1,CY(I)-1) - (CX(I)+1,CY(I)+1),,B
6000    NEXT
6000    NEXT
6010    IF TQ=1 THEN GOTO 6030
6020    GOTO 6100
6030    FOR I= 1 TO N
6040    FX(I)=50+(FX(I)-XO)*IX
6050    FY(I)=170-(FY(I)-YO)*IY
6060    NEXT
6070    M=N-1
6080    FOR I* 1 TO M
6090    LINE (FX(I),FY(I))-(FX(I+1),FY(I+1))
6095    NEXT
```

```
6096    YY=2*(ABS(SD))*(ABS(IY))
6097    LINE (600,100)-<600,100-YY)
6098    LINE (599,100-YY) - (601,100-YY)
6099    LINE (599,100) - <601,100)
6130    RETURN
7000    SCREEN 0,0,0
7020    PRINT "THEN PLEASE PROVIDE INCRIMENTS OF THE PARAMETERS"
7030    PRINT:PRINT:PRINT
7040    INPUT "         INCRIMENT IN a =";INA(1)
7050    INPUT "         INCRIMENT IN b =";INA(2)
7060    INPUT "         INCRIMENT IN d =";INA(3)
7065    INPUT "         INCRIMENT IN alpha=";INA(4)
7070    GOSUB 4000
7080    PRINT #3,CHR$(&H10)"incriments are: ina = ";INA(1);" inb • ";INA(2);" ir
c = ";INA(3)
7090    PRINT #3,CHR$(&H10) : PRINT #3,CHR$(&H10)
7100    PRINT #3,CHR$(&H10) TAB(5);"  a ";TAB(20);"  b ";TAB(35);"  d ";TAB(5
0);" MSD "
7110    PRINT "                    PLEASE WAIT
7120    GOSUB 800
7130    MSD0=RMSD
7140    DSUM=0
7150    FOR J= 1 TO 4
7160    A(J)=A(J)+.01*INA(J)
7170    GOSUB 800
7180 DMSD(J) = (RMSD-MSD0) / (.01*INA(J))
7190    DBMSD(J)=DMSD(J)*INA(J)
7200 DSUM=DSUM+DBMSD( J) ^ 2
7210    A(J)=A(J)-.01*INA(J)
7220    NEXT J
7230    DSUM=SQR(DSUM)
7240    FOR J=1 TO 4
7250    GAMA(J)=DBMSD(J)/DSUM
7260    NEXT J
7270    FOR J= 1 TO  4
7280    A(J)=A(J)-GAMA(J)*INA(J)
7290    NEXT J
7300    GOSUB 800
7310    MSD1=RMSD
7315    GOSUB 4000
7320    IF MSD1>=MSD0 THEN GOTO 7370
7330    IMPR=(MSD0-MSD1)/MSD0
7340    IF IMPR<.05 THEN GOTO 7370
7350    MSD0=MSD1
7360    GOTO 7270
7370    MSD0=MSD1
7380    IF IMPR<.01 THEN GOTO 7400
7390    GOTO  7150
7400    PRINT #3,CHR$(&H10) TAB(5);A(1);TAB(20);A(2);TAB(35);A(3);TAB(50);RMSD
7405    PRINT #3,CHR$(&H10)"  GRADIENT SEARCH HAS CONVERGED TO 1% ACCURACY"
7410    PRINT #3,CHR$(&H10)
7420    GOSUB 4000
7430    PRINT "DO YOU WANT TO START GRID SEARCH (Y/N)?"
7450    PP$=INKEY$: IF PP$="y" THEN GOTO 415
7460    IF PP$="n" THEN GOTO 760
7470    GOTO 7450
```